

**Ligand-Modulated Palladium-Mediated Oxidation Reactions: Thermodynamic
Considerations and Mechanistic Insights.**

By

David L. Bruns

A dissertation submitted in partial fulfillment of
the requirements for the degree of

Doctor of Philosophy

(Chemistry)

At the

UNIVERSITY OF WISCONSIN-MADISON

2022

Date of final oral examination: 01/21/2022

The dissertation is approved by the following members of the Final Oral Committee:

Shannon S. Stahl, Professor, Chemistry

Tehshik Yoon, Professor, Chemistry

John F. Berry, Professor, Chemistry

Zachary K. Wickens, Assistant Professor, Chemistry

Abstract

Homogeneous palladium-catalyzed oxidation reactions are a powerful way to introduce functionality into organic molecules and streamline the synthesis of pharmaceuticals, agrochemicals, and commodity chemicals. In recent decades, the use of ancillary ligands has greatly improved the scope and applicability of Pd-catalyzed oxidation reactions, where they modulate catalyst activity, selectivity, and stability. Despite extensive studies cataloguing the mechanistic roles that ligands play, little attention has been given to how ancillary ligands modulate thermodynamic aspects of Pd-catalyzed oxidation reactions. Herein are reported studies of Pd-mediated oxidation reactions, with particular emphasis on how ancillary ligands modulate the thermodynamic properties of Pd catalysts and how those properties are made manifest in Pd-mediated oxidations.

Chapter 1 introduces some foundational concepts in aerobic oxidation catalysis, particularly that of overpotential and its relation to how the oxidative driving force derived from O₂ can have a profound influence on chemoselectivity in aerobic oxidation reactions. Chapter 2 describes a mechanistic study of the effects of ancillary ligands on Pd^{II/0} reduction potentials. Chapter 3 presents comparative kinetic and thermodynamic studies of Pd-mediated hydroquinone and alcohol oxidation reactions. Chapter 4 explores the development of a novel ligand-supported Pd catalyst for the oxidative homocoupling of thiophenes with relevance to the synthesis of functional materials.

Acknowledgements

I am deeply privileged to have had the opportunity to be advised by Shannon Stahl. He has a contagious passion for science and embodies scholarly excellence. Thank you, Shannon, for being a scientist I can seek to emulate without reserve.

My Stahl lab colleagues have likewise been exemplary role models, both scientifically and personally. It has been wonderful working with such kind people who are always willing to lend a hand, and to them I give many thanks. I extend a special thank you to Chase Salazar, Josh Buss, and Alex Stamoulis who always challenge me to think deeply about chemistry and made even the worst days in lab a pleasure. The UW-Madison Chemistry community—from my fellow students, to the faculty and staff—is truly phenomenal. During the past five years I have been surrounded by some of the kindest, most thoughtful, and smartest individuals I could ever hope to know, and I can't imagine having had a better graduate school experience anywhere else.

Mom and Dad, you have been constant sources of unqualified love and support. You are among the most talented and hard-working people I know, and I count it a special blessing to call you my parents. Thank you, Lauren, for coming first and setting the bar so high that I must constantly stretch myself to keep pace with you. Nonnie and Poppie, though you aren't here to read this, you have been utterly foundational in instilling in me a tenacious curiosity of the world around me, and for that my thankfulness knows no end. To my church family, thank you for support, encouragement, love, and leadership. Finally, thank you to my incredible wife Julianne. You have sacrificed so much for me and I hope you know how deeply I appreciate it and how deeply I love you for it. By your example, you constantly push me to grow in kindness, patience, and love. I am so happy to call you my wife.

Table of Contents:

Abstract.....	i
Acknowledgements	ii
Table of Contents:	iii
Table of Figures:.....	v
Table of Schemes:	viii
Table of Tables:.....	viii
Table of Equations:.....	ix
Abbreviations and Acronyms	xi
Chapter 1: The Role of Overpotential in Homogeneous Aerobic Oxidation Catalysis.....	1
1.1 Abstract	2
1.2 Introduction	3
1.3 Oxidation Reactions Involving Hydride Transfer	7
1.4 Tuning Overpotential for Chemoselective Pd-Catalyzed Aerobic Oxidations	13
1.5 Reductive Activation of O ₂ : <i>in situ</i> Generation of Organic Peroxides.....	17
1.6 Conclusions	21
1.7 Acknowledgements	22
1.8 References	22
Chapter 2: Can Donor Ligands Make Pd(OAc)₂ a Stronger Oxidant? Access to Elusive Palladium(II) Reduction Potentials and Effects of Ancillary Ligands via Palladium(II)/Hydroquinone Redox Equilibria.....	32
2.1 Abstract	33
2.2 Introduction	33
2.3 Results and Discussion.....	36
2.4 Conclusion.....	52
2.5 Acknowledgements	53
2.6 References	53
Chapter 3: Thermodynamic-Kinetic Comparison of Palladium(II)-Mediated Alcohol and Hydroquinone Oxidation	66
3.1 Abstract	67
3.2 Introduction	67
3.3 Results and Discussion.....	70
3.4 Conclusion.....	78
3.5 Acknowledgements	78
3.6 References	78
Chapter 4: Pd-Catalyzed Aerobic Oxidative Coupling of Thiophenes: Synergistic Benefits of Phenanthroline Dione and a Cu Cocatalyst	85
4.1 Abstract	86
4.2 Introduction	86
4.3 Results and Discussion.....	88
4.4 Conclusion.....	95
4.5 Acknowledgements	96
4.6 References	96
Appendix A: Supporting Information for Chapter 2.....	105
A.1 General Considerations	106

A.2	Ligand Screens	106
A.3	Approach to Equilibrium Plots.....	107
A.4	Equilibrium Constant Measurements	109
A.5	Quinone Exchange Measurements	112
A.6	Quinone/hydroquinone Reduction Potential Determination by Open Circuit Potential (OCP) Measurements	119
A.7	Synthesis of (bathocuproine)Pd Complexes	121
A.8	NMR Spectroscopic Data.....	124
A.9	Crystal Structure Data	129
A.10	Computational Data	132
A.11	References.....	146
Appendix B: Supporting Information for Chapter 3		149
B.1	General Considerations	150
B.2	Kinetic Studies: ⁴ Fb _n OH Oxidation	150
B.3	Kinetic Isotope Effect: ⁴ Fb _n OH Oxidation	153
B.4	Carboxylate Dependence: ⁴ Fb _n OH Oxidation	154
B.5	Temperature Dependence: ⁴ Fb _n OH Oxidation	154
B.6	Kinetic Studies: ⁷ BuH ₂ Q Oxidation.....	155
B.7	Kinetic Isotope Effect: ⁷ BuH ₂ Q Oxidation	158
B.8	Temperature Dependence: ⁷ BuH ₂ Q Oxidation	160
B.9	Carboxylate Dependence: ⁷ BuH ₂ Q Oxidation	161
B.10	Estimation of pK _a of 4-trifluoromethylbenzoic acid	161
B.11	Synthesis of (bc)Pd(O ₂ CR) ₂ complexes	162
B.12	Synthesis of deuterated ⁴ Fb _n OH substrates.....	165
B.13	NMR Spectroscopic Data.....	167
B.14	References	172
Appendix C: Supporting Information for Chapter 4		173
C.1	General Considerations	174
C.2	Procedures for Aerobic Oxidative Thiophene C–H Thiophene Homocoupling	175
C.3	Optimization of Aerobic Oxidative Thiophene C–H Thiophene Homocoupling	176
C.4	Attempted Thiophene C–H Homocoupling with Reported Aerobic Conditions	184
C.5	Synthetic Applications: Gram Scale Coupling of 1a and Use of Lower Catalyst Loading	185
C.6	Initial Rate Dependence on Catalyst Components	185
C.7	Kinetic Isotope Effect Studies.....	188
C.8	H/D Exchange Studies	190
C.9	Assessment of Non-Redox Active Metal Acetate Salts.....	192
C.10	Catalyst Characterization by ¹ H NMR Spectroscopy.....	193
C.11	Synthetic Procedures and Characterization Data	197
C.12	NMR Spectra of Isolated Products.....	205
C.13	References	226
Appendix D: A Thermodynamically Stable Palladium Catalyst for the Aerobic Oxidation of Organic Molecules		229
D.1	Introduction	230
D.2	Results and Discussion.....	232
D.2.1	Ligand screens	233
D.2.2	Solvent screens	235
D.2.3	Metal additive screens	241
D.2.4	Quinone screens.....	242

D.2.5	Temperature, O ₂ pressure, time, and added glass bead screens.....	244
D.2.6	Organic oxidation screen.....	245
D.3	Conclusions and future directions.....	249
D.4	Experimental.....	250
D.5	References.....	251

Table of Figures:

Figure 1.1. (A) Common oxidants used in organic oxidation reactions and their standard reduction potentials (vs SHE). (B) Common organic oxidation reactions and their standard reduction potentials (vs SHE). (C) Potential scale for O₂ reduction and common organic substrates.4

Figure 1.2. Comparison of (A) Pt-catalyzed H₂/O₂ fuel cell and (B) a catalyzed aerobic oxidation reaction and the associated potentials of the corresponding catalyzed half-reactions.....6

Figure 1.3. (A) NO_x/Oxoammonium-catalyzed organic oxidation reactions and (B) Cu/TEMPO-catalyzed alcohol oxidation reactions.9

Figure 1.4. (A) NO_x/DDQ and (B) [Ru(phd)₃]²⁺-based oxidation catalyst systems.12

Figure 1.5. (A) Pd^{0/II} and (B) Pd^{II/IV} mediated aerobic oxidation reactions.15

Figure 1.6. (A) Reductive activation of O₂ in nature. (B) Aerobic generation of hypervalent iodine reagents. (C) Pd catalyzed C–N bond formation mediated by solvent autoxidation. (C) The Mukaiyama Epoxidation18

Figure 2.1. Representative ancillary nitrogen-based ligands encountered in Pd-catalyzed oxidation reactions and considered in the present study.....36

Figure 2.2. (A) Ligand effects on the Pd(OAc)₂-mediated oxidation of ^tBuH₂BQ. Conversion determined by ¹H NMR spectroscopy using methyl-3,5-dinitrobenzoate (dioxane/AcOD-*d*₄) or 1,3,5-trimethoxybenzene (CDCl₃/AcOD-*d*₄) as an internal standard. ^a20 mM pyridine used. (B) X-ray crystal structure of (bc)Pd(^tBuBQ). H-atoms and solvent molecules omitted for clarity. See Section A.9 of Appendix A for full details.39

Figure 2.3. Approach-to-equilibrium concentration data. A: Forward Reaction: oxidation of ^tBuH₂BQ by DAF/Pd(OAc)₂ to form ^tBuBQ and [Pd^I(μ-DAF)(OAc)]₂. Reaction conditions: [Pd(OAc)₂] = 13.5 mM; [DAF] = 13.5 mM; [^tBuH₂BQ] = 6.75 mM. B: Reverse Reaction: oxidation of [Pd^I(μ-DAF)(OAc)]₂ by ^tBuBQ to form ^tBuH₂BQ and DAF/Pd(OAc)₂. [Pd^I(μ-DAF)(OAc)]₂ = 6.75 mM; [^tBuBQ] = 6.75 mM. C. Linear free energy relationship of log(*K*_{eq}) *E*_{Q/H₂Q}(dioxane/AcOH). Reaction conditions: [DAF] = 13.5 mM; [Pd(OAc)₂] = 13.5 mM; [H₂Q] = variable (see Appendix A sections A.3 and A.4 for details).41

Figure 2.4. Equilibrium reaction of (bc)Pd(OAc)₂/^tBuH₂BQ and (bc)Pd(^tBuBQ). Reaction conditions: A: Forward: [(bc)Pd(OAc)₂] = 10.0 mM; [^tBuH₂BQ] = 10.0 mM. B: Reverse: [(bc)Pd(^tBuBQ)] = 10 mM C. Linear free energy relationship of log(*K*_{eq}) and *E*_{Q/H₂Q}(CHCl₃/AcOH). Reaction conditions: [(bc)Pd(OAc)₂] = 10.0 mM [H₂Q] = variable (see sections A.3 and A.4 of Appendix A for details).43

Figure 2.5. A. Energy diagram for reaction of (L)Pd(OAc)₂ and hydroquinone. Energies of (L)Pd(OAc)₂ complexes are reported relative to (phen)Pd(OAc)₂. B. Scale showing calculated reduction potentials for (L)Pd(OAc)₂ complexes.47

Figure 3.1. Kinetic analysis of (bc)Pd(OAc)₂-mediated oxidation of ^tBuH₂Q, including (a) [(bc)Pd(OAc)₂] dependence, (b) [^tBuH₂Q] dependence, and (c) kinetic isotope effect obtained via independent rate measurement. See sections B.6 and B.7 in Appendix B for experimental details.....71

Figure 3.2. Kinetic analysis of (bc)Pd(OAc) ₂ -mediated oxidation of ⁴ Fb ₃ OH, including (a) [(bc)Pd(OAc) ₂] dependence (b) [⁴ Fb ₃ OH] dependence, and kinetic isotopic effects determined by (c) independent rate measurements of ⁴ Fb ₃ OH and ⁴ FPhCD ₂ OH and (d) an intramolecular competition experiment with ⁴ FPhC(H)(D)OH. See sections B.2 and B.3 in Appendix B for experimental details.....	72
Figure 3.3. Rate dependence of ⁴ Fb ₃ OH oxidation by (bc)Pd(O ₂ CR) ₂ on (a) pK _a (DMSO) of RCO ₂ H and (b) on percent buried volume. Rate dependence of ¹ BuH ₂ Q oxidation by (bc)Pd(O ₂ CR) ₂ on (c) pK _a (DMSO) of RCO ₂ H and (d) on percent buried volume. [‡] Percent buried volume values obtained from PR ₃ ligands (see text for details).....	74
Figure 3.4. Free energy diagram for (bc)Pd(OAc) ₂ -mediated oxidation of ⁴ Fb ₃ OH and ¹ BuH ₂ Q.	75
Figure 4.1. (A) Commercial organic polymers for materials science applications containing a 2,2'-bithiophene unit. (B) Precedent for Pd-catalyzed oxidative homocoupling of 2-bromo-3-alkylthiophenes with stoichiometric AgI oxidants, and (C) aerobic oxidation method targeted in the present study.....	87
Figure 4.2. Ligand Effects in Pd/Cu-Cocatalyzed Aerobic C–H Homocoupling of 2-Bromo-3-Hexylthiophene. Conditions: 0.17 mmol 2-bromo-3-hexylthiophene, 5 mol% ligand (for L5-L11 and phd) or 10 mol% ligand (L1-L4), 0.25 mL in DMSO. Yields determined by HPLC.....	89
Figure 4.3. Assessment of Catalytic Components on Thiophene C–H Homocoupling. Conditions: 1a (1.1 mmol), catalyst (3 mol%), 1.0 mL in DMSO, 1.1 atm pO ₂ , 120 °C, 16 hr.....	90
Figure 4.4. Substrate Scope for Phd/Pd(OAc) ₂ -Catalyzed Aerobic Oxidative Coupling of Thiophenes. Conditions: Substrate (1.1 mmol, 1.1 M), 3 mol% each Pd(OAc) ₂ , phd, Cu(OAc) ₂ •H ₂ O, BQ, 1 mL reaction volume in DMSO, 120 °C, 1.1 atm O ₂ , 16 hr. ¹ H NMR yields, with isolated yields in parentheses. ^a Solvent was a 1.2:1 mixture DMSO: CyOAc. ^b 100 °C. ^c 5 mol% catalyst. ^d Mn(OAc) ₂ •4H ₂ O used instead of Cu(OAc) ₂ •H ₂ O. ^e 24 hr. ^f R = 2-(butyl)octyl; obtained with ~7% unidentified impurity (see section C.11 of Appendix C for details). ^g isolated in 9:1 ratio with monodeprotected 3p (see Section C.11 of Appendix C for details).....	91
Figure 4.5. Mechanistic experiments probing the effect of Cu(OAc) ₂ loading on the rate (A) and the role of Cu(OAc) ₂ on C–H activation and C–C coupling (B).	93
Figure 4.6. Proposed structure of catalytically active phd-supported Cu/Pd heterobimetallic complex....	95
Figure A.1. Variable temperature ¹ H NMR Spectra for exchange of ¹ BuBQ with (bc)Pd(MeBQ). Asterisk (*) denotes unidentified, temperature-dependent peak. See above text for details.	115
Figure A.2. Variable temperature ¹ H NMR Spectra for exchange of MeBQ with (bc)Pd(BQ).	117
Figure A.3. Variable temperature ¹ H NMR Spectra for exchange of BQ with (bc)Pd(CIBQ).....	118
Figure A.4. Open circuit potential measurements (vs. Fc ⁺⁰) for 1:1 mixtures of Q/H ₂ Q in 3:1 1,4-dioxane:AcOH with tetrabutylammonium tetrafluoroborate supporting electrolyte (500 mM).	120
Figure A.5. Open circuit potential measurements (vs. Fc ⁺⁰) for 1:1 mixtures of Q/H ₂ Q derivatives in chloroform/AcOH (1.5 M AcOH) with tetrabutylammonium hexafluorophosphate supporting electrolyte (500 mM).	121
Figure A.6. Single XRD structure of (bc)Pd(¹ BuBQ).....	131
Figure B.1. Initial rate of formation of 4-fluorobenzaldehyde vs ⁴ Fb ₃ OH concentration.....	151
Figure B.2. Initial rate of formation of 4-fluorobenzaldehyde vs (bc)Pd(OAc) ₂ concentration.....	151
Figure B.3. Initial rate of formation of 4-fluorobenzaldehyde vs [¹ BuBQ]	152
Figure B.4. Kinetic isotope effect: Initial rate of formation of 4-fluorobenzaldehyde from ⁴ Fb ₃ OH and ⁴ FPhCD ₂ OH.....	153

Figure B.5. Eyring plot for (bc)Pd(OAc) ₂ -mediated ⁴ F ₇ BnOH oxidation	155
Figure B.6. Dependence of initial rate of formation of (bc)Pd(^t BuBQ) on [^t BuH ₂ Q]. (a) representative UV/Vis spectral stack for formation of (bc)Pd(^t BuBQ) and (b) initial rate dependence on [^t BuH ₂ Q]	156
Figure B.7. Initial rate of formation of (bc)Pd(^t BuBQ) vs [(bc)Pd(OAc) ₂].....	157
Figure B.8. Initial rate of formation of (bc)Pd(^t BuBQ) vs [^t BuBQ].	157
Figure B.9. Time course and initial rate data for formation of (bc)Pd(^t BuBQ) from ^t BuH ₂ Q and ^t BuD ₂ Q. (a.) and (c.) represent time course and initial rate data before time adjustment. (b.) and (d.) represent time course and initial rate data after time adjustment	159
Figure B.10. Eyring plot for (bc)Pd(OAc) ₂ -mediated ^t BuH ₂ Q oxidation.....	160
Figure B.11. Carboxylic acid pK _a (DMSO) vs phenol pK _a (DMSO)	162
Figure C.1. Comparison of spectroscopic yields of selected substrates from Figure 4.4 to spectroscopic yields from conditions adapted from Wang's aerobic thiophene C–H homocoupling.....	184
Figure C.2. Dependence on [BQ] and Initial-Rate Time Course. Standard conditions: 33 mM catalyst ([Pd(OAc) ₂], [Cu(OAc) ₂ ·H ₂ O], [phd], [BQ]), 1.1 M [2a] (0.55 mmol), 1.1 atm pO ₂ , 0.50 mL in DMSO, 120 °C. Standard conditions were employed, except for varied [BQ].	186
Figure C.3. Rate Dependence on pO ₂ . Conditions: 33 mM catalyst ([Pd(OAc) ₂], [Cu(OAc) ₂ ·H ₂ O], [phd], [BQ]), 1.1 M [2a] (1.1 mmol), 1.1 atm pO ₂ or ambient air, 1.0 mL in DMSO, 120 °C.....	186
Figure C.4. Rate dependence on 1a. Conditions: 33 mM catalyst ([Pd(OAc) ₂], [Cu(OAc) ₂ ·H ₂ O], [phd], [BQ]), varying [2a] (1.1 mmol), 1.1 atm pO ₂ or ambient air, 0.5 mL in DMSO, 120 °C.	187
Figure C.5. Initial rate data for formation of 2a from 1a (black) or 1a-d ₁ (red) at [Cu(OAc) ₂] = 8.25 mM	189
Figure C.6. Initial rate data for formation of 2a from 1a (black) or 1a-d ₁ (red) at [Cu(OAc) ₂] = 33 mM	189
Figure C.7. Initial rate data for formation of 2a from 1a (black) or 1a-d ₁ (red) at [Cu(OAc) ₂] = 110 mM	189
Figure C.8. ¹ H NMR spectra of the crude reaction mixtures from H/D exchange of 1a with DOAc.	191
Figure C.9. ² H NMR spectra of the crude reaction mixtures from H/D exchange of 1a with DOAc.....	192
Figure C.10. Plot of titration of Pd(OAc) ₂ with phd as monitored by ¹ H NMR spectroscopy.....	194
Figure C.11. Titration experiment involving addition of phd into a solution of Pd(OAc) ₂ in DMSO. Pd(OAc) ₂ /phd species is denoted by 'a'; free phd is denoted by 'b'; free Pd(OAc) ₂ is denoted by 'c'; * denotes methyl 3,5-dinitrobenzoate internal standard.	194
Figure C.12. ¹ H NMR Spectral Studies of phd-Pd/Cu(OAc) ₂ Mixtures ¹ H NMR spectra of mixtures of (1) phd + Pd(OAc) ₂ + Cu(OAc) ₂ ; (2) phd + Cu(OAc) ₂ ; (3) phd + Pd(OAc) ₂ in DMSO-d ₆ (all components 33 mM). Spectra are clipped vertically to amplify the phd resonances. NMR parameters =500 MHz, DMSO-d ₆ , 8 scans, 2 dummy scans, T1 relaxation delay: 10 seconds	196
Figure C.13. ¹ H NMR spectra of mixtures of (1) phen + Pd(OAc) ₂ + Cu(OAc) ₂ ; (2) phen + Cu(OAc) ₂ ; (3) phen + Pd(OAc) ₂ in DMSO-d ₆ (all components 33 mM). Spectra are clipped vertically to amplify the phd resonances. NMR parameters =500 MHz, DMSO-d ₆ , 8 scans, 2 dummy scans, T1 relaxation delay: 10 seconds.....	197
Figure D.1. Pourbaix Diagram for Pd and acetaldehyde, with relevant Wacker Process conditions	232

Table of Schemes:

Scheme 2.1. Role of Benzoquinone as a (Co-)Oxidant in Palladium-Catalyzed Oxidation Reactions	34
Scheme 2.2. Determination of (L)Pd(OAc) ₂ Reduction Potentials in Dioxane/AcOH (L = DAF) and CHCl ₃ /AcOH (L = bc)	45
Scheme 2.3. Ligand-Based Structure Contributions to Modulation of Pd ^{II} Reduction Potentials	50
Scheme 2.4. Thermodynamic Considerations for Pd ^{II} -Catalyzed Oxidation Reactions	51
Scheme 3.1. Redox Half Reactions in Pd-catalyzed Oxidations with Benzoquinone as the Oxidant.	68
Scheme 3.2. Comparison of Redox Potentials for Pd ^{II/0} , BQ/H ₂ Q, and PhCHO/PhCH ₂ OH.	68
Scheme 3.3. (bc)Pd(OAc) ₂ -Mediated Oxidation of ^t BuH ₂ Q and ^{4F} BnOH.	69
Scheme 3.4. Proposed Mechanisms for (A) Hydroquinone and Benzyl Alcohol Oxidation Mediated by (bc)Pd(OAc) ₂ and (B) Oxidation of Pd ⁰ by Benzoquinone in the Presence of Acid ²¹	76
Scheme D.1. Generic mechanism of Pd catalyzed aerobic oxidation reaction	231

Table of Tables:

Table A.1. Determination of equilibrium constants for Equation A.1	110
Table A.2. Determination of equilibrium constants for Equation A.2 with ^t BuH ₂ BQ.....	111
Table A.3. Determination of equilibrium constants for Equation A.2 with MeH ₂ BQ.....	112
Table A.4. Determination of equilibrium constants for Equation A.2 with H ₂ BQ.....	112
Table A.5. Determination of equilibrium constants for Equation A.2 with ClH ₂ BQ	112
Table A.6. Equilibria data and van't Hoff plot for exchange of ^t BuBQ with (bc)Pd(MeBQ).....	116
Table A.7. Equilibria data and van't Hoff plot for exchange of MeBQ with (bc)Pd(BQ).....	118
Table A.8. Equilibria data and van't Hoff plot for exchange of BQ with (bc)Pd(ClBQ).	119
Table A.9. Crystal data and structure refinement for (bc)Pd(^t BuBQ)	131
Table B.1. Initial rate data for formation of 4-fluorobenzaldehyde with variable [^{4F} BnOH]	151
Table B.2. Initial rate data for formation of 4-fluorobenzaldehyde with variable [(bc)Pd(OAc) ₂].....	152
Table B.3. Initial rate data for formation of 4-fluorobenzaldehyde with variable [(bc)Pd(OAc) ₂]	152
Table B.4. Initial rate data for formation of 4-fluorobenzaldehyde with (bc)Pd(O ₂ CR) ₂ complexes.....	154
Table B.5. Initial rate data for formation of (bc)Pd(^t BuBQ) with variable [^t BuH ₂ Q].....	156
Table B.6. Initial rate data for formation of (bc)Pd(^t BuBQ) with variable [(bc)Pd(OAc) ₂].....	157
Table B.7. Initial rate data for formation of (bc)Pd(^t BuBQ) with variable [^t BuBQ]	158
Table B.8. Initial rate data for formation of (bc)Pd(^t BuBQ) from (bc)Pd(O ₂ CR) ₂ complexes.....	161
Table B.9. pK _a values for 4-substituted phenols and carboxylic acids	162
Table C.1. Assessment of Alternative Reaction Conditions: 50 °C.....	176
Table C.2. Assessment of Alternative Reaction Conditions: 120 °C.....	177

Table C.3. Monodentate Pyridine Screening	178
Table C.4. Bidentate Ligand Screening	180
Table C.5. Cu Cocatalyst Screening	181
Table C.6. Pd Catalyst Screening	182
Table C.7. Catalyst Component Screening.....	183
Table C.8. Compiled initial rate data for formation of 2a from 1a and 1a-d₁ under varying [Cu(OAc) ₂].	188
Table C.9. Results of H/D Exchange Studies from ¹ H NMR Analysis	191
Table C.10. Acetate Salt Additive Screen	192
Table C.11. Concentrations of Species in phd Titration.....	193
Table D.1. Ligand screen for Pd corrosion	234
Table D.2. Solvent screen for Pd corrosion	236
Table D.3. Solvent screen with AcOH cosolvent for Pd corrosion	238
Table D.4. Solvent screen with TFAH cosolvent for Pd corrosion	239
Table D.5. Metal additive screen for Pd corrosion	242
Table D.6. Quinone screen for Pd corrosion.....	243
Table D.7. Temperature, O ₂ pressure, and glass bead screen with best corrosion conditions	244
Table D.8. Effect of time on Pd corrosion	245
Table D.9. Benzyl alcohol oxidation to benzaldehyde by corroded Pd solutions	246
Table D.10. Styrene oxidation to acetophenone by corroded Pd solutions	247
Table D.11. 4-phenylcyclohexanone dehydrogenation to 4-phenylcyclohexenone by corroded Pd solutions	248

Table of Equations:

Equation 2.1. Reaction of DAF/Pd(OAc) ₂ with ^t BuH ₂ BQ.....	37
Equation 2.2. Equilibrium expression for reaction of DAF/Pd(OAc) ₂ and ^t BuH ₂ BQ.....	41
Equation 2.3. Equilibrium expression for reaction of (bc)Pd(OAc) ₂ with hydroquinones	43
Equation A.1.	110
Equation A.2.	111
Equation A.3.	113
Equation A.4.	114
Equation A.5.	114
Equation D.1. General reaction scheme for Pd dissolution experiments	233
Equation D.2. Reaction scheme for ligand screen.....	234

Equation D.3. Reaction scheme for solvent screen	236
Equation D.4. Reaction scheme for AcOH cosolvent screen	238
Equation D.5. Reaction scheme for TFAH cosolvent screen	239
Equation D.6. Reaction scheme for transition metal salt additive screen	242
Equation D.7. Reaction scheme for quinone screen	243
Equation D.8. Reaction scheme for temperature, O ₂ pressure and glass beads	244
Equation D.9. Reaction scheme for time reaction time screen	245
Equation D.10. Reaction scheme for corrosion-oxidation sequence with benzyl alcohol substrate	246
Equation D.11. Reaction scheme for corrosion-oxidation sequence with styrene substrate	247
Equation D.12. Reaction scheme for corrosion-oxidation sequence with 4-phenylcyclohexanone substrate	248

Abbreviations and Acronyms

2,6-Me ₂ BQ	2,6-dimethyl-1,4-benzoquinone
2,6-Me ₂ H ₂ Q	2,6-dimethyl-1,4-hydroquinone
AcOH	acetic acid
bc	2,9-dimethyl-4,7-diphenyl-1,10-phenanthroline
bphen	4,7-diphenyl-1,10-phenanthroline
Bpy	2,2'-bipyridine
BQ	1,4-benzoquinone
CIBQ	2-chloro-1,4-benzoquinone
ClH ₂ Q	2-chloro-1,4-hydroquinone
DAF	4,5-diazafluoren-9-one
DCM	dichloromethane
DDQ	2,3-dichloro-5,6-dicyano- <i>p</i> -benzoquinone
DFT	density-functional theory
dmbpy	6,6'-dimethyl-2,2'-bipyridine
dmphen	2,9-dimethyl-1,10-phenanthroline
DMSO	dimethyl sulfoxide
equiv	equivalent(s)
ESI	electrospray ionization
H ₂	molecular hydrogen
HOR	hydrogen oxidation reaction
HRMS	high-resolution mass spectrometry
KIE	kinetic isotope effect
MeBQ	2-methyl-1,4-benzoquinone
MeH ₂ Q	2-methyl-1,4-hydroquinone
mol%	mole percent
NADH	nicotinamide adenine dinucleotide
NHE	normal hydrogen electrode
NMR	nuclear magnetic resonance
O ₂	molecular oxygen
ORR	oxygen reduction reaction
phd	1,10-phenanthroline-5,6-dione
phen	1,10-phenanthroline
PSI	pound-force per square inch
py	pyridine
SHE	standard hydrogen electrode
^t AmylOH	<i>tert</i> -amyl alcohol
TBHBQ	4- <i>tert</i> -butyl-2-hydroxybenzoquinone
TBHP	<i>tert</i> -butyl hydroperoxide

¹ BuBQ	<i>tert</i> -butyl-1,4-benzoquinone
¹ BuH ₂ Q	<i>tert</i> -butyl-1,4-hydroquinone
TEMPO	Tetramethylpiperidine <i>N</i> -oxyl
THF	tetrahydrofuran
⁴ FbOH	4-fluorobenzyl alcohol

Chapter 1: The Role of Overpotential in Homogeneous Aerobic Oxidation Catalysis

This work was prepared with Alexios G. Stamoulis.

1.1 Abstract

Oxidation reactions are an indispensable tool for synthetic chemists. However, many oxidation reactions demand the use of harsh and hazardous stoichiometric oxidants. The catalytic aerobic oxidation of organic molecules has the ability to streamline the synthesis of complex molecules and obviate many of the challenges associated with using chemical oxidants in synthesis. A key challenge in using O_2 as an oxidant in the context of complex molecules is chemoselectivity. In this work, we analyze a selection of catalytic aerobic oxidation reactions in the context of overpotential as it relates to the oxygen reduction reaction (ORR) and the oxidation of organic substrates. Overpotential, a concept widely employed in the field of electrocatalysis, provides a useful framework for understanding the importance of thermodynamic considerations in aerobic oxidations. We highlight several examples where catalysts facilitate the selective oxidation of organic molecules using O_2 as a terminal oxidant by modulating the amount of oxidative power that is derived from O_2 . Catalyst systems that operate at low overpotential with respect to ORR, and high overpotential with respect to substrate oxidation, demonstrate promiscuous substrate oxidation by capturing a greater amount of oxidative potential from O_2 , enabling high-energy reaction pathways such as direct electron- and hydride-transfer pathways. Other catalyst systems that operate at high overpotential with respect to ORR, and low overpotential with respect to substrate oxidation, demonstrate greater chemoselectivity and functional group compatibility by effectively "wasting" some of dioxygen's oxidative potency and operating via mechanisms that circumvent high-energy pathways in favor more inherently selective low-energy mechanisms. We also show that switches in chemoselectivity can be achieved by changing the overpotential at which the catalyst system operates, modulating selectivity between products with high and low reduction potentials. Finally, we demonstrate that reductive

activation of O₂ to generate high potential organic peroxides enables the synthesis of high-potential products and obviates the need for strong stoichiometric oxidants. Analysis of catalytic aerobic oxidation reactions through the lens of overpotential should provide a useful framework for the design of selective aerobic oxidation reactions.

1.2 Introduction

The oxidation of organic molecules is a powerful means to introduce functionality and streamline chemical synthesis in the commodity chemical, agrochemical, fine chemical, and pharmaceutical industries.¹⁻⁴ Most industrially relevant oxidation reactions involve the formal dehydrogenation of a substrate or the formal dehydrogenative coupling between a C–H bond and another C–H bond or heteroatom–H bond. Many oxidation reactions require use of harsh oxidants such as ozone, peroxides, and chromium and osmium salts that pose considerable safety hazards and/or generate (super)stoichiometric amounts of waste, including environmentally toxic heavy metal salts. However, the widespread use of these strong oxidants belies the fact that the thermodynamic driving forces required for the oxidation of a wide variety of substrates are small relative to the potentials of the oxidants used (Figure 1.1).⁵ For example, the thermodynamic potential for the dehydrogenation of isopropanol to acetone is 0.12 V vs SHE, while the 2 H⁺/2 e⁻ reduction potential of benzoquinone (BQ) is 0.69 V vs SHE, representing an excess oxidative driving force of >0.5 V.

Dioxygen is the ideal oxidant. It is inexpensive, readily accessible, produces only environmentally benign byproducts (water), and is amenable to large-scale applications. Indeed, it sees widespread use as an oxidant in commodity chemical synthesis where it is one of the only economically viable oxidants.³ Although the unmediated aerobic oxidation of organic molecules (i.e. autoxidation) can be employed in select cases to oxidize organic molecules to value-added

products (e.g. the Cumene process), this strategy is limited to substrates that undergo site-selective radical reactions. Therefore, the development of catalysts to impart selectivity in the aerobic functionalization of more complex molecules, such as pharmaceuticals and agrochemicals, represents a significant challenge. However, addressing the selectivity challenge raises a fundamental stoichiometry problem: how can O_2 —a $4 H^+/4 e^-$ oxidant—be used to perform the $2 H^+/2 e^-$ oxidations most commonly implemented in synthetic contexts?

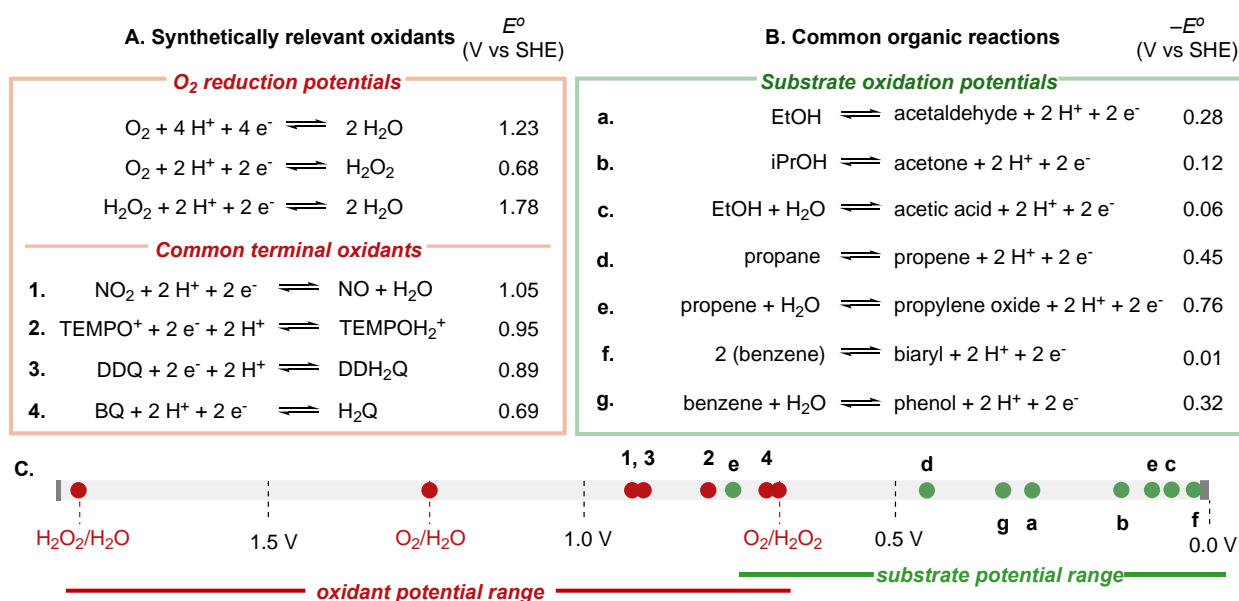


Figure 1.1. (A) Common oxidants used in organic oxidation reactions and their standard reduction potentials (vs SHE). (B) Common organic oxidation reactions and their standard reduction potentials (vs SHE). (C) Potential scale for O_2 reduction and common organic substrates.

There are two distinct $2 H^+/2 e^-$ redox couples associated with O_2 reduction: O_2 reduction to H_2O_2 (0.68 V vs SHE) and H_2O_2 reduction to H_2O (1.78 V vs SHE), with the net $4 H^+/4 e^-$ reduction of O_2 to H_2O at 1.23 V vs SHE.⁶ In principle, the O_2/H_2O_2 couple provides suitable thermodynamic driving force for most organic oxidations (cf. Figure 1.1). But having sufficient driving force for a reaction is a necessary but ultimately insufficient condition to promote effective

aerobic oxidation catalysis. In a typical aerobic oxidation reaction, there are two half reactions of central importance: substrate oxidation and oxygen reduction. Successful catalysis demands that both reactions be kinetically competent, and there are significant kinetic challenges associated with the O₂ reduction reaction (ORR). O₂ reduction to H₂O₂ involves five substrates—O₂, 2 H⁺, and 2 e⁻—and O₂ to water involves nine.⁶ The kinetic hurdles associated with this deceptively simple reaction are exemplified in the context of H₂/O₂ fuel cells: high kinetic barriers associated with the 4 H⁺/4 e⁻ reduction of O₂ at the cathode surface severely limit a fuel cell's efficiency and, therefore, energy output.⁷

One metric widely used to compare the relative performance of ORR catalysts is overpotential, defined as the difference between the thermodynamic potential of the 4 H⁺/4 e⁻ O₂/H₂O couple (1.23 V vs NHE) and the empirically observed potential at which ORR occurs (Figure 1.2A).⁸ The ORR overpotential (η_{ORR}) contributes to energetic losses incurred in the cell and is directly related to the amount of energy that can be harvested relative to the theoretical maximum of 1.23 V vs SHE for a H₂/O₂ fuel cell. (It should be noted that although there are kinetic challenges associated with the H₂ oxidation reaction (HOR) at the anode, these are negligible compared to those encountered for the oxygen reduction reaction, hence the small value for E°_{HOR} in Figure 1.2A.) The overpotential of ORR is highly dependent on the catalyst fixed to the electrode surface. State of the art Pt catalysts are capable of performing ORR at approximately 0.9 V vs NHE, as defined by the onset potential for ORR, although the potential at which ORR occurs varies based on factors such as the current density at which the ORR is performed. Because of prohibitive costs, a tremendous amount of research has been dedicated to the development of ORR catalysts that operate at low overpotential without the need for expensive Pt-group catalysts.⁹

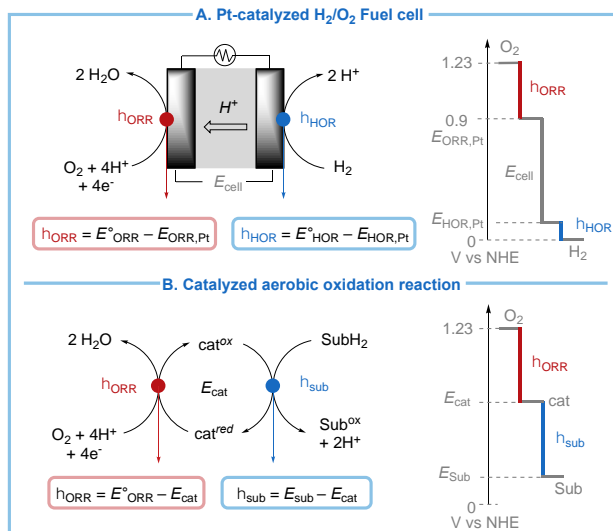


Figure 1.2. Comparison of (A) Pt-catalyzed H₂/O₂ fuel cell and (B) a catalyzed aerobic oxidation reaction and the associated potentials of the corresponding catalyzed half-reactions.

The success of catalytic aerobic oxidation reactions and H₂/O₂ fuel cells hinges on effective transfer of protons and electrons from a substrate to O₂. In fuel cells, the substrate is H₂ (or other hydrogen carriers like NH₃ or MeOH), while in organic oxidation reactions the substrate is a functional group in an organic molecule. This similarity between fuel cells and catalytic aerobic organic oxidation reactions allows for the extension of the concept of overpotential to the latter process. In the case of catalytic aerobic oxidation reactions, there are two relevant overpotential values that can be defined. The first is the difference in potential between the thermodynamic potential of ORR and the thermodynamic potential of the redox active catalyst involved in ORR (η_{ORR}), and this is the same as the overpotential for ORR in a fuel cell. The second is the difference in the thermodynamic potentials of the redox active catalyst directly involved in substrate oxidation and the organic substrate (η_{sub}), and this value is analogous to HOR. A large η_{sub} indicates a large thermodynamic driving force for the oxidation of substrate by the catalyst, while a smaller value represents a smaller driving force.

This work analyzes a selection of catalytic aerobic oxidation reactions in the context of η_{ORR} and η_{sub} , with a particular emphasis on how these values influence chemoselectivity. It also explores how reductive activation of O_2 as a means to generate thermodynamically potent and kinetically reactive peroxide species is an important strategy for the formation of high reduction potential products.

1.3 Oxidation Reactions Involving Hydride Transfer

TEMPO versus Cu/TEMPO catalyzed oxidation reactions. Oxoammonium and *N*-oxyl based oxidant systems see widespread use in organic synthesis for a wide variety of transformations,^{10,11} including alcohol^{12–16} and amine^{17,18} oxidation, oxidative cleavage of ethers,^{19,20} and C–H oxidation reactions (Figure 1.3A).^{21,22} Though they are often employed as stoichiometric oxidants, catalytic variants have been developed using terminal oxidants such as NaOCl ,²³ oxone,²⁴ and hypervalent iodine,²⁵ or can be turned over electrochemically.¹¹ Oxoammonium-mediated alcohol oxidation either proceeds via a direct bimolecular hydride transfer from alcohol to oxoammonium (under acidic conditions) or through the intermediacy of an alcohol/oxoammonium adduct, followed by intramolecular hydride transfer (under basic conditions, Figure 1.3A).¹³ Direct hydride transfer mechanisms to oxoammonium have likewise been implicated in mediated electrochemical Shono-type oxidations of piperidines and related heterocycles.²⁶

Tetramethylpiperidine *N*-oxyl (TEMPO) is the prototypical example of an oxoammonium oxidant and has a standard potential of 0.95 V vs SHE for the $\text{H}^+ / 2 \text{e}^-$ reduction of TEMPO^+ to TEMPOH.^{27,28} The high potential values oxoammonium reagents typically display has two important consequences on their synthetic and catalytic applications. The first is that oxoammonium reagents have inherently small η_{ORR} values, since the oxoammonium potential lies

close to the $\text{O}_2/\text{H}_2\text{O}$ potential. Consequently, regeneration of TEMPO^+ from TEMPOH generally requires the use of a strong chemical oxidant. At 1.23 V, the $4 \text{H}^+/4 \text{e}^-$ reduction of O_2 to H_2O has sufficient driving force to facilitate oxidation of TEMPOH to TEMPO^+ , with a η_{ORR} of 0.28 V. However, kinetic limitations make the direct regeneration of TEMPOH from TEMPO^+ with O_2 challenging. It is also worth noting that conditions that can only perform the $2 \text{H}^+/2\text{e}^-$ reduction of O_2 to H_2O_2 at 0.68 V would result in a η_{ORR} of -0.27 V, making the regeneration of TEMPO^+ prohibitively uphill. While the direct aerobic regeneration of TEMPO^+ is not practically feasible, the aerobic oxidation of TEMPOH can be achieved by means of the addition of cocatalytic NO_x (Figure 1.3A), whose $2 \text{H}^+/2 \text{e}^-$ standard potential is 1.05 V (NO_2/NO). The reduction of O_2 to H_2O by cocatalytic NO_x is kinetically facile and involves two high potential $1 \text{H}^+/1 \text{e}^-$ steps: the $1 \text{H}^+/1 \text{e}^-$ NO_2/HNO_2 couple is 1.06 V vs SHE and the $1 \text{H}^+/1 \text{e}^-$ HNO_2/NO couple is 1.04 V vs SHE.²⁹ By reducing O_2 to water at the NO_2/NO potential, an η_{ORR} value of only 0.18 V is achieved. Thus, much of the oxidative driving force of O_2 needed to regenerate TEMPO^+ from TEMPOH is captured, while bypassing the thermodynamically unfavorable $2 \text{H}^+/2 \text{e}^-$ reduction of O_2 with TEMPOH . This strategy enables the electrochemical reduction of O_2 with overpotentials as low as 300 mV in acetonitrile, rivalling the state-of-the-art ORR catalysts employed in fuel cells.²⁹ In an organic chemistry context, the use of $\text{NO}_x/\text{TEMPO}^+$ catalyst systems enabled the aerobic oxidation of alcohols, the oxidation of primary amines to nitriles, as well as the oxidative cleavage or α -C-H functionalization of ethers and cyclic amines (Figure 1.3A).^{30,31}

The second consequence of their high reduction potentials is that oxoammonium reagents possess large η_{sub} values. For instance, the η_{sub} values for the oxidation of ethanol to acetaldehyde, and isopropanol to acetone with TEMPO^+ are 0.67 V and 0.83 V, respectively. These large values have direct implications on chemoselectivity. The presence of multiple oxidatively sensitive

functional groups in a given molecule presents a challenge for selective oxidation with a reagent that has little ability to discriminate between functional groups, due to the large driving force available and the consequent high-energy mechanistic pathways that the large driving forces enable, such as direct hydride- and electron-transfer mechanisms.

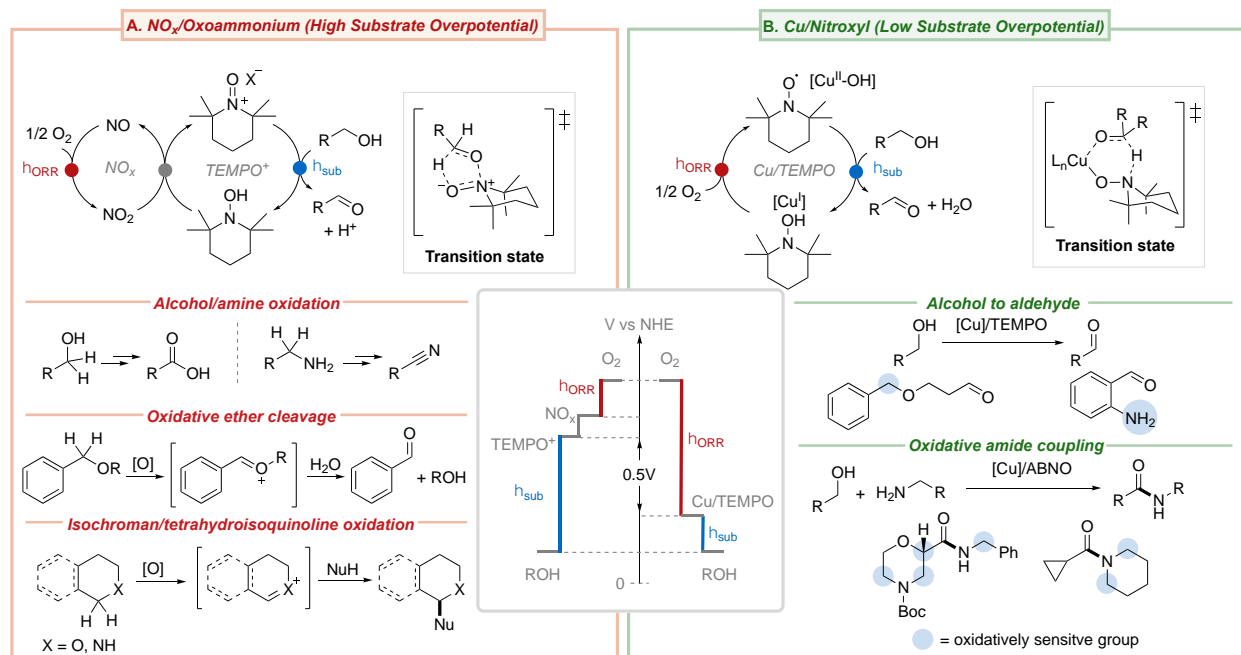


Figure 1.3. (A) NO_x /Oxoammonium-catalyzed organic oxidation reactions and (B) Cu/TEMPO-catalyzed alcohol oxidation reactions.

In contrast to oxoammonium mediated oxidation reactions, Cu/nitroxyl catalyzed aerobic oxidation reactions demonstrate exquisite selectivity for alcohol oxidation, even in the presence of other oxidatively sensitive functional groups such as amines and activated C–H bonds (Figure 1.3B).³² Mechanistic studies of Cu/nitroxyl catalyzed alcohol oxidations implicate the formation of a key $\text{L}_n\text{Cu}(\text{alkoxide})(\text{nitroxyl})$ intermediate. Net hydride transfer occurs from this intermediate via the 6-membered TS structure shown in Figure 1.3B to generate product, $\text{L}_n\text{Cu}^{\text{I}}$, and TEMPOH.^{33–35} Reaction of $\text{L}_n\text{Cu}^{\text{I}}$ and TEMPOH with O_2 regenerates $\text{L}_n\text{Cu}^{\text{II}}$ and TEMPO. A key

mechanistic difference becomes apparent upon comparison of oxoammonium and Cu/nitroxyl mediated oxidation reactions. While in oxoammonium-mediated oxidations the oxoammonium oxidation state is requisite, Cu/TEMPO catalyzed alcohol oxidations do not access TEMPO⁺. Instead, Cu^{II} and TEMPO—each one-electron oxidants—work cooperatively to facilitate net hydride transfer to generate carbonyl product.

Electrochemical studies of the Cu/nitroxyl-mediated catalyst system reveals that the substrate oxidation occurs at the Cu^{III/I} potential, 0.5 V below the TEMPO/TEMPO⁺ potential.³⁶ Since under aerobic conditions ORR occurs at Cu^{III/I}, η_{ORR} for Cu/TEMPO catalyzed alcohol oxidation is at least 0.5 V lower than η_{ORR} for NO_x/TEMPO. The η_{sub} value for a primary alcohol such as ethanol is therefore no greater than 0.17 V, a considerably smaller value than η_{sub} for TEMPO⁺ of 0.67 V. By effectively "wasting" ~0.5 V of O₂'s oxidative driving force, Cu/TEMPO is a milder oxidant that, via cooperative catalysis, allows for an inner-sphere mechanism that bypasses the high-energy intermediates involved in the direct hydride-transfer pathways operative with TEMPO⁺ as the oxidant. Consequently, a substantially lower η_{sub} is required for Cu/TEMPO relative to TEMPO⁺, resulting in a greater tolerance for oxidatively sensitive functional groups.

Quinone-catalyzed oxidations: DDQ versus amine oxidase mimics. The effect of η_{ORR} and η_{sub} on chemoselectivity is also illustrated in quinone-mediated oxidations. Like oxoammonium and oxyl-based oxidation systems, quinone-mediated oxidations see widespread utility in chemical synthesis.³⁷ 2,3-dichloro-5,6-dicyano-*p*-benzoquinone (DDQ) is a prominent example of a quinone-based oxidant. With a 2 H⁺/2 e⁻ standard reduction potential of 0.89 V vs SHE it provides sufficient thermodynamic driving force to perform most commonly encountered organic oxidation reactions, including alcohol and amine oxidations, oxidative deprotection of alcohols, dehydrogenation of saturated heterocycles, and oxidative C–C coupling (Figure 1.4A).³⁷

While DDQ has historically been used as a stoichiometric oxidant, variants using catalytic quantities of DDQ have emerged, though catalytic regeneration of DDQ from DDQH₂ is not trivial and demands the use of high potential oxidants such as hypervalent iodine reagents and MnO₂. In analogy to oxoammonium reagents, DDQ's high potential raises challenges in the context of selective aerobic oxidation catalysis. First, its small η_{ORR} value makes aerobic regeneration difficult. The direct aerobic regeneration of DDQ encounters the same challenges as the aerobic regeneration of TEMPO⁺: the direct aerobic oxidation of DDH₂Q is challenging, in part because of inadequate driving force of the intermediate 2 H⁺/2e⁻ reduction of O₂ to H₂O₂. The same strategy used to regenerate TEMPO⁺ using O₂ as a terminal oxidant can be employed for DDQ-catalyzed oxidations, employing NO_x cocatalysis to enable efficient aerobic regeneration of DDQ from DDQH₂, operating at η_{ORR} of 0.18 V.

Like oxoammonium reagents, DDQ's high potential and consequently large η_{sub} enables mechanistic pathways not accessible to lower potential quinones, including direct electron- and hydride-transfer (Figure 1.4A), and introduces challenges with regards to selective oxidation in the presence of multiple oxidatively sensitive functional groups. This is evident in the DDQ mediated dehydrogenation of 5-bromo-1-methylindoline to the corresponding indole, in which the presence of oxidatively sensitive additives including diphenylmethane, dihydrobenzofuran, dihydrobenzopyran, allylic alcohols, cyclic amides, and N-boc-pyrrolidine are not well tolerated: in addition to formation of the desired indole product, considerable consumption of the additives is observed (Figure 1.4B).³⁸

Lower potential quinones likewise see widespread use as oxidants in synthesis and are often encountered as redox active cofactors in biologically mediated oxidations.³⁹ Synthetic derivatives, such as 4-*tert*-butyl-2-hydroxybenzoquinone (TBHBQ),⁴⁰ (phd)ZnX₂ (phd = 1,10-

phenanthroline-5,6-dione),⁴¹ and $[\text{Ru}(\text{phd})_3]^{2+}$ have been shown to be effective catalysts for the aerobic oxidative dehydrogenation of amines.⁴² $[\text{Ru}(\text{phd})_3]^{2+}$ catalyzes aerobic dehydrogenation of indolines using O_2 as a terminal oxidant and $\text{Co}(\text{salophen})$ as a redox cocatalyst (Figure 1.4B).³⁸ The reaction proceeds via indoline addition to a carbonyl of the *o*-quinone moiety of the phd ligand on $[\text{Ru}(\text{phd})_3]^{2+}$, followed by an ene-type hydride-transfer mechanism to generate product and the reduced quinone. $\text{Co}(\text{salophen})$ oxidizes the reduced phd ligand in the presence of O_2 to regenerate the catalyst. High yields of dehydrogenated products are obtained with a variety of saturated nitrogen heterocycles under mild reaction conditions. In contrast to DDQ-mediated oxidations, oxidatively sensitive additives do not diminish the yield and are recovered in high yield.

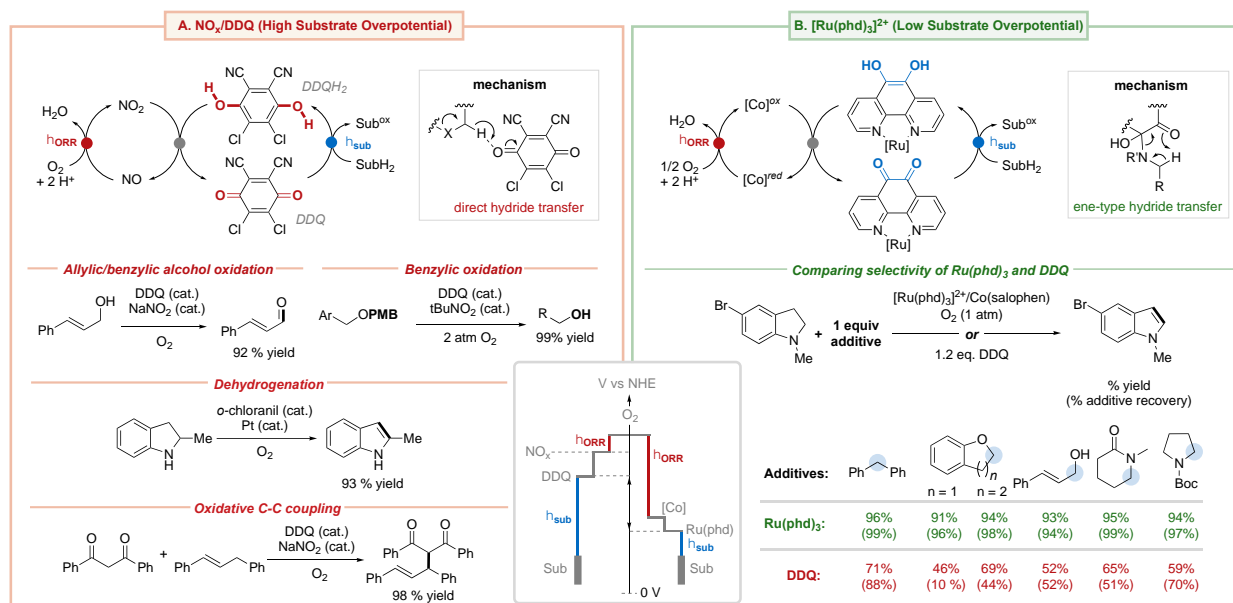


Figure 1.4. (A) NO_x/DDQ and (B) $[\text{Ru}(\text{phd})_3]^{2+}$ -based oxidation catalyst systems.

The enhanced chemoselectivity of $[\text{Ru}(\text{phd})_3]^{2+}$ relative to DDQ can be explained by an evaluation of η_{ORR} and η_{sub} values. The η_{ORR} for NO_x cocatalysis has already been established at 0.18 V. In the context of molecular electrocatalysts for ORR, studies of N_2O_2 -ligated Co

complexes have shown that they reduce O_2 to H_2O_2 with overpotentials as low as 90 mV,⁴³ indicating that η_{ORR} for the $Co/[Ru(phd)_3]^{2+}$ catalyst system is no smaller than ~ 0.55 V. Thus, N_2O_2 -ligated Co complexes such as $Co(salophen)$ reduce O_2 at a much lower potential (that is, with a larger η_{ORR}) relative to NO_x , reducing the amount of oxidizing power from O_2 available for substrate oxidation. While precise values for the $2 H^+/2 e^-$ reduction potential of $[Ru(phd)_3]^{2+}$ are not available, the one-electron reduction potential of $[Ru(phd)_3]^{2+}$ at -0.59 V vs $Fc^{+/0}$ is significantly lower than that of DDQ ($1 e^- E_{1/2} = 0.14$ V vs $Fc^{+/0}$),⁴⁴ a difference of 0.73 V, indicating a substantial difference in η_{sub} for the oxidation of a given substrate. The large η_{sub} value exhibited by DDQ enables high-energy reaction pathways such as direct electron- and hydride-transfer mechanisms, resulting in promiscuous substrate oxidation. In contrast, $[Ru(phd)_3]^{2+}$ has a significantly smaller η_{sub} , and only those mechanisms that proceed via lower energy pathways—such as inner-sphere ene-type hydride—are accessible, resulting in enhanced chemoselectivity.

1.4 Tuning Overpotential for Chemoselective Pd-Catalyzed Aerobic Oxidations

Palladium catalyst facilitate a diverse array of dehydrogenation and dehydrogenative coupling reactions. Mechanistically, they can be generically represented by two half reactions, substrate oxidation by Pd^{n+} and reoxidation of $Pd^{(n-2)+}$ by an external oxidant such as O_2 , benzoquinone, and Cu^{II} and Ag^I salts.^{45–48} Pd-catalyzed oxidations typically proceed via a $Pd^{0/II}$ cycle, although recent methods have been developed proposing $Pd^{II/IV}$ cycles, accessed with strong oxidants such as peroxides, to carry out demanding oxidation reactions like dehydrogenative C–H oxygenation and alkylation reactions not accessible via traditional $Pd^{0/II}$ catalysis.^{49–51} The complementary selectivity achieved via $Pd^{0/II}$ and $Pd^{II/IV}$ catalyzed reaction manifolds represents a particularly illustrative case study for how overpotential is an important consideration in the design

of catalytic aerobic oxidation reactions, and this section will focus on demonstrating how these redox manifolds can be manipulated in order to promote the desired reactivity.

Our group has had a long-standing interest in synthetic and mechanistic aspects of Pd-catalyzed oxidative biaryl coupling reactions.⁵² Mechanistic studies have shown that the reaction proceeds via C–H activation of Ar–H by $L_nPd(OAc)_2$ to generate $L_nPd(OAc)(Ar)$, followed by transmetallation between two $L_nPd(OAc)(Ar)$ to form $L_nPd(OAc)_2$ and $L_nPd(Ar)_2$. The latter undergoes reductive elimination to form Ar–Ar, and L_nPd^0 reacts with O_2 in the presence of AcOH to form H_2O_2 and regenerate $L_nPd(OAc)_2$ (Figure 1.5B). At 0.01 V vs SHE, the oxidative homocoupling of benzene to generate biphenyl is nearly thermoneutral, and the overall driving force for the reaction is 1.22 V and 0.67 V with respect to the O_2/H_2O and O_2/H_2O_2 couples, respectively. Either redox couple provides substantial driving force for the reaction; however, the reaction is mediated by a Pd-catalyst, and the feasibility is dependent on whether Pd is thermodynamically capable of performing the oxidation. While the reduction potentials of many ligand-supported Pd catalysts are not well-defined, we recently showed that with the appropriate ligand, their potentials can reach as high as the BQ/ H_2Q potential (0.69 V vs SHE), and by extension the O_2/H_2O_2 potential (0.68 V vs SHE). However, $Pd^{II/0}$ redox potentials are ligand-dependent and vary by at least ~400 mV, and they are generally expected to be lower than 0.69 V.⁵³ Consequently, η_{sub} for oxidative coupling of benzene is expected to be no larger than 0.67 V, that value representing an extreme upper boundary.

While the $Pd^{0/II}$ manifold provides sufficient thermodynamic driving force for most organic oxidation reactions, there are some classes of reactions that would likely be limited by $Pd^{0/II}$ catalyst potentials, such as kinetically challenging C–O bond formation reactions like aryl C–H oxygenation. At 0.32 V vs SHE, the dehydrogenative coupling of water and benzene to generate

phenol is considerably more thermodynamically demanding than benzene homocoupling, and the most oxidizing palladium catalyst operating at the Pd^{0/II} manifold would have η_{sub} of ~ 0.38 V. In principle, higher oxidation state catalytic manifolds such as Pd^{II/IV} provide larger η_{sub} values that could facilitate the kinetically challenging C–O reductive elimination step featured in the reaction.

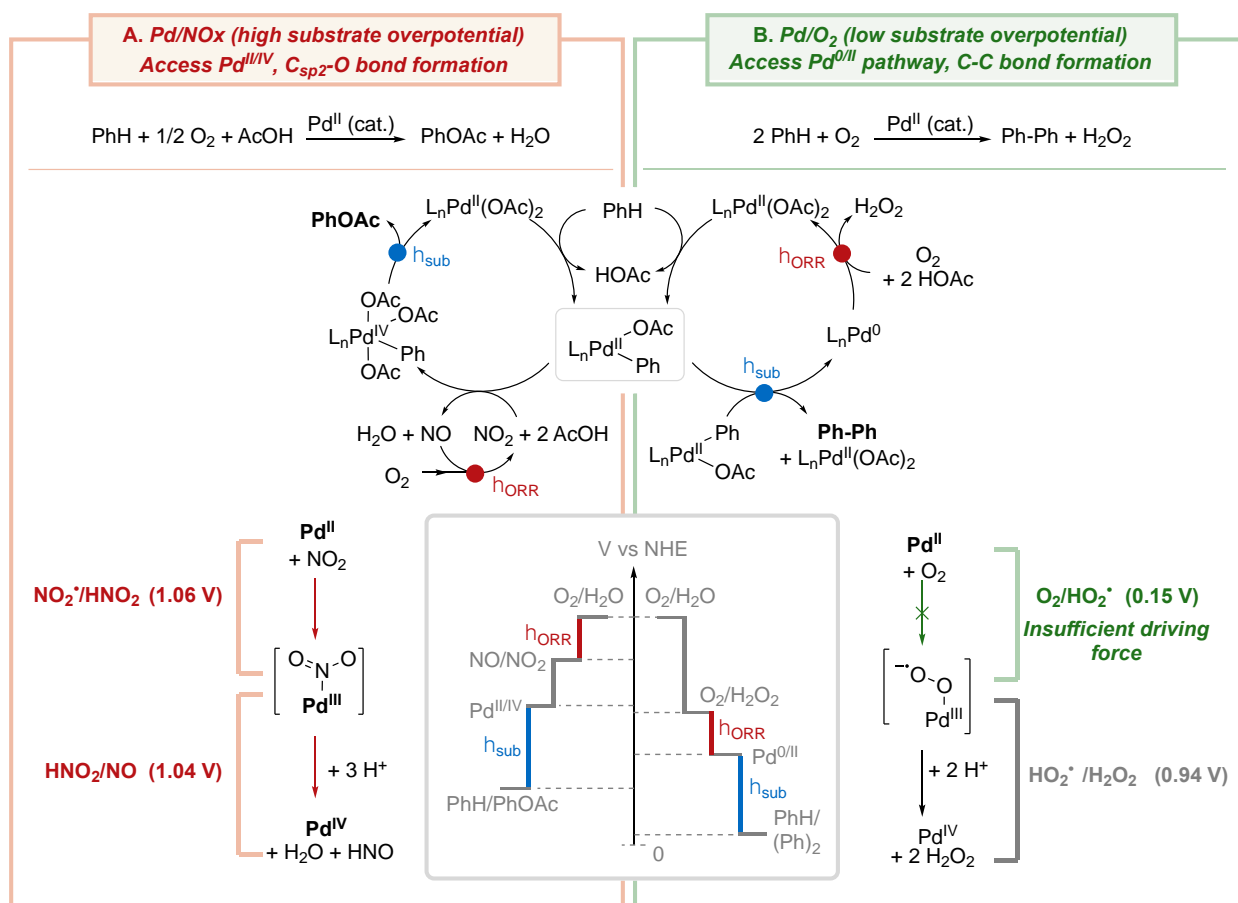


Figure 1.5. (A) Pd^{0/II} and (B) Pd^{II/IV} mediated aerobic oxidation reactions.

In the context of aerobic oxidation catalysis, direct access to higher oxidation states of Pd (Pd^{III} and Pd^{IV}) is not achievable with O₂⁵⁴ and requires oxidants such as hypervalent iodine or organic peroxides like TBHP.⁵⁵ This observation can be rationalized by the following considerations. First, the two-electron oxidation of Pd^{II} by O₂ would access the O₂/H₂O₂ manifold

at 0.68 V, and this potential is likely insufficient, considering the upper limit for Pd^{0/II} potentials approximate this value. Second, the oxidation of Pd^{II} by O₂ involves the intermediacy of Pd^{III}-O₂. The initial 1 H⁺/1 e⁻ reduction of O₂ is 0.15 V vs SHE, well below the value of the Pd^{0/II} couple, indicating that this intermediate step is likely prohibitively uphill (Figure 1.5B).

In contrast, Pd's higher oxidation states can be accessed with NO_x, which replaces the unfavorable intermediate single-electron transfer step with O₂ with more potent ones: the 1 H⁺/1 e⁻ NO₂/HNO₂ couple is 1.06 V vs SHE and the 1 H⁺/1 e⁻ HNO₂/NO couple is 1.04 V vs SHE. Our lab and others have shown that introduction of NO_x-generating additives to aerobic Pd-catalyzed oxidation reactions can facilitate the formation of products not typically observed with more traditional Pd^{0/II} cycles.⁵⁶⁻⁶² One such example is the oxidative coupling of benzene and acetic acid in the presence of O₂ and fuming HNO₃ to form phenyl acetate (Figure 1.5A). The reaction is proposed to begin with C-H activation of benzene by Pd(OAc)₂ to generate Pd(OAc)(Ar), which reacts with NO₂ and AcOH to form Pd^{IV}(OAc)₃(Ar). Reductive elimination of acetate and aryl ligands yields phenyl acetate and regenerates the Pd(OAc)₂ catalyst. Pd(OAc)(Ar) is a common intermediate in benzene homocoupling and benzene acetoxylation and represents a mechanistic branching point: in the absence of NO_x, it transmetallates with another equivalent of Pd(OAc)(Ar) in route to biphenyl, while its presence affords phenyl acetate. By helping capture a larger share of the oxidative driving force from O₂ (i.e. by operating with a smaller η_{ORR}), NO_x cocatalysis enables access to higher Pd oxidation states, facilitating an otherwise kinetically and thermodynamically challenging C-O reductive elimination step, and achieving selectivity that is complementary to the C-C coupling observed in its absence.

1.5 Reductive Activation of O₂: *in situ* Generation of Organic Peroxides

Aerobic oxidation reactions are challenging on a number of fundamental levels. There is a simple stoichiometry problem: while most organic oxidation reactions are net 2 H⁺/2 e⁻ dehydrogenations, O₂ is a 4 e⁻/4 H⁺ oxidant, and reaction design must be considered with that constraint in mind. Further complicating the challenge, O₂ is a ground-state open-shell species and kinetically reluctant to react directly with most closed-shell organic molecules (much to the benefit of all living things). Finally, the potential of the initial 2 H⁺/2 e⁻ reduction of O₂ to H₂O₂ (0.68 V) is significantly lower than subsequent reduction of H₂O₂ to H₂O (1.78 V), so even catalyst systems that manage to address the first two issues must contend with the fact that they are thermodynamically limited to 0.68 V. Nature has perfected a strategy to obviate these challenges: reductive activation of O₂. Broadly speaking, reductive activation involves using a sacrificial 2 H⁺/2 e⁻ reductant to generate a thermodynamically potent and reactive 2 H⁺/2 e⁻ oxidant in the form of a peroxy species. Monooxygenase enzymes use NADH or related reductants to generate reactive metal-peroxy and -oxo species from O₂-bound metal centers in the enzyme active site to perform myriad catalytic reactions (Figure 1.6A).⁶³ In the context of organic synthesis, the reductive activation of O₂ with aliphatic aldehydes or other organic reductants has been implemented for a variety of oxidation reactions including generation of hypervalent iodine reagents,^{64,65} C–H amination,⁶⁶ and alkene epoxidation.^{67,68}

Leveraging autoxidation to access hypervalent iodine reagents *in situ*. Hypervalent iodine reagents are strong oxidants and are commonly used in synthetic chemistry.⁶⁹ They are typified by bis(acetoxy)iodobenzene (BAIB, 0.91 V vs SHE)⁷⁰ and are commonly generated by oxidation of iodobenzene with strong oxidants such as persulfate, periodate, and permanganate, with potentials at 2.08, 1.59, and 1.49 V vs SHE, respectively.^{5,71} While O₂ provides sufficient

driving force to generate many hypervalent iodine reagents, it is generally ineffective for directly generating $\text{PhI}(\text{OAc})_2$. Indeed, accessing the $2\text{H}^+/2\text{e}^-$ PhI/BAIB couple (0.91 V) is thermodynamically unfeasible with the corresponding $2\text{H}^+/2\text{e}^-$ reduction of O_2 to H_2O_2 (0.68 V). On the other hand, peroxides provide the thermodynamic driving force to generate hypervalent iodine reagents and reductive activation of O_2 provides a means to overcome the kinetic challenge of coupling the 4-electron reduction of O_2 to the 2-electron oxidation of iodobenzene.

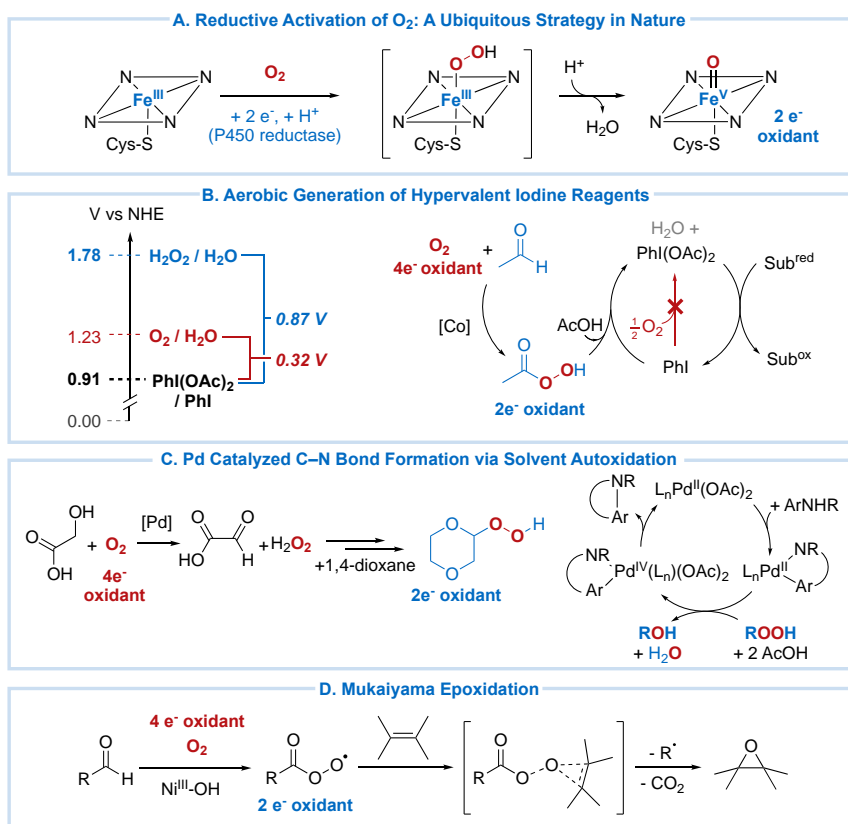


Figure 1.6. (A) Reductive activation of O_2 in nature. (B) Aerobic generation of hypervalent iodine reagents. (C) Pd catalyzed C–N bond formation mediated by solvent autoxidation. (D) The Mukaiyama Epoxidation

Recently, the Powers group demonstrated reductive activation of O_2 for the aerobic generation of hypervalent iodine reagents (Figure 1.6B).^{72,73} The autoxidation of acetaldehyde with

CoCl₂ as an initiator generates acyl hydroperoxide—a thermodynamically potent and reactive 2 e⁻ oxidant—which reacts with aryl iodides in the presence of acetic acid to generate ArI(OAc)₂.⁷⁴ The *in situ* aerobic generation of hypervalent iodine reagents from aryl iodides demonstrated compatibility with a variety of organic oxidation reactions including alkene oxidation and C–H oxygenation, bromination, and amidation. This strategy also supports the use of catalytic quantities of aryl iodide. The aerobic generation of hypervalent oxidants obviates the need for harsh stoichiometric oxidants and expands opportunities for the use of dioxygen in sustainable organic synthesis.

1,4-Dioxane autoxidation for *in situ* generation of alkyl hydroperoxides in Pd-catalyzed C–H amination. Pd-catalyzed aryl C–N bond forming reactions, such as the Buchwald-Hartwig coupling, have revolutionized chemical synthesis. An appealing alternative route is Pd-catalyzed oxidative aryl C–H amination, a more step economical approach than traditional cross-coupling methods. A major drawback to this strategy is that strong stoichiometric oxidants such as oxone, hypervalent iodine, and [F⁺] are often required to oxidize Pd^{II} to Pd^{IV} in order to facilitate the challenging C–N bond formation.⁵⁵ The *in situ* reductive activation of O₂ to generate organic peroxides is a viable means to generate strong peroxide oxidants capable generating Pd^{IV} en route to C–N coupled products. Indeed, our lab has implemented this strategy for the (DAF)Pd(OAc)₂ catalyzed (DAF = 4,5-diazafluoren-9-one) intramolecular oxidative C–H amination of *N*-benzenesulfonyl-2-aminobiphenyl (**1**) to *N*-benzenesulfonylcarbazole (**2**) in 1,4-dioxane solvent (Figure 1.6C).⁷⁵

Initial experiments for the (DAF)Pd(OAc)₂-catalyzed cyclization of **1** yielded **2** in 44% yield. Close inspection of the reaction mixture revealed that significant quantities of 2-hydroperoxy-1,4-dioxane were present in an aged bottle of 1,4-dioxane, and experiments showed

that **2** could be formed in comparable yields with peroxides such as *tert*-butylhydroperoxide. Additional control experiments showed that introduction of glycolic acid, an oxidative decomposition product of 1,4-dioxane, promoted the reaction and formed **2** in 81% yield. Based on these results, it was proposed that aerobic Pd-mediated oxidation of glycolic acid generates 2-hydroperoxy-2-hydroacetic acid. Upon O–O scission, this peroxide initiates radical chain autoxidation of 1,4-dioxane to 2-hydroperoxy-1,4-dioxane, and this species was proposed to be responsible for the generation of Pd^{IV} en route to product **2**. These observations demonstrate that reductive activation of O₂ via autoxidation of 1,4-dioxane solvent is an effective strategy for accessing aerobic high-valent Pd catalysis for challenging oxidation reactions.

Autoxidation of aldehydes for alkene epoxidation (Mukaiyama Epoxidation). The epoxidation of alkenes is among the most thermodynamically demanding organic oxidation reactions, exemplified by propylene oxide whose standard $2\text{H}^+ / 2\text{e}^-$ reduction potential is 0.76 V vs SHE (cf. Figure 1.1B).⁵ Strongly oxidizing reagents such as NaOCl, oxone, and organic peroxides are typically employed in their synthesis, often in the presence of a transition metal catalyst.^{76,77} As is the case with hypervalent iodine reagents, the O₂/H₂O₂ potential is thermodynamically incapable of supporting epoxide formation.

Since H₂O₂ and other organic peroxides are commonly employed as oxidants in olefin epoxidation reactions, the reductive activation of O₂ with an organic reductant to generate an organic peroxide is a viable means of utilizing O₂ as a terminal oxidant in a way that bypasses the direct use of hazardous peroxide reagents. The Mukaiyama epoxidation, the Ni-catalyzed aerobic epoxidation of alkenes, is a prominent example of this strategy. First reported in 1990, the Mukaiyama epoxidation uses a Ni^{II} catalyst to mediate the formation of epoxides from substituted olefins in the presence of an aliphatic alcohol additive and O₂ under mild conditions (Figure 1.6D).

⁷⁸ Later studies found that aldehydes, generated by *in situ* alcohol oxidation, were superior additives,⁷⁹ and subsequent mechanistic studies showed that the Ni catalyst initiates aldehyde autoxidation to generate an acylperoxyl radical. These highly oxidizing species are proposed as the species primarily responsible for alkene epoxidation via O-atom transfer.⁸⁰ The Muyaayama epoxidation is a prime example of how to effectively utilize O₂ as an oxidant for thermodynamically challenging oxidation reactions.

1.6 Conclusions

Overpotential, a metric largely reserved to the field of electrocatalysis, provides a useful framework for rationalizing chemoselectivity when applied to catalytic aerobic oxidation reactions. The proper use of catalysts and cocatalysts can enable the synthetic chemist to modulate the amount oxidative power harvested from O₂ and change the mechanistic pathways available for the dehydrogenation of organic substrates and thereby control the chemoselectivity of aerobic oxidation reactions. By operating at small η_{ORR} , larger amounts of oxygen's oxidative power can be utilized, ensuring larger η_{sub} values and enabling mechanistic pathways that facilitate thermodynamically and kinetically challenging dehydrogenation reactions. In contrast, by choosing catalyst systems with large η_{ORR} , there are consequently smaller η_{sub} values, and this is advantageous in the context of the selective oxidation of organic molecules by limiting the oxidant to mechanistic pathways that are specially tuned to specific functional groups. One way to maximize the oxidative driving force extracted from O₂ is by means of reductive activation to generate peroxides, which can in turn participate in a variety of thermodynamically challenging organic oxidation reactions. We anticipate that considerations of overpotential and O₂ reduction mechanisms will prove useful in the development of selective catalytic aerobic oxidation reactions.

1.7 Acknowledgements

The contributions of Alex Stamoulis to the generation of figures and editing the text of this work are gratefully acknowledged.

1.8 References

1. Liquid Phase Aerobic Oxidation Catalysis; Stahl, S. S., Alsters, P. L., Eds.; Wiley-VCH Verlag GmbH & Co. KGaA: Weinheim, Germany, 2016.
2. Caron, S.; Dugger, R. W.; Ruggeri, S. G.; Ragan, J. A.; Ripin, D. H. B. Large-Scale Oxidation in the Pharmaceutical Industry. *Chem. Rev.* **2006**, *106*, 2943-2989.
3. Cavani, F.; Teles, J. H. Sustainability in Catalytic Oxidation: An Alternative Approach or a Structural Evolution? *ChemSusChem* **2009**, *2*, 508-534.
4. Burns, N. Z.; Baran, P. S.; Hoffmann, R. W. Redox Economy in Organic Synthesis. *Angew. Chem. Int. Ed.* **2009**, *48*, 2854-2867.
5. Nutting, J. E.; Gerken, J. B.; Stamoulis, A. G.; Bruns, D. L.; Stahl, S. S. "How Should I Think about Voltage? What is Overpotential?": Establishing and Organic Chemistry Intuition for Electrochemistry. *J. Org. Chem.* **2021**, *86*, 15875-15885.
6. Pegis, M. L.; Wise, C. F.; Martin, D. J.; Mayer, J. M. Oxygen Reduction by Homogeneous Molecular Catalysts and Electrocatalysts. *Chem. Rev.* **2018**, *118*, 2340-2391.
7. Chen, W.; Huang, J.; Wei, J.; Zhou, D.; Cai, J.; He, Z-H.; Chen, Y-X. Origins of High Onset Overpotential of Oxygen Reduction Reaction at Pt-Based Electrocatalysts: A Mini Review. *Electrochemistry Communications* **2018**, *96*, 71-76.
8. Appel, A. M.; Helm, M. L. Determining the Overpotential for a Molecular Electrocatalyst. *ACS Catal.* **2014**, *4*, 630-633.

9. Gewirth, A. A.; Thorum, M. S. Electroreduction of Dioxygen for Fuel-Cell Applications: Materials and Challenges. *Inorg. Chem.* **2010**, *49*, 3557-3566.
10. Merbouth, N.; Bobbitt, J. M.; Brückner, C. Preparation of Tetramethylpiperidine-1-Oxoammonium Salts and Their Use as Oxidants in Organic Chemistry. A Review. *Org. Prep. Proced. Int.* **2004**, *36* 1-31.
11. Nutting, J. E.; Raifee, M.; Stahl, S. S. Tetramethylpiperidine *N*-Oxyl (TEMPO), Phthalimide *N*-Oxyl (PINO), and Related *N*-Oxyl Species: Electrochemical Properties and Their Use in Electrocatalytic Reactions. *Chem. Rev.* **2018**, *118*, 4834-4885.
12. Semmelhack, M. F.; Schmid, C. R.; Cortés, D. A.; Chou, C. S. Oxidation of Alcohols to Aldehydes with Oxygen and Cupric Ion, Mediated by Nitrosonium Ion. *J. Am. Chem. Soc.* **1984**, *106*, 3374-3376.
13. Bobbitt, J. M.; Brückner, C.; Merbouh, N. Oxoammonium- and Nitroxide-Catalyzed Oxidations of Alcohols. In *Organic Reactions*; Wiley: Hoboken, NJ, 2009; pp 103– 424
14. Hoover, J. M.; Stahl, S. S. Highly Practical Copper(I)/TEMPO Catalyst System for Chemoselective Aerobic Oxidation of Primary Alcohols. *J. Am. Chem. Soc.* **2011**, *133*, 16901-16910.
15. Zultanski, S. L.; Zhao, J.; Stahl, S. S. Practical Synthesis of Amides via Copper/ABNO-Catalyzed Aerobic Oxidative Coupling of Alcohols and Amines. *J. Am. Chem. Soc.* **2016**, *138*, 6416-6419.
16. Raifee, M.; Konz, Z. M.; Graaf, M. D.; Koolman, H. F.; Stahl, S. S. Electrochemical Oxidation of Alcohols and Aldehydes to Carboxylic Acids Catalyzed by 4-Acetamide-TEMPO: An Alternative to "Anelli" and "Pinnick" Oxidations. *ACS Catal.* **2018**, *8*, 6738-6744.

17. Kim, J.; Stahl, S. S. Cu/Nitroxyl-Catalyzed Aerobic Oxidation of Primary Amines into Nitriles at Room Temperature. *ACS Catal.* **2013**, *3*, 1652-1656.
18. Facile Oxidation of Primary Amines to Nitriles Using an Oxoammonium Salt. *Org. Lett.* **2014**, *16*, 6484-6487.
19. Pradhan, P. P.; Bobbitt, J. M.; Bailey, W. F. Oxidative Cleavage of Benzylic and Related Ethers, Using an Oxoammonium Salt. *J. Org. Chem.* **2009**, *74*, 9524-9527.
20. Kelly, C. B.; Ovian, J. M.; Cywar, R. M.; Gosselin, T. R.; Wiles, R. J.; Leadbeater, N. E. Oxidative Cleavage of Allyl Ethers by an Oxoammonium Salt. *Org. Biomol. Chem.* **2015**, *13*, 4255-4259.
21. Richter, H.; Rohlmann, R.; García Mancheño, O. Catalyzed Selective Direct α - and γ -Alkylation of Aldehydes with Cyclic Benzyl Ethers by Using $T^+BF_4^-$ in the Presence of an Inexpensive Organic Acid or Anhydride. *Chem. Eur. J.* **2011**, *17*, 11622-11627.
22. Richter, H.; Fröhlich, R.; Daniliuc, C.-G.; García Mancheño, O. Mild Metal-Free Tandem α -Alkylation/Cyclization of *N*-Benzyl Carbamates with Simple Olefins. *Angew. Chem. Int. Ed.* **2012**, *51*, 8656-8660.
23. Anelli, P. L.; Banfi, S.; Montanari, F.; Quici, S. Oxidation of Diols with Alkali Hypochlorites Catalyzed by Oxoammonium Salts Under Two-Phase Conditions. *J. Org. Chem.* **1989**, *54*, 2970-2972.
24. Bolm, C.; Magnus, A. S.; Hildebrand, J. P. Catalytic Synthesis of Aldehydes and Ketones under Mild Conditions Using TMEPO/Oxone. *Org. Lett.* **2000**, *2*, 1173-1175.

25. De Mico, A.; Margarita, R.; Parlanti, L.; Vescovi, A.; Piancatelli, G. A Versatile and Highly selective Hypervalent Iodine (III)/2,2,6,6-Tetramethyl-1-piperidinyloxy-Mediated Oxidation of Alcohols to Carbonyl Compounds. *J. Org. Chem.* **1997**, *62*, 6974-6977.
26. Lennox, A. J. J.; Goes, S. L.; Webster, M. P.; Koolman, H. F.; Djuric, S. W.; Stahl, S. S. Electrochemical Aminoxy-Mediated α -Cyanation of Secondary Piperidines for Pharmaceutical Building Block Diversification. *J. Am. Chem. Soc.* **2018**, *140*, 11227-11231.
27. Gerken, J. B.; Pang, Y. Q.; Lauber, M. B.; Stahl, S. S. Structural Effects on the pH-Dependent Redox Properties of Organic Nitroxyls: Pourbaix Diagrams for TEMPO, ABNO, and Three TEMPO Analogs. *J. Org. Chem.* **2018**, *83*, 7323-7330.
28. Merbouth, N.; Bobbitt, J. M.; Brückner, C. Preparation of Tetramethylpiperidine-1-Oxoammonium Salts and Their Use as Oxidants in Organic Chemistry. A Review. *Org. Prep. Proced. Int.* **2004**, *36* 1-31.
29. Gerken, J. B.; Stahl, S. S. High-Potential Electrocatalytic O₂ Reduction with Nitroxyl/NO_x Mediators: Implications for Fuel Cells and Aerobic Oxidation Catalysis. *ACS Cent. Sci.* **2015**, *1*, 234-243.
30. Wertz, S.; Studer, A. Nitroxide-Catalyzed Transition-Metal-Free Aerobic Oxidation Processes. *Green Chem.* **2013**, *15*, 3116-3134.
31. Cao, Q.; Dornan, L. M.; Rogan, L.; Hughes, N. L.; Muldoon, M. J. Aerobic Oxidation Catalysis with Stable Radicals. *Chem. Commun.* **2014**, *50*, 4524-4543.
32. Ryland, B. L.; Stahl, S. S. Practical Aerobic Oxidations of Alcohols and Amines with Homogeneous Copper/TMEPO and Related Catalyst Systems. *Angew. Chem. Int. Ed.* **2014**, *53*, 8824-8838.

33. Hoover, J. M.; Ryland, B. L.; Stahl, S. S. Copper/TEMPO-Catalyzed Aerobic Alcohol Oxidation: Mechanistic Assessment of Different Catalyst Systems. *ACS Catal.* **2013**, *3*, 2599-2605.
34. Hoover, J. M.; Ryland, B. L.; Stahl, S. S. Mechanism of Copper(I)/TEMPO-Catalyzed Aerobic Alcohol Oxidation. *J. Am. Chem. Soc.* **2013**, *135*, 2357-2367.
35. Ryland, B. L.; McCann, S. D.; Brunold, T. C.; Stahl, S. S. Mechanism of Alcohol Oxidation Mediated by Copper(II) and Nitroxyl Radicals. *J. Am. Chem. Soc.* **2014**, *136*, 12166-12173.
36. Badalyan, A.; Stahl, S. S. Cooperative Electrocatalytic Alcohol Oxidation with Electron-Proton-Transfer Mediators. *Nature* **2016**, *535*, 406-410.
37. Wendlandt, A. E.; Stahl, S. S. Quinone-Catalyzed Selective Oxidation of Organic Molecules. *Angew. Chem. Int. Ed.* **2015**, *54*, 14638-14658.
38. Li, B.; Wendlandt, A. E.; Stahl, S. S. Replacement of Stoichiometric DDQ with a Low Potential *o*-Quinone Catalyst Enabling Aerobic Dehydrogenation of Tertiary Indolines in Pharmaceutical Intermediates. *Org. Lett.* **2019**, *21*, 1176-1181.
39. Wendlandt, A. E.; Stahl, S. S. Quinone-Catalyzed Selective Oxidation of Organic Molecules. *Angew. Chem. Int. Ed.* **2015**, *54*, 14638-14658.
40. Wendlandt, A. E.; Stahl, S. S. Chemoselective Organocatalytic Aerobic Oxidation of Primary Amines to Secondary Imines. *Org. Lett.* **2012**, *14*, 2850-2853.
41. Wendlandt, A. E.; Stahl, S. S. Bioinspired Aerobic Oxidation of Secondary Amines and Nitrogen Heterocycles with a Bifunctional Quinone Catalyst. *J. Am. Chem. Soc.* **2014**, *136*, 506-512.

42. Wendlandt, A. E.; Stahl, S. S. Modular *o*-Quinone Catalyst System for Dehydrogenation of Tetrahydroquinolines under Ambient Conditions. *J. Am Chem. Soc.* **2014**, *136*, 11910-11913.
43. Wang, Y.-H.; Pegis, M. L.; Mayer, J. M.; Stahl, S. S. Molecular Cobalt Catalysts for O₂ Reduction: Low-Overpotential Production of H₂O₂ and Comparison with Iron-Based Catalysts. *J. Am. Chem. Soc.* **2017**, *139*, 16458-16461.
44. Li, B.; Wendlandt, A. E.; Stahl, S. S. Replacement of Stoichiometric DDQ with a Low Potential *o*-Quinone Catalyst Enabling Aerobic Dehydrogenation of Tertiary Indolines In Pharmaceutical Intermediates. *Org. Lett.* **2019**, *21*, 1176-1181.
45. Stahl, S. S. Palladium-Catalyzed Oxidation of Organic Chemicals with O₂. *Science*, **2005**, 1824-1826.
46. Stahl, S. S. Palladium Oxidase Catalysis: Selective Oxidation of Organic Chemicals by Direct Dioxygen-Coupled Turnover. *Angew. Chem. Int. Ed.* **2004**, *43*, 3400-3420.
47. Wang, D.; Weinstein, A. B.; White, P. B.; Stahl, S. S. Ligand-Promoted Palladium-Catalyzed Aerobic Oxidation Reactions. *Chem. Rev.* **2018**, *118*, 2636-2679.
48. Vasseur, A.; Muzart, J.; Le Bras, J. Ubiquitous Benzoquinones, Multitalented Compounds for Palladium-Catalyzed Oxidative Reactions. *Eur. J. Org. Chem.* **2015**, 4053-4069.
49. Zhuang, Z.; Yu, J.-Q. Lactonization as a General Route to β -C(*sp*³)-H Functionalization. *Nature* **2019**, *577*, 656-660.
50. Zhuang, Z.; Herron, A. N.; Fan, Z.; Yu, J.-Q. Ligand-Enabled Monoselective β -C(*sp*³)-H Acyloxylation of Free Carboxylic Acids Using a Practical Oxidant. *Nature* **2020**, *142*, 6769-6776.

51. Zhuang, Z.; Herron, A. N.; Liu, S.; Yu, J.-Q. Rapid Construction of Tetralin, Chromane, and Indane Motifs via Cyclative C–H/C–H Coupling: Four-Step Total Synthesis of (±)-Russujaponol F. *J. Am Chem. Soc.* **2021**, *143*, 687-692.
52. Wang, D.; Izawa, Y.; Stahl, S. Rapid Pd-Catalyzed Aerobic Oxidative Coupling of Arenes: Evidence for Transmetalation between Two Pd(II)-Aryl Intermediates. *J. Am Chem. Soc.* **2014**, *136*, 9914-9917.
53. Bruns, D. L.; Musaev, D. G.; Stahl, S. Can Donor Ligands Make Pd(OAc)₂ a Stronger Oxidant? Access to Elusive Palladium(II) Reduction Potentials and Effects of Ancillary Ligands via Palladium(II)/Hydroquinone Redox Equilibria. *J. Am Chem. Soc.* **2020**, *142*, 19678-19688.
54. Aerobic generation of Pd^{III} from Pd^{II} has been observed in complexes with strongly donating ligand spheres. See: Khusnutdinova, J. R.; Rath, P. N.; Mirica, L. M. The Aerobic Oxidation of a Pd(II) Dimethyl Complex Leads to Selective Ethane Elimination from a Pd(III) Intermediate. *J. Am. Chem. Soc.* **2012**, *134*, 2414-2422.
55. Sehnal, P.; Taylor, R. J. K.; Fairlamb, I. J. S. Emergence of Palladium(IV) Chemistry in Synthesis and Catalysis. *Chem. Rev.* **2010**, *110*, 824-889.
56. Zultanski, S. L.; Stahl, S. S. Palladium-Catalyzed Aerobic Acetoxylation of Benzene Using NO_x-Based Redox Mediators. *J. Organomet. Chem.* **2015**, *793*, 263-268.
57. Tissue, T.; Downs, W. J. Palladium(II)-Catalysed Nitration of Benzene. *Chem. Commun.* **1969**, *793*, 263-268.
58. An, Z.; Pan, X.; Liu, X.; Han, X.; Bao, X. Combined Redox Couples for Catalytic Oxidation of Methane by Dioxygen at Low Temperatures. *J. Am. Chem. Soc.* **2006**, *128*, 16028-16029.

59. Stowers, K. J.; Kubota, A.; Sanford, M. S. Nitrate as a Redox Co-Catalyst for the Aerobic Pd-Catalyzed Oxidation of Unactivated sp^3 -C–H Bonds. *Chem. Sci.* **2012**, *3*, 3192-3195.
60. Zhang, W.; Lou, S.; Liu, Y.; Xu, Z. Palladium-Catalyzed Chelation-Assisted Aromatic C–H Nitration: Regiospecific Synthesis of Nitroarenes Free from the Effect of the Orientation Rules. *J. Org. Chem.* **2013**, *78*, 5932-5948.
61. Majhi, B.; Kundu, D.; Ahammed, S.; Ranu, B. C. tert-Butyl Nitrite Mediated Regiospecific Nitration of (E)-Azoarenes through Palladium-Catalyzed Directed C–H Activation. *Chem. Eur. J.* **2014**, *20*, 9862-9866.
62. Wickens, Z. K.; Guzman, P.; Grubbs, R. H. Aerobic Palladium-Catalyzed Diacetoxylation of Alkenes Enabled by Catalytic Nitrite. *Angew. Chem. Int. Ed.* **2015**, *54*, 236-240.
63. Huang, X.; Groves, J. T. Oxygen Activation and Radical Transformations in Heme Proteins and Metalloporphyrins. *Chem. Rev.* **2018**, *118*, 2491-2553.
64. Maity, A.; Hyun, S.-M.; Powers, D. C. Oxidase Catalysis via Aerobically Generated Hypervalent Iodine Intermediates. *Nat. Chem.* **2018**, *10*, 200-204.
65. Maity, A.; Hyun, S.-M.; Wortman, A. K.; Powers, D. C. Oxidation Catalysis via an Aerobically Generated Dess-Martin Periodinane Analogue. *Angew. Chem. Int. Ed.* **2018**, *57*, 7205-7209.
66. Weinstein, A. B.; Stahl, S. S. Palladium Catalyzed Aryl C–H Amination with O_2 via *in situ* Formation of Peroxide-Based Oxidant(s) from Dioxane. *Catal. Sci. Technol.* **2014**, *4*, 1-4.
67. Mukaiyama, T.; Takai, T.; Yamada, T.; Rhode, O. Nickel(II) Complex Catalyzed Epoxidation of Olefins with Molecular Oxygen and Primary Alcohol. *Chem. Lett.* **1990**, 1661-1664.

68. Yamada, T.; Takai, T.; Rhode, O.; Mukaiyama, T. Highly Efficient Method for Epoxidation of Olefins with Molecular Oxygen and Aldehydes Catalyzed by Nickel(II) Complexes. *Chem. Lett.* **1991**, *20*, 1-4.
69. Zhdankin, V. V.; Stang, P. J. Chemistry of Polyvalent Iodine. *Chem. Rev.* **2008**, *108*, 5299-5358.
70. Radzhabov, M. R.; Sheremetev, A. B.; Pivina, T. S. Oxidative ability of organic iodine(III) reagents: a theoretical assessment. *New J. Chem.*, **2020**, *44*, 7051-7057.
71. Lide, D. R. ed. (2006). CRC Handbook of Chemistry and Physics (87th ed.). Boca Raton, FL: CRC Press. ISBN 0-8493-0487-3.
72. Maity, A.; Hyun, S.-M.; Powers, D. C. Oxidase Catalysis via Aerobically Generated Hypervalent Iodine Intermediates. *Nat. Chem.* **2018**, *10*, 200-204.
73. Maity, A.; Hyun, S.-M.; Wortman, A. K.; Powers, D. C. Oxidation Catalysis via an Aerobically Generated Dess-Martin Periodinane Analogue. *Angew. Chem. Int. Ed.* **2018**, *57*, 7205-7209.
74. Hyun, S.-M.; Yuan, M.; Maity, A.; Gutierrez, O.; Powers, D. C. The Role of Iodanyl Radicals as Critical Chain Carriers in Aerobic Hypervalent Iodine Chemistry. *Chem.* **2019**, *5*, 2388-2404.
75. Weinstein, A. B.; Stahl, S. S. Palladium-Catalyzed Aryl C-H Amination with O₂ via *in situ* Formation of Peroxide-Based Oxidant(s) from Dioxane. *Catal. Sci. Technol.* **2014**, *4*, 4301-4307.
76. Jørgensen, K. A. Transition-Metal-Catalyzed Epoxidations. *Chem. Rev.* **1989**, *89*, 431-458.
77. Xia, Q.-H.; Ge, H.-Q.; Ye, C.-P.; Liu, Z.-M.; Su, K.-X. Advances in Homogeneous and Heterogeneous Catalytic Asymmetric Epoxidation. *Chem. Rev.* **2005**, *105*, 1603-1662.

78. Mukaiyama, T.; Takai, T.; Yamada, T.; Rhode, O. Nickel(II) Complex Catalyzed Epoxidation of Olefins with Molecular Oxygen and Primary Alcohol. *Chem. Lett.* **1990**, 1661-1664.
79. Yamada, T.; Takai, T.; Rhode, O.; Mukaiyama, T. Highly Efficient Method for Epoxidation of Olefins with Molecular Oxygen and Aldehydes Catalyzed by Nickel(II) Complexes. *Chem. Lett.* **1991**, 1-4.
80. Wentzel, B. B.; Alsters, P. L.; Feiters, M. C.; Nolte, R. J. M. Mechanistic Studies on the Mukaiyama Epoxidation. *J. Org. Chem.* **2004**, *69*, 3453-3464.

**Chapter 2: Can Donor Ligands Make Pd(OAc)₂ a Stronger
Oxidant? Access to Elusive Palladium(II) Reduction
Potentials and Effects of Ancillary Ligands via
Palladium(II)/Hydroquinone Redox Equilibria.**

This work is published:

Bruns, D. L.; Musaev, D. G.; Stahl, S. S. *J. Am. Chem. Soc.* **2020**, *142*, 19678-19688.

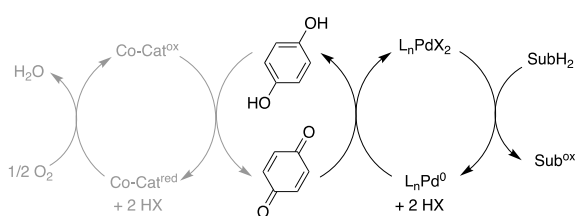
2.1 Abstract

Palladium(II)-catalyzed oxidation reactions represent an important class of methods for selective modification and functionalization of organic molecules. This field has benefitted greatly from the discovery of ancillary ligands that expand the scope, reactivity, and selectivity in these reactions; however, ancillary ligands also commonly poison these reactions. The different influences of ligands in these reactions remain poorly understood. For example, over the 60-year history of this field, the Pd^{II/0} redox potentials for catalytically relevant Pd complexes have never been determined. Here, we report the unexpected discovery of (L)Pd^{II}(OAc)₂-mediated oxidation of hydroquinones, the microscopic reverse of quinone-mediated oxidation of Pd⁰ commonly employed in Pd^{II}-catalyzed oxidation reactions. Analysis of redox equilibria arising from the reaction of (L)Pd(OAc)₂ and hydroquinones (L = bathocuproine, 4,5-diazafluoren-9-one), generating reduced (L)Pd species and benzoquinones, provides the basis for determination of (L)Pd^{II}(OAc)₂ reduction potentials. Experimental results are complemented by density functional theory calculations to show how a series of nitrogen-based ligands modulate the (L)Pd^{II}(OAc)₂ reduction potential, thereby tuning the ability of Pd^{II} to serve as an effective oxidant of organic molecules in catalytic reactions.

2.2 Introduction

The field of homogeneous palladium catalyzed reactions for organic synthesis originated in 1959 with the discovery of the Wacker process, which features palladium(II)-catalyzed oxidative coupling of ethylene and water to generate acetaldehyde.¹ Subsequent research efforts led to the discovery of numerous other oxidation reactions, including Wacker-type oxidative coupling of alkenes with diverse heteroatom and carbon-based nucleophiles;²⁻⁵ oxidative 1,4-difunctionalization of conjugated dienes;⁶ aromatic and allylic C–H oxidation reactions, including

oxidative biaryl coupling,^{7,8} Fujiwara-Moritani coupling of arenes and alkenes,^{9,10} and allylic acetoxylation.¹¹ These reactions typically employed palladium(II) catalysts with a stoichiometric oxidant to support reoxidation of Pd⁰ to Pd^{II}, enabling catalytic turnover. The original Wacker process and various other reactions proved compatible with O₂ as the oxidant, but 1,4-benzoquinone (BQ) emerged as one of the most widely used oxidants, including as a stoichiometric oxidant and as a redox-active co-catalyst (Scheme 2.1).^{12–17}



Scheme 2.1. Role of Benzoquinone as a (Co-)Oxidant in Palladium-Catalyzed Oxidation Reactions

Catalysts used during the first several decades of this field primarily consisted of palladium(II) salts dissolved in polar solvents, but more recent efforts have emphasized ligand-supported catalysts. Oxidatively stable nitrogen donors, such as pyridine and phenanthroline, are among the most common class of ancillary ligands, but other examples include tertiary amines, sulfoxides, and *N*-heterocyclic carbenes. Ancillary ligands can impart multiple benefits to these reactions, including (1) facilitating catalyst turnover with O₂ rather than other stoichiometric oxidants, often without the need for redox co-catalysts; (2) enhancing catalyst stability by inhibiting decomposition of Pd⁰ into inactive nanoparticles or heterogeneous Pd; and (3) modulating chemo-, regio-, and stereoselectivity in synthetic oxidation reactions of alcohols, alkenes, C–H bonds, and other functional groups.¹⁸

Ancillary ligands play a crucial role in many homogeneous catalytic reactions; however, their use in Pd-catalyzed homogeneous oxidation reactions is somewhat paradoxical. Pd^{II} is the primary oxidant of the organic substrate, and coordination of electron-donating ligands to Pd^{II} is expected to make Pd^{II} a weaker oxidant. This consideration could explain why "ligand-free" catalyst systems dominated much of the early literature and synthetic applications within the field. Even in recent studies, ancillary donor ligands are commonly found to inhibit catalyst turnover.^{19–23} Yet, direct insights into the influence of ligands on Pd^{II/0} redox potentials are almost entirely lacking, and ligand selection is largely guided by intuitive concepts and empirical screening. Catalytically relevant Pd^{II} complexes, such as (L)PdX₂ species (L = bidentate ancillary donor ligand or two monodentate ligands; X = OAc, Cl, or other anionic ligand), exhibit complex electrochemical behavior that complicates acquisition of such insights.^{24–27} Cyclic voltammetry studies yield irreversible waves arising from the different coordination environments of the corresponding Pd^{II} and Pd⁰ species and/or from the formation of metastable species via one-electron redox steps and, therefore, the data do not provide reliable thermodynamic information.²⁸

Here, we present the first analysis of ligand effects on Pd^{II/0} redox potentials for (L)Pd(OAc)₂ complexes, using prototypical nitrogen-donor ligands commonly employed in Pd-catalyzed oxidation reactions. These ligands include pyridine (py), 2,2'-bipyridine (bpy), 1,10-phenanthroline (phen), bathophenanthroline (bphen; 4,7-diphenyl-1,10-phenanthroline), 6,6'-dimethyl-2,2'-bipyridine (dmbpy), 2,9-dimethyl-1,10-phenanthroline (dmphen), bathocuproine (bc; 2,9-dimethyl-4,7-diphenyl-1,10-phenanthroline), and 4,5-diazafluoren-9-one (DAF) (Figure **2.1**). This study originates from an unexpected observation that certain ligated Pd(OAc)₂ complexes oxidize 1,4-hydroquinone (H₂BQ) to BQ, reversing the redox reaction featured in BQ-promoted Pd-catalyzed oxidation reactions (cf. Scheme **2.1**). This reactivity provides the basis for

unprecedented redox equilibria between palladium complexes and benzoquinone derivatives. Experimental and computational analysis of these reactions shows how the ancillary ligand structure modulates Pd^{II} redox potentials, sometimes in non-intuitive ways, and enables construction of a redox potential scale for the different (L)Pd(OAc)₂ complexes.

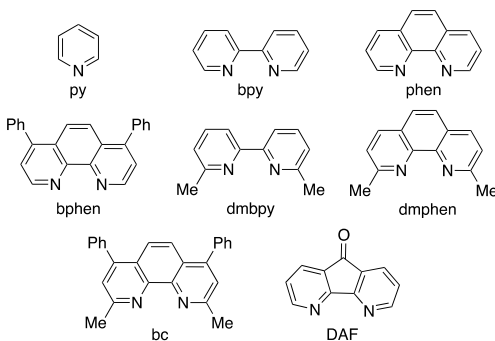


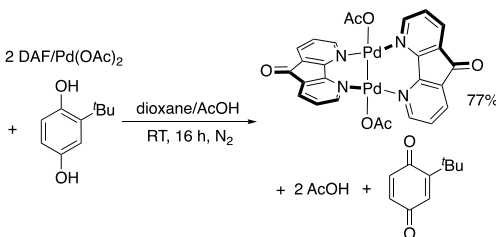
Figure 2.1. Representative ancillary nitrogen-based ligands encountered in Pd-catalyzed oxidation reactions and considered in the present study.

2.3 Results and Discussion

Background context and discovery of (L)Pd(OAc)₂-mediated oxidation of hydroquinone. In a 2010 study of Pd(OAc)₂-catalyzed allylic acetoxylation, we noted that DAF enabled good reactivity with O₂ as the sole oxidant,²⁹ while little or no catalytic turnover was observed with other ancillary nitrogen ligands (e.g., Figure 2.1). Beneficial effects of DAF have been noted in other Pd-catalyzed oxidation reactions,^{23,30–40} and mechanistic studies highlight important ways in which DAF facilitates catalytic turnover, including its kinetic lability and access to multiple coordination modes.^{23,29,41,42} In other reactions, ligands with methyl groups adjacent to the coordinating nitrogen atoms, including dmbpy, dmphen, and bc, have been shown to be effective. Mechanistic studies show that these ligands disfavor formation of inactive binuclear complexes^{43–46} and undergo facile κ^2 – κ^1 interconversion to open coordination sites at the Pd^{II}

center.²³ A factor not considered or investigated in these studies is the influence of the ancillary ligand on the Pd^{II/0} redox potential. Ligands that raise the reduction potential of Pd^{II} will increase the thermodynamic driving force for the substrate oxidation half-reaction and facilitate catalytic turnover (steps associated with substrate oxidation by Pd^{II} are often turnover limiting).¹⁸

An opportunity to probe the influence of ligands on the Pd^{II/0} redox potential arose unexpectedly from recent observations made while expanding on the synthetic utility of DAF/Pd(OAc)₂-catalyzed allylic oxidations.⁴⁷ We noted that benzoquinones could enhance the catalytic performance of DAF/Pd(OAc)₂, even in the absence of other redox active co-catalysts (cf. Scheme 2.1). This result suggested possible synergistic redox reactivity between Pd^{II} and BQ, including Pd^{II}-mediated oxidation of hydroquinone.^{48–52} This possibility was not explored at the time, but provides the basis for the present investigation. A hydroquinone derivative, 2-*tert*-butyl-1,4-hydroquinone (^tBuH₂BQ), was combined with DAF and Pd(OAc)₂ in dioxane:AcOH (3:1 vol:vol) under conditions resembling those used in the original study of DAF/Pd(OAc)₂-catalyzed allylic oxidation. The initial yellow-orange solution changed to deep-red upon standing at room temperature for several hours, and ¹H NMR analysis of the final products revealed the previously characterized Pd^I dimer, [Pd^I(μ-DAF)(OAc)]₂,^{42,53} and 2-*tert*-butyl-1,4-benzoquinone (^tBuBQ). The ^tBuBQ was obtained in 77% yield, when accounting for Pd as a one-electron oxidant (Equation 2.1; see Appendix A: for details).



Equation 2.1. Reaction of DAF/Pd(OAc)₂ with ^tBuH₂BQ

This result prompted us to test whether other ancillary ligands support the Pd^{II}-mediated oxidation of ^tBuH₂BQ. Two different solvent systems, dioxane:acetic acid-*d*₄ (3:1) and chloroform-*d*₁/1.5 M acetic acid-*d*₄, were used to account for differences in the solubility properties of the different Pd/ligand combinations and the use of dioxane and chlorinated solvents in the previous catalytic studies.^{29,47} The reactions were conducted by adding 2 equiv of ^tBuH₂BQ to solutions of L/Pd(OAc)₂ (L:Pd = 1:1 for bidentate ligands and 2:1 for pyridine) in the two solvent systems. The solutions were analyzed by ¹H NMR spectroscopy after 24 h at ambient temperature under N₂ (Figure **2.2A**).

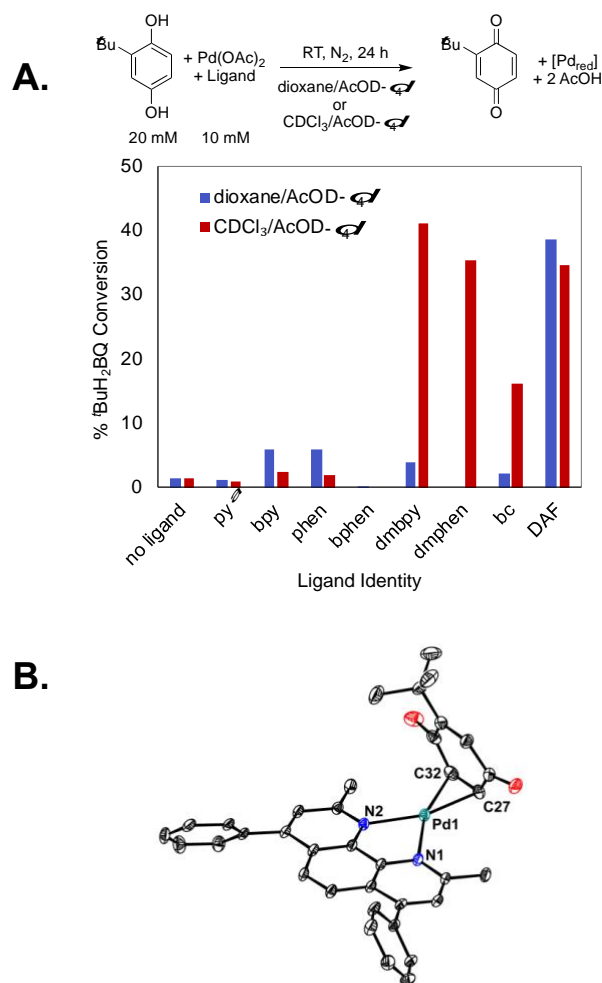


Figure 2.2. (A) Ligand effects on the Pd(OAc)₂-mediated oxidation of ^tBuH₂BQ. Conversion determined by ¹H NMR spectroscopy using methyl-3,5-dinitrobenzoate (dioxane/AcOD-*d*₄) or 1,3,5-trimethoxybenzene (CDCl₃/AcOD-*d*₄) as an internal standard. ^a20 mM pyridine used. (B) X-ray crystal structure of (bc)Pd(^tBuBQ). H-atoms and solvent molecules omitted for clarity. See Section A.9 of Appendix A: for full details.

In both solvents, very little ^tBuH₂BQ conversion was observed in the absence of ancillary ligand and with py, bpy, phen, and bphen as ligands (< 10%), together with small amounts of Pd black. In dioxane/AcOD-*d*₄, very low ^tBuH₂BQ conversions were also observed with dmbpy, dmphen, and bc; however, 39% ^tBuH₂BQ conversion was observed with DAF. No Pd black was observed in this reaction, and identification of [Pd^I(μ-DAF)(OAc)]₂ as the reduced Pd product indicates that the 39% conversion corresponds to a 77% yield with respect to Pd^{III}, as noted above.

In $\text{CDCl}_3/\text{AcOD-}d_4$, several ligands led to productive conversion of ${}^t\text{BuH}_2\text{BQ}$: dmbpy, dmphen, bc, and DAF led to ${}^t\text{BuH}_2\text{BQ}$ conversions of 41%, 36%, 16%, and 35%, respectively. All of these reaction solutions exhibited a color change, from yellow-orange to deep red. The red solution with DAF was attributed to the same Pd^{I} dimer observed in dioxane:AcOH (cf. Equation 2.1), although significant Pd black formation was also observed. Analysis of the products obtained from reactions with dmbpy, dmphen, and bc by ${}^1\text{H}$ NMR spectroscopy revealed four distinct resonances associated with the *tert*-butyl group and three ring protons for ${}^t\text{BuBQ}$, but the peaks were shifted upfield relative to free ${}^t\text{BuBQ}$. Crystals were obtained from the reaction of ${}^t\text{BuH}_2\text{BQ}$ and (bc) $\text{Pd}(\text{OAc})_2$, and X-ray diffraction analysis revealed the identity of (bc) $\text{Pd}(\eta^2\text{-}{}^t\text{BuBQ})$ as the product of the reaction (Figure 2.2B).^{54–58} Similar species were evident in the ${}^1\text{H}$ NMR spectra with the dmbpy and dmphen ligands, but the products were less stable and led to relatively rapid Pd black formation. Consequently, subsequent studies focused on the reactions of DAF- and bc-ligated Pd complexes.

Characterization of redox equilibria between DAF/ $\text{Pd}(\text{OAc})_2$ and hydroquinones. The partial conversion observed in the reaction of ${}^t\text{BuH}_2\text{BQ}$ and DAF/ $\text{Pd}(\text{OAc})_2$ described above raised the possibility that an equilibrium is established between the reagents and products. To explore this possibility, the reaction between ${}^t\text{BuH}_2\text{BQ}$ and DAF/ $\text{Pd}(\text{OAc})_2$ was monitored by ${}^1\text{H}$ NMR spectroscopy. Only partial conversion to ${}^t\text{BuBQ}$ and $[\text{Pd}^{\text{I}}(\mu\text{-DAF})(\text{OAc})]_2$ (Figure 2.3A) was observed, and the same product mixture was obtained when the reverse reaction was analyzed, starting with independently prepared $[\text{Pd}^{\text{I}}(\mu\text{-DAF})(\text{OAc})]_2$ and ${}^t\text{BuBQ}$ (Figure 2.3B). These observations confirm equilibration between the oxidized and reduced Pd and quinone species, and the final concentrations indicate an equilibrium constant of 305 M for the reaction in Equation 2.1, according to the expression in Equation 2.2.

$$K_{\text{eq}} = \frac{[\text{Pd}(\mu\text{-DAF})(\text{OAc})_2] \cdot [{}^t\text{BuBQ}] \cdot [\text{AcOH}]^2}{[\text{DAF}/\text{Pd}(\text{OAc})_2]^2 \cdot [{}^t\text{BuH}_2\text{BQ}]}$$

Equation 2.2. Equilibrium expression for reaction of DAF/Pd(OAc)₂ and ^tBuH₂BQ

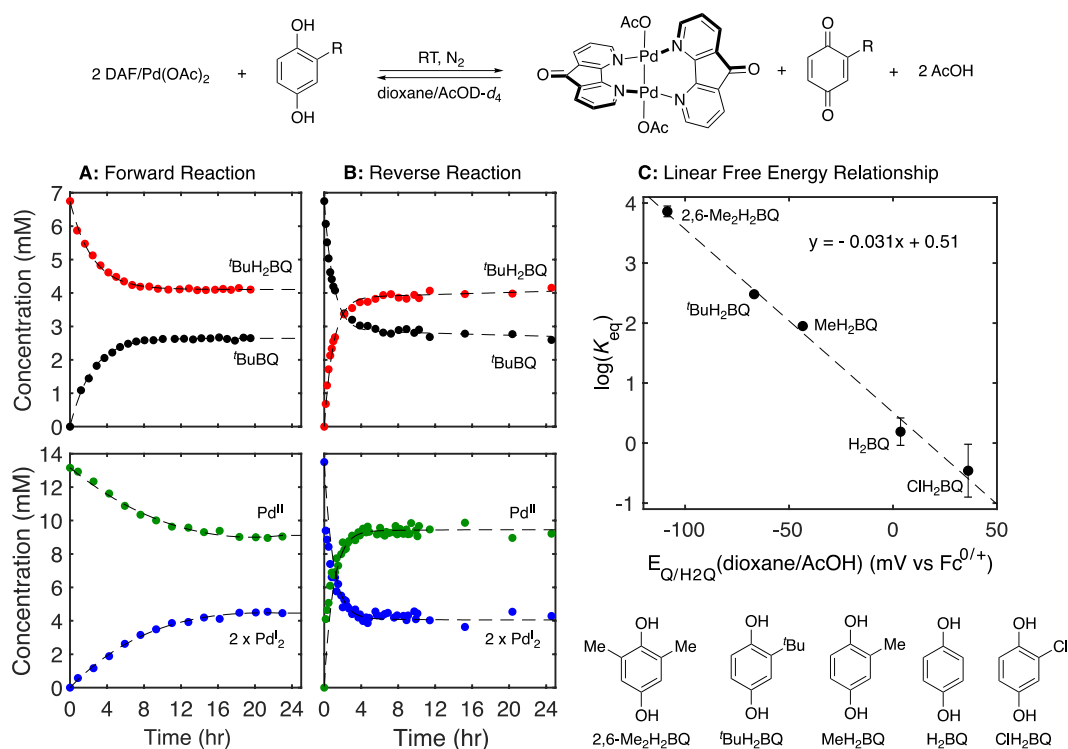


Figure 2.3. Approach-to-equilibrium concentration data. A: Forward Reaction: oxidation of ^tBuH₂BQ by DAF/Pd(OAc)₂ to form ^tBuBQ and [Pd^I(μ-DAF)(OAc)]₂. Reaction conditions: [Pd(OAc)₂] = 13.5 mM; [DAF] = 13.5 mM; [^tBuH₂BQ] = 6.75 mM. B: Reverse Reaction: oxidation of [Pd^I(μ-DAF)(OAc)]₂ by ^tBuBQ to form ^tBuH₂BQ and DAF/Pd(OAc)₂. [Pd^I(μ-DAF)(OAc)]₂ = 6.75 mM; [^tBuBQ] = 6.75 mM. C. Linear free energy relationship of log(*K*_{eq}) *E*_{Q/H₂Q}(dioxane/AcOH) (mV vs Fc^{0/+}). Reaction conditions: [DAF] = 13.5 mM; [Pd(OAc)₂] = 13.5 mM; [H₂Q] = variable (see Appendix A sections A.3 and A.4 for details).

Similar data were then obtained with a series of other hydroquinone derivatives in their reaction with DAF/Pd(OAc)₂ in dioxane/AcOD-*d*₄, with the equilibrium concentrations of species analyzed by ¹H NMR spectroscopy. The equilibrium constants obtained from these experiments follow a logical trend, with more electron-rich hydroquinones exhibiting higher equilibrium

constants: 2,6-Me₂H₂BQ ($K_{\text{eq}} = 7241 \text{ M}$), ^tBuH₂BQ ($K_{\text{eq}} = 305 \text{ M}$; see above), MeH₂BQ, ($K_{\text{eq}} = 90 \text{ M}$), H₂BQ ($K_{\text{eq}} = 1 \text{ M}$) and ClH₂BQ ($K_{\text{eq}} = 0.4 \text{ M}$). One-electron and 2H⁺/2e⁻ redox potentials for these quinones have been reported in the literature; however, the values were obtained under different conditions.⁵⁹ Efforts to obtain potentials under the present reaction conditions were complicated by irreversible cyclic voltammograms, but reliable values could be obtained by performing open circuit potential measurements with 1:1 mixtures of the corresponding hydroquinone/benzoquinone species.⁶⁰ Reduction potentials determined by this method, designated $E_{\text{Q}/\text{H}_2\text{Q}}$ (dioxane/AcOH), are as follows: 2,6-Me₂BQ: -109 mV, ^tBuBQ: -67 mV, MeBQ: -43 mV, BQ: 4 mV, ClBQ: 36 mV, all referenced to Fc⁺⁰ (see section A.6 of Appendix A for details). A plot of $\log(K_{\text{eq}})$ versus $E_{\text{Q}/\text{H}_2\text{Q}}$ (dioxane/AcOH) for the different quinones exhibits a linear correlation with a negative slope, reflecting the larger K_{eq} values for quinones with lower redox potentials (Figure 2.3C). [Nomenclature note: The abbreviation "Q/H₂Q" is used when referring generically to (hydro)quinone species, while "BQ/H₂BQ" specifically refers to the unsubstituted 1,4-(hydro)benzoquinone derivatives.

Characterization of redox equilibria between (bc)Pd(OAc)₂ and hydroquinones. The well behaved reaction between ^tBuH₂BQ and (bc)Pd(OAc)₂ was also monitored by ¹H NMR spectroscopy, and an equilibrium mixture of (bc)Pd(OAc)₂, ^tBuH₂BQ, and (bc)Pd(^tBuBQ) was obtained. Analysis of the reverse reaction, starting with (bc)Pd(^tBuBQ) in the presence of AcOD-*d*₄ cosolvent, led to the same equilibrium mixture (Figure 2.4A and Figure 2.4B).

Similar behavior was observed when the reactions were conducted with other hydroquinones. An exception was observed in the reaction of (bc)Pd(OAc)₂ with 2,6-Me₂H₂BQ, which generated substantial amounts of Pd black, probably reflecting the comparative instability of the Pd⁰ complex of the 2,6-disubstituted quinone. For the other four quinones, equilibrium

constants were determined according to the expression in Equation 2.3, with the following values: ${}^t\text{BuH}_2\text{BQ}$ ($K_{\text{eq}} = 129 \text{ M}$), MeH_2BQ , ($K_{\text{eq}} = 30 \text{ M}$), H_2BQ ($K_{\text{eq}} = 3 \text{ M}$) and ClH_2BQ ($K_{\text{eq}} = 0.5 \text{ M}$).

$$K_{\text{eq}} = \frac{[(bc)\text{Pd}(\text{RBQ})] \cdot [\text{AcOH}]^2}{[(bc)\text{Pd}(\text{OAc})_2] \cdot [\text{RH}_2\text{BQ}]}$$

Equation 2.3. Equilibrium expression for reaction of $(bc)\text{Pd}(\text{OAc})_2$ with hydroquinones

The $2\text{H}^+/2\text{e}^- \text{Q}/\text{H}_2\text{Q}$ redox potentials were re-determined in this different solvent system via open circuit potential measurements, as described above (see section A.6 in Appendix A for details). The values differ slightly (16-31 mV lower) from those measured in dioxane: ${}^t\text{BuBQ} = -98 \text{ mV}$, $\text{MeBQ} = -74 \text{ mV}$, $\text{BQ} = -13 \text{ mV}$, and $\text{ClBQ} = 10 \text{ mV}$ vs. $\text{Fc}^{+/0}$. The plot of $\log(K_{\text{eq}})$ versus $E_{\text{Q}/\text{H}_2\text{Q}}(\text{CHCl}_3/\text{AcOH})$ for the different quinones again exhibits a linear correlation with a negative slope, reflecting larger K_{eq} values for quinones with lower redox potentials (Figure 2.4C).

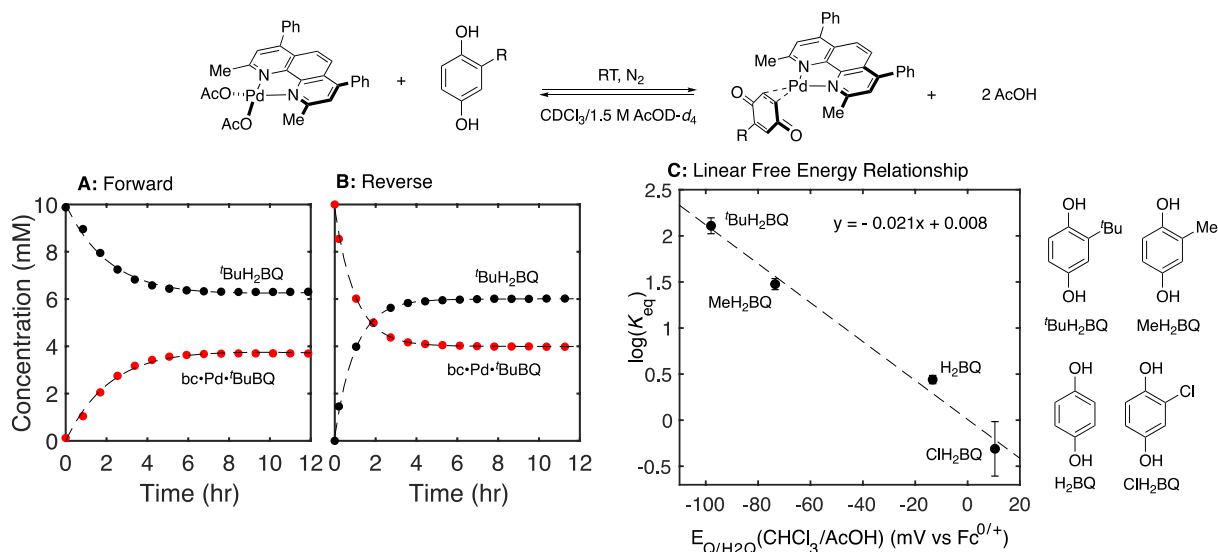


Figure 2.4. Equilibrium reaction of $(bc)\text{Pd}(\text{OAc})_2/{}^t\text{BuH}_2\text{BQ}$ and $(bc)\text{Pd}({}^t\text{BuBQ})$. Reaction conditions: A: Forward: $[(bc)\text{Pd}(\text{OAc})_2] = 10.0 \text{ mM}$; $[{}^t\text{BuH}_2\text{BQ}] = 10.0 \text{ mM}$. B: Reverse: $[(bc)\text{Pd}({}^t\text{BuBQ})] = 10 \text{ mM}$. C. Linear free energy relationship of $\log(K_{\text{eq}})$ and

$E_{Q/H_2Q}(CHCl_3/AcOH)$. Reaction conditions: $[(bc)Pd(OAc)_2] = 10.0$ mM $[H_2Q] =$ variable (see sections A.3 and A.4 of Appendix A for details).

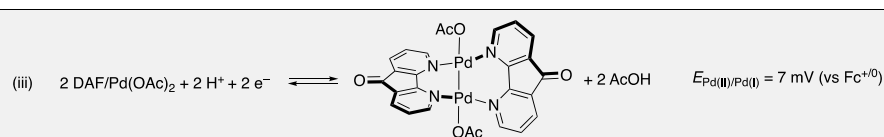
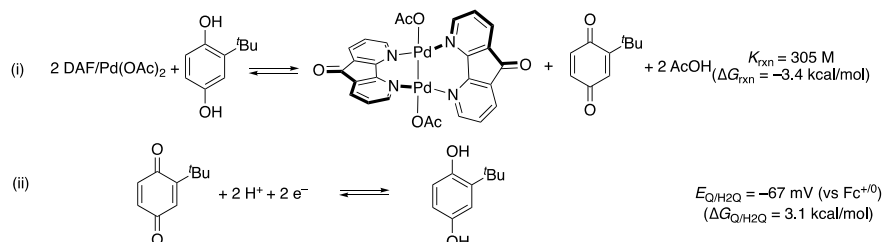
The somewhat smaller slope of this plot, relative to that in Figure 2.3C, may be rationalized by enhanced stability of the Pd^0 complexes with more electron-deficient quinones, which will partially offset the more favorable oxidation of more electron-rich hydroquinones.

Quantitative Analysis of Ligand Effects on Palladium(II) Reduction Potentials. These well-behaved redox equilibria provide unique access to quantitative ligand effects on Pd^{II} reduction potentials. With DAF as the ancillary ligand, the Q/H_2Q reduction potentials and Pd^{II}/Pd^I redox equilibria with different (hydro)quinones may be used to create thermodynamic cycles that allow determination the $2H^+/2e^-$ reduction potential associated with the conversion of 2 $DAF/Pd(OAc)_2$ into $[Pd^I(\mu-DAF)(OAc)]_2 + 2$ AcOH. The analysis depicted in Scheme 2.2A shows a thermodynamic cycle using $^tBuH_2BQ/^tBuBQ$ as representative (hydro)quinone reagents. The $Pd^{III/I}$ potential is obtained by adding the free energy (ΔG) values from the reaction of $DAF/Pd^{II}(OAc)_2$ and tBuH_2BQ and the $^tBuBQ/^tBuH_2BQ$ reduction potential, followed by conversion of ΔG into ΔE using the Nernst equation. Similar analysis of the reactions with all five (hydro)quinone derivative led to an average $E_{Pd(II)/Pd(I)}$ value of 12 ± 7 mV vs $Fc^{+/0}$. We note that the $E_{Pd(II)/Pd(I)}$ value could also be obtained from the linear free energy correlation in Figure 2.2, by identifying the Q/H_2Q potential corresponding to $\log(K_{eq}) = 0$. The value of $E_{Pd(II)/Pd(I)} = 17$ mV obtained by this approach is within experimental error of the result obtained in Scheme 2.2A.

Determination of the reduction potential of $(bc)Pd(OAc)_2$ is a bit more complex due to coordination of the quinone to Pd^0 . The lack of free quinone as a product results in an undefined quinone/hydroquinone redox potential; however, this issue may be addressed by including an additional quinone-exchange equilibrium at Pd^0 (c.f. Scheme 2.2Bii). The latter reaction allows a

thermodynamic cycle to be created for determination of the $2\text{H}^+/2\text{e}^-$ reduction potential of (bc)Pd(OAc)₂/BQ to (bc)Pd⁰(BQ) + 2 AcOH.

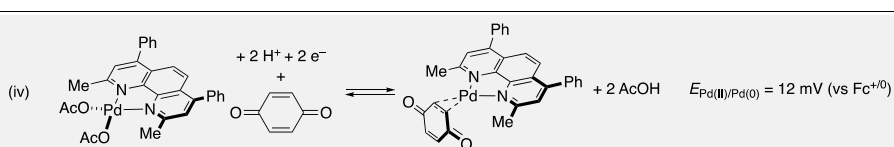
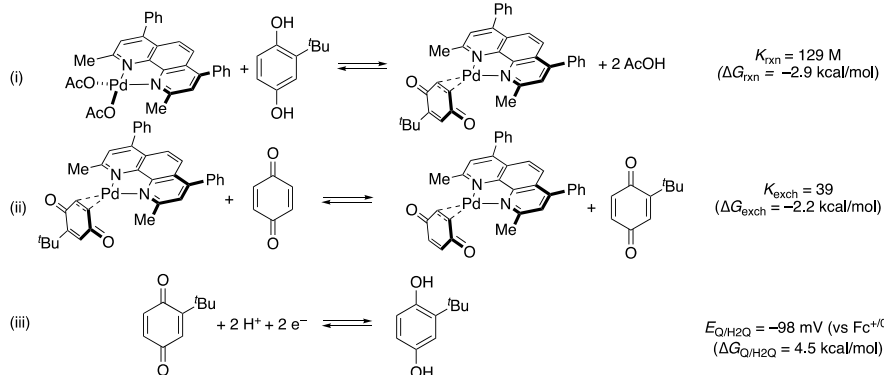
A. Thermodynamic Cycle for Determination of DAF/Pd(OAc)₂ Reduction Potential in dioxane/AcOD-*d*₄



Quinone	K_{rxn} (M)	$E_{\text{Q}/\text{H}_2\text{Q}}$ (mV vs $\text{Fc}^{+/0}$)	$E_{\text{Pd(II)}/\text{Pd(I)}}$ (mV vs $\text{Fc}^{+/0}$)
2,6-Me ₂ BQ	7241	-109	6
tBuBQ	305	-67	7
MeBQ	90	-43	14
BQ	1	4	9
ClBQ	0.4	36	23

average
 $E_{\text{Pd(II)}/\text{Pd(I)}} = 12 \pm 7 \text{ mV}$
 vs $\text{Fc}^{+/0}$

B. Thermodynamic Cycle for Determination of (bc)Pd(OAc)₂ Reduction Potential In $\text{CDCl}_3/1.5 \text{ M AcOD-}d_4$



Quinone	K_{rxn}	K_{exchange}	$E_{\text{Q}/\text{H}_2\text{Q}}$ (mV vs $\text{Fc}^{+/0}$)	$E_{\text{Pd(II)}/\text{Pd(0)}}$ (mV vs $\text{Fc}^{+/0}$)
tBuBQ	129	39	-98	12
MeBQ	30	12	-74	2
BQ	3	1	-13	-0.3
ClBQ	0.5	0.1	10	-29

average
 $E_{\text{Pd(II)}/\text{Pd(0)}} = -4 \pm 18 \text{ mV}$
 vs $\text{Fc}^{+/0}$

Scheme 2.2. Determination of (L)Pd(OAc)₂ Reduction Potentials in Dioxane/AcOH (L = DAF) and $\text{CHCl}_3/\text{AcOH}$ (L = bc)

To complete this analysis, equilibrium constants were measured for the exchange of different quinones at the (bc)Pd⁰ fragment (see section A.5 in Appendix A for details).^{56,61} A representative thermodynamic cycle, using the equilibrium exchange of BQ and ^tBuBQ at Pd⁰ and ^tBuH₂BQ/^tBuBQ as a reference redox couple, is depicted in Scheme 2.2B. The reaction free energies may be summed, and the resulting ΔG value may then be used to obtain the $E_{\text{Pd(II)/Pd(0)}}$ value. Use of four different reference Q/H₂Q potentials and Pd⁰-BQ/Q exchange equilibrium constants led to an average value of $E_{\text{Pd(II)/Pd(0)}} = -4 \pm 18 \text{ mV vs Fc}^{+/0}$.

DFT Computational Analysis of Ligand Effects on Pd^{II/0} Reduction Potentials.

Palladium/quinone redox equilibria were not experimentally accessible for all of the ligands in Figure 2.1 due to complications arising from poor solubility and/or instability of the Pd⁰-quinone complexes. To address these cases, density functional theory (DFT) calculations were employed, using experimental data for the DAF- and bc-ligated Pd(OAc)₂ complexes as benchmarks. These calculations were conducted at the B3LYP-D3(BJ)/[6-31G(d,p) + Lanl2dz (Pd)] level of theory, with the corresponding Hay-Wadt effective core potential for Pd. Bulk solvent effects were incorporated at the IEF-PCM level (chloroform, $\epsilon = 4.7113$).⁶²⁻⁷¹ The calculated thermodynamic data are reported at a temperature of 298.15 K.

DFT data were used to analyze the thermodynamics for oxidation of H₂BQ by the different (L)Pd(OAc)₂ complexes (**1**) for L = phen, bpy, py, dmphen, dmbpy, and DAF, leading to the formation of (L)Pd⁰(BQ) complexes (**2**). Initial calculations probed the free energies of ligand exchange for the reaction of different ligands with (phen)Pd(OAc)₂ (ΔG_L ; Figure 2.5A-*i*). The resulting values show that the different ancillary ligands can lead to substantial changes in the relative stability the (L)Pd(OAc)₂ complexes. Each of these complexes was then used to calculate

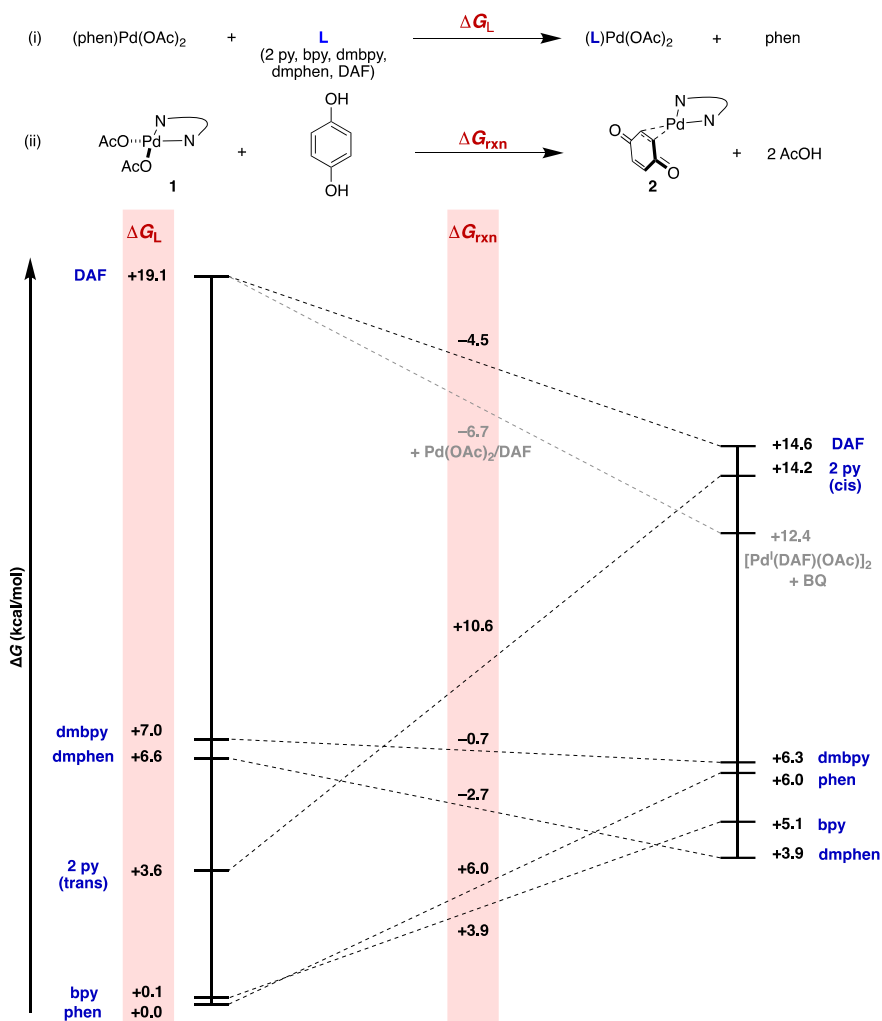
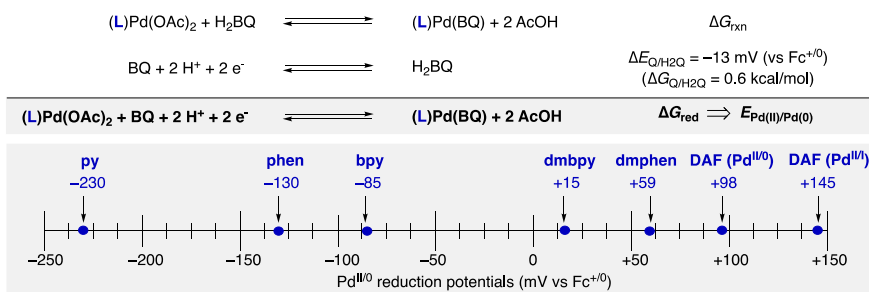
A. Energy Diagram for Reaction of (L)Pd(OAc)₂ and Hydroquinone

B. Calculated Reduction Potentials for (L)Pd(OAc)₂ Complexes


Figure 2.5. A. Energy diagram for reaction of (L)Pd(OAc)₂ and hydroquinone. Energies of (L)Pd(OAc)₂ complexes are reported relative to (phen)Pd(OAc)₂. B. Scale showing calculated reduction potentials for (L)Pd(OAc)₂ complexes.

the reaction free energy for oxidation of H₂BQ to afford (L)Pd⁰(BQ) and 2 equiv of AcOH (ΔG_{rxn} , Figure 2.5A-ii). This reaction is endergonic for L = py, bpy, and phen, with calculated free energies of the reactions of $\Delta G_{\text{rxn}} = +10.6$, $+6.0$, and $+3.9$ kcal/mol, respectively. The reaction of H₂BQ with (L)Pd(OAc)₂ complexes with L = dmbpy, dmphen and DAF are exergonic, with $\Delta G_{\text{rxn}} = -0.7$, -2.7 , and -4.5 kcal/mol, respectively. We also computed the free energy for the reaction of 2 (DAF)Pd(OAc)₂ with H₂BQ to generate [Pd^I(μ -DAF)(OAc)]₂ and free BQ. This reaction proved to be even more exergonic than formation of the (DAF)Pd⁰(BQ) adduct ($\Delta G = -6.7$ kcal/mol; Figure 2.5A - gray reaction in energy diagram), consistent with experimentally observed formation of the Pd^I dimer, rather than a (DAF)Pd⁰-BQ adduct. More broadly, these results show good qualitative alignment with the experimental ligand effects on the reaction of Pd(OAc)₂ with ^tBuH₂BQ CHCl₃/AcOD-*d*₄, (cf. Figure 2.2) in which little or no reaction was observed with L = py, bpy, and phen, while ^tBuH₂BQ oxidation was observed with L = dmbpy, dmphen, and DAF.

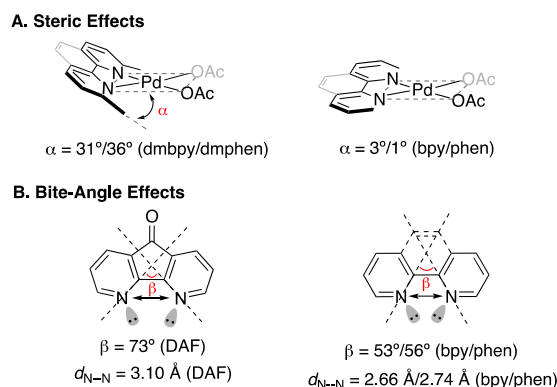
Ligand-based differences in energies are more significant for the Pd^{II} complexes than the Pd⁰ complexes. This behavior is evident, for example, from the effect of adding methyl groups adjacent to nitrogen in the bpy and phen ligands. The (L)Pd(OAc)₂ complexes with L = dmbpy and dmphen, are approximately 7 kcal/mol higher in energy than the analogs with L = bpy and phen, while the corresponding (L)Pd⁰(BQ) complexes for L = bpy, phen, dmbpy and dmphen span a range of energies of only 2.4 kcal/mol, with the dmphen complex having the lowest energy. Pyridine has intermediate stability among the different non-DAF ligands but leads to a particularly unstable Pd⁰(BQ) complex.

The calculated ΔG_{rxn} values (see Figure 2.5A-i) together with the experimental 2H⁺/2e⁻ BQ/H₂BQ reduction potential (-13 mV vs Fc⁺⁰) may be used to determine reduction potentials for each of the (L)Pd(OAc)₂ complexes, resembling the approach illustrated in Scheme 2.2. The

results reveal that the ligands lead to (L)Pd(OAc)₂ reduction potentials that span 375 mV (Figure 2.5B): L = DAF (to form [Pd^I(DAF)(μ-OAc)]₂): +145 mV; L = DAF (to form (DAF)Pd(BQ)): +98 mV; L = dmphen: +59 mV; L = dmbpy: +15 mV; L = bpy: -85 mV; L = phen: -130 mV; L = py: -230 mV.

Summary and Implications of Ligand Effects on Palladium(II) Reduction Potentials.

The above data show that the ancillary ligand can significantly impact the Pd^{II} reduction potential and provide, for the first time, a quantitative assessment of this effect for catalytically relevant Pd complexes. Several specific results warrant further commentary. The methyl groups of the dmbpy and dmphen ligands increase the Pd^{II} reduction potential by 100 and 189 mV, respectively, relative to the corresponding bpy and phen complexes. This effect rationalizes the ability of dmbpy- and dmphen-ligated Pd(OAc)₂ to promote more favorable oxidation of H₂Q derivatives relative to the bpy- and phen-ligated complexes (cf. Figure 2.2). This ligand-based increase in redox potential also implicates a thermodynamic contribution to the success of dmbpy and dmphen ligands in Pd-catalyzed aerobic oxidations, including alcohol oxidation,⁴³⁻⁴⁶ aza-Wacker,²³ and oxidative Heck reactions.⁷²⁻⁷⁴ The higher energy of the dmbpy- and dmphen-ligated Pd(OAc)₂, relative to the bpy- and phen-ligand complexes, arises from destabilizing steric interactions between the ligand methyl groups and the acetate groups, which distort the coordination geometry of the planar ligand, forcing it out of the Pd^{II} square plane (Scheme 2.3A). This geometrical distortion has been noted in previously reported crystal structures of these complexes;^{23,75,76} however, the work here provides the first insight into the impact of this effect on the Pd^{II} reduction potential.



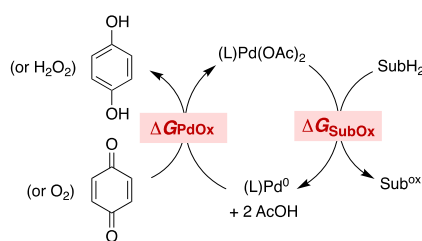
Scheme 2.3. Ligand-Based Structure Contributions to Modulation of Pd^{II} Reduction Potentials

The thermodynamic influence of DAF is even more profound and especially reflects the destabilization of Pd^{II}, rationalized by distortion of the bite angle of DAF relative to conventional bpy and phen ligands (Scheme 2.3B).^{23,41} Insights from the present study rationalize some of the unusual kinetic behavior that has been observed in DAF/Pd(OAc)₂-catalyzed oxidation reactions. For example, aza-Wacker and allylic oxidation exhibit a kinetic burst at the beginning of the reaction when DAF is used as an ancillary ligand.^{42,53} This burst phase arises from stoichiometric substrate oxidation by the DAF/Pd(OAc)₂ species and generates the Pd^I dimer, [Pd^I(DAF)(μ-OAc)]₂. This burst is followed by a slower steady-state phase of the reaction, and mechanistic data indicate that the steady-state turnover features a more conventional Pd^{II/0} cycle.⁴² The relative rates of the initial burst and steady-state phases of the reaction align with the different driving force provided by the Pd^{II/I} vs Pd^{II/0} redox processes, in which the stronger driving force for the Pd^{II/I} process contributes to the more rapid rate.

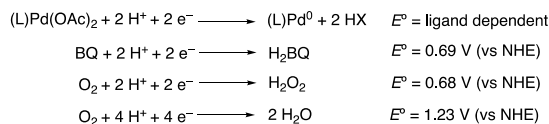
More generally, the observations here illustrate how ligands may be used to modulate the Pd^{II} reduction potential and thereby impact the driving force for oxidation reactions mediated by palladium(II) (ΔG_{SubOx} , Scheme 2.4A). The majority of Pd^{II}-catalyzed oxidation reactions feature turnover-limiting steps associated with the substrate oxidation half-reaction (e.g., reductive

elimination, transmetalation, β -hydride elimination).¹⁸ Ligands such as dmbpy, dmphen, and DAF that increase the Pd^{II} reduction potential will provide additional driving force for the net half-reaction, likely promoting faster rates and more effective substrate oxidation. Such benefits will ultimately reach a limit, however, controlled by the thermodynamics of the Pd oxidation half-reaction (ΔG_{PdOx} , Scheme 2.4A).

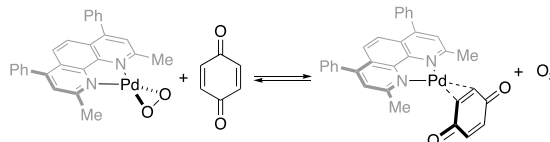
A. Free Energies of Redox Half-Reactions



B. Free Energies of Redox Half-Reactions



C. Quinone/O₂ Exchange Reaction at bc-Ligated Pd Center (ref. 78)



Scheme 2.4. Thermodynamic Considerations for Pd^{II}-Catalyzed Oxidation Reactions

Benzoquinone has been widely used as an oxidant for this reaction, but the present study reveals that, in some cases, the relative reduction potential of Pd^{II} and BQ can invert, and BQ will not have sufficient driving force for reoxidation of the Pd catalyst. Hints of this behavior are evident in Pd-oxidation reactions that are inhibited by BQ,^{77,78} and certain cases in which oxidation of the Pd catalyst is turnover-limiting.⁴² Such insights have direct implications for the use of O₂ as an oxidant because the 2H⁺/2e⁻ reduction potential of O₂ to H₂O₂ is virtually identical to that of

BQ to H₂BQ (0.68/0.69 V vs NHE, Scheme 2.4B). This relationship is evident in the nearly isoergic exchange of BQ and O₂ that has been observed at a bc-ligated Pd center (Scheme 2.4C).^{79,80} On the other hand, the 4H⁺/4e⁻ reduction of O₂ to water provides additional driving force (1.23 V) relative to the 2H⁺/2e⁻ process (Scheme 2.4B). Mechanisms capable of leveraging this O₂ reduction pathway provide a strategy to expand the scope and utility of Pd-catalyzed aerobic oxidation reactions.⁸¹⁻⁸⁶

2.4 Conclusion

The present study provides unique insights into the influence of ancillary ligands on Pd^{II} reduction potentials, arising from the unexpected discovery that certain ligands enable equilibrium-controlled oxidation of hydroquinone derivatives. Oxidation of hydroquinone by Pd^{II} is opposite to the direction of reactivity usually encountered in Pd-catalyzed oxidation reactions, where BQ is often used as a stoichiometric or co-catalytic reagent to re-oxidize the Pd catalyst. A noteworthy outcome of this study is the insight that coordination of electron-donating ancillary ligands do not necessarily lower the reduction potential of Pd(OAc)₂. Three of the (L)Pd(OAc)₂ complexes studied here (L = 2 py, bpy, and phen), in addition to Pd(OAc)₂ itself, did not promote oxidation of ^tBuH₂BQ, while (L)Pd(OAc)₂ complexes with four other ligands (L = dmbpy, dmphen, bc, and DAF) promoted this oxidation reaction. Experimental and computational analysis of the ligand effects show that this series of common nitrogen-based ligands leads to 2H⁺/2e⁻ reduction potentials for (L)Pd(OAc)₂ complexes that vary by 375 mV, with values falling both above and below the 2H⁺/2e⁻ reduction potentials for BQ derivatives.

These results have important implications for further development of Pd-catalyzed oxidation reactions by highlighting the thermodynamic influence of ancillary ligands on the Pd^{II} reduction potential. The insights point to the value of identifying new ligands that destabilize Pd^{II}

via steric effects (as with dmbpy, dmphen, and bc) or electronic effects (as with DAF), thereby increasing the driving force for substrate oxidation by Pd^{II}. The results of this study, however, also show that such efforts will need to be complemented by consideration of the oxidant used in the reaction to ensure that both substrate and Pd oxidation half-reactions are favorable and effective.

2.5 Acknowledgements

We benefited from a number of valuable discussions with Josh Buss and Chase Salazar (UW-Madison) and assistance from Ilia Guzei and Amelia Wheaton (UW-Madison) with X-ray diffraction data analysis. Funding for the experimental work was provided by the National Science Foundation (CHE-1665120 and CHE-1953926; SSS), and computational studies were supported by the NSF-CCI Center for C–H Functionalization (CHE-1700982, DGM). Spectroscopic instrumentation was supported by a gift from Paul J. Bender, NSF (CHE1048642), and the NIH (1S10 OD020022-1). DGM gratefully acknowledges the use of resources of the Cherry L. Emerson Center for Scientific Computation (Emory University).

2.6 References

1. Smidt, J.; Hafner, W.; Jira, R.; Sedlmeier, J.; Sieber, R.; Rüttinger, R.; Kojer, H. Catalytic Reactions of Olefins on Compounds of the Platinum Group. *Angew. Chem.* **1959**, *71*, 176-182.
2. Zeni, G.; Larock, R. C. Synthesis of Heterocycles via Palladium π -Olefin and π -Alkyne Chemistry. *Chem. Rev.* **2004**, *104*, 2285-2309.
3. Beccalli, E. M.; Broggini, G.; Martinelli, M.; Sottocornola, S. C–C, C–O, C–N Bond Formation on sp² Carbon by Pd(II)-Catalyzed Reactions Involving Oxidant Agents. *Chem. Rev.* **2007**, *107*, 5318-5365.

4. Minatti, A.; Muñiz, K. Intramolecular Aminopalladation of Alkenes as a Key Step to Pyrrolidines and Related Heterocycles. *Chem. Soc. Rev.* **2007**, *36*, 1142-1152.
5. McDonald, R. I.; Liu, G. S.; Stahl, S. S. Palladium(II)-Catalyzed Alkene Functionalization via Nucleopalladation: Stereochemical Pathways and Enantioselective Catalytic Applications. *Chem. Rev.* **2011**, *111*, 2981-3019.
6. Bäckvall, J.-E. In *Metal-Catalyzed Cross-Coupling Reactions*, 2nd ed.; de Meijere A., Diederich F., Eds. Wiley-VCH: Weinheim, **2004**; Vol. 2, p 479-529.
7. Yeung, C. S.; Dong, V. M. Catalytic Dehydrogenative Cross-Coupling: Forming Carbon-Carbon Bonds by Oxidizing Two Carbon-Hydrogen Bonds. *Chem. Rev.* **2011**, *111*, 1215-1292.
8. Liu, C.; Zhang, H.; Shi, W.; Lei, A. Bond Formations between Two Nucleophiles: Transition Metal Catalyzed Oxidative Cross-Coupling Reactions. *Chem. Rev.* **2011**, *111*, 1780-1824.
9. Jia, C.; Kitamura, T.; Fujiwara, Y. Catalytic Functionalization of Arenes via C-H Bond Activation. *Acc. Chem. Res.* **2001**, *34*, 633-639.
10. Le Bras, J.; Muzart, J. Intermolecular Dehydrogenative Heck Reactions. *Chem. Rev.* **2011**, *111*, 1170-1214.
11. Liron, F.; Oble, J.; Lorion, M. M.; Poli, G. Direct Allylic Functionalization Through Pd-Catalyzed C-H Activation. *Eur. J. Org. Chem.* **2014**, 5863-5883.
12. Moiseev, I. I.; Vargaftik, M. N.; Syrkin, Y. K. On the Mechanism of the Reaction of Palladium Salts with Olefins in Hydroxyl-Containing Solutions. *Dokl. Akad. Nauk SSSR* **1960**, *133*, 377-380.

13. Heumann, Åkermark, B. Oxidation with Palladium Salts: Catalytic Preparation of Allyl Acetates from Monoolefins Using a Three-Component Oxidation System. *Angew. Chem. Int. Ed.* **1984**, *23*, 453-454.
14. Bäckvall, J.-E.; Awasthi, A. K.; Renko, Z. D. Biomimetic Aerobic 1,4-Oxidation of 1,3-Dienes Catalyzed by Cobalt Tetraphenylporphyrin-Hydroquinone-Palladium(II). An Example of Triple Catalysis. *J. Am. Chem. Soc.* **1987**, *109*, 4750-4752.
15. Popp, B. V., Stahl, S. S. Palladium-Catalyzed Oxidation Reactions: Comparison of Benzoquinone and Molecular Oxygen as Stoichiometric Oxidants. *Top. Organomet. Chem.* **2007**, *22*, 149-189.
16. Piera, J.; Bäckvall, J.-E. Catalytic Oxidation of Organic Substrates by Molecular Oxygen and Hydrogen Peroxide by Multistep Electron Transfer—A Biomimetic Approach. *Angew. Chem. Int. Ed.* **2008**, *47*, 3506-3523.
17. Vasseur, A.; Muzart, J.; Le Bras, J. Ubiquitous Benzoquinones, Multitalented Compounds for Palladium-Catalyzed Oxidative Reactions. *Eur. J. Org. Chem.* **2015**, 4053-4069.
18. Wang, D.; Weinstein, A. B.; White, P. B.; Stahl, S. S. Ligand-Promoted Palladium-Catalyzed Aerobic Oxidation Reactions. *Chem. Rev.* **2018**, *118*, 2636-2679.
19. Steinhoff, B. A.; Guzei, I. A.; Stahl, S. S. Mechanistic Characterization of Aerobic Alcohol Oxidation Catalyzed by Pd(OAc)₂/Pyridine Including Identification of the Catalyst Resting State and the Origin of Nonlinear [Catalyst] Dependence. *J. Am. Chem. Soc.* **2004**, *126*, 11268-11278.

20. Schultz, M. J.; Alder, R. S.; Zierkiewicz, W.; Privalov, T.; Sigman, M. S. Using Mechanistic and Computational Studies to Explain Ligand Effects in the Palladium-Catalyzed Aerobic Oxidation of Alcohols. *J. Am. Chem. Soc.* **2005**, *127*, 8499-8507.
21. Zhang, Y.-H.; Shi, B.-F.; Yu, J.-Q. Pd(II)-Catalyzed Olefination of Electron-Deficient Arenes Using 2,6-Dialkylpyridine Ligands. *J. Am. Chem. Soc.* **2009**, *131*, 5072-5074.
22. Izawa, Y.; Stahl, S. S. Aerobic Oxidative Coupling of *o*-Xylene: Discovery of 2-Fluoropyridine as a Ligand to Support Selective Pd-Catalyzed C–H Functionalization. *Adv. Synth. Catal.* **2010**, *352*, 3223-3229.
23. White, P. B.; Jaworski, J. N.; Zhu, G. H.; Stahl, S. S. Diazafluorenone-Promoted Oxidation Catalysis: Insights into the Role of Bidentate Ligands in Pd-Catalyzed Aerobic Aza-Wacker Reactions. *ACS Catal.* **2016**, *6*, 3340-3348.
24. Parry, E. P.; Oldham, K. B. Electrochemistry of Palladium(II) Ion in Ammonia and Pyridine Media. *Anal. Chem.* **1968**, *40*, 1031-1036.
25. Wan, C. C.; Lai, C. K.; Wang, Y. Y. A Study of the Reduction of Chelated Palladium on Mercury Electrode. *Bull. Chem. Soc. Jpn.* **1991**, *64*, 635-640.
26. Azzabi, M., Jutand, A., Amatore, C. Role and Effects of Halide Ions on the Rates and Mechanisms of Oxidative Addition of Iodobenzene to Low-Ligated Zerovalent Palladium Complexes Pd⁰(PPh₃)₂. *J. Am. Chem. Soc.* **1991**, *113*, 8375-8384.
27. Van Asselt, R., Elsevier, C. J., Jutand, A., Amatore, C. Divalent Palladium and Platinum Complexes Containing Rigid Bidentate Nitrogen Ligands and Electrochemistry of the Palladium Complexes. *Organometallics*. **1997**, *16*, 317-328.

28. A rare case of well-behaved Pd^{II/0} electrochemistry has been reported for tetraphosphine-ligated Pd complexes; however, these complexes are rather different from the catalyst species employed in conventional oxidative and non-oxidative coupling reactions. See: Raebiger, J.W., Miedaner, A., Curtis, C.J., Miller, S.M., Anderson, O.P., DuBois, D.L. Using Ligand Bite Angles to Control the Hydricity of Palladium Diphosphine Complexes. *J. Am. Chem. Soc.* **2004**, *126*, 5502-5514.
29. Campbell, A.N., White, P. B., Guzei, Ilia, A. G., Stahl, S.S. Allylic C–H Acetoxylation with 4,5-diazafluorenone-Ligated Palladium Catalyst: A Ligand-Based Strategy to Achieve Aerobic Catalytic Turnover. *J. Am. Chem. Soc.* **2010**, *132*, 15116-15119.
30. Campbell, A. N.; Meyer, E. B.; Stahl, S. S. Regiocontrolled Aerobic Oxidative Coupling of Indoles and Benzene Using Pd Catalysts with 4,5-Diazafluorene Ligands. *Chem. Commun.* **2011**, *47*, 10257-10259.
31. Xiao, B.; Gong, T.-J.; Liu, Z.-J.; Liu, J.-H.; Luo, D.-F.; Xu, J.; Liu, L. Synthesis of Dibenzofurans via Palladium-Catalyzed Phenol-Directed C–H Activation/C–O Cyclization. *J. Am. Chem. Soc.* **2011**, *133*, 9250-9253.
32. Gao, W.; He, Z. Q.; Qian, Y.; Zhao, J.; Huang, Y. General Palladium-Catalyzed Aerobic Dehydrogenation to Generate Double Bonds. *Chem. Sci.* **2012**, *3*, 883-886.
33. Diao, T.; Wadzinski, T. J.; Stahl, S. S. Direct Aerobic α,β -Dehydrogenation of Aldehydes and Ketones with a Pd(TFA)₂/4,5-Diazafluorenone Catalyst. *Chem. Sci.* **2012**, *3*, 887-891.
34. Piotrowicz, M.; Zakrzewski, J. Aerobic Dehydrogenative Heck Reaction of Ferrocene with a Pd(OAc)₂/4,5-Diazafluoren-9-one Catalyst. *Organometallics* **2013**, *32*, 5709-5712.

35. Buter, J.; Moezelaar, R.; Minnaard, A. J. Enantioselective Palladium Catalyzed Conjugate Additions of Ortho-Substituted Arylboronic Acids to β,β -Disubstituted Cyclic Enones: Total Synthesis of Herbertenediol, Enokipodin A and Enokipodin B. *Org. Biomol. Chem.* **2014**, *12*, 5883-5890.
36. Piotrowicz, M.; Zakrzewski, J.; Métivier, R.; Brosseau, A.; Makal, A.; Wóznia, K. Aerobic Palladium(II)-Catalyzed Dehydrogenative Heck Reaction in the Synthesis of Pyrenyl Fluorophores. A Photophysical Study of β -Pyrenyl Acrylates in Solution and in the Solid State. *J. Org. Chem.* **2015**, *80*, 2573-2581.
37. Vasseur, A.; Laugel, C.; Harakat, D.; Muzart, J.; Le Bras, J. Ligand-Promoted Reactivity of Alkenes in Dehydrogenative Heck Reactions of Furans and Thiophenes. *Eur. J. Org. Chem.* **2015**, *5*, 944-948.
38. Kim, H. T.; Ha, H.; Kang, G.; Kim, O. S.; Ryu, H.; Biswas, A. K.; Lim, S. M.; Baik, M.-H.; Joo, J. M. Ligand-Controlled Regiodivergent C–H Alkenylation of Pyrazoles and its Application to the Synthesis of Indazoles. *Angew. Chem. Int. Ed.* **2017**, *56*, 16262-16266.
39. Kim, T. H.; Lee, W.; Kim, E.; Joo, J. M. C–H Alkenylation of Pyrroles by Electronically Matching Ligand Control. *Chem. Asian. J.* **2018**, *13*, 2418-2422.
40. Zheng, Y.; Xiao, L.; Xie, Q.; Shao, L. Palladium-Catalyzed Synthesis of β,β -Diaryl α,β -Unsaturated Ketones. *Synthesis* **2019**, *51*, 1455-1465.
41. White, P. B.; Jaworski, J. N.; Fry, C. G.; Dolinar, B. S.; Guzei, I. A.; Stahl, S. S. Structurally Diverse Diazafluorene-Ligated Palladium(II) Complexes and Their Implications for Aerobic Oxidation Reactions. *J. Am. Chem. Soc.* **2016**, *138*, 4869-4880.

42. Jaworski, J. N.; Kozack, C. V.; Tereniak, S. J.; Knapp, S. M.; Landis, C. R.; Miller, J. T.; Stahl, S. S. Operando Spectroscopic and Kinetic Characterization of Aerobic Allylic C–H Acetoxylation Catalyzed by Pd(OAc)₂/4,5-Diazafluoren-9-one. *J. Am. Chem. Soc.* **2019**, *141*, 10462-10474.
43. ten Brink, G. J.; Arends, I. W. C. E.; Hoogenraad, M.; Verspui, G.; Sheldon, R. A. Catalytic Conversions in Water. Part 23: Steric Effects and Increased Substrate Scope in the Palladium-Neocuproine Catalyzed Aerobic Oxidation of Alcohols in Aqueous Solvents. *Adv. Synth. Catal.* **2003**, *345*, 1341-1352.
44. Conley, N. R.; Labios, L. A.; Pearson, D. M.; McCrory, C. C. L.; Waymouth, R. M. Aerobic Alcohol Oxidation with Cationic Palladium Complexes: Insights into Catalyst Design and Decomposition. *Organometallics* **2007**, *26*, 5447-5453.
45. Painter, R. M.; Pearson, D. M.; Waymouth, R. M. Selective Catalytic Oxidation of Glycerol to Dihydroxyacetone. *Angew. Chem. Int. Ed.* **2010**, *49*, 9456-9459.
46. Chung, K.; Banik, S. M.; De Crisci, A. G.; Pearson, D. M.; Blake, T. R.; Olsson, J. V.; Ingram, A. J.; Zare, R. N.; Waymouth, R. M. Chemoselective Pd-Catalyzed Oxidation of Polyols: Synthetic Scope and Mechanistic Studies. *J. Am. Chem. Soc.* **2013**, *135*, 7593-7602.
47. Kozack, C. V.; Sowin, J. A.; Jaworski, J. N.; Iosub, A. V.; Stahl, S. S. Aerobic Acyloxylation of Allylic C–H Bonds Initiated by a Pd(0) Precatalyst with 4,5-Diazafluoren-9-one as an Ancillary Ligand. *ChemSusChem* **2019**, *12*, 3003-3007.
48. Rispoli, P. L.; Coe, J. S. Kinetics of the Oxidation of Benzene-1,4-Diol by Palladium(II) Compounds in Aqueous Solution. *Dalton. Trans.* **1976**, 2215-2218.

49. Toshikazu, H.; Toshihide, M.; Mitsuru, O.; Yoshiki, O. Redox System of Palladium-Trimethyl Ester of Coenzyme PQQ. *Chem. Lett.* **1989**, *18*, 785-786.
50. Toshikazu, H.; Toshihide, M.; Mitsuru, O.; Yoshiki, O. Trimethyl Ester of Coenzyme PQQ in Redox Reactions with Transition Metals. An Efficient System for the Palladium-Catalyzed Ring-Opening Reaction of α,β -Epoxy silane *Chem. Lett.* **1991**, *20*, 299-302.
51. Zheng, B.; Schmidt, M. A.; Eastgate, M. D. Synergistic Catalysis: Pd(II) Catalyzed Oxidation of 1,4-Dihydroquinones in the Pd(II) Catalyzed 1,4-Oxidation of Cyclic 1,3-Dienes. *J. Org. Chem.* **2016**, *81*, 3112-3118.
52. Horak, K. T.; Agapie, T. Dioxygen Reduction by a Pd(0)-Hydroquinone Diphosphine Complex. *J. Am. Chem. Soc.* **2016**, *138*, 3443-3452.
53. Jaworski, J. N.; McCann, S. D.; Guzei, I. A.; Stahl, S. S. Detection of Palladium(I) in Aerobic Oxidation Catalysis. *Angew. Chem. Int. Ed.* **2017**, *56*, 3605-3610.
54. Milani, B.; Anzilutti, A.; Vicentini, L.; Sessanta o Santi, A.; Zangrando, E.; Geremia, S.; Mestroni, G. Bis-Chelated Palladium(II) Complexes with Nitrogen-Donor Chelating Ligands are Efficient Catalyst Precursors for the CO/Styrene Copolymerization Reaction. *Organometallics.* **1997**, *16*, 5064-5075.
55. Klein, R. A.; Witte, P.; van Belzen, R.; Fraanje, J.; Goubitz, K.; Numan, M.; Schenk, H.; Ernisting, J. M.; Elsevier, C. J. Monodentate and Bridging Coordination of 3,3'-Annelated 2,2'-Bipyridines in Zerovalent Palladium- and Platinum-*p*-Quinone Complexes. *Eur. J. Inorg. Chem.* **1998**, 319-330.
56. Canovese, L.; Visentin, F.; Chessa, G.; Uguagliati, P.; Dolmella, A. Synthesis, Characterization and X-Ray Structural Determination of Palladium(0)-Olefin Complexes

- Containing Pyridine-Thioethers Ancillary Ligands. Equilibria and Rates of Olefin and Ligand Exchange. *J. Organomet. Chem.* **2000**, *601*, 1-15.
57. Canovese, L.; Visentin, F. Synthesis, Stability and Reactivity of Palladium(0)-Olefin Complexes Bearing Labile or Hemi-Labile Ancillary Ligands and Electron-poor Olefins. *Inorg. Chim. Acta.* **2010**, *363*, 2375-2386.
58. Canovese, L.; Visentin, F.; Santo, C.; Bertolasi, V. Low Valent Palladium Benzoquinone Complexes Bearing Different Spectator Ligands. The Versatile Coordinative Capability of Benzoquinone. *J. Organomet. Chem.* **2014**, *749*, 379-386.
59. Huynh, M. T.; Anson, C. W.; Cavell, A. C.; Stahl, S. S.; Hammes-Schiffer, S. Quinone 1 e⁻ and 2 e⁻/2 H⁺ Reduction Potentials: Identification and Analysis of Deviations from Systematic Scaling Relationships. *J. Am. Chem. Soc.* **2016**, *138*, 15903-15910.
60. A systematic presentation of this methodology was recently reported: Wise, C. F.; Agarwal, R. G.; Mayer, J. M. Determining Proton-Coupled Standard Potentials and X-H Bond Dissociation Free Energies in Nonaqueous Solvents Using Open-Circuit Potential Measurements *J. Am Chem Soc.* **2020**, *142*, 10681-10691.
61. Van Asselt, R.; Elsevier, C. J.; Zerovalent Palladium and Platinum Complexes Containing Rigid Bidentate Nitrogen Ligands and Alkenes: Synthesis, Characterization, Alkene Rotation and Substitution Reactions/X-ray Crystal Structure of [Bis((2,6-diisopropylphenyl)imino)-acenaphthene](maleic anhydride)palladium(0). *Inorg. Chem.* **1994**, *33*, 1521-1531.
62. Frisch, M. J.; Trucks, G. W.; Schlegel, H. B.; Scuseria, G. E.; Robb, M. A.; Cheeseman, J. R.; Scalmani, G.; Barone, V.; Mennucci, B.; Petersson, G. A.; Nakatsuji, H.; Caricato, M.; Li, X.; Hratchian, H. P.; Izmaylov, A. F.; Bloino, J.; Zheng, G.; Sonnenberg, J. L.; Hada, M.; Ehara,

- M.; Toyota, K.; Fukuda, R.; Hasegawa, J.; Ishida, M.; Nakajima, T.; Honda, Y.; Kitao, O.; Nakai, H.; Vreven, T.; Montgomery, J. A., Jr.; Peralta, J. E.; Ogliaro, F.; Bearpark, M.; Heyd, J. J.; Brothers, E.; Kudin, K. N.; Staroverov, V. N.; Kobayashi, R.; Normand, J.; Raghavachari, K.; Rendell, A.; Burant, J. C.; Iyengar, S. S.; Tomasi, J.; Cossi, M.; Rega, N.; Millam, M. J.; Klene, M.; Knox, J. E.; Cross, J. B.; Bakken, V.; Adamo, C.; Jaramillo, J.; Gomperts, R.; Stratmann, R. E.; Yazyev, O.; Austin, A. J.; Cammi, R.; Pomelli, C.; Ochterski, J. W.; Martin, R. L.; Morokuma, K.; Zakrzewski, V. G.; Voth, G. A.; Salvador, P.; Dannenberg, J. J.; Dapprich, S.; Daniels, A. D.; Farkas, Ö.; Foresman, J. B.; Ortiz, J. V.; Cioslowski, J.; Fox, D. J., *Gaussian 09, Revision D.01*, Gaussian, Inc., Wallingford CT, **2009**.
63. Hay, P. J.; Wadt, W. R. Ab Initio Effective Core potentials for Molecular Calculations. Potentials for the Transition Metal Atoms Sc to Hg. *J. Chem. Phys.* **1985**, *82*, 270-283.
64. Wadt, W. R.; Hay, P. J. Ab Initio Effective Core Potentials for Molecular Calculations. Potentials for Main Group Elements Na to Bi. *J. Chem. Phys.* **1985**, *82*, 284-298.
65. Becke, A. D. Density-functional Exchange-energy Approximation with Correct Asymptotic Behavior. *Phys. Rev. A* **1988**, *38*, 3098-3100.
66. Lee, C.; Yang, W.; Parr, R. G. Development of the Colle-Salvetti Correlation-energy Formula into a Functional of the Electron Density. *Phys. Rev. B* **1988**, *37*, 785-789.
67. Becke, A. D. A New Mixing of Hartree-Fock and Local Density Functional Theories. *J. Chem. Phys.* **1993**, *98*, 1372-1377.
68. Grimme, S.; Antony, J.; Ehrlich, S.; Krieg, H. A Consistent and Accurate Ab Initio Parametrization of Density Functional Dispersion Correction (DFT-D) for the 94 Elements H-Pu. *J. Chem. Phys.* **2010**, *132*, 154104.

69. Cancès, E.; Mennucci, B.; Tomasi, J. A New Integral Equation Formalism for the Polarizable Continuum Model: Theoretical Background and Applications to Isotropic and Anisotropic Dielectrics. *J. Chem. Phys.* **1997**, *107*, 3032-3041.
70. Mennucci, B.; Tomasi, J. Continuum Solvation Models: A New Approach to the Problem of Solute's Charge Distribution and Cavity Boundaries. *J. Chem. Phys.* **1997**, *106*, 5151-5158.
71. Scalmani, G.; Frisch, M. J. Continuous Surface Charge Polarizable Continuum Models of Solvation. I. General Formalism. *J. Chem. Phys.* **2010**, *132*, 114110.
72. Andappan, M. M. S.; Nilsson, P.; Larhed, M. The First Ligand-Modulated Oxidative Heck Vinylation. Efficient Catalysis with Molecular Oxygen as Palladium(0) Oxidant. *Chem. Commun.* **2004**, 218-219.
73. Lindh, J.; Enquist, P.; Pilotti, Å.; Nilsson, P.; Larhed, M. Efficient Palladium(II) Catalysis under Air. Base-Free Oxidative Heck Reactions at Room Temperature or with Microwave Heating. *J. Org. Chem.* **2007**, *72*, 7957-7962.
74. Zheng, C.; Wang, D.; Stahl, S. Catalyst-Controlled Regioselectivity in the Synthesis of Branched Conjugated Dienes via Aerobic Oxidative Heck Reactions. *J. Am. Chem. Soc.* **2012**, *134*, 16496-16499.
75. Moulin, S.; Pellerin, O.; Toupet, L.; Paul, F. Formation of Six-membered Palladacycles from Phenanthroline Pd(II) Bisacetate Precursors and Phenylisocyanate. *C. R. Chime* **2014**, *17*, 521-525.
76. Milani, B.; Alessio, E.; Mestroni, G.; Sommazzi, A.; Garbassi, F.; Zangrando, E.; Bresciani-Pahor, N.; Randaccio, L. Synthesis and Characterization of Monochelated Carboxylatopalladium(II) Complexes with Nitrogen-donor Chelating Ligands. Crystal

- Structures of Diaceto(1,10-phenanthroline)- and Diaceto(2,9-dimethyl-1,10-phenanthroline)-Palladium(II). *J. Chem. Soc. Dalton Trans.* **1994**, 1903-1911.
77. Pattillo, C. C.; Strambeanu, I. I.; Calleja, P.; Vermeulen, N. A.; Mizuno, T.; White, M. C. Aerobic Linear Allylic C–H Amination: Overcoming Benzoquinone Inhibition. *J. Am. Chem. Soc.* **2016**, *138*, 1265-1272.
78. Salazar, C. A.; Flesch, K. N.; Zhou, P. S.; Musaev, D. G.; Stahl, S. S. Palladium-Catalyzed C–H Oxidative Arylation Accessing High Turnover with O₂. *Science* **2020**, *370*, 1454-1460.
79. Popp, B. V.; Stahl, S. S. “Oxidatively Induced” Reductive Elimination of Dioxygen from an η^2 -Peroxopalladium(II) Complex Promoted by Electron-Deficient Alkenes. *J. Am. Chem. Soc.* **2006**, *128*, 2804-2805.
80. Popp, B. V.; Thorman, J. L.; Stahl, S. S. Similarities Between the Reactions of Dioxygen and Alkenes with Palladium(0)- Relevance to the Use of Benzoquinone and Molecular Oxygen as Stoichiometric Oxidants in Palladium-Catalyzed Oxidation Reactions. *J. Mol. Cat. A: Chem.* **2006**, *251*, 2-7.
81. Khusnutdinova, J. R.; Rath, P. N.; Mirica, L. M. The Aerobic Oxidation of a Pd(II) Dimethyl Complex Leads to Selective Ethane Elimination from a Pd(III) Intermediate. *J. Am. Chem. Soc.* **2012**, *134*, 2414-2422.
82. Gerken, J. B.; Stahl, S. S. Similarities High-Potential Electrocatalytic O₂ Reduction with Nitroxyl/NO_x Mediators: Implications for Fuel Cells and Aerobic Oxidation Catalysis. *ACS Cent. Sci.* **2015**, *1*, 234-243.
83. Zultanski, S. L.; Stahl, S. S. Palladium-Catalyzed Aerobic Acetoxylation of Benzene Using NO_x-Based Redox Mediators. *J. Organomet. Chem.* **2015**, *793*, 263-268.

84. Ingram, A. J.; Walker, K.L; Zare, R. N.; Waymouth, R. M. Catalytic Role of Multinuclear Palladium–Oxygen Intermediates in Aerobic Oxidation Followed by Hydrogen Peroxide Disproportionation. *J. Am. Chem. Soc.* **2015**, *137*, 13632-13646.
85. Anson, C. W.; Stahl, S. S. Cooperative Electrocatalytic O₂ Reduction Involving Co(salophen) with *p*-Hydroquinone as an Electron–Proton Transfer Mediator. *J. Am. Chem. Soc.* **2017**, *139*, 18472-18475.
86. Maity, A.; Hyun, S.-M.; Powers, D. C. Oxidase Catalysis via Aerobically Generated Hypervalent Iodine Intermediates. *Nat. Chem.* **2018**, *10*, 200-204.

**Chapter 3: Thermodynamic-Kinetic Comparison of
Palladium(II)-Mediated Alcohol and Hydroquinone
Oxidation**

3.1 Abstract

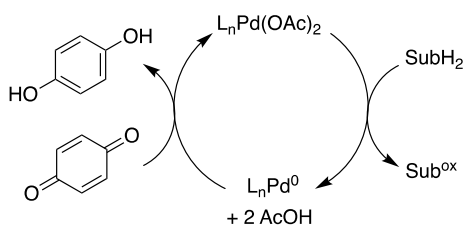
Palladium(II) catalysts promote oxidative dehydrogenation and dehydrogenative coupling of many organic molecules. Oxidations of alcohols to aldehydes or ketones are prominent examples. Hydroquinone (H₂Q) oxidation to benzoquinone (BQ) is conceptually related to alcohol oxidation, but it is significantly more challenging thermodynamically. The BQ/H₂Q redox potential is sufficiently high that BQ is often used as an oxidant in Pd-catalyzed oxidation reactions. Chapter 2 showed that certain ancillary ligands can raise the Pd^{II/0} redox potential sufficiently to reverse this reactivity, enabling (L)Pd^{II}(OAc)₂ to oxidize hydroquinone to benzoquinone. Here, we investigate the oxidation of 2-*tert*-butyl-1,4-hydroquinone (^tBuH₂Q) and 4-fluorobenzyl alcohol (^{4F}BnOH), mediated by (bc)Pd(OAc)₂ (bc = bathocuproine). Although alcohol oxidation is thermodynamically favored over H₂Q oxidation by more than 400 mV, the oxidation of ^tBuH₂Q proceeds several orders of magnitude faster than ^{4F}BnOH oxidation. Kinetic and mechanistic studies reveal that these reactions feature different rate-limiting steps. Alcohol oxidation proceeds via rate-limiting β-hydride elimination from a Pd^{II}-alkoxide intermediate, while H₂Q oxidation features rate-limiting isomerization from an O-to-C-bound Pd^{II}-hydroquinonate species. The enhanced rate of H₂Q oxidation reflects the kinetic facility of O–H relative to C–H bond cleavage.

3.2 Introduction

Palladium(II)-catalyzed oxidation reactions are a versatile class of reactions in organic chemistry that enable diverse transformations, including alcohol oxidation, oxidative coupling of alkenes with heteroatom nucleophiles, oxidative C–C coupling reactions, among others.^{1–15} These reactions typically feature two redox half-reactions, consisting of Pd^{II}-mediated substrate oxidation and reoxidation of Pd⁰ to Pd^{II} by various oxidants,¹⁶ including O₂¹⁷ and benzoquinone

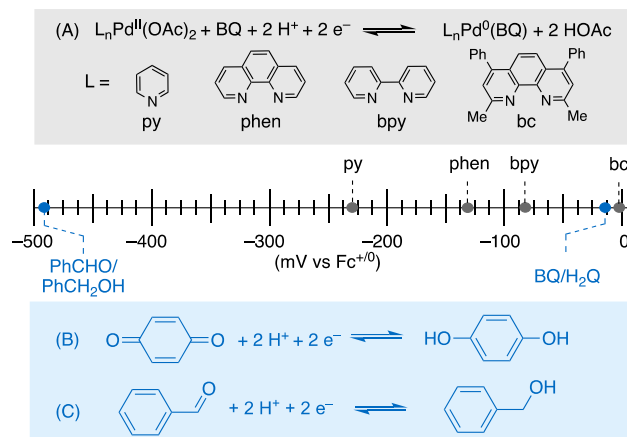
(BQ) (Scheme 3.1).^{18,19} Ancillary ligands, such as amines and mono- and bidentate pyridine derivatives, are increasingly common in Pd-catalyzed oxidation reactions. These ligands can influence both redox half-reactions, for example, by stabilizing the Pd catalyst, enhancing the rate of catalyst reoxidation, or modulating the chemo-, regio-, or stereoselectivity of substrate oxidation.¹⁵

Scheme 3.1. Redox Half Reactions in Pd-catalyzed Oxidations with Benzoquinone as the Oxidant.



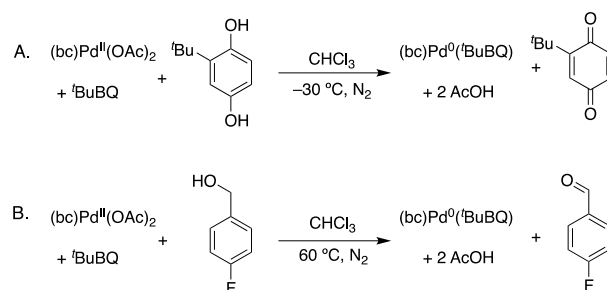
Chapter 2 reported an experimental and computational study of the influence of ancillary ligands on the Pd^{II/0} redox potential.²⁰ This study was made possible by the unexpected finding that certain ligands, such as bathocuproine (bc), increase the Pd^{II/0} potential sufficiently to allow oxidation of hydroquinone (H₂Q) by (L)Pd^{II}(OAc)₂, inverting the typical redox reactivity between Pd^{II/0} and BQ/H₂Q.^{21–23} Analysis of equilibria between (L)Pd^{II}(OAc)₂/H₂Q and (L)Pd⁰(BQ)/2 AcOH provided the basis for determination of formal redox potentials for various (L)Pd^{II}(OAc)₂ complexes (Scheme 3.2A) relative to potentials associated with the BQ/H₂Q and PhCHO/PhCH₂OH redox reactions (Scheme 3.2B and C).^{20,24,25}

Scheme 3.2. Comparison of Redox Potentials for Pd^{II/0}, BQ/H₂Q, and PhCHO/PhCH₂OH.



Observation of (bc)Pd(OAc)₂-mediated oxidation of hydroquinone provides a unique opportunity to compare thermodynamic-kinetic relationships between oxidative dehydrogenation of H₂Q and alcohols. The redox potential for BQ/H₂Q is ~400-500 mV higher than that of PhCHO/PhCH₂OH (Scheme 3.2),²⁵ but qualitative observations revealed that H₂Q oxidation is much more rapid than PhCH₂OH oxidation. This contra-thermodynamic kinetic behavior prompted us to pursue a quantitative comparison of the relative rates and probe the mechanisms of these two conceptually similar dehydrogenation reactions. Here, we report an investigation of stoichiometric oxidation of *tert*-butylhydroquinone (*t*BuH₂Q) to *tert*-butylbenzoquinone (*t*BuBQ) and 4-fluorobenzyl alcohol (^{4F}BnOH) to 4-fluorobenzaldehyde, mediated by (bc)Pd(OAc)₂ (Scheme 3.3). Both reactions are conducted in the presence of *tert*-butylbenzoquinone (*t*BuBQ) to ensure that they have identical Pd^{II/0} reagents/products, [(bc)Pd(OAc)₂]/[(bc)Pd⁰(BQ)]. This study of stoichiometric alcohol oxidation by Pd^{II} complements multiple mechanistic studies of *catalytic* alcohol oxidation with Pd^{II} catalysts,^{6,26–33} while mechanistic studies of Pd^{II}-mediated oxidation of hydroquinone in the absence of a secondary oxidant are unprecedented.²²

Scheme 3.3. (bc)Pd(OAc)₂-Mediated Oxidation of *t*BuH₂Q and ^{4F}BnOH.



3.3 Results and Discussion

Kinetic investigation of $(bc)Pd(OAc)_2$ -mediated hydroquinone oxidation. We initiated our investigation with a kinetic analysis of $(bc)Pd(OAc)_2$ -mediated oxidation of tBuH_2Q at $-30\text{ }^\circ\text{C}$ in chloroform by UV-visible spectroscopy (monitoring appearance of an absorption band at 420 nm; see Figure B.6 in Appendix B). This hydroquinone derivative was used instead of the parent H_2Q because of its higher solubility in chloroform. The reaction forms the known complex, $(bc)Pd^0({}^tBuBQ)$.²⁰ The concentration of $(bc)Pd(OAc)_2$ was varied from 0.25-1.25 mM, with $[{}^tBuH_2Q]$ fixed at 4 mM and $[{}^tBuBQ]$ at 1 mM. Then, $[{}^tBuH_2Q]$ was varied from 1-10 mM, with $[(bc)Pd(OAc)_2]$ and $[{}^tBuBQ]$ fixed at 1 mM each. Comparison of the initial rates under each of these conditions revealed a first-order dependence on $[(bc)Pd(OAc)_2]$ and $[{}^tBuH_2Q]$ (Figure 3.1a and b). The reaction was unaffected by changes to $[{}^tBuBQ]$ over a range of 1-8 mM concentration (See Appendix B, Figure B.8). No deuterium kinetic isotope effect was evident from independent rate measurements with tBuH_2Q and tBuD_2Q ($k_H/k_D = 1.0 \pm 0.2$, Figure 3.1c; care was taken to avoid O–D exchange with sources of "H" in the glassware; see B.7 in Appendix B: for details).

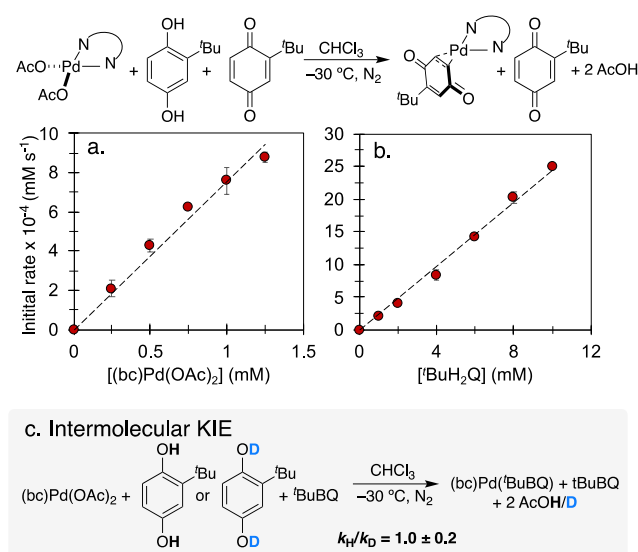


Figure 3.1. Kinetic analysis of (bc)Pd(OAc)₂-mediated oxidation of *t*BuH₂Q, including (a) [(bc)Pd(OAc)₂] dependence, (b) [*t*BuH₂Q] dependence, and (c) kinetic isotope effect obtained via independent rate measurement. See sections B.6 and B.7 in Appendix B: for experimental details.

Kinetic investigation of (bc)Pd(OAc)₂-mediated alcohol oxidation. Similar kinetic analysis was conducted for (bc)Pd(OAc)₂-mediated oxidation of ⁴Fb_nOH. Use of this substrate facilitated analysis of the reaction by ¹⁹F NMR spectroscopy, although most kinetic data were acquired by UPLC analysis of reaction aliquots. The concentration of (bc)Pd(OAc)₂ was varied from 2-12 mM, [⁴Fb_nOH] and [*t*BuBQ] fixed at 40 mM and 10 mM. Then, [⁴Fb_nOH] was varied from 10-160 mM, while fixing [(bc)Pd(OAc)₂] and [*t*BuBQ] at 10 mM each. Comparison of the initial rates under each of these conditions revealed a first-order dependence on [(bc)Pd(OAc)₂] and [⁴Fb_nOH] (Figure 3.2a and b). The reaction was unaffected by changes to [*t*BuBQ] (see Appendix B: Figure B.3). A deuterium kinetic isotope effect of $k_H/k_D = 2.0 \pm 0.3$ was observed from the comparison of independent rates measured with ⁴Fb_nOH and ⁴FbPhCD₂OH as the substrate. An intramolecular kinetic isotope of $k_H/k_D = 2.8 \pm 0.3$ was obtained from oxidation of ⁴FbPhC(H)(D)OH (Figure 3.2c and d). These KIEs are similar to those observed for Pd-catalyzed alcohol oxidation with bc-ligated Pd catalysts.²⁶

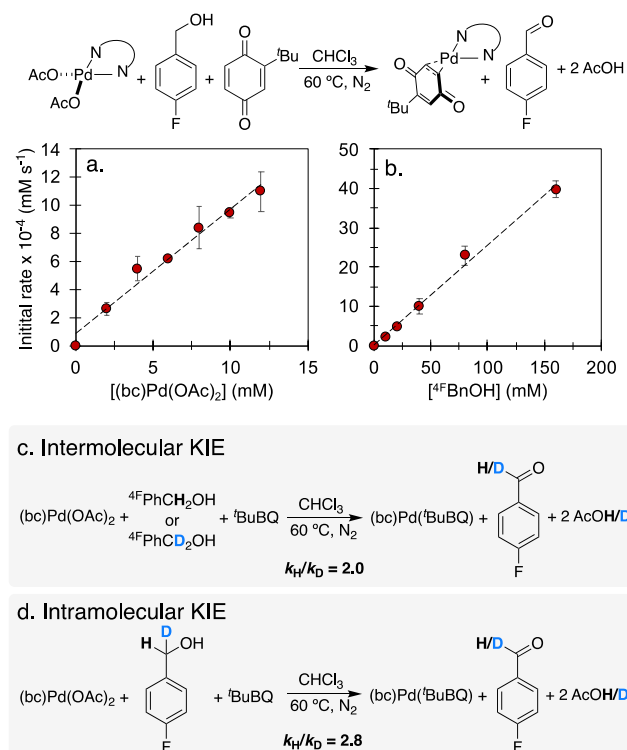


Figure 3.2. Kinetic analysis of (bc)Pd(OAc)₂-mediated oxidation of ⁴F-BnOH, including (a) [(bc)Pd(OAc)₂] dependence (b) [⁴F-BnOH] dependence, and kinetic isotopic effects determined by (c) independent rate measurements of ⁴F-BnOH and ⁴F-PhCD₂OH and (d) an intramolecular competition experiment with ⁴F-PhC(H)(D)OH. See sections B.2 and B.3 in Appendix B: for experimental details.

Carboxylate electronic and steric effects and temperature analysis of hydroquinone and alcohol oxidation rates. A series of bc-supported Pd carboxylate complexes, (bc)Pd(O₂CR)₂, were used to probe steric and electronic effects for oxidation of ^tBuH₂Q and ⁴F-BnOH. The carboxylate ligands included 4-trifluoromethylbenzoate, benzoate, 4-*tert*-butylbenzoate, acetate, and pivalate. Electronic parameters correspond to the pK_a values of the conjugate acids of the carboxylates, which range from 10.1 to 12.6 (DMSO values).^{34–37} Relative steric effects were assessed by using a proxy value corresponding to the percent buried volume reported for PR₃ groups (R = ⁴CF₃Ph, Ph, ⁴*t*BuPh, Me, ^tBu) at 2 Å in (R₃P)AuCl complexes.^{38,39}

Initial rates of ^tBuH₂Q oxidation were obtained with the different (bc)Pd(O₂CR)₂ complexes. A plot of log(rate) versus carboxylate pK_a values revealed a slope of 0.06 with a poor correlation (R² = 0.04) (Figure 3.3a), indicating the rate is not strongly correlated with the basicity of the carboxylate ligand. A relatively good correlation was observed, however, between log(rate) versus the buried volume parameter for the carboxylate ligands (R² = 0.86) (Figure 3.3b), indicating that the rate of ^tBuH₂Q oxidation by (bc)Pd(O₂CR)₂ is sensitive to the steric profile of the carboxylate ligand.

An analogous set of experiments was performed for ⁴FbNOH oxidation. In this case, the Brønsted plot exhibits a much better correlation (R² = 0.99) with a positive slope (0.37) (Figure 3.3c), indicating that the reaction is promoted by more basic carboxylate ligands. On the other hand, the corresponding assessment of steric effects (Figure 3.3d) exhibits a very poor correlation (R² = 0.02), indicating that steric effects of the carboxylate ligand play little role in ⁴FbNOH oxidation.

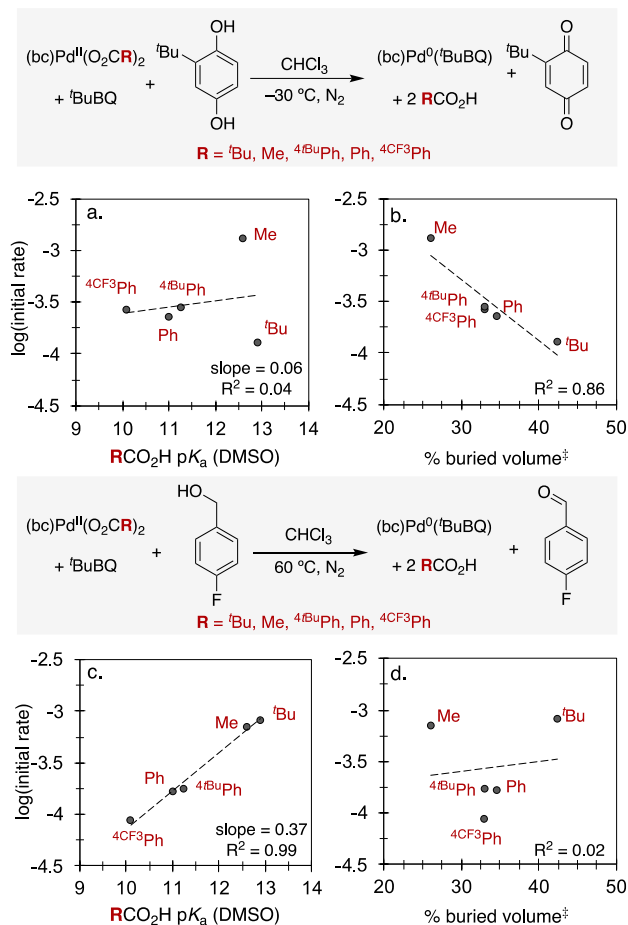


Figure 3.3. Rate dependence of ${}^4\text{FBnOH}$ oxidation by $(bc)\text{Pd}(\text{O}_2\text{CR})_2$ on (a) pK_a (DMSO) of RCO_2H and (b) on percent buried volume. Rate dependence of ${}^t\text{BuH}_2\text{Q}$ oxidation by $(bc)\text{Pd}(\text{O}_2\text{CR})_2$ on (c) pK_a (DMSO) of RCO_2H and (d) on percent buried volume. ‡ Percent buried volume values obtained from PR_3 ligands (see text for details).

The studies described thus far have employed different temperatures for investigation of ${}^t\text{BuH}_2\text{Q}$ and ${}^4\text{FBnOH}$ oxidation reactions, $-30\text{ }^\circ\text{C}$ and $60\text{ }^\circ\text{C}$, respectively. These different temperatures highlight the faster rate of ${}^t\text{BuH}_2\text{Q}$ oxidation. In order to permit quantitative comparison at a single temperature, both reactions were analyzed over a range of temperatures, from $-40 - 0\text{ }^\circ\text{C}$ for ${}^t\text{BuH}_2\text{Q}$ and $+30 - +60\text{ }^\circ\text{C}$ for ${}^4\text{FBnOH}$. The resulting data were then subjected to Eyring analysis to obtain activation free energies at 298 K: $\Delta G^\ddagger_{{}^t\text{BuH}_2\text{Q}}(298\text{ K}) = 17.1\text{ kcal/mol}$ and $\Delta G^\ddagger_{{}^4\text{FBnOH}}(298\text{ K}) = 23.1\text{ kcal/mol}$. The values, which quantify the kinetic facility of ${}^t\text{BuH}_2\text{Q}$

over $^4\text{F}\text{BnOH}$ oxidation may be compared to the overall reaction free energies of reaction with $(\text{bc})\text{Pd}(\text{OAc})_2$, which strongly favor $^4\text{F}\text{BnOH}$ over $^t\text{BuH}_2\text{Q}$ oxidation: $\Delta G^\circ_{^t\text{BuH}_2\text{Q}}(298\text{ K}) = -2.9$ kcal/mol²⁰ and $\Delta G^\circ_{^4\text{F}\text{BnOH}}(298\text{ K}) = \text{approx. } -22$ kcal/mol (the latter estimated from the difference in reported reduction potentials of $^t\text{BuBQ}$ and benzaldehyde^{24,25}). Both sets of energetic values are depicted in the energy diagram in Figure 3.4.

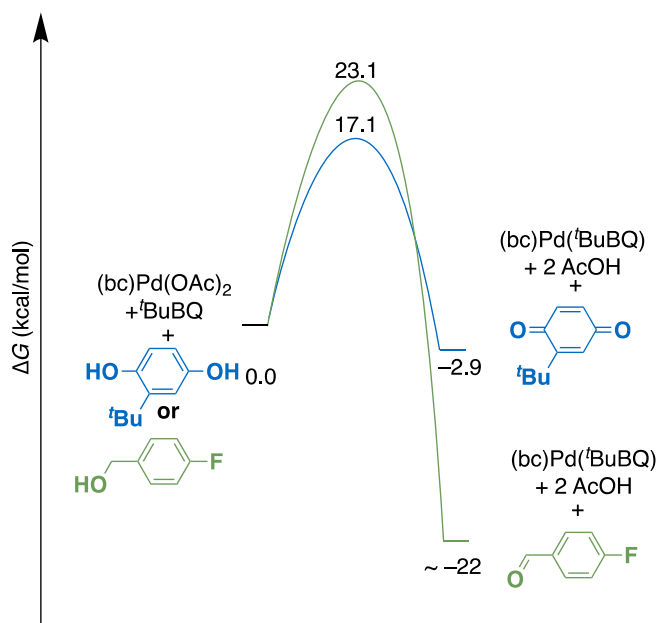
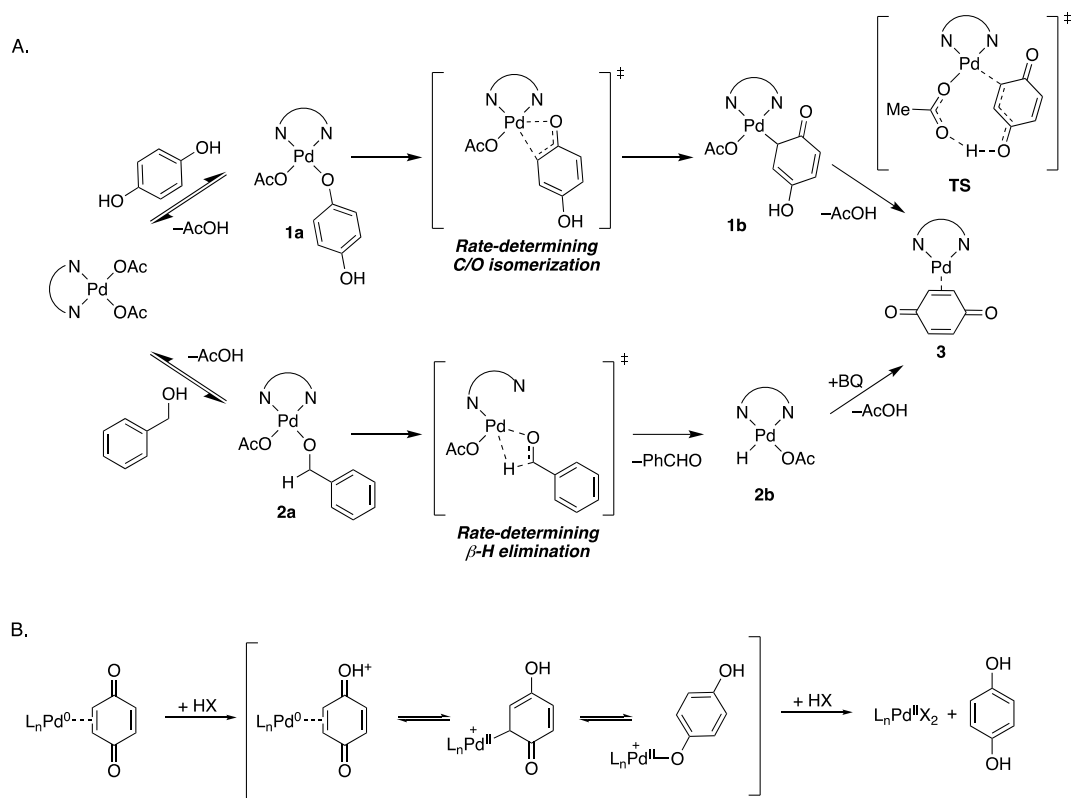


Figure 3.4. Free energy diagram for $(\text{bc})\text{Pd}(\text{OAc})_2$ -mediated oxidation of $^4\text{F}\text{BnOH}$ and $^t\text{BuH}_2\text{Q}$.

Mechanistic analysis. The kinetic data elaborated above provide a foundation for understanding the origin of the contra-thermodynamic outcome depicted in Figure 3.4. The data reveal both similarities and differences between $(\text{bc})\text{Pd}(\text{OAc})_2$ -mediated oxidation of $^t\text{BuH}_2\text{Q}$ and $^4\text{F}\text{BnOH}$. Both reactions feature a first-order dependence on $[(\text{bc})\text{Pd}(\text{OAc})_2]$ and $[\text{substrate}]$, but they exhibit different KIEs and show different electronic and steric effects. Mechanisms that rationalize these observations are depicted in Scheme 3.4A.

Scheme 3.4. Proposed Mechanisms for (A) Hydroquinone and Benzyl Alcohol Oxidation Mediated by (bc)Pd(OAc)₂ and (B) Oxidation of Pd⁰ by Benzoquinone in the Presence of Acid²¹



Oxidation of ^tBuH₂Q by (bc)Pd(OAc)₂ (Scheme 3.4A, top) is proposed to begin with formation of a Pd^{II}-(O-hydroquinonate) species **1a** via proton-coupled ligand exchange³⁰ between acetate and ^tBuH₂Q, followed by rate-limiting isomerization to the Pd^{II}-(C-hydroquinonate) species **1b**. These steps rationalize (a) the rate law, with a first order dependence on [Pd] and [^tBuH₂Q], and (b) the lack of a primary kinetic isotope effect, since H/D reactivity is incorporated in an equilibrium step expected to have negligible equilibrium isotope effect. The lack of systematic correlation between the rate and carboxylate pK_a suggests proton transfer steps are not involved in the rate-limiting step, while the carboxylate steric influence, favoring less sterically hindered carboxylates, is rationalized by rate-limiting isomerization of the hydroquinonate to the more hindered C-bound isomer **1b**. The reaction concludes with an intramolecular redox reaction involving proton transfer

from the phenolic O–H of **1b** to the carboxylate, coupled to two-electron transfer to Pd. This step forms the (bc)Pd⁰(BQ) product **3**. This mechanism corresponds to the microscopic reverse of the mechanism proposed by Bäckvall for acid-promoted oxidation of well-defined Pd⁰(BQ) complexes (Scheme 3.4B).²¹

The oxidation of ⁴Fb_nOH (Scheme 3.4A, bottom) is similarly proposed to begin with proton-coupled exchange of ⁴Fb_nOH with acetate at (bc)Pd(OAc)₂ to generate Pd-alkoxide **1b**. The kinetic isotope effect data, however, suggest that β -hydride elimination to generate Pd^{II}-hydride **2b** is rate-limiting. The electronic dependence on the carboxylate ligand suggests that formation of the Pd^{II}-alkoxide **2a** also contributes the reaction rate.⁶ Subsequent loss (formally, reductive elimination) of acetic acid from **2b** in the presence of ^tBuBQ forms the Pd-quinone product **3**. The kinetic facility of this step,⁴⁰ enhanced further by the ability of quinones to promote H–O₂CR reductive elimination from Pd^{II}(H)(O₂CR) complexes,⁴¹ rationalizes the zero-order dependence of the reaction rate on [^tBuBQ].

To summarize, ⁴Fb_nOH oxidation has a significantly higher kinetic barrier than ^tBuH₂Q oxidation, even though the net reaction of ⁴Fb_nOH is more favorable by approximately 20 kcal/mol. At least two factors support faster rates of ^tBuH₂Q oxidation. The first step in both reactions involves proton-coupled ligand substitution between the substrate and a carboxylate ligand, and H₂Q is significantly more acidic than benzyl alcohol (aqueous pK_a value of H₂Q is ~5 units lower than the pK_a of benzyl alcohol).^{42,43} Thus, the pre-equilibrium formation of a Pd^{II}-hydroquinonate intermediate will be strongly favored relative to formation of a Pd^{II}-alkoxide. The difference in relative rates, however, ultimately arises from the difference in relative energies of the rate-limiting transition states. The data indicate that the transition state for hydroquinonate isomerization is lower in energy than the transition state for Pd^{II}-alkoxide β -hydride elimination.

Net hydride transfer from the hydroquinonate intermediate, involving proton transfer to carboxylate and two-electron transfer to Pd, is sufficiently facile that it proceeds after the rate-limiting isomerization step. This step is undoubtedly facilitated by the polarity of the O–H bond of the hydroquinonate, which facilitates proton transfer, relative to cleavage of the C–H bond involved in β -hydride elimination from the alkoxide.⁴⁴

3.4 Conclusion

The mechanistic studies of (bc)Pd(OAc)₂-mediated oxidation of ⁴Fb_nOH and ¹BuH₂Q outlined above illuminate the kinetic and thermodynamic relationships between these reactions. The oxidation of ⁴Fb_nOH is approximately 20 kcal/mol more favorable than the oxidation of ¹BuH₂Q. Nonetheless, the activation energy for ⁴Fb_nOH oxidation is substantially higher than that for ¹BuH₂Q oxidation ($\Delta\Delta G^\ddagger = 6$ kcal/mol), resulting in ¹BuH₂Q oxidation proceeding several orders of magnitude faster than ⁴Fb_nOH oxidation at room temperature. Mechanistic data provide insights into the different rate-limiting steps for these reactions, which feature β -hydride elimination for ⁴Fb_nOH oxidation and isomerization from an *O*-to-*C*-bound hydroquinonate in ¹BuH₂Q oxidation. This study represents the first mechanistic analysis of hydroquinone by Pd^{II} complexes, and it was made possible by the identification of ancillary ligands that increasing the Pd^{II/0} redox potential sufficiently to support oxidation of hydroquinones.

3.5 Acknowledgements

Funding was provided by the National Science Foundation (CHE-1953926; SSS). Spectroscopic instrumentation was supported by a gift from Paul J. Bender, NSF (CHE1048642), and the NIH (1S10 OD020022-1).

3.6 References

1. Smidt, J.; Hafner, W.; Jira, R.; Sedlmeier, J.; Sieber, R.; Rüttinger, R.; Kojer, H. Catalytic Reactions of Olefins on Compounds of the Platinum Group. *Angew. Chem.* **1959**, *71*, 176-182.
2. Sheldon, R. A.; Arends, I. W. C. E.; ten Brink, G.-J.; Dijkman, A. Green, Catalytic Oxidations of Alcohols. *Acc. Chem. Res.* **2002**, *35*, 774-781.
3. Muzart, J. Palladium-Catalysed Oxidation of Primary and Secondary Alcohols. *Tetrahedron* **2003**, *59*, 5789-5816.
4. Stahl, S. S. Palladium Oxidase Catalysis: Selective Oxidation of Organic Chemicals by Direct Dioxygen-Coupled Turnover. *Angew. Chem. Int. Ed.* **2004**, *43*, 3400-3420.
5. Zeni, G.; Larock, R. C. Synthesis of Heterocycles via Palladium π -Olefin and π -Alkyne Chemistry. *Chem. Rev.* **2004**, *104*, 2285-2309.
6. Sigman, M. S.; Jensen, D. R. Ligand-Modulated Palladium-Catalyzed Aerobic Alcohol Oxidations. *Acc. Chem. Res.* **2006**, *39*, 221-229.
7. Beccalli, E. M.; Brogini, G.; Martinelli, M.; Sottocornola, S. C-C, C-O, C-N Bond Formation on sp^2 Carbon by Pd(II)-Catalyzed Reactions Involving Oxidant Agents. *Chem. Rev.* **2007**, *107*, 5318-5365.
8. Minatti, A.; Muñiz, K. Intramolecular Aminopalladation of Alkenes as a Key Step to Pyrrolidines and Related Heterocycles. *Chem. Soc. Rev.* **2007**, *36*, 1142-1152.
9. Karimi, B.; Zamani, A. Recent Advances in the Homogeneous Palladium-Catalyzed Aerobic Oxidation of Alcohols. *J. Iran. Chem. Soc.* **2008**, *5*, S1-S20.
10. Chen, X.; Engle, K. M.; Wang, D.-H.; Yu, J.-Q. Palladium(II)-Catalyzed C-H Activation/C-C Cross-Coupling Reactions: Versatility and Practicality. *Angew. Chem. Int. Ed.* **2009**, *48*, 5094-5115.

11. Yeung, C. S.; Dong, V. M. Catalytic Dehydrogenative Cross-Coupling: Forming Carbon–Carbon Bonds by Oxidizing Two Carbon–Hydrogen Bonds. *Chem. Rev.* **2011**, *111*, 1215-1292.
12. Liu, C.; Zhang, H.; Shi, W.; Lei, A. Bond Formations between Two Nucleophiles: Transition Metal Catalyzed Oxidative Cross-Coupling Reactions. *Chem. Rev.* **2011**, *111*, 1780-1824.
13. McDonald, R. I.; Liu, G.; Stahl, S. S. Palladium(II)-Catalyzed Alkene Functionalization via Nucleopalladation: Stereochemical Pathways and Enantioselective Catalytic Applications. *Chem. Rev.* **2011**, *111*, 2981-3019.
14. Liron, F.; Oble, J.; Lorion, M. M.; Poli, G. Direct Allylic Functionalization Through Pd-Catalyzed C–H Activation. *Eur. J. Org. Chem.* **2014**, 5863-5883.
15. Wang, D., Weinstein, A. B.; White, P. B.; Stahl, S. S. Ligand-Promoted Palladium-Catalyzed Aerobic Oxidation Reactions. *Chem. Rev.* **2018**, *118*, 2636-2679.
16. Heumann, A.; Jens, K.-J.; Réglie, M. Palladium Complex Catalyzed Oxidation Reactions. *Prog. Inorg. Chem.* **1994**, *42*, 483-576.
17. Stahl, S. S. Palladium-Catalyzed Oxidation of Organic Chemicals with O₂. *Science* **2005**, *309*, 1824-1826.
18. Piera, J.; Bäckvall, J.-E. Catalytic Oxidation of Organic Substrates by Molecular Oxygen and Hydrogen Peroxide by Multistep Electron Transfer—A Biomimetic Approach. *Angew. Chem. Int. Ed.* **2008**, *47*, 3506-3523.
19. Liu, J.; Guðmundsson, A.; Bäckvall, J.-E. Efficient Aerobic Oxidation of Organic Molecules by Multistep Electron Transfer. *Angew. Chem. Int. Ed.* **2021**, *60*, 15686-15704.

20. Bruns, D. L.; Musaev, D. G.; Stahl, S. S. Can Donor Ligands Make Pd(OAc)₂ a Stronger Oxidant? Access to Elusive Palladium(II) Reduction Potentials and Effects of Ancillary Ligands via Palladium(II)/Hydroquinone Redox Equilibria. *J. Am. Chem. Soc.* **2020**, *142*, 19678-19688.
21. Grennberg, H.; Gogoll, A.; Bäckvall, J.-E. Acid-Induced Transformation of Palladium(0)–Benzoquinone Complexes to Palladium(II) and Hydroquinone. *Organometallics* **1993**, *12*, 1790-1793.
22. An earlier precedent features Pd^{II}-mediated oxidation of hydroquinone in the absence of a secondary oxidant, although the thermodynamics are likely influenced by the formation of metallic Pd as the final product. See the following: Coe, J. S.; Rispoli, P. L. Kinetics of the Oxidation of Benzene-1,4-Diol by Palladium(II) Compounds in Aqueous Solution. *J. Chem. Soc., Dalton. Trans.* **1976**, 2215-2218.
23. See also: Horak, K. T.; Agapie, T. Dioxygen Reduction by a Pd(0)–Hydroquinone Diphosphine Complex. *J. Am. Chem. Soc.* **2016**, *138*, 3443-3452.
24. Huynh, M. T.; Anson, C. W.; Cavell, A. C.; Stahl, S. S.; Hammes-Schiffer, S. Quinone 1 e⁻ and 2 e⁻/2 H⁺ Reduction Potentials: Identification and Analysis of Deviations from Systematic Scaling Relationships. *J. Am. Chem. Soc.* **2016**, *138*, 15903-15910.
25. The estimated standard potential for benzyl alcohol oxidation under the present conditions is deduced from the difference between previously reported standard potentials for PhCHO/PhCH₂OH and BQ/H₂Q. Although this estimate is imperfect, any errors (e.g., due to relative differences in solvation energy) are expected to be relatively minor and will not alter the analysis here. See the following references: (a) Wang, Y.; Gonell, S.; Mathiyazhagan, U.

- R.; Liu, Y.; Wang, D.; Miller, A. J. M.; Meyer, T. J. Simultaneous Electrosynthesis of Syngas and an Aldehyde from CO₂ and an Alcohol by Molecular Electrocatalysis. *ACS Appl. Energy Mater.* **2019**, *2*, 97-101. (b) Nutting, J. E.; Gerken, J. B.; Stamoulis, A. G.; Bruns, D. L.; Stahl, S. S. "How Should I Think about Voltage? What is Overpotential?": Establishing an Organic Chemistry Intuition for Electrochemistry. *J. Org. Chem.* **2021**, *86*, 15875-15885.
26. ten Brink, G.-J.; Arends, I. W. C. E.; Sheldon, R. A. Catalytic Conversions in Water. Part 21: Mechanistic Investigations on the Palladium-Catalysed Aerobic Oxidation of Alcohols in Water. *Adv. Synth. Catal.* **2002**, *344*, 355-369.
27. Steinhoff, B. A.; Fix, S. R.; Stahl, S. S. Mechanistic Study of Alcohol Oxidation by the Pd(OAc)₂/O₂/DMSO Catalyst System and Implications for the Development of Improved Aerobic Oxidation Catalysts. *J. Am. Chem. Soc.* **2002**, *124*, 766-767.
28. Steinhoff, B. A.; Stahl, S. S. Ligand-Modulated Palladium Oxidation Catalysis: Mechanistic Insights into Aerobic Alcohol Oxidation with the Pd(OAc)₂/Pyridine Catalyst System. *Org. Lett.* **2002**, *4*, 4179-4181.
29. Mueller, J. A.; Sigman, M. S. Mechanistic Investigations of the Palladium-Catalyzed Aerobic Oxidative Kinetic Resolution of Secondary Alcohols Using (-)-Sparteine. *J. Am. Chem. Soc.* **2003**, *125*, 7005-7013
30. Steinhoff, B. A.; Guzei, I. A.; Stahl, S. S. Mechanistic Characterization of Aerobic Alcohol Oxidation Catalyzed by Pd(OAc)₂/Pyridine Including Identification of the Catalyst Resting State and the Origin of Non-Linear [Catalyst] Dependence. *J. Am. Chem. Soc.* **2004**, *126*, 11268-11278.

31. Mueller, J. A.; Cowell, A.; Chandler, B. D.; Sigman, M. S. Origin of Enantioselection in Chiral Alcohol Oxidation Catalyzed by Pd[(-)-sparteine]Cl₂. *J. Am. Chem. Soc.* **2005**, *127*, 14817-14824.
32. Arends, I. W. C. E.; ten Brink, G.-J.; Sheldon, R. A. Palladium-Neocuproine Catalyzed Aerobic Oxidation of Alcohols in Aqueous Solvents *J. Mol. Catal. A: Chem.* **2006**, *251*, 246-254.
33. Steinhoff, B. A.; Stahl, S. S. Mechanism of Pd(OAc)₂/DMSO-Catalyzed Aerobic Alcohol Oxidation: Mass-Transfer-Limitation Effects and Catalyst Decomposition Pathways. *J. Am. Chem. Soc.* **2006**, *128*, 4348-4355.
34. For pK_a of acetic acid and benzoic acid in DMSO: Bordwell, F. G. Equilibrium Acidities in Dimethyl Sulfoxide Solution. *Acc. Chem. Res.* **1988**, *21*, 456-463.
35. For pK_a of pivalic acid in DMSO: Bartnicka, H.; Bojanowska, I.; Kalinowski, M. K. Solvent Effect on the Dissociation Constants of Aliphatic Carboxylic Acids. *Aust. J. Chem.* **1991**, *44*, 1077-1084.
36. For pK_a of 4-*tert*-butylbenzoic acid in DMSO: Kulhánek, J.; Decouzon, M.; Gal, J.-F.; Maria, P.-C.; Fiedler, P.; Jiménez, P.; Roux, M.-V.; Exner, O. Steric Effects and Steric Hindrance to Resonance in *tert*-Butylbenzoic Acids in the Gas Phase and in Solution. *Eur. J. Org. Chem.* **1999**, 1589-1594.
37. The pK_a of 4-trifluoromethylbenzoic acid is not available in DMSO and was estimated by interpolating a linear fit of the pK_a values of *para*-substituted phenols and carboxylic acids with known pK_a values in DMSO. See Appendix B., Section B.10 for details. See also, ref. 34 and the following: (a) Bordwell, F. G.; Cheng, J.-P. Substituent Effects on the Stabilities of

- Phenoxyl Radicals and the Acidities of Phenoxyl Radical Cations. *J. Am. Chem. Soc.* **1991**, *113*, 1736-1743. (b) Maran, F.; Celadon, D.; Severin, M. G.; Vianello, E. Electrochemical Determination of the pK_a of Weak Acids in *N,N*-Dimethylformamide. *J. Am. Chem. Soc.* **1991**, *113*, 9320-9329.
38. Clavier, H; Nolan, S. P. Percent Buried Volume for Phosphine and *N*-Heterocyclic Carbene Ligands: Steric Properties in Organometallic Chemistry. *Chem. Commun.* **2010**, *46*, 841-861.
39. Note that buried volumes for 4-*tert*-butylbenzoic acid and 4-trifluoromethylbenzoic acid are not available and are assumed to be the same as that of 4-methylbenzoic acid.
40. Konnick, M. M.; Stahl, S. S. Reaction of Molecular Oxygen with a Pd^{II}-Hydride to Produce a Pd^{II}-Hydroperoxide: Experimental Evidence for an HX-Reductive-Elimination Pathway. *J. Am. Chem. Soc.* **2008**, *130*, 5753–5762.
41. Decharin, N.; Stahl, S. S. Benzoquinone-Promoted Reaction of O₂ with a Pd^{II}-Hydride. *J. Am. Chem. Soc.* **2011**, *133*, 5732-5735.
42. Bishop, C. A.; Tong, L. K. J. Equilibria of Substituted Semiquinones at High pH. *J. Am. Chem. Soc.* **1965**, *87*, 501-505.
43. Takahashi, S.; Cohen, L. A.; Miller, H. K.; Peake, E. G. Calculation of the pK_a Values of Alcohols from σ^* Constants and from the Carbonyl Frequencies of Their Esters. *J. Org. Chem.* **1971**, *36*, 1205-1209.
44. Kramarz, K. W.; Norton, J. R. Slow Proton-Transfer Reactions in Organometallic and Bioinorganic Chemistry. *Prog. Inorg. Chem.* **1994**, *42*, 1-65.

**Chapter 4: Pd-Catalyzed Aerobic Oxidative Coupling of
Thiophenes: Synergistic Benefits of Phenanthroline Dione
and a Cu Cocatalyst**

This work is published:

Tereniak, S. J.; Bruns, D. L.; Stahl, S. S. *J. Am. Chem. Soc.* **2020**, *142*, 20318-20323.

This work was done with Dr. Steve Tereniak. We contributed equally to this project.

4.1 Abstract

Substituted bithiophenes are prominent fragments in functional organic materials, and they are ideally prepared via direct oxidative C–H/C–H coupling. Here, we report a novel Pd^{II} catalyst system, employing 1,10-phenanthroline-5,6-dione (phd) as the ancillary ligand, that enables aerobic oxidative homocoupling of 2-bromothiophenes and other related heterocycles. These observations represent the first use of phd to support Pd-catalyzed aerobic oxidation. The reaction also benefits from a Cu(OAc)₂ co-catalyst, and mechanistic studies show that Cu promotes C–C coupling, implicating a role for Cu^{II} different from its conventional contribution to reoxidation of the Pd catalyst.

4.2 Introduction

Palladium-catalyzed oxidative C–H/C–H coupling of (hetero)arenes¹ provides efficient access to biaryl monomers used in high-performance polymers. Ancillary ligands often improve the Pd catalyst performance when O₂ is used as the oxidant.^{2,3} An important commercial application of this concept is featured in the homocoupling of dimethyl phthalate, generating a biphenyl tetracarboxylate precursor to the polyimide resin, Upilex.^{4,5} The patented catalyst system of Ube Industries consists of Pd(OAc)₂ and phenanthroline (phen), and uses Cu(OAc)₂ as a cocatalyst.⁶ This reaction has attracted considerable recent attention, with efforts focused on use of alternative arene feedstocks, such as *o*-xylene, identification of new catalyst systems and ancillary ligands, and mechanistic studies.^{7–14} 2,2'-Bithiophenes represent another important target for oxidative coupling reactions. These motifs are prevalent in organic materials, with applications ranging from organic solar cells^{15,16} to organic light-emitting diodes¹⁷ and organic field effect transistors (Figure 4.1A).¹⁸ Pd-catalyzed oxidative homocoupling of thiophenes has precedent;^{19–}²⁶ however, the most effective substrates, including those compatible with aerobic conditions,

consist of electron-rich derivatives that are less useful in organic materials applications. Substrates that feature bromide or other electron-withdrawing substituents are unreactive or perform poorly under existing oxidative homocoupling conditions. A rare exception, reported by Mori and coworkers, enables oxidative homocoupling of 2-bromothiophenes and other derivatives (Figure 4.1B);^{19,20} however, it requires Ag^I as the stoichiometric oxidant.

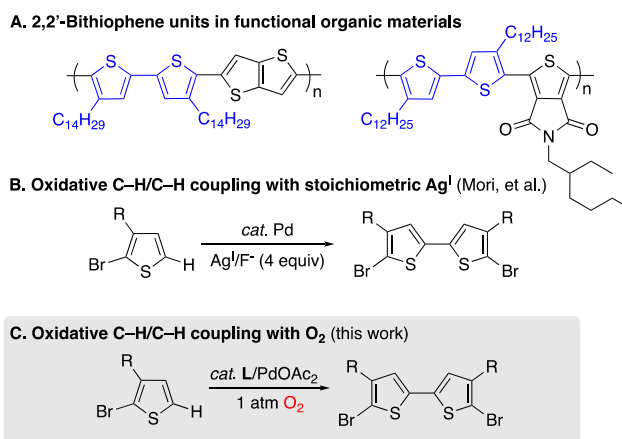


Figure 4.1. (A) Commercial organic polymers for materials science applications containing a 2,2'-bithiophene unit. (B) Precedent for Pd-catalyzed oxidative homocoupling of 2-bromo-3-alkylthiophenes with stoichiometric Ag^I oxidants, and (C) aerobic oxidation method targeted in the present study

The present study was motivated by the prospect of identifying a ligand-supported Pd catalyst system that enables use of O₂ as the oxidant, while retaining good reactivity with 2-bromothiophenes and related electron-deficient heterocycles (Figure 4.1C). The resulting catalyst system showcases the utility of 1,10-phenanthroline-5,6-dione (phd) as ligand that has not been used previously in Pd-catalyzed aerobic oxidations. The discovery of this catalyst system, the substrate scope, and mechanistic insights are reported herein.

4.3 Results and Discussion

Our initial efforts focused on evaluating Pd catalyst compositions and reaction conditions for oxidative homocoupling of 2-bromo-3-hexylthiophene (**1a**) with O₂ to afford 5,5'-dibromo-4,4'-dihexyl-2,2'-bithiophene **2a**. Substrate **1a** was selected because alkyl groups are commonly featured as solubilizing groups in thiophene-containing organic electronic materials, and bromide substituents are often desired for subsequent coupling steps to access oligomeric or polymeric products.²⁷ Several previously reported conditions for aerobic C–H/C–H biaryl coupling were screened,^{7,22,28} but these proved ineffective (see section C.3 of Appendix C for full screening data). For example, **2a** was obtained in only 4% yield when using the previously reported Pd-catalyzed aerobic conditions effective for the homocoupling of electron-rich thiophenes. On the other hand, promising reactivity was observed by combining features of the commercial oxidative homocoupling of dimethyl phthalate,²⁹ including use of an ancillary nitrogen ligand and Cu(OAc)₂ cocatalyst, and the use of DMSO as the solvent (Figure 4.2). In a survey of different ancillary ligands, electron-rich pyridine derivatives led to higher yields of **2a** over electron-deficient pyridines (**L3** vs **L1**, Figure 4.2). Bidentate nitrogen-donor ligands, including 2,2'-bipyridine, 1,10-phenanthroline, and 4,5-diazafluoren-9-one (**L8**), afforded similar, moderate yields (26-57%). In contrast, 1,10-phenanthroline-5,6-dione (phd) led to a good yield of **2a** (80%). Phd has been used previously as a catalyst itself for the aerobic oxidation of amines,³⁰⁻³² but this is the first successful use of phd in Pd-catalyzed aerobic oxidation reactions.³³ Pd salts with anionic ligands less basic than acetate (trifluoroacetate, nitrate) were less effective, while those with similar or higher basicity (benzoate, propionate, pivalate) performed very similarly to Pd(OAc)₂.

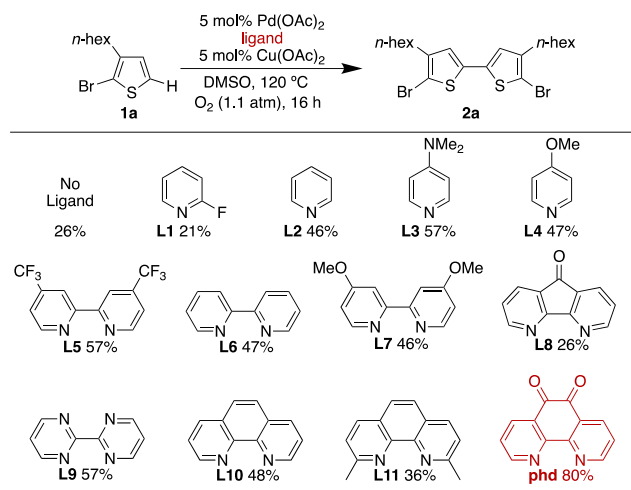


Figure 4.2. Ligand Effects in Pd/Cu-Cocatalyzed Aerobic C–H Homocoupling of 2-Bromo-3-Hexylthiophene. Conditions: 0.17 mmol 2-bromo-3-hexylthiophene, 5 mol% ligand (for L5-L11 and phd) or 10 mol% ligand (L1-L4), 0.25 mL in DMSO. Yields determined by HPLC.

When the loadings of Pd(OAc)₂, phd, and Cu(OAc)₂ were lowered to 3 mol%, the yield of **2a** could be improved to 85% by including 3 mol% 1,4-benzoquinone (BQ). Systematic assessment of the different catalyst components (Figure 4.3) highlighted the importance of each of the catalyst components to access **2a** in good yield. High conversion of thiophene starting material was observed with Pd(OAc)₂/Cu(OAc)₂ but little product was obtained, suggesting phd promotes selective formation of product **2a**. The ternary catalyst system, composed of Pd(OAc)₂/Cu(OAc)₂/phd, led to a substantially improved yield (64%). As the inclusion of 3 mol% BQ does not affect the initial rate of the reaction (see Figure C.2 in section C.6 of Appendix C), the enhanced yield of **2a** is attributed to improved catalyst stability.

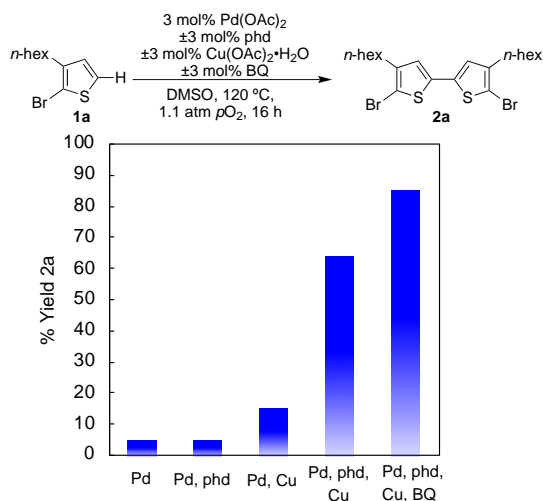


Figure 4.3. Assessment of Catalytic Components on Thiophene C–H Homocoupling. Conditions: **1a** (1.1 mmol), catalyst (3 mol%), 1.0 mL in DMSO, 1.1 atm pO_2 , 120 °C, 16 hr.

The optimized catalyst system, consisting of 3 mol% $Pd(OAc)_2$ /phd, $Cu(OAc)_2$, and BQ was then tested in the oxidative homocoupling of a series of thiophenes and related heterocycles (Figure 4.4). Several 2-halo-3-alkylthiophenes **1a-1c** react smoothly to afford 2,2'-bithiophenes that are useful as intermediates or precursors to intermediates in materials synthesis.^{34,35} A terthiophene **3c** was isolated as a by-product from the coupling reaction of **1c** (see C.11 in Appendix C). A 74% yield of **2d** was observed when using cyclohexyl acetate as a cosolvent to enhance the solubility of **1d**. 2-Chloro- and 2-bromothiophenes **1e** and **1f** benefited from a lowered reaction temperature (100 °C). Dihalogenated substrates gave moderate-to-good yields (**2g-2i**). The 3,3'-difluorobithiophene **2i** is a noteworthy product because fluorination in this position has been shown to enhance solar cell power conversion efficiency.^{36,37} Benzo[*b*]thiophenes^{38–40} also underwent oxidative coupling to afford **2j** and **2k**.

The 3,3'-diester derivative **2l** is a precursor for materials used in organic solar cell applications.⁴¹ Products **2m-2p** show that the catalyst system affords moderate-to-good yields with both electron-deficient and electron-rich substrates. Product **2p** is a precursor to 5,5'-

bis(carbaldehyde)-2,2'-bithiophene, a common intermediate in Knoevenagel condensations, Horner-Wadsworth-Emmons and Wittig olefinations used to prepare conjugated polymers.^{42–45} A 2,2'-bithiophene substrate **1q** was coupled in good yield at 100 °C to yield quaterthiophene derivative **2q**, suggesting that the catalyst has promise for the synthesis of oligothiophene intermediates. Bithiazole **2r** has been utilized as an intermediate for the synthesis of organic field effect transistors, although it was accessed in modest yield (29%). The phd/Pd catalyst system represents an important advance over the previous non-ligated Pd(OAc)₂ aerobic catalyst system.²² The latter method was evaluated for a number of the important substrates in Figure 4.4 (**1a**, **1b**, **1l**, **1p**, and **1q**). In each case, the product yield was < 10%.

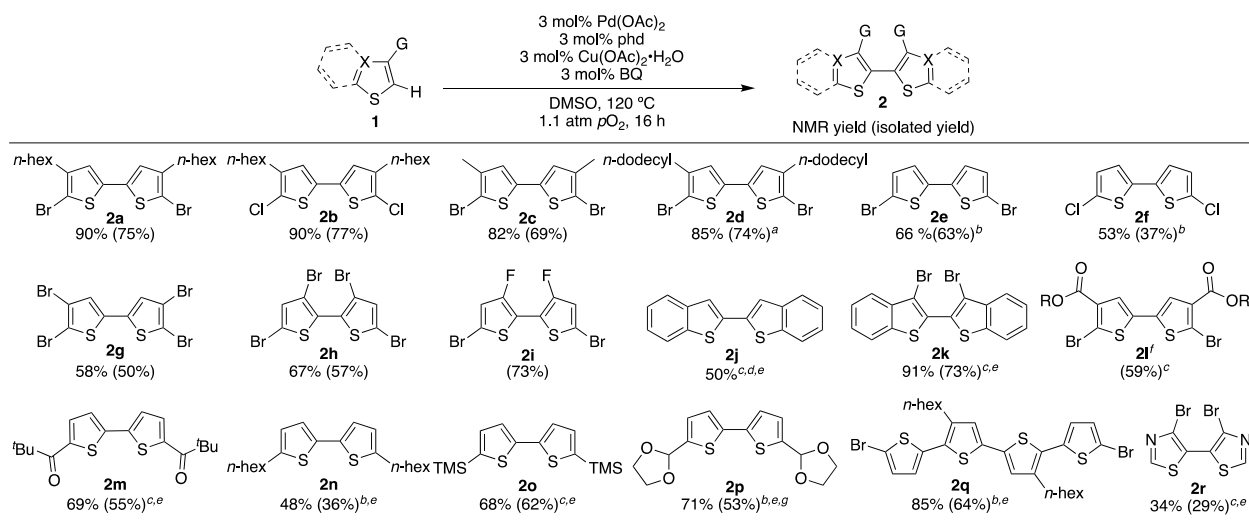


Figure 4.4. Substrate Scope for Phd/Pd(OAc)₂-Catalyzed Aerobic Oxidative Coupling of Thiophenes. Conditions: Substrate (1.1 mmol, 1.1 M), 3 mol% each Pd(OAc)₂, phd, Cu(OAc)₂·H₂O, BQ, 1 mL reaction volume in DMSO, 120 °C, 1.1 atm O₂, 16 hr. ¹H NMR yields, with isolated yields in parentheses. ^aSolvent was a 1.2:1 mixture DMSO: CyOAc. ^b100 °C. ^c5 mol% catalyst. ^dMn(OAc)₂·4H₂O used instead of Cu(OAc)₂·H₂O. ^e24 hr. ^fR = 2-(butyl)octyl; obtained with ~7% unidentified impurity (see section C.11 of Appendix C for details). ^gisolated in 9:1 ratio with monodeprotected 3p (see Section C.11 of Appendix C for details)

A gram-scale oxidative coupling of **1a** under the standard conditions generated **2a** in 90% isolated yield. Moreover, the coupling of **1a** was performed with Pd(OAc)₂ and phd loadings of 0.5 mol%, with Cu(OAc)₂ and BQ at 13 and 3 mol% loading, respectively. A 70% ¹H NMR yield of **2a** was obtained under these conditions. Both of these results have important implications for larger scale applications of this chemistry.

Several observations provide insight into the role of phd as an ancillary ligand. When [phd] is varied at a fixed loading of 3 mol% Pd(OAc)₂ and Cu(OAc)₂, the reaction rate increases linearly with [phd] until it maximizes at a phd: Pd ratio of approximately 1:1 (Figure 4.5A.i). The rate diminishes beyond this phd loading, and catalysis is completely inhibited at a phd: Pd ratio of 3:1. Complementary data were observed at a higher Cu(OAc)₂ loading (12 mol%), while maintaining 3 mol% Pd(OAc)₂. The rate again maximizes at a phd: Pd ratio of approximately 1:1 and decreases beyond this ratio. These results, together with NMR titration experiments showing that phd binds tightly to Pd(OAc)₂ in 1:1 stoichiometry (see Figure C.10 and Figure C.11 in Appendix C), suggest that phd coordinates preferentially to Pd rather than Cu in the catalytic reaction.⁴⁶

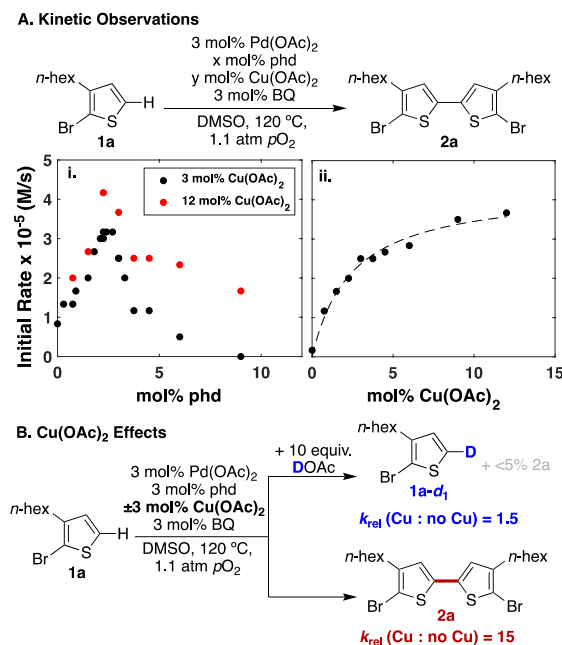


Figure 4.5. Mechanistic experiments probing the effect of Cu(OAc)₂ loading on the rate (A) and the role of Cu(OAc)₂ on C–H activation and C–C coupling (B).

A primary deuterium kinetic isotope effect (KIE) is observed when the homocouplings of **1a** and **1a-d₁** (deuterium at the C5 position) are monitored under standard conditions [3 mol% Pd(OAc)₂ and Cu(OAc)₂]: $k_{\text{H}}/k_{\text{D}} = 2.9 \pm 0.1$. Changing the Cu(OAc)₂ loading has little impact on the KIE: $k_{\text{H}}/k_{\text{D}} = 2.4 \pm 0.1$ and 2.6 ± 0.2 at 0.75 mol% and 10 mol% Cu(OAc)₂, respectively. These KIE values, which resemble those observed in other Pd-catalyzed C–H oxidation reactions,^{47–52} and a first-order dependence of the catalytic rate on [**1a**] (cf. Figure C.4 in Appendix C) indicate that C–H activation is the catalytic turnover-limiting step.

Other experiments provide insights into the role of Cu(OAc)₂. Cu^{II} salts are commonly used as redox cocatalysts to promote Pd catalyst reoxidation by O₂; however, less conventional roles in which Cu^{II} influences substrate oxidation steps mediated by Pd^{II} have also been documented.⁵³ The data in Figure 4.5A.i show that the rate is faster at higher Cu(OAc)₂ loading, and systematic variation of [Cu(OAc)₂] reveals a saturation dependence (Figure 4.5A.ii). Addition

of 10 equiv DOAc inhibits biaryl coupling, but it leads to deuterium incorporation into the C5 position of **1a**, consistent with reversible C–H activation of thiophene under these conditions. Cu(OAc)₂ has only moderate impact on the H/D exchange, increasing deuterium incorporation by a factor of 1.5 after 30 min (28% vs 42%; Figure 4.5B, top). The H/D exchange and KIE data indicate that Cu(OAc)₂ has minimal influence on C–H activation. On the other hand, Cu(OAc)₂ has a major impact on C–C coupling: the oxidative coupling rate of **1a** differs by a factor of 15 in the presence and absence of 3 mol% Cu(OAc)₂ (25×10^{-6} vs 1.7×10^{-6} M/s) (Figure 4.5B, bottom). ¹H NMR spectroscopic data provide evidence for direct interaction between Cu(OAc)₂ and (phd)Pd(OAc)₂ in solution, likely involving the dione fragment of the Pd-bound phd ligand.^{54–60} This evidence was obtained by comparing the effect of adding 1 equiv Cu(OAc)₂ to solutions of (phen)Pd(OAc)₂ and (phd)Pd(OAc)₂ in DMSO-*d*₆. Whereas Cu(OAc)₂ has very little effect on the spectrum of (phen)Pd(OAc)₂, it leads to the appearance of multiple new paramagnetically shifted peaks (upfield and downfield) in the spectrum of (phd)Pd(OAc)₂ (see Figure C.12 and Figure C.13 in Appendix C).

Collectively, the kinetic and spectroscopic data suggest that Cu^{II} influences C–C coupling in a non-redox role. Such roles could include serving as a Lewis acid to promote activation of a second thiophene in a sequential C–H/C–H coupling pathway, promoting transmetalation of a thiophenyl group between two (phd)Pd^{II}-Ar^{Het} intermediates, or promoting reductive elimination from the (phd)Pd(Ar^{Het})₂ intermediate present in either mechanism. Support for this non-redox/Lewis acid role was obtained by replacing Cu^{II} with redox inactive Mg^{II} and Zn^{II} acetate salts. The Mg^{II} and Zn^{II} salts are not as effective as Cu^{II}, but the 35% and 30% yields of **2a**, respectively, are significantly better than the 5% yield of **2a** obtained in the absence of a metal cocatalyst (see **Error! Reference source not found.**). The improved performance of Cu^{II} relative

to Zn^{II} and Mg^{II} is consistent with its enhanced Lewis acidity (cf. Irving-Williams series), which could support more favorable interaction with the phd dione fragment. This secondary binding site in the phd ligand provides a rationale for the superior performance of phd relative to the other ligands in Figure 4.2, and we postulate that a phd-bridged bimetallic species, $(\text{AcO})_2\text{Cu}(\text{phd})\text{Pd}(\text{OAc})_2$ (Figure 4.6), exhibits kinetic advantages over more conventional bimetallic interactions, such as those involving bridging acetate ligands.

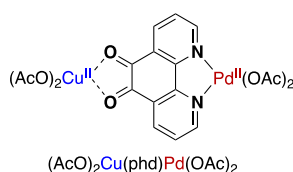


Figure 4.6. Proposed structure of catalytically active phd-supported Cu/Pd heterobimetallic complex

4.4 Conclusion

The results described herein highlight a unique synergistic catalyst system for Pd-catalyzed aerobic oxidative C–H/C–H coupling. 1,10-Phenanthroline-5,6-dione serves as a conventional bidentate ligand for $\text{Pd}(\text{OAc})_2$, while engaging $\text{Cu}(\text{OAc})_2$ as a cooperative partner via interaction with the dione fragment of the ligand backbone. The data implicate an important non-redox role for Cu^{II} in the C–C coupling reaction. Additional studies have been initiated to gain further insights into this unique catalyst system and the catalytic mechanism, but we anticipate that these results will have impact beyond the homocoupling of thiophene. Efforts to pursue these opportunities have also been initiated.

4.5 Acknowledgements

This work was funded by the NSF through the CCI Center for Selective C–H Functionalization (CHE-1205646 and CHE-1700982) and by the NIH (NRSA fellowship award F32 GM119214 to S.J.T.). We acknowledge the NSF (CHE-9709065) and the Paul and Margaret Bender Fund for support of the NMR facility. We acknowledge the NIH (1S10 OD020022-1) for mass spectrometry support.

4.6 References

1. Yang, Y.; Lan, J.; You, J. Oxidative C–H/C–H Coupling Reactions between Two (Hetero)Arenes. *Chem. Rev.* **2017**, *117*, 8787–8863.
2. Stahl, S. S. Palladium Oxidase Catalysis: Selective Oxidation of Organic Chemicals by Direct Dioxygen-Coupled Turnover. *Angew. Chem. Int. Ed.* **2004**, *43*, 3400–3420.
3. Wang, D.; Weinstein, A. B.; White, P. B.; Stahl, S. S. Ligand-Promoted Palladium-Catalyzed Aerobic Oxidation Reactions. *Chem. Rev.* **2018**, *118*, 2636–2679.
4. Takeoshi, T. Polyimides. In *Advances in Polymer Science*; Springer-Verlag: Berlin, Germany, 1990; Vol. 94, pp 2–22
5. Kreuz, J. A.; Edman, J. R. Polyimide Films. *Adv. Mater.* **1998**, *10*, 1229–1232.
6. Itatani, H.; Shiotani, A.; Fujimoto, M. Method for Producing Biphenyltetracarboxylic esters. U. S. Patent 4,581,469. April 8, 1986.
7. Izawa, Y.; Stahl, S. S. Aerobic Oxidative Coupling of *o*-Xylene: Discovery of 2-Fluoropyridine as a Ligand to Support Selective Pd-Catalyzed C–H Functionalization. *Adv. Synth. Catal.* **2010**, *352*, 3223–3229.

8. Wang, D.; Stahl, S. S. Pd-Catalyzed Aerobic Oxidative Biaryl Coupling: Non-Redox Cocatalysis by Cu(OTf)₂ and Discovery of Fe(OTf)₃ as a Highly Effective Cocatalyst. *J. Am. Chem. Soc.* **2017**, *139*, 5704–5707.
9. Álvarez-Casao, Y.; van Slagmaat, C. A. M. R.; Verzijl G. K. M.; Lefort, L.; Alsters, P. L.; Fernández-Ibáñez, M. Á. Palladium-Catalyzed Cross-Dehydrogenative Coupling of *o*-Xylene: Evidence of a New Rate-Limiting Step in the Search for Industrially Relevant Conditions. *ChemCatChem.* **2018**, *10*, 2620–2626.
10. Ishida, T.; Aikawa, S.; Mise, Y.; Akebi, R.; Hamasaki, A.; Honma, T.; Ohashi, H.; Tsuji, T.; Yamamoto, Y.; Miyasaka, M.; Yokoyama, T.; Tokunaga, M. Direct C–H Arene Homocoupling Over Gold Nanoparticles Supported on Metal Oxides. *ChemSusChem* **2015**, *8*, 695–701.
11. Erdmann, N.; Su, Y.; Bosmans, B.; Hessel, V.; Noël, T. Palladium-Catalyzed Aerobic Oxidative Coupling of *o*-Xylene in Flow: A Safe and Scalable Protocol for Cross-Dehydrogenative Coupling. *Org. Process. Res. Dev.* **2016**, *20*, 831–835.
12. Hirano, M.; Sano, K.; Kanazawa, Y.; Komine, N.; Meano, Z.; Mitsudome, T.; Takaya, H. Mechanistic Insights on Pd/Cu-Catalyzed Dehydrogenative Coupling of Dimethyl Phthalate. *ACS Catal.* **2018**, *8*, 5827–5841.
13. Van Velthoven, N.; Waitschat, S.; Chavan, S. M.; Liu, P.; Smolders, S.; Vercammen, J.; Bueken, B.; Bals, S.; Lillerud, K. P.; Stock, N.; De Vos, D. E. Single-Site Metal-Organic Framework Catalysts for the Oxidative Coupling of Arenes *via* C–H/C–H Activation. *Chem. Sci.* **2019**, *10*, 3616–3622.

14. Kanzawa, Y.; Mitsudome, T.; Takaya, H.; Hirano, M. Pd/Cu-Catalyzed Dehydrogenative Coupling of Dimethyl Phthalate: Synchrotron Radiation Sheds Light on the Cu Cycle Mechanism. *ACS Catal.* **2020**, *10*, 5909–5919.
15. Cheng, Y.-J.; Yang, S.-H.; Hsu, C.-S. Synthesis of Conjugated Polymers for Organic Solar Cell Applications. *Chem. Rev.* **2009**, *109*, 5868–5923.
16. Mishra, A.; Bäuerle, P. Small Molecule Organic Semiconductors on the Move: Promises for Future Solar Energy Technology. *Angew. Chem. Int. Ed.* **2012**, *51*, 2020–2067.
17. Meng, H.; Perepichka, I.; Perepichka, D. Thiophene-Based Materials for Electroluminescent Applications. In *Handbook of Thiophene-Based Materials: Applications in Organic Electronics and Photonics*; Perepichka, D., Perepichka, I., Eds.; John Wiley & Sons, Ltd.: West Sussex, United Kingdom, 2009; pp 695–756.
18. Facchetti, A. Electroactive Oligothiophenes and Polythiophenes for Organic Field Effect Transistors. In *Handbook of Thiophene-Based Materials: Applications in Organic Electronics and Photonics*; Perepichka, I., Perepichka, D., Eds.; John Wiley & Sons, Ltd.: West Sussex, United Kingdom, 2009; pp 595–646.
19. Masui, K.; Ikegami, H.; Mori, A. Palladium-Catalyzed C–H Homocoupling of Thiophenes: Facile Construction of Bithiophene Structure. *J. Am. Chem. Soc.* **2004**, *126*, 5074–5075.
20. Takahashi, M.; Masui, K.; Sekiguchi, H.; Kobayashi, N.; Mori, A.; Funahashi, M.; Tamaoki, N. Palladium-Catalyzed C–H Homocoupling of Bromothiophene Derivatives and Synthetic Application to Well-Defined Oligothiophenes. *J. Am. Chem. Soc.* **2006**, *128*, 10930–10933.
21. He, C.-Y.; Wang, Z.; Wu, C.-Z.; Qing, F.-L.; Zhang, X. Pd-Catalyzed Oxidative Cross-Coupling Between Two Electron Rich Heteroarenes. *Chem. Sci.* **2013**, *4*, 3508–3513.

22. Li, N.-N.; Zhang, Y.-L.; Mao, S.; Gao, Y.-R.; Guo, D.-D.; Wang, Y.-Q. Palladium-Catalyzed C–H Homocoupling of Furans and Thiophenes Using Oxygen as the Oxidant. *Org. Lett.* **2014**, *16*, 2732–2735.
23. Lotz, M. D.; Camasso, N. M.; Canty, A. J.; Sanford, M. S. Role of Silver Salts in Palladium-Catalyzed Arene and Heteroarene C–H Functionalization Reactions. *Organometallics* **2017**, *36*, 165–171.
24. P, S.; Sau, S. C.; Vardhanapu, P. K.; Mandal, S. K. Halo-Bridged Abnormal NHC Palladium(II) Dimer for Catalytic Dehydrogenative Cross-Coupling Reactions of Heteroarenes. *J. Org. Chem.* **2018**, *83*, 9403–9411.
25. Wang, L.; Carrow, B. P. Oligothiophene Synthesis by a General C–H Activation Mechanism: *Electrophilic Concerted Metalation–Deprotonation (eCMD)*. *ACS. Catal.* **2019**, *9*, 6821–6836.
26. Shinde, V. N.; Bhuvanesh, N.; Kumar, A.; Joshi, H. Design and Syntheses of Palladium Complexes of NNN/CNN Pincer Ligands: Catalyst for Cross Dehydrogenative Coupling Reaction of Heteroarenes. *Organometallics* **2020**, *39*, 324–333.
27. McCullough, R. D. The Chemistry of Conducting Polythiophenes. *Adv. Mater.* **1998**, *10*, 93–116.
28. Campbell, A. N.; Meyer, E. B.; Stahl, S. S. Regiocontrolled Aerobic Oxidative Coupling of Indoles and Benzene Using Pd Catalysts with 4,5-Diazafluorene Ligands. *Chem. Commun.* **2011**, *47*, 10257–10259.
29. Itatani, H.; Shiotani, A.; Fujimoto, M. Method for Producing Biphenyltetracarboxylic esters. U. S. Patent 4,581,469. April 8, 1986.

30. Wendlandt, A. E.; Stahl, S. S. Bioinspired Aerobic Oxidation of Secondary Amines and Nitrogen Heterocycles with a Bifunctional Quinone Catalyst. *J. Am. Chem. Soc.* **2014**, *136*, 506–512.
31. Wendlandt, A. E.; Stahl, S. S. Modular *o*-Quinone Catalyst System for Dehydrogenation of Tetrahydroquinolines under Ambient Conditions. *J. Am. Chem. Soc.* **2014**, *136*, 11910–11913.
32. Li, B.; Wendlandt, A. E.; Stahl, S. S. Replacement of Stoichiometric DDQ with a Low Potential *o*-Quinone Catalyst Enabling Aerobic Dehydrogenation of Tertiary Indolines in Pharmaceutical Intermediates. *Org. Lett.* **2019**, *21*, 1176–1181.
33. In one previous case, it was used with benzoquinone as the stoichiometric oxidant: Ding, D.; Zhu, G.; Jiang, X. Ligand-Controlled Palladium(II)-Catalyzed Regiodivergent Carbonylation of Alkynes: Syntheses of Indolo[3,2-*c*]coumarins and Benzofuro[3,2-*c*]quinolinones. *Angew. Chem. Int. Ed.* **2018**, *57*, 9028–9032.
34. Verswyvel, M.; Monnaie, F.; Koeckelberghs, G. AB Block Copoly(3-Alkylthiophenes): Synthesis and Chiroptical Behavior. *Macromolecules* **2011**, *44*, 9489–9498.
35. McCulloch, I.; Heeney, M.; Bailey, C.; Genevicius, K.; MacDonald, I.; Shkunov, M.; Sparrowe, D.; Tierney, S.; Wagner, R.; Zhang, W.; Chabinyc, M. L.; Kline, R. J.; McGehee, M. D.; Toney, M. F. Liquid-Crystalline Semiconducting Polymers with High Charge-Carrier Mobility. *Nat. Mater.* **2006**, *5*, 328–333.
36. Zhang, Q.; Kelly, M. A.; Bauer, N.; You, W. The Curious Case of Fluorination of Conjugated Polymers for Solar Cells. *Acc. Chem. Res.* **2017**, *50*, 2401–2409.
37. Kawashima, K.; Fukuhara, T.; Suda, Y.; Suzuki, Y.; Koganezawa, T.; Yoshida, H.; Ohkita, H.; Osaka, I.; Takimiya, K. Implication of Fluorine Atom on Electronic Properties, Ordering

- Structures, and Photovoltaic Performance in Naphthobisthiadiazole-Based Semiconducting Polymers. *J. Am. Chem. Soc.* **2016**, *138*, 10265–10275.
38. Qi, T.; Guo, Y.; Liu, Y.; Xi, H.; Zhang, H.; Gao, X.; Liu, Y.; Lu, K.; Du, C.; Yu, G.; Zhu, D. Synthesis and Properties of the *anti* and *syn* Isomers of Dibenzothieno[*b,d*]pyrrole. *Chem. Commun.* **2008**, 6227–6229.
39. Dienes, Y.; Eggenstein, M.; Kárpáti, T.; Sutherland, T. C.; Nyulászi, L.; Baumgartner, T. Phosphorus-Based Heteropentacenes: Efficiently Tunable Materials for Organic n-Type Semiconductors. *Chem. Eur. J.* **2008**, *14*, 9878–9889.
40. Zhao, Y.; Hao, W.; Ma, W.; Zang, Z.; Zhang, H.; Liu, X.; Zou, S.; Zhang, H.; Liu, W.; Gao, J. Easily-Soluble Heteroacene Bis(benzothieno)silole Derivatives for Sensing of Nitro Explosives. *New J. Chem.* **2014**, *38*, 5754–5760.
41. Zhang, M.; Guo, X.; Ma, W.; Ade, H.; Hou, J. A Polythiophene Derivative with Superior Properties for Practical Application in Polymer Solar Cells. *Adv. Mater.* **2014**, *26*, 5880–5885.
42. Leclerc, N.; Michaud, A.; Sirois, K.; Morin, J.-F.; Leclerc, M. Synthesis of 2,7-Carbazolenevinylene-Based Copolymers and Characterization of Their Photovoltaic Properties. *Adv. Funct. Mater.* **2006**, *16*, 1694–1704.
43. Zrig, S.; Koeckelberghs, G.; Verbiest, T.; Andrioletti, B.; Rose, E.; Persoons, A.; Asselberghs, I.; Clays, K. Λ -Type Regioregular Oligothiophenes: Synthesis and Second-Order NLO Properties. *J. Org. Chem.* **2007**, *72*, 5855–5858.
44. Bhuwalka, A.; Mike, J. F.; Intemann, J. J.; Ellern, A.; Jeffries-EL, M. A Versatile and Efficient Synthesis of Bithiophene-Based Dicarboxaldehydes from a Common Synthon. *Org. Biomol. Chem.* **2015**, *13*, 9462–9470.

45. Brzeczek, A.; Piwowar, K.; Domagała, W.; Mikołajczyk, M. M.; Walczak, K.; Wagner, P. Systematic Elongation of Thienyl Linkers and Their Effect on Optical and Electrochemical Properties in Carbazole–BODIPY Donor–Acceptor Systems. *RSC Adv.* **2016**, *6*, 36500–36509.
46. A recent mechanistic study of the oxidative coupling of dimethyl phthalate suggests phenanthroline remains bound to Pd(OAc)₂ in the presence of Cu(OAc)₂. See ref. 14. We note that addition of 1–3 equiv of thiophene **2a** to the NMR solutions does not perturb the Pd/Cu/phd speciation.
47. Davidson, J. M.; Triggs, C. Reaction of Metal Ion Complexes with Hydrocarbons. Part I. ‘Palladation’ and Some Other New Electrophilic Substitution Reactions. The Preparation of Palladium(I). *J. Chem. Soc. A* **1968**, *0*, 1324–1330.
48. Kashima, M.; Yoshimoto, H.; Itatani, H. Isotope Effect of Aromatic Coupling Reaction Catalyzed by Palladium Acetate. *J. Catal.* **1973**, *29*, 92–98.
49. Wang, D.; Izawa, Y.; Stahl, S. S. Pd-Catalyzed Aerobic Oxidative Coupling of Arenes: Evidence for Transmetalation between Two Pd(II)-Aryl Intermediates. *J. Am. Chem. Soc.* **2014**, *136*, 9914–9917.
50. Hennessy, E. J.; Buchwald, S. L. Synthesis of Substituted Oxindoles from α -Chloroacetanilides via Palladium-Catalyzed C–H Functionalization. *J. Am. Chem. Soc.* **2003**, *125*, 12084–12085.
51. Campeau, L.-C.; Parisien, M.; Jean, A.; Fagnou, K. Catalytic Direct Arylation with Aryl Chlorides, Bromides, and Iodides: Intramolecular Studies Leading to New Intermolecular Reactions. *J. Am. Chem. Soc.* **2006** *128*, 581–590.

52. Chiong, H. A.; Pham, Q.-N.; Daugulis, O. Two Methods for Direct *ortho*-Arylation of Benzoic Acids. *J. Am. Chem. Soc.* **2007**, *129*, 9879–9884.
53. See ref. 8 and references cited therein.
54. Fox, G. A.; Bhattacharya, S.; Pierpont, C. G. Structural and Electrochemical Properties of Binuclear Complexes Containing 1,10-Phenanthroline-5,6-Diolate as a Bridging Ligand. *Inorg. Chem.* **1991**, *30*, 2895–2899.
55. Hill, P. M.; Lee, L. Y.; Younkin, T. R.; Orth, S. D.; McElwee-White, L. Synthesis and Electrochemical Oxidation of Bridged Ruthenium/Platinum Complexes of 1,10-Phenanthroline-5,6-Diolate. *Inorg. Chem.* **1997**, *36*, 5655-5657.
56. Calderazzo, F.; Marchetti, F.; Pampaloni, G.; Passarelli, V. Co-ordination Properties of 1,10-Phenanthroline-5,6-Dione Towards Group 4 and 5 Metals in Low and High Oxidation States. *J. Chem. Soc., Dalton Trans.* **1999**, 4389–4396.
57. Calderazzo, F.; Pampaloni, G.; Passarelli, V. 1,10-Phenanthroline-5,6-dione as a Building Block for the Synthesis of Homo- and Heterometallic complexes. *Inorg. Chim. Acta* **2002**, *330*, 136–142.
58. Shavaleev, N. M.; Moorcraft, L. P.; Pope, S. J. A.; Bell, Z. R.; Faulkner, S.; Ward, M. D. Sensitized Near-Infrared Emission from Complexes of Yb^{III}, Nd^{III} and Er^{III} by Energy-Transfer from Covalently Attached Pt^{II}-Based Antenna Units. *Chem. Eur. J.* **2003**, *9*, 5283-5291.
59. Fujihara, T.; Okamura, R.; Wada, T.; Tanaka, K. Coordination Ability of 1,10-Phenanthroline-5,6-Dione: Syntheses and Redox Behavior of a Ru(II) Complex with an o-Quinoid Moiety and of Bridged Ru(II)–M(II) Complexes (M = Pd, Pt). *Dalton Trans.* **2003**, 3221–3226.

60. Hickson, J. R.; Horsewill, S. J.; Bamforth, C.; McGuire, J.; Wilson, C.; Sproules, S.; Farnaby, J. H. The Modular Synthesis of Rare-Earth Transition Metal Heterobimetallic Complexes Utilizing a Redox-Active Ligand. *Dalton Trans.* **2018**, *47*, 10692–10701.

Appendix A: Supporting Information for Chapter 2

A.1 General Considerations

All manipulations were carried out in a glovebox or using standard Schlenk line technique unless specified otherwise. All chemicals and solvents were purchased from commercially available sources. Substituted benzoquinones were purified by sublimation. 1,4-dioxane was distilled from sodium benzophenone ketyl radical and stored under inert atmosphere. Chloroform and D-chloroform were dried over calcium hydride and stored under inert atmosphere. Palladium acetate was purchased from Sigma-Aldrich and used without further purification, although the purity of the Pd(OAc)₂ was confirmed by ¹H NMR spectroscopic analysis because Pd(OAc)₂ is occasionally contaminated with NO₂ substituting an acetate ligand.¹ Palladium dimer [Pd^I(μ-DAF)(OAc)]₂ was prepared according to literature procedure.² All NMR spectra were obtained on Bruker-Avance 400, 500, or 600 MHz spectrometers. Attenuated total reflectance FTIR (ATR-FTIR) data were collected on a Bruker Tensor 27 on a Pike Technologies diamond ATR stage.

A.2 Ligand Screens

Ligand Screen for Conversion of ^tBuH₂BQ with Pd(OAc)₂/L in dioxane/d₄-AcOD

Stock solutions of ligands were prepared in dichloromethane such that a 100 μL aliquot contained 0.008 mmol of ligand (0.016 mmol for pyridine). A stock solution of Pd(OAc)₂ (18.2 mg, 0.081 mmol) in dichloromethane (1.0 mL) was prepared. 100 μL of ligand stock solution and 100 μL of Pd(OAc)₂ stock solution were transferred to scintillation vials, the dichloromethane was removed *in vacuo*, and the vials were transferred to a glovebox. A stock solution of ^tBuH₂BQ (67.3 mg, 0.405 mmol) and internal standard (1,3,5-trimethoxybenzene; 22.7 mg, 0.134 mmol) in dioxane:AcOD-*d*₄ mixture (3:1 vol:vol, 10.0 mL) was prepared. Into each of the vials containing Pd(OAc)₂/L was added 600 μL of the ^tBuH₂BQ solution. The solutions were stirred for approximately 1 h before being transferred to NMR tubes and were allowed to stand for 24 h before

^1H NMR spectra were collected (8 scans, 2 dummy scans, 16 s T1 relaxation delay). The ^tBu peak of remaining $^t\text{BuH}_2\text{BQ}$ was integrated relative to internal standard to quantify conversion.

Ligand Screen for Conversion of $^t\text{BuH}_2\text{BQ}$ with $\text{Pd}(\text{OAc})_2/\text{L}$ in $\text{CDCl}_3/d_4\text{-AcOD}$

Stock solutions of ligands (0.06 mmol in 1000 μL dichloromethane), $^t\text{BuH}_2\text{BQ}$ (0.06 mmol in 1000 μL inhibitor-free THF), $\text{Pd}(\text{OAc})_2$ (0.09 mmol in 1500 μL dichloromethane) and methyl-3,5-dinitrobenzoate internal standard (0.18 mmol in the same 1500 μL solution as $\text{Pd}(\text{OAc})_2$) were prepared. The $^t\text{BuH}_2\text{BQ}$ stock solution (100 μL) was added to a scintillation vial and the solvent was removed under reduced pressure. Into separate vials were added 100 μL of the ligand stock solutions and 100 μL of the $\text{Pd}(\text{OAc})_2$ /internal standard stock solutions and the solvent was removed *in vacuo*. The vials were then transferred into a glovebox and the solid mixtures of $\text{Pd}(\text{OAc})_2$ /ligand/internal standard were dissolved in 600 μL of a 1.5 M solution of $\text{AcOD-}d_4$ in CDCl_3 . Each of these solutions was transferred to the vials containing $^t\text{BuH}_2\text{BQ}$ and stirred until homogeneous, after which they were transferred to NMR tubes, capped, and allowed to stand at ambient temperature in the glovebox for 16 h before collecting ^1H NMR spectra. The ^tBu peak of remaining $^t\text{BuH}_2\text{BQ}$ was integrated relative to internal standard to quantify conversion.

A.3 Approach to Equilibrium Plots

$(\text{DAF})\text{Pd}(\text{OAc})_2/[\text{Pd}^{\text{I}}(\mu\text{-DAF})(\text{OAc})]_2$ (See Figure 3 in the manuscript)

For “Forward” Direction: In a glove box, a 2.0 mL stock solution of $\text{Pd}(\text{OAc})_2$ (6.1 mg, 0.027 mmol), 4,5-diazfluorenone (DAF, 4.9 mg, 0.027 mmol), and internal standard (3,5-dinitromethylbenzoate; 6.1 mg, 0.027 mmol) in 2.0 mL of a 3:1 mixture (vol:vol) of dioxane: $\text{AcOD-}d_4$ was prepared. A separate stock solution of $^t\text{BuH}_2\text{BQ}$, (13.5 mg, 0.081 mmol, in 1.0 mL of dichloromethane) was prepared, and 50 μL of this solution was transferred to a 6 mL scintillation vial. The dichloromethane was removed *in vacuo*, the $^t\text{BuH}_2\text{BQ}$ was dissolved in a

600 μL portion of the $\text{Pd}(\text{OAc})_2/\text{DAF}/\text{internal standard}$ stock solution and quickly transferred to an NMR tube. The tube was capped, removed from the glove box, and frozen in liquid nitrogen. The sample was kept frozen until data collection commenced. ^1H NMR spectra were collected every 15 min for the first 10 h and every 2.5 h for the remaining 14 h of the experiment (T_1 relaxation delay of 21 s.). The DAF ligand signals were integrated relative to internal standard to quantify $[\text{Pd}^{\text{I}}(\mu\text{-DAF})(\text{OAc})_2]$ and the tert-butyl signal of $^t\text{BuH}_2\text{BQ}$ and $^t\text{BuBQ}$ were integrated to quantify quinone concentration. Equilibrium constants were calculated according to Equation 2.2 in Chapter 2.

For “Reverse” direction: In a glove box, a stock solution of $[\text{Pd}^{\text{I}}(\mu\text{-DAF})(\text{OAc})_2]$ (7.0 mg, 0.010 mmol) and internal standard (3,5-dinitromethylbenzoate; 4.6 mg, 0.020 mmol) in 1.5 mL of dioxane: $\text{AcOD-}d_4$ was prepared. A separate stock solution of $^t\text{BuBQ}$ (13.5 mg, 0.081 mmol, in 1.0 mL of dichloromethane) was prepared, and 50 μl of this solution was transferred to a 6 mL scintillation vial before the dichloromethane was removed *in vacuo*. The $^t\text{BuBQ}$ was dissolved in a 600 μL portion of the $[\text{Pd}^{\text{I}}(\mu\text{-DAF})(\text{OAc})_2]$ /internal standard stock solution and quickly transferred to an NMR tube, which was capped, removed from the purge box, and frozen in liquid nitrogen. The sample was kept frozen until data collection commenced. ^1H NMR Spectra were collected every 5 min for the first 10 h and approximately every 2.5 h for the remaining 14 h of the experiment (T_1 relaxation delay of 21 s).

(Bathocuproine) $\text{Pd}(\text{OAc})_2$ /(bathocuproine) $\text{Pd}(\text{RBQ})$ (See Figure 4 in the manuscript)

For “Forward” Direction: In a glovebox, a stock solution of $(\text{bc})\text{Pd}(\text{OAc})_2$ (7.3 mg, 0.12 mmol) in 1.0 mL of 1.5 M $\text{AcOD-}d_4$ in CDCl_3 was prepared. A separate solution of $^t\text{BuH}_2\text{BQ}$ (8.3 mg, 0.05 mmol) and methyl-3,5-dinitrobenzoate internal standard (11.3 mg, 0.05 mmol) in 1.0 mL of 1.5 M $\text{AcOD-}d_4$ in CDCl_3 was prepared. A 400 μL aliquot of the $(\text{bc})\text{Pd}(\text{OAc})_2$ solution was

injected to an NMR tube and capped with a septum cap. Just before the sample was inserted into the NMR spectrometer, 100 μL of the $^t\text{BuH}_2\text{BQ}$ /internal standard solution was injected through the septum cap and shaken well to ensure good mixing. The NMR tube was inserted into the spectrometer and data collection was commenced (spectra collected every 5 min with 4 s T1 relaxation delay). The time between the injection and the first spectrum was recorded. To quantify concentration, the tert-butyl peaks of the (bc)Pd($^t\text{BuBQ}$) and $^t\text{BuH}_2\text{BQ}$ were integrated relative to internal standard.

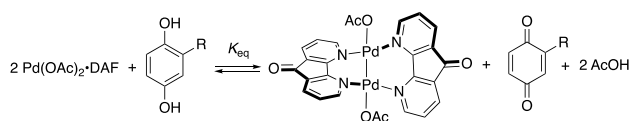
For “Reverse” direction: A stock solution of methyl-3,5-dinitrobenzoate internal standard (12.2 mg, 0.054 mmol) in 5.0 mL of CDCl_3 was prepared. A separate stock solution of (bc)Pd(η^2 - $^t\text{BuBQ}$) (7.1 mg, 0.011 mmol) in 1.0 mL of the internal standard stock solution was prepared. Into an NMR tube was injected 550 μL of the (bc)Pd(η^2 - $^t\text{BuBQ}$) solution, which was capped with a septum cap and taken to the NMR spectrometer. Just before the sample was inserted into the spectrometer, 51 μL of $\text{AcOD-}d_4$ was injected. The tube was shaken to ensure good mixing and inserted into the spectrometer before data collection was commenced (spectra collected every 5 min with 4 s T1 relaxation delay). The time between the injection and the first spectrum was recorded.

A.4 Equilibrium Constant Measurements



Stock solutions of $\text{Pd}(\text{OAc})_2$ (13.6 mg, 0.606 mmol in 750 μL of dichloromethane), DAF (14.8 mg, 0.081 mmol in 1.0 mL of dichloromethane), and internal standard (methyl 3,5-dinitrobenzoate; 18.3 mg, 0.081 mmol in 1.0 mL of dichloromethane) were prepared. Into 5 separate 6 mL scintillation vials, 100 μL of each of the stock solutions were apportioned and the dichloromethane was removed *in vacuo* and transferred to a glove box. Stock solutions of the

substituted hydroquinones (2,6-dimethylhydroquinone, 2-tertbutylhydroquinone, 2-methylhydroquinone, hydroquinone, and 2-chlorohydroquinone) were prepared (0.081 mmol in 1.0 mL dichloromethane). Into 5 separate 6 mL scintillation vials, 100 μ L of each of the solutions were apportioned before the dichloromethane was removed *in vacuo* and transferred to a glove box. The Pd(OAc)₂/DAF/internal standard mixture was dissolved in 600 μ L of dioxane:AcOD-*d*₄. The substituted hydroquinones were then dissolved in the Pd(OAc)₂/DAF/internal standard solution and then transferred to an NMR tube and allowed to stand for 24 h in the glovebox at ambient temperature before NMR spectra were collected. The DAF ligand signals were integrated to quantify [Pd^I(μ -DAF)(OAc)]₂ and the tert-butyl signal of ¹BuH₂BQ and ¹BuBQ were integrated to quantify quinone concentration. Equilibrium constants were calculated according to Equation 2.2 in the Chapter 2. Error analysis was conducted by means of standard propagation of error calculations. For $x = \log(a)$: $S_x = 0.434[S_a/a]$, where a is random variable, S_x = standard deviation of x , S_a = standard deviation of a .



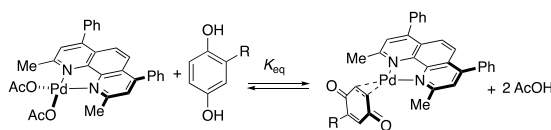
Equation A.1

Table A.1. Determination of equilibrium constants for Equation A.1

Hydroquinone	Equivalents RH ₂ BQ (relative to total [Pd])	K_{eq}	K_{eq} average	std dev	$\log(K_{eq})$	error
2,6-Me ₂ H ₂ BQ	0.5	8292.2	7241.5	1486.0	3.9	0.1
2,6-Me ₂ H ₂ BQ	3.0	6190.7				
¹ BuH ₂ BQ	0.5	305.9	305.2	0.9	2.5	0.001
¹ BuH ₂ BQ	3.0	304.6				
MeH ₂ BQ	0.5	91.7	90.0	2.4	2.0	0.01
MeH ₂ BQ	3.0	88.3				
H ₂ BQ	0.5	1.0	1.5	0.8	0.2	0.2
H ₂ BQ	3.0	2.1				
ClH ₂ BQ	0.5	0.1	0.4	0.4	-0.5	0.4
ClH ₂ BQ	3.0	0.6				

(bc)Pd(OAc)₂/(bc)Pd(η²-BQ)

A stock solution of Pd(OAc)₂ (33.7 mg, 0.15 mmol), bathocuproine (54.1 mg, 0.15 mmol), and methyl-3,5,-dinitrobenzoate internal standard (67.84 mg, 0.30 mmol) in 15 mL of a 1.5 M solution of AcOD-d₄ in CDCl₃ was prepared in a glovebox. A separate stock solution of ^tBuH₂BQ (14.9 mg, 0.09 mmol) was prepared in 2.0 mL of dichloromethane, and with an airtight Hamilton syringe 50 μL, 100 μL, 200 μL, 300 μL, and 400 μL of this solution were transferred into 5 separate 4 mL vials. The dichloromethane was removed *in vacuo*, and the vials were moved to the glovebox. To each vial of ^tBuH₂BQ was added 600 μL of the Pd(OAc)₂/bc/internal standard solution. Once the ^tBuH₂BQ dissolved, the solution was transferred to and NMR tube and allowed to stand at room temperature for 16 h in the glove box before ¹H NMR spectra were recorded. An analogous procedure was repeated for MeH₂BQ, H₂BQ, and ClH₂BQ. Equilibrium constants were calculated according to Equation 2.3 in Chapter 2. Error analysis was conducted by means of standard propagation of error calculations. For $x = \log(a)$: $S_x = 0.434[S_a/a]$, where a is random variable, S_x = standard deviation of x , S_a = standard deviation of a .

**Equation A.2****Table A.2.** Determination of equilibrium constants for Equation A.2 with ^tBuH₂BQ

Hydroquinone	Equivalents RH ₂ BQ (relative to total [Pd])	K _{eq}	K _{eq} average	std dev	log(K _{eq})	error
^t BuH ₂ BQ	0.5	87.2	128.6	25.5	2.1	0.09
^t BuH ₂ BQ	1.0	149.9				
^t BuH ₂ BQ	2.0	134.9				
^t BuH ₂ BQ	3.0	123.4				
^t BuH ₂ BQ	4.0	147.7				

Table A.3. Determination of equilibrium constants for Equation A.2 with MeH₂BQ

Hydroquinone	Equivalents RH ₂ BQ (relative to total [Pd])	K_{eq}	K_{eq} average	std dev	$\log(K_{\text{eq}})$	error
MeH ₂ BQ	0.5	25.6	29.9	4.1	1.5	0.06
MeH ₂ BQ	1.0	26.1				
MeH ₂ BQ	2.0	32.8				
MeH ₂ BQ	3.0	30.0				
MeH ₂ BQ	4.0	35.1				

Table A.4. Determination of equilibrium constants for Equation A.2 with H₂BQ

Hydroquinone	Equivalents RH ₂ BQ (relative to total [Pd])	K_{eq}	K_{eq} average	std dev	$\log(K_{\text{eq}})$	error
H ₂ BQ	0.5	2.3	2.8	0.3	0.4	0.05
H ₂ BQ	1.0	2.8				
H ₂ BQ	2.0	3.1				
H ₂ BQ	3.0	2.8				
H ₂ BQ	4.0	2.8				

Table A.5. Determination of equilibrium constants for Equation A.2 with ClH₂BQ

Hydroquinone	Equivalents RH ₂ BQ (relative to total [Pd])	K_{eq}	K_{eq} average	std dev	$\log(K_{\text{eq}})$	error
ClH ₂ BQ	0.5	0.0*	0.5	0.3	-0.3	0.3
ClH ₂ BQ	1.0	0.9				
ClH ₂ BQ	2.0	0.4				
ClH ₂ BQ	3.0	0.5				
ClH ₂ BQ	4.0	0.6				

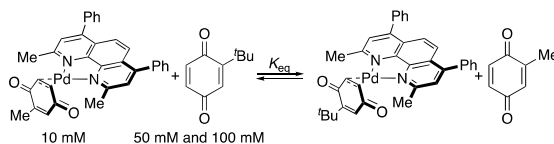
* No measurable concentration of (bc)Pd(η^2 -ClBQ) complex with only 0.5 equivalents of ClH₂BQ.

A.5 Quinone Exchange Measurements

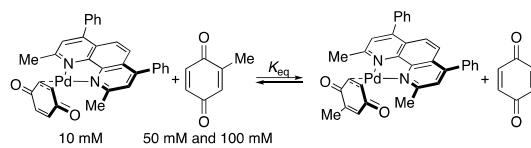
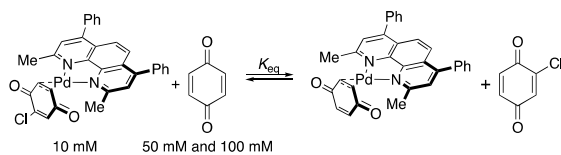
For the reaction shown in Equation A.3 below: Into a two separate 4 mL vials, (bc)Pd(OAc)₂ (3.51 mg, 0.006 mmol) and 2-MeH₂BQ (0.74 mg, 0.006 mmol) were dissolved in 500 μ L of CDCl₃ [the Pd⁰(quinone) adducts were generated *in situ* to avoid complications associated with their isolation, which in some cases proved challenging because of decomposition of the products on concentration]. The formation of the corresponding (bc)Pd(η^2 -2-MeBQ) adduct was allowed to proceed to completion (~20 min) before 5 equivalents ^tBuBQ (4.93 mg, 0.03 mmol) and 10 equivalents ^tBuBQ (9.85 mg, 0.06 mmol) were added to each respective vial as 100 μ L solutions. The reactions reach equilibrium rapidly but were allowed to stand overnight before ¹H

NMR spectra were collected at $-60\text{ }^{\circ}\text{C}$, $-50\text{ }^{\circ}\text{C}$, $-40\text{ }^{\circ}\text{C}$, and $-30\text{ }^{\circ}\text{C}$. Analogous procedures were followed for Equation A.4 and Equation A.5.

The exchange reactions were carried out at low temperature because exchange kinetics on the NMR time scale at room temperature caused significant broadening that precluded reliable integration. In the case of $(bc)\text{Pd}(\eta^2\text{-}^t\text{BuBQ})$, MeBQ was determined to be a more convenient exchange partner, as the equilibrium exchange of BQ with $(bc)\text{Pd}(\eta^2\text{-}^t\text{BuBQ})$ favored $(bc)\text{Pd}(\eta^2\text{-BQ})$ such that reliable integration of $(bc)\text{Pd}(\eta^2\text{-}^t\text{BuBQ})$ could not be obtained. For $(bc)\text{Pd}(^t\text{BuBQ})$ and $(bc)\text{Pd}(\text{MeBQ})$ the tert-butyl and methyl peaks were integrated to determine concentrations when the resolution was sufficiently good. Otherwise, the protons of the bound quinone were integrated. For $(bc)\text{Pd}(\eta^2\text{-BQ})$ and $(bc)\text{Pd}(\eta^2\text{-ClBQ})$ the ring protons were integrated to determine concentration. The polynomial baseline correction feature of MestReNova 12.0.1 was used for baseline correction. In the exchange reaction of $^t\text{BuBQ}$ with $(bc)\text{Pd}(\text{MeBQ})$, the formation of a small unidentified peak with a temperature dependent chemical shift is observed between ~ 5.6 and 6.3 ppm (denoted with asterisk (*)) in top spectral stack in Figure A.1). The identity of the unknown peak was not the subject of thorough investigation. However, since the chemical shift of the peak is temperature dependent, while the peaks of the Pd-quinone complexes are not, we conclude that it is not associated with the Pd-quinone complexes. We speculate that it results from an exchangeable proton (e.g. from acetic acid) present in the reaction mixture or impurity in the $^t\text{BuBQ}$ starting material.



Equation A.3

**Equation A.4****Equation A.5**

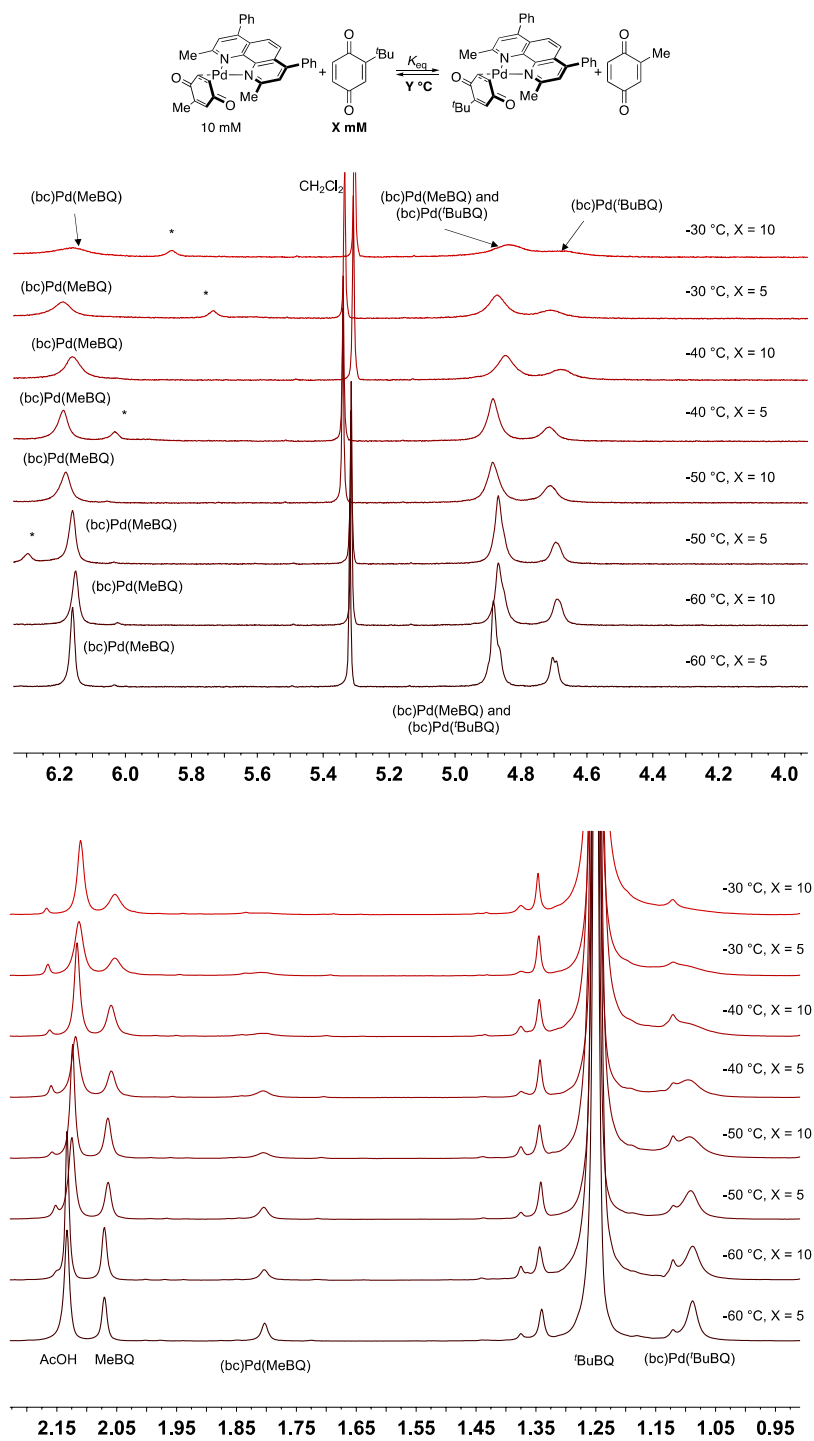


Figure A.1. Variable temperature ^1H NMR Spectra for exchange of $t\text{BuBQ}$ with $(bc)\text{Pd}(\text{MeBQ})$. Asterisk (*) denotes unidentified, temperature-dependent peak. See above text for details.

Table A.6. Equilibria data and van't Hoff plot for exchange of ^tBuBQ with (bc)Pd(MeBQ).

Temp (°C)	[^t BuBQ] (mM)	K_{eq}	avg.
-60	50	0.15	0.15
	100	0.15	
-50	50	0.17	0.17
	100	0.16	
-40	50	0.21	0.19
	100	0.16	
-30	50	0.23	0.20
	100	0.17	

$y = -504.47x + 0.4727$
 $R^2 = 0.991$

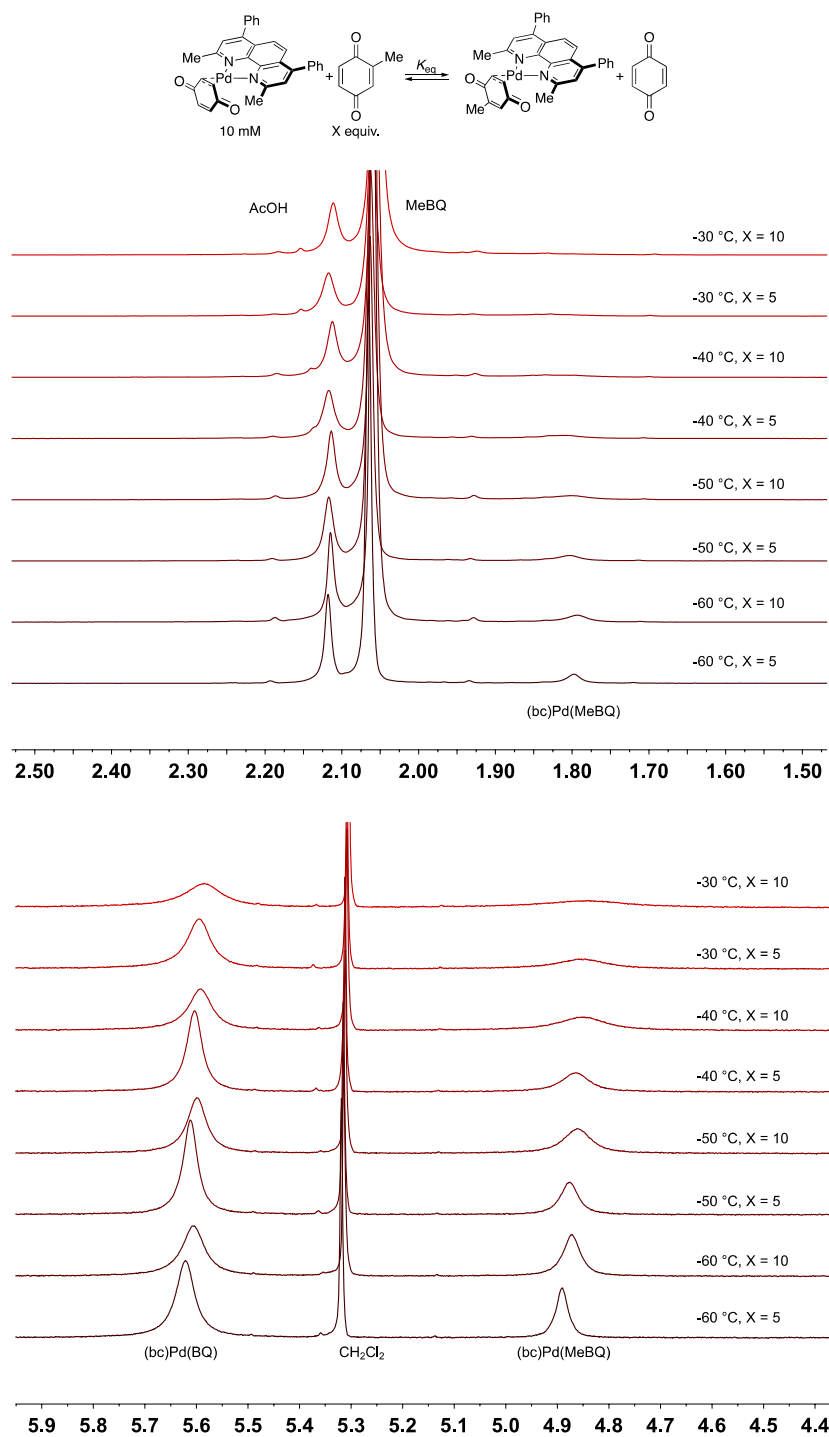


Figure A.2. Variable temperature ^1H NMR Spectra for exchange of MeBQ with (bc)Pd(BQ).

Table A.7. Equilibria data and van't Hoff plot for exchange of MeBQ with (bc)Pd(BQ).

Temp (°C)	[MeBQ] (mM)	K_{eq}	avg.
-60	50	0.051	0.051
	100	0.052	
-50	50	0.052	0.054
	100	0.055	
-40	50	0.057	0.057
	100	0.057	
-30	50	0.071	0.062
	100	0.054	

$y = -327.69x - 1.4414$
 $R^2 = 0.9802$

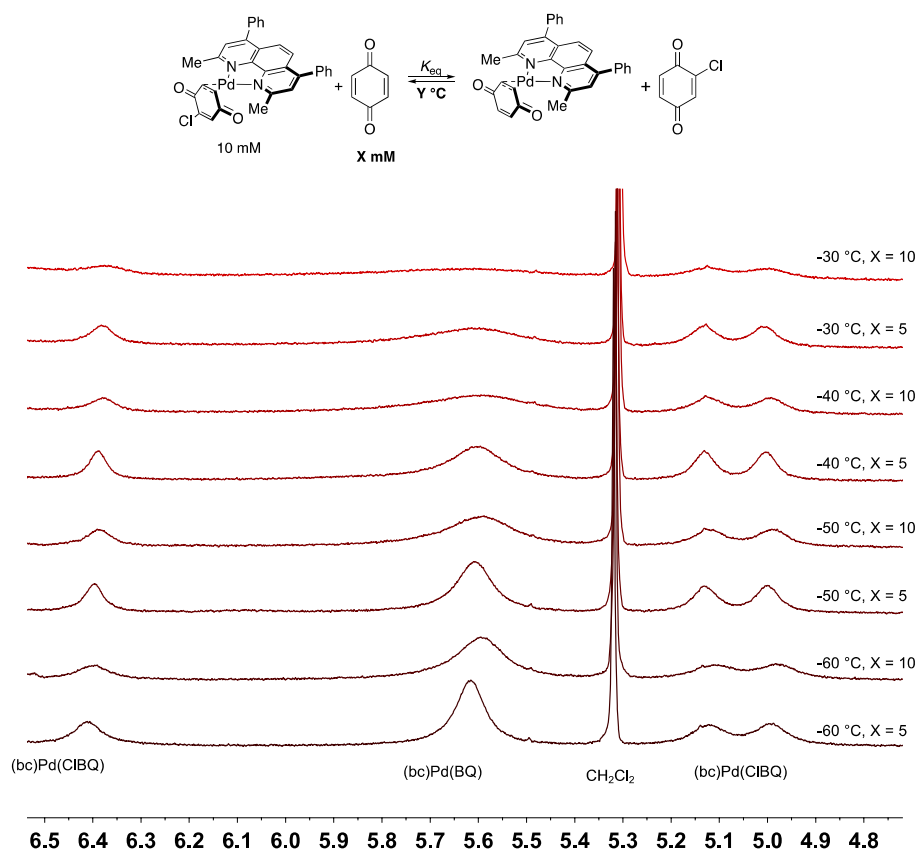
**Figure A.3.** Variable temperature ¹H NMR Spectra for exchange of BQ with (bc)Pd(CIBQ).

Table A.8. Equilibria data and van't Hoff plot for exchange of BQ with (bc)Pd(CIBQ).

Temp (°C)	[BQ] (mM)	K_{eq}	avg.
-60	50	0.052	0.050
	100	0.048	
-50	50	0.057	0.054
	100	0.052	
-40	50	0.064	0.058
	100	0.052	
-30	50	0.062	0.066
	100	0.071	

$y = -483.89x - 0.7405$
 $R^2 = 0.9806$

A.6 Quinone/hydroquinone Reduction Potential Determination by Open Circuit Potential (OCP) Measurements

General considerations: Open circuit potentials measurements and cyclic voltammetry measurements were performed at room temperature using a Pine Potentiostat/Galvanostat. The experiments were carried out in a three-electrode cell configuration with a glassy carbon working electrode (3 mm diameter) and a platinum wire counter electrode. The potentials were measured versus an Ag/AgCl reference electrode (all electrodes from BASi).

Measurements in 1,4-dioxane/AcOH: A 500 mM solution of tetrabutylammonium tetrafluoroborate (TBAB) in a 3:1 mixture of 1,4-dioxane:AcOH (vol:vol) was prepared. Equimolar quantities of BQ and H₂Q (0.1 mmol) were weighed into separate vials. The BQ and H₂Q were dissolved in 10 mL of the TBAB solution and the solution was purged with nitrogen for several minutes. An initial CV was recorded before the OCP was measured for 30-40 min. Following the OCP measurement, a second CV was recorded. Ferrocene was added to the BQ/H₂Q solution and a CV was recorded for reference. The value for the OCP was obtained from the average of the data following an initial equilibration period (approximately 200 s).

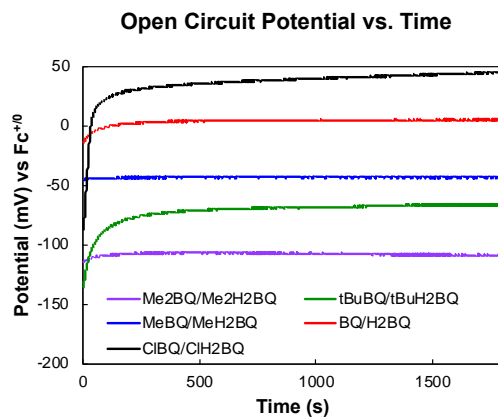


Figure A.4. Open circuit potential measurements (vs. $\text{Fc}^{+/0}$) for 1:1 mixtures of Q/H₂Q in 3:1 1,4-dioxane:AcOH with tetrabutylammonium tetrafluoroborate supporting electrolyte (500 mM).

Measurements in chloroform/AcOH: A 500 mM solution of tetrabutylammonium hexafluorophosphate (TBAP) in a 1.5 M solution of AcOH in chloroform was prepared. Equimolar quantities of BQ and H₂Q (0.1 mmol) were weighed into separate vials. The BQ and H₂Q were dissolved in 10 mL of the TBAP solution and the solution was purged with nitrogen for several minutes. An initial CV was recorded before the OCP was measured for 30-40 min. Following the OCP measurement, a second CV was recorded. Ferrocene was added to the BQ/H₂BQ solution and a CV was recorded for reference. In the case of 2-chlorobenzoquinone, ClBQ/ClH₂BQ redox events obscured the peaks of the ferrocene couple, so the ferrocene reference was recorded in fresh solvent free of quinone immediately following the measurement of the OCP. The value for the OCP was obtained from the average of the data following an initial equilibration period (approximately 200 s).

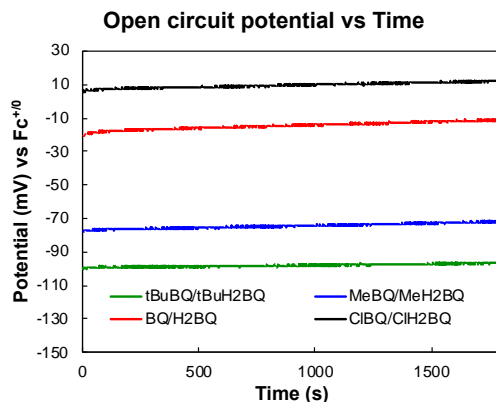


Figure A.5. Open circuit potential measurements (vs. $\text{Fc}^{+/0}$) for 1:1 mixtures of Q/H₂Q derivatives in chloroform/AcOH (1.5 M AcOH) with tetrabutylammonium hexafluorophosphate supporting electrolyte (500 mM).

A.7 Synthesis of (bathocuproine)Pd Complexes

Synthesis of (bathocuproine)Pd(OAc)₂: Palladium acetate (1.56 g, 6.94 mmol) and bathocuproine (2.5 g, 6.94 mmol) were dissolved in 25 mL of dichloromethane and stirred at room temperature overnight under air. The solvent was removed *in vacuo* to yield (bc)Pd(OAc)₂ (4.0 g, 98% yield).

¹H NMR (500 MHz, Chloroform-*d*) δ 7.79 (s, 2H), 7.559-7.52 (m, 6H), 7.49-7.44 (m, 4H), 7.42 (s, 2H), 2.99 (s, 6H), 2.03 (s, 6H)

¹³C NMR (126 MHz, CDCl₃) δ 178.57, 164.87, 150.99, 148.38, 135.55, 129.87, 129.40, 129.21, 126.99, 126.65, 124.39, 24.88, 23.09.

Synthesis of (bc)Pd(^tBuBQ): Into an over-dried 100 mL Teflon stoppered bomb flask equipped with a stir bar was added ^tBuH₂BQ (71.0 mg, 0.427 mmol) and (bc)Pd(OAc)₂ (250 mg, 0.427 mmol). The flask was evacuated, filled with 50 mL chloroform, and stirred at room temperature overnight. Chloroform was removed *in vacuo*, 10 mL of toluene were added and the red-orange solid was stirred for about 10 min before the toluene was removed *in vacuo* to remove acetic acid that is a byproduct of the reaction. This process was repeated three times. The flask was

transferred to a glovebox, where the solid was dissolved in chloroform (~10 mL) and filtered through a pad of Celite filter powder. The chloroform was removed under reduced pressure, and the resulting red-orange solid was washed with pentane (~20 mL) and toluene (~5 mL) to yield (bc)Pd(^tBuBQ) (223.5 mg, 83% yield). Single crystals suitable for X-ray diffraction were grown from vapor diffusion of pentane into a saturated toluene solution of Pd(bathocuproine)(^tBuBQ).

¹H NMR (500 MHz, Chloroform-*d*) δ 7.81 (s, 2H), 7.63 (d, *J* = 3.1 Hz, 2H), 7.58-7.52 (m, 6H), 7.52 – 7.45 (m, 3H), 6.15 (d, *J* = 2.2 Hz, 1H), 4.78 (dd, *J* = 7.0, 2.2 Hz, 1H), 4.64 (d, *J* = 6.9 Hz, 1H), 3.08 (s, 3H), 3.02 (s, 3H), 1.14 (s, 9H).

¹³C{¹H} NMR (126 MHz, CDCl₃) δ 191.39, 190.71, 162.61, 157.14, 150.02, 146.72, 146.69, 136.88, 136.84, 134.13, 129.59, 129.55, 129.33, 129.31, 129.01, 126.20, 126.01, 125.91, 125.81, 123.65, 123.60, 57.49, 55.91, 35.21, 29.40, 28.57, 28.41.

FTIR (ATR, cm⁻¹): 1583 (C=O), 1610 (C=O)

Synthesis of (bc)Pd(MeBQ): (bc)Pd(OAc)₂ (100 mg, 0.171 mmol) and MeH₂BQ (21.22 mg, 0.171 mmol) were dissolved in ~20 mL of chloroform in a 100 mL Teflon stoppered bomb flask and stirred at room temperature overnight. Pentane was vacuum transferred to the reaction to precipitate the product before it was moved to a glovebox. The resulting brown solid was washed with pentane, toluene and THF to yield the yield 32 mg of (bc)Pd(MeBQ) (32% yield).

¹H NMR (400 MHz, Chloroform-*d*) δ 7.80 (s, 2H), 7.62 (s, 2H), 7.59 – 7.42 (m, 10H), 6.15 (s, 1H), 4.78 (s, 2H), 3.07 (s, 3H), 3.05 (s, 3H), 1.84 (s, 3H).

¹³C{¹H} NMR (126 MHz, CDCl₃) δ 191.49, 191.02, 166.45, 162.65, 151.07, 150.09, 148.89, 146.72, 146.60, 136.83, 135.69, 135.48, 130.01, 129.54, 129.32, 126.92, 126.11, 126.00, 124.29, 123.62, 55.87, 28.39, 28.08, 16.95

FTIR (ATR, cm⁻¹): 1603 (C=O), 1613 (C=O)

Synthesis of (bc)Pd(BQ): (bc)•Pd(OAc)₂ (100 mg, 0.171 mmol) and H₂BQ (18.9 mg, 0.171 mmol) were dissolved in ~30 mL of chloroform in a 100 mL Teflon stoppered bomb flask and stirred at room temperature overnight. Pentane was vacuum transferred to the reaction to precipitate the product before it was moved to a glovebox. The resulting brown solid was washed with pentane to yield 34.1 mg of (bc)Pd(BQ) (35% yield). The product decomposed upon removal of solvent, so rigorous drying was forgone, hence the substantial pentane peak in the NMR spectra. ¹H NMR (400 MHz, Chloroform-*d*) δ 7.81 (s, 2H), 7.63 (s, 2H), 7.59 – 7.46 (m, 10H), 5.55 (s, 4H), 3.06 (s, 6H). ¹³C{¹H} NMR (126 MHz, CDCl₃) δ 190.41, 162.47, 150.06, 146.58, 136.63, 129.39, 129.21, 128.90, 126.01, 123.52, 116.14, 28.06.

FTIR (ATR, cm⁻¹): 1642 (C=O)

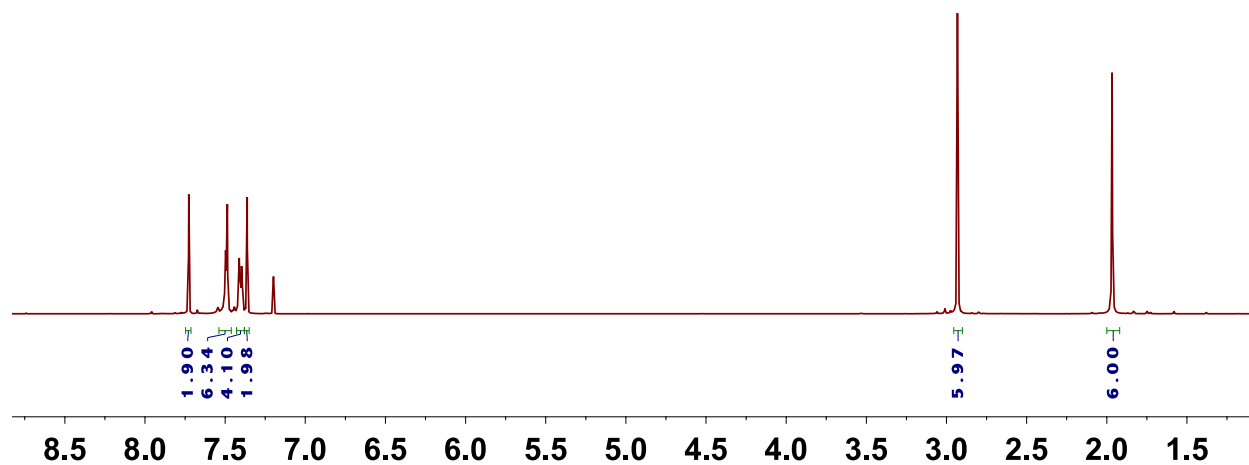
Synthesis of (bc)Pd(CIBQ): (bc)Pd(OAc)₂ (100 mg, 0.171 mmol) and ClH₂BQ (24.7 mg, 0.171 mmol) were dissolved in ~20mL of chloroform and stirred at room temperature overnight. The product was precipitated out of solution with pentane and the resulting brown solid was washed with pentane, toluene, and THF to yield (bc)Pd(CIBQ) in 69% yield (71.9 mg) as a brown solid.

¹H NMR (400 MHz, Chloroform-*d*) δ 7.82 (s, 2H), 7.63 (s, 2H), 7.60 – 7.45 (m, 10H), 6.33 (s, 1H), 5.13 (d, *J* = 7.3 Hz, 1H), 5.01 (d, *J* = 7.4 Hz, 1H), 3.04 (s, 3H), 3.02 (s, 3H). ¹³C{¹H} NMR (126 MHz, CDCl₃) δ 188.76, 182.88, 162.76, 162.66, 150.38, 136.71, 129.53, 129.40, 129.06, 126.14, 125.14, 67.09, 66.82, 28.24, 28.09.

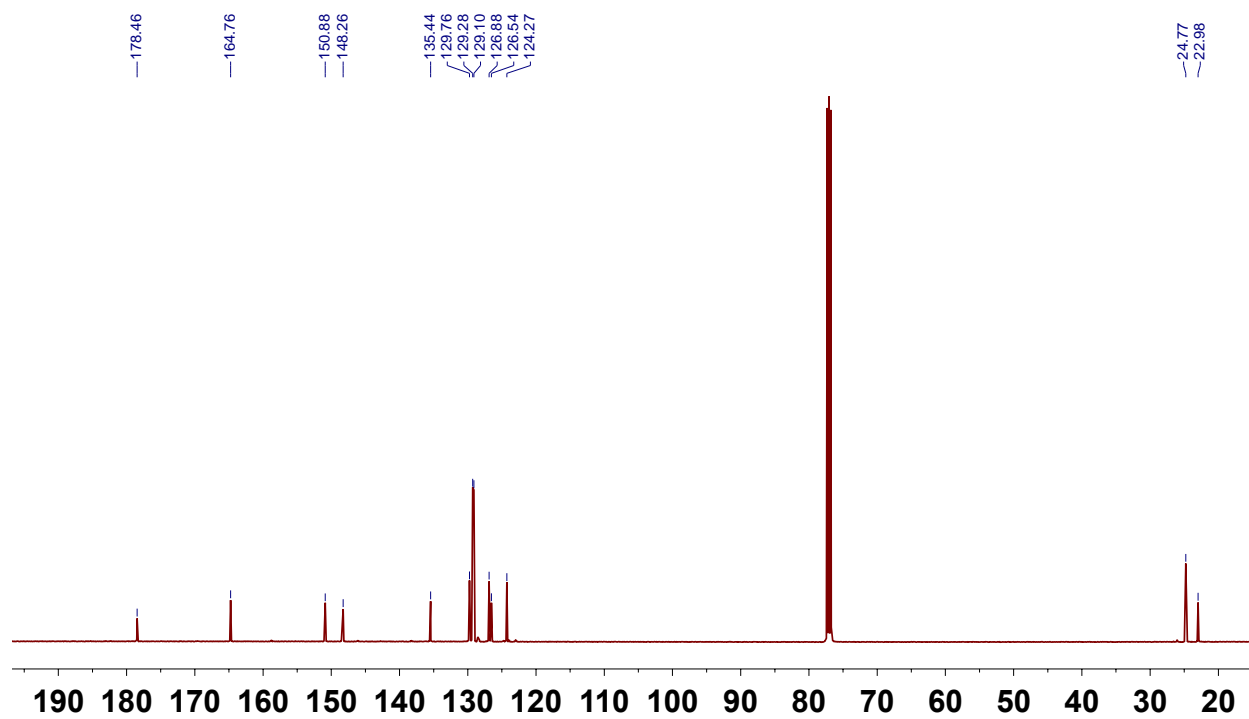
FTIR (ATR, cm⁻¹): 1620 (C=O), 1642 (C=O)

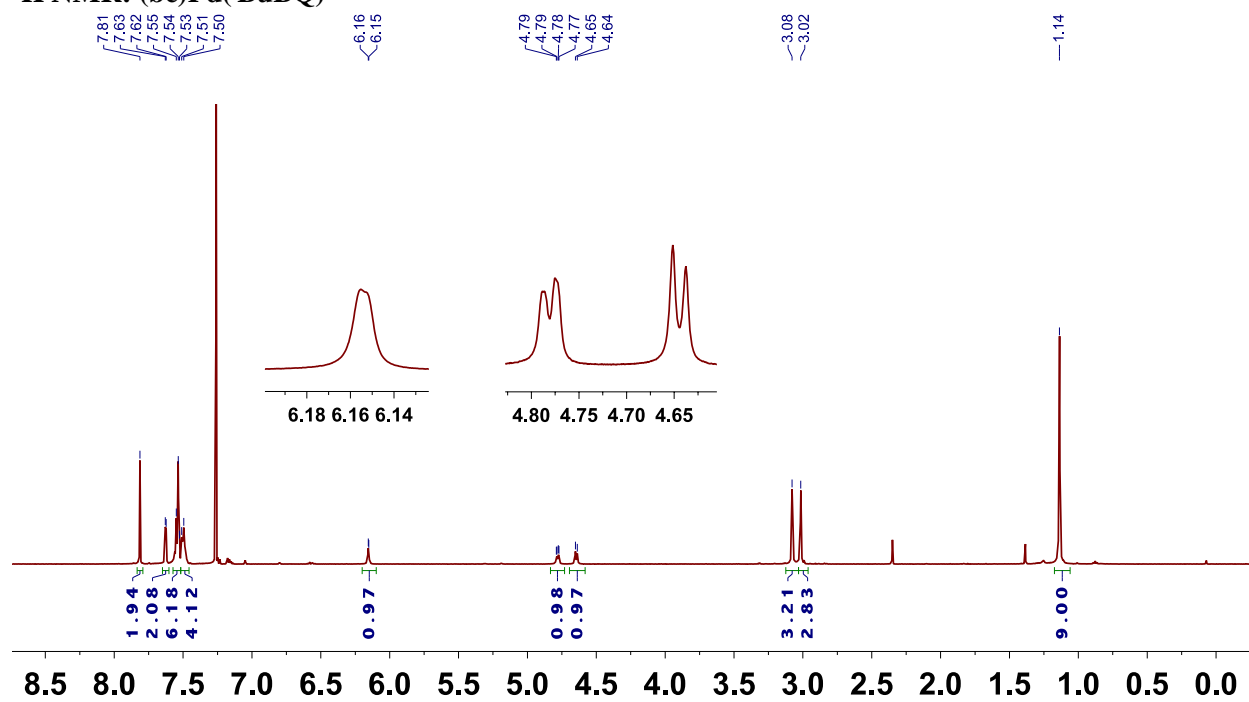
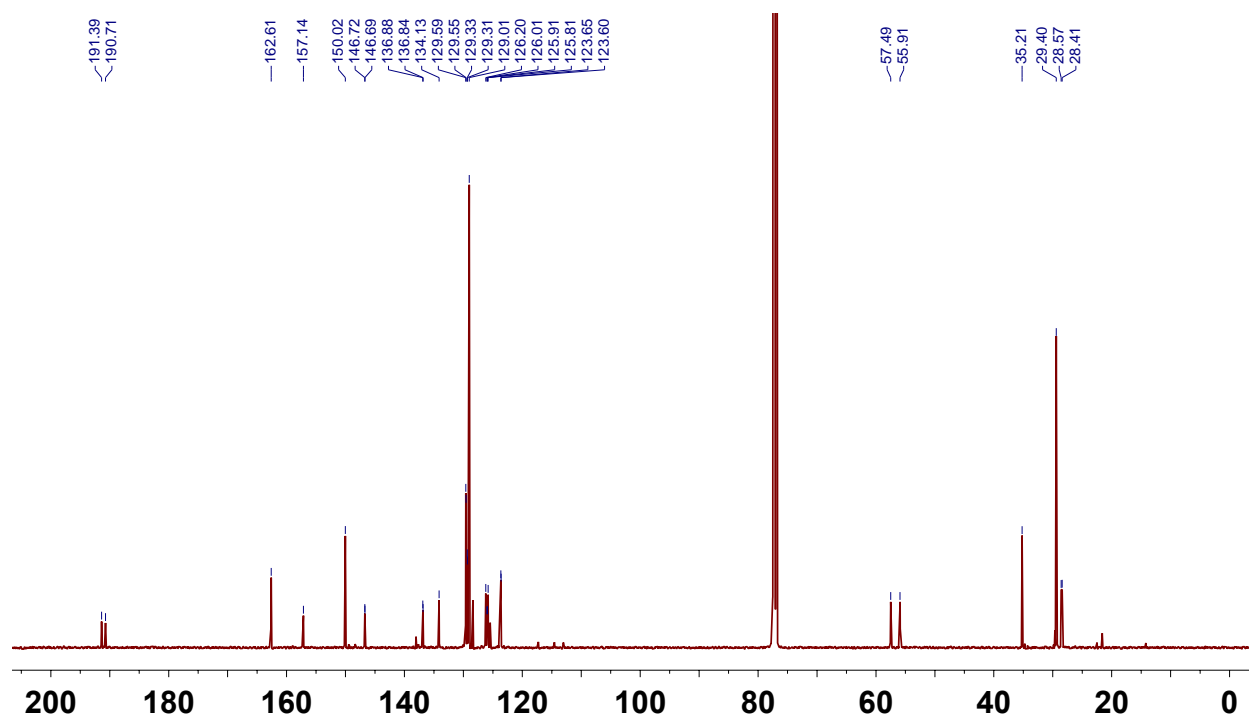
A.8 NMR Spectroscopic Data

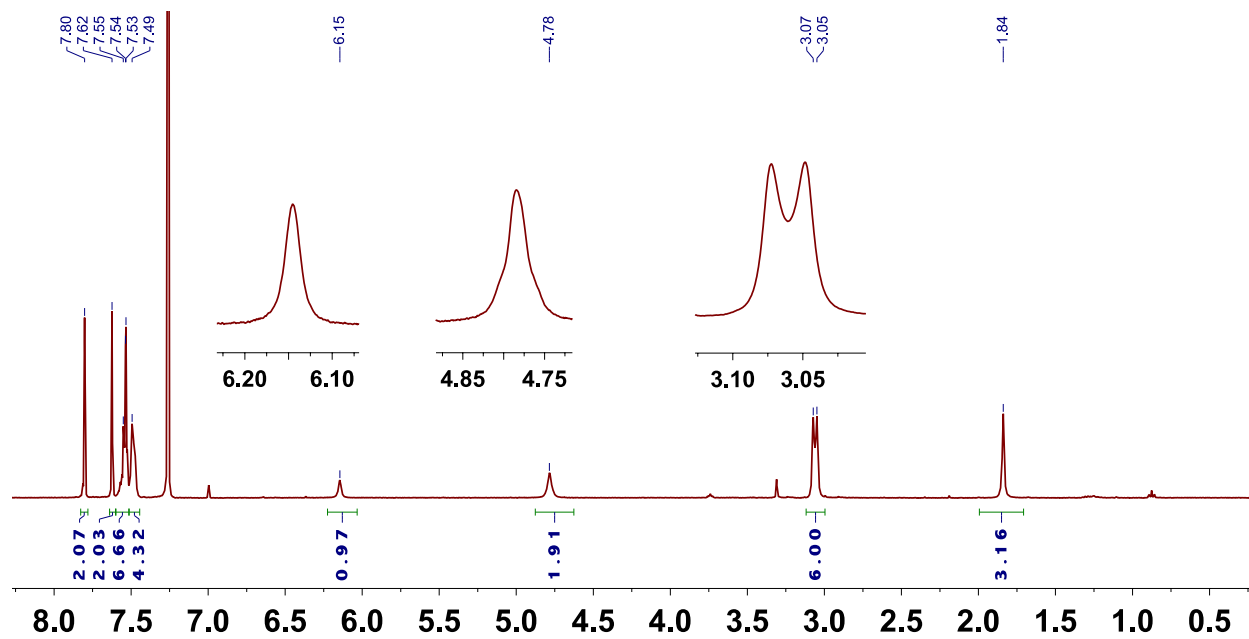
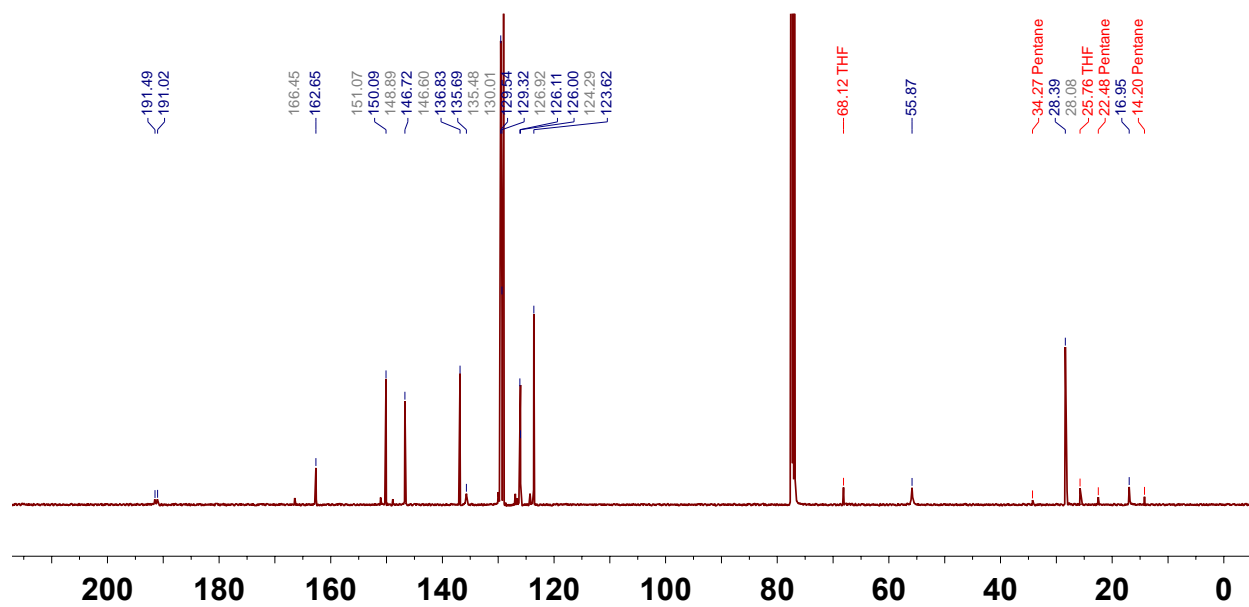
^1H NMR: (bc)Pd(OAc)₂

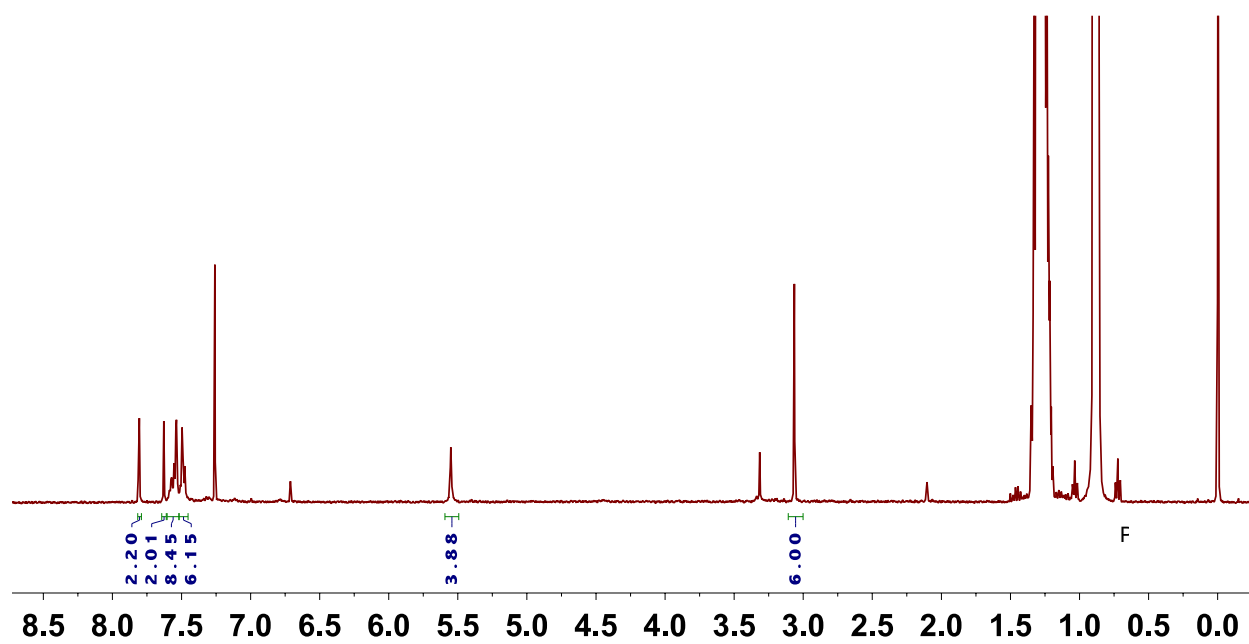
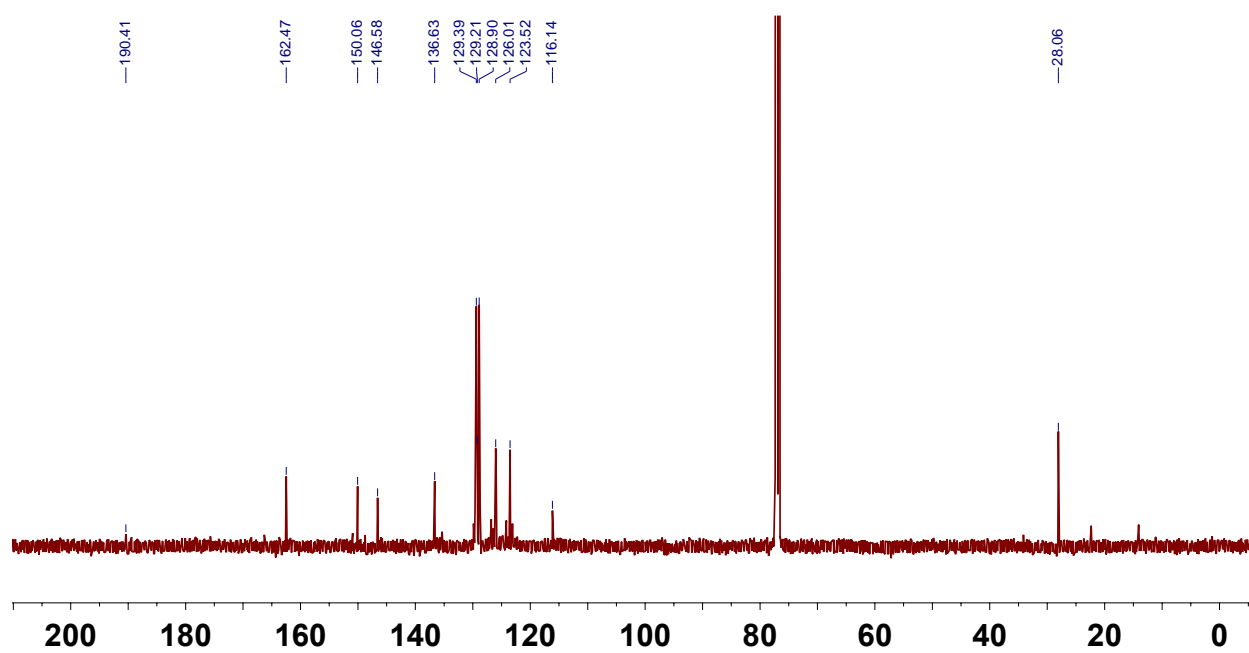


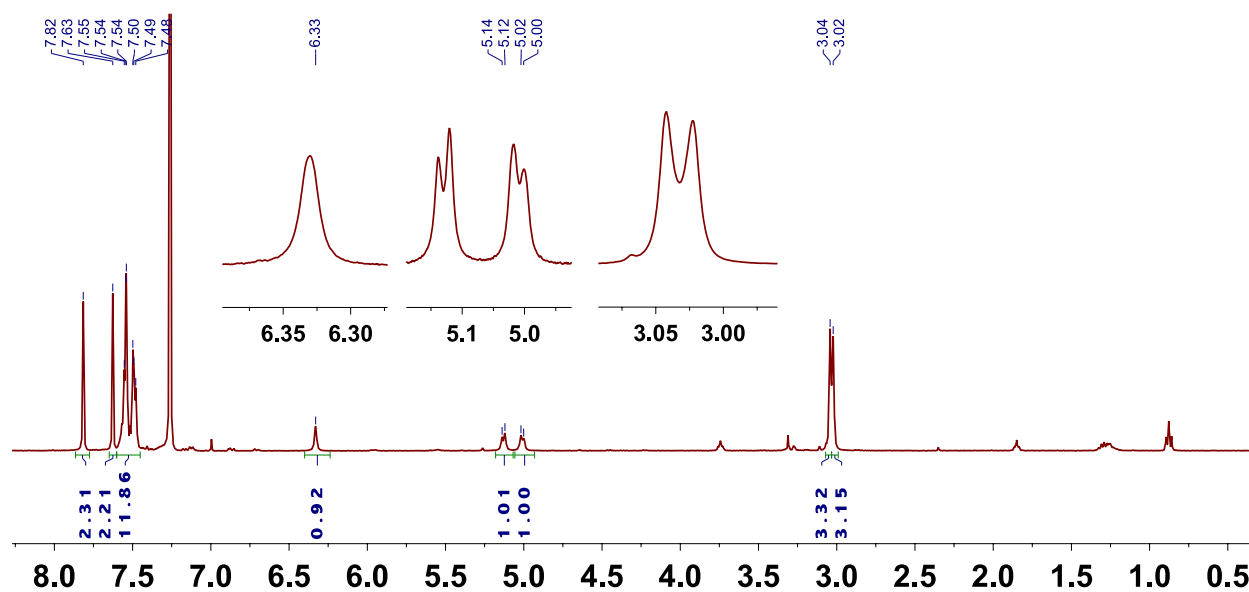
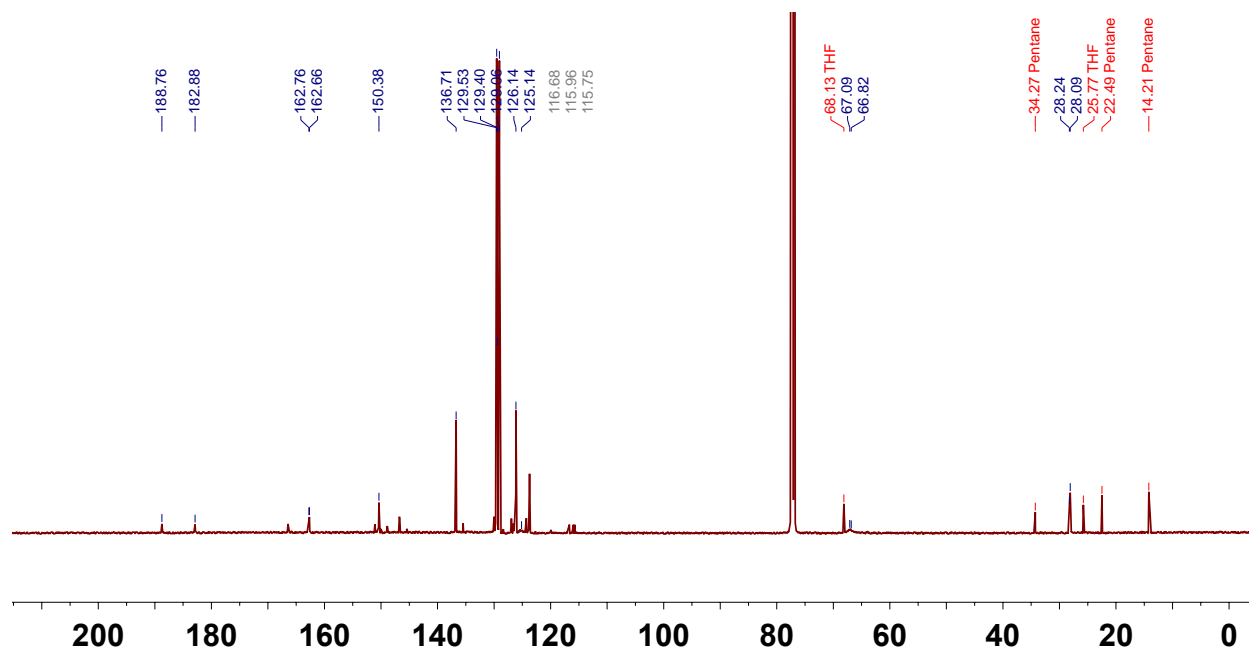
$^{13}\text{C}\{^1\text{H}\}$ NMR: (bc)Pd(OAc)₂



^1H NMR: (bc)Pd(BuBQ) $^{13}\text{C}\{^1\text{H}\}$ NMR: (bc)Pd(BuBQ)

^1H NMR: (bc)Pd(MeBQ) **$^{13}\text{C}\{^1\text{H}\}$ NMR: (bc)Pd(MeBQ)**

^1H NMR: (bc)Pd(BQ) **$^{13}\text{C}\{^1\text{H}\}$ NMR: (bc)Pd(BQ)**

^1H NMR: (bc)Pd(CIBQ) $^{13}\text{C}\{^1\text{H}\}$ NMR: (bc)Pd(CIBQ)

A.9 Crystal Structure Data

Data Collection: An orange crystal with approximate dimensions 0.12 x 0.09 x 0.01 mm³ was selected under oil under ambient conditions and attached to the tip of a MiTeGen MicroMount©. The crystal was mounted in a stream of cold nitrogen at 100(1) K and centered in the X-ray beam by using a video camera. The crystal evaluation and data collection were performed on a Bruker Quazar SMART APEXII diffractometer with Mo K α ($\lambda = 0.71073$ Å) radiation and the diffractometer.

The initial cell constants were obtained from three series of ω scans at different starting angles. Each series consisted of 12 frames collected at intervals of 0.5° in a 6° range about ω with the exposure time of 20 s per frame. The reflections were successfully indexed by an automated indexing routine built in the APEXII program suite. The final cell constants were calculated from a set of 9981 strong reflections from the actual data collection. The data were collected by using the full sphere data collection routine to survey the reciprocal space to the extent of a full sphere to a resolution of 0.83 Å. A total of 75418 data were harvested by collecting 4 sets of frames with 0.5° scans in ω and ϕ with exposure times of 120 sec per frame. These highly redundant datasets were corrected for Lorentz and polarization effects. The absorption correction was based on fitting a function to the empirical transmission surface as sampled by multiple equivalent measurements.

Structure Solution and Refinement: The systematic absences in the diffraction data were consistent for the space group $P1$ and $P\bar{1}$ that yielded chemically reasonable and computationally stable results of refinement.^{3,4}

A successful solution by charge-flipping provided most non-hydrogen atoms from the E-map. The remaining non-hydrogen atoms were located in an alternating series of least-squares cycles and difference Fourier maps. All non-hydrogen atoms were refined with anisotropic

displacement coefficients. All hydrogen atoms were included in the structure factor calculation at idealized positions and were allowed to ride on the neighboring atoms with relative isotropic displacement coefficients.

The asymmetric unit contains one molecule of the palladium complex shown in Figure A.6 and 2.5 molecules of toluene. The toluene molecules occupy three positions within the asymmetric unit. Toluene molecule C37-C43 is fully occupied and has two disordered components (major occupancy: 61.5(7)%). Toluene molecule C44-C50 is fully occupied and has two disordered components (major occupancy: 58.2(8)%). Toluene molecule C51-C57 resides on an inversion center and is half occupied. All toluene molecules were constrained to have an idealized geometry⁵ and thermal parameter constraints were used on the disordered toluene molecules in order to obtain a chemically reasonable and computationally stable refinement.

The final least-squares refinement of 442 parameters against 10640 data resulted in residuals R (based on F2 for $I \geq 2\sigma$) and wR (based on F2 for all data) of 0.0510 and 0.1363, respectively. The final difference Fourier map featured 2 peaks of residual electron density (2.59 e/A³) in vicinity of Pd in chemically unreasonable positions and were considered noise.

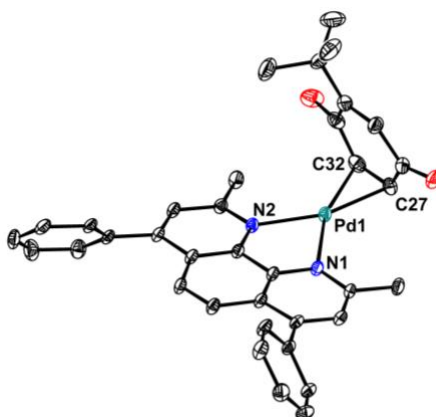


Figure A.6. Single XRD structure of (bc)Pd(*t*BuBQ)

Table A.9. Crystal data and structure refinement for (bc)Pd(*t*BuBQ)

Identification code	stahl246_c
Empirical formula	C ₃₆ H ₃₂ N ₂ O ₂ Pd (2.5 C ₇ H ₈)
Formula weight	1722.74
Temperature/K	100
Crystal system	triclinic
Space group	<i>P</i> $\bar{1}$
<i>a</i> /Å	10.619(3)
<i>b</i> /Å	13.727(4)
<i>c</i> /Å	14.993(5)
α /°	85.713(16)
β /°	80.258(13)
γ /°	82.221(16)
Volume/Å ³	2131.1(12)
<i>Z</i>	1
ρ_{calc} mg/mm ³	1.342
μ /mm ⁻¹	0.572
<i>F</i> (000)	898
Crystal size/mm ³	0.12 × 0.09 × 0.01
Radiation	MoK α (λ = 0.71073)
2 Θ range for data collection	2.3154 to 28.2760°
Index ranges	-14 ≤ <i>h</i> ≤ 14, -18 ≤ <i>k</i> ≤ 17, -20 ≤ <i>l</i> ≤ 19
Reflections collected	44651
Independent reflections	10640 [R _{int} = 0.0439, R _{sigma} = 0.0404]
Data/restraints/parameters	10640/0/442
Goodness-of-fit on <i>F</i> ²	1.077
Final <i>R</i> indexes [<i>I</i> ≥ 2 σ (<i>I</i>)]	<i>R</i> ₁ = 0.0510, <i>wR</i> ₂ = 0.1302
Final <i>R</i> indexes [all data]	<i>R</i> ₁ = 0.0606, <i>wR</i> ₂ = 0.1363
Largest diff. peak/hole / e Å ⁻³	2.59/-1.539

A.10 Computational Data

Computational Procedure: Geometry optimizations and frequency calculations for all reported structures were performed with the Gaussian 09 suite of programs⁶ at the B3LYP-D3(BJ)/[6-31G(d,p) + Lanl2dz (Pd)] level of theory with the corresponding Hay-Wadt effective core potential for Pd, and Grimme's empirical dispersion-correction (D3) with Becke-Johnson (BJ) damping for B3LYP.⁷⁻¹² Frequency analysis was used to characterize each minimum with zero imaginary frequency. Bulk solvent effects were incorporated for all calculations (including the geometry optimization and frequency calculations) using the self-consistent reaction field polarizable continuum model (IEF-PCM).¹³⁻¹⁵ As a solvent we chose chloroform ($\epsilon = 4.7113$). Calculated cartesian coordinates of all studied systems are given below.

Computational Structures and Coordinates

H₂BQ

O 4.45305900 -0.86146400 1.03417100
 C 4.66532500 -0.53487200 2.34911300
 C 4.58289200 0.77678600 2.82801300
 C 4.97646700 -1.57143600 3.23362000
 C 4.80898200 1.04861700 4.17658300
 H 4.34190500 1.58979300 2.14795600
 C 5.20255900 -1.29960500 4.58219000
 H 5.03923800 -2.58686600 2.85668400
 C 5.12012300 0.01205200 5.06109100
 H 4.74622100 2.06404800 4.55351700
 H 5.44355800 -2.11261100 5.26224400
 O 5.33239900 0.33864700 6.37603000
 H 5.53541600 -0.46505100 6.87337700
 H 4.25001800 -0.05776800 0.53683000

BQ

O 4.71524800 -0.58956300 1.06285100
 C 4.79725700 -0.43853600 2.27846700
 C 4.72065500 0.91021400 2.89337200
 C 4.97578200 -1.59801500 3.18772000
 C 4.80983400 1.07520300 4.22241600
 H 4.58975800 1.74238000 2.20891300
 C 5.06496100 -1.43302300 4.51676400
 H 5.02904100 -2.57380700 2.71536500
 C 4.98841800 -0.08426900 5.13166100

H 4.75652600 2.05099100 4.69477600
H 5.19581100 -2.26519500 5.20122700
O 5.07018100 0.06673500 6.34729900

AcOH

C -1.68307800 2.56092600 1.48944900
O -2.24174000 2.59552400 0.25868600
C -2.06637500 3.76590600 2.30582200
H -1.59598800 3.71090100 3.28637900
H -1.75245200 4.67845000 1.79120200
H -3.15378300 3.80892800 2.41528000
O -0.96591000 1.65138100 1.85492400
H -1.95251700 1.79195600 -0.20688500

py

C -1.86615700 -1.74287100 -1.61577200
C -1.99595100 -2.77236900 -2.54878700
N -1.10495500 -0.65519400 -1.80864700
C -1.29799200 -2.67139600 -3.75205000
C -0.44030400 -0.57325800 -2.97070500
C -0.50219100 -1.54692100 -3.96868200
H -1.37238000 -3.45157400 -4.50331900
H 0.05951000 -1.42234400 -4.88838400
H -2.62794300 -3.62753500 -2.33392700
H 0.17309100 0.31467800 -3.11200000
H -2.39921100 -1.79420400 -0.66827900

bpy

C -2.83785600 -0.80583600 1.80451700
N -2.31303300 -0.74000200 0.57669600
C -2.27256800 -1.87008400 -0.15362100
C -2.74824300 -3.09496600 0.33784700
C -3.29234100 -3.14625800 1.61873800
C -3.34369900 -1.97609900 2.37349700
H -3.66064700 -4.08463900 2.02114800
H -3.75775500 -1.96536800 3.37586200
C -1.69001700 -1.77404000 -1.52317500
C -2.16083100 -2.59345300 -2.56007400
N -0.70848200 -0.87183700 -1.71080700
C -1.58868400 -2.48254000 -3.82490100
C -0.16962900 -0.77772500 -2.93074600
C -0.56598700 -1.55646200 -4.01970300
H -1.94191400 -3.10223200 -4.64303800
H -0.08916600 -1.43319500 -4.98601900
H -2.97476600 -3.28756400 -2.38464100
H -2.67247900 -3.99398800 -0.26289400
H 0.62500000 -0.04291300 -3.04668900
H -2.85908400 0.12668800 2.36557800

dmbpy

C -2.66102000 -0.85699200 1.89520800

N -2.21104700 -0.77683000 0.63327800
C -2.19992900 -1.88579600 -0.12483900
C -2.63396400 -3.12921100 0.35750400
C -3.10016800 -3.21075900 1.66612100
C -3.11806100 -2.05963000 2.44962900
H -3.43574100 -4.16009200 2.07204100
H -3.47356600 -2.08697400 3.47423300
C -1.69423700 -1.74829700 -1.52210500
C -2.22234700 -2.54092300 -2.55162800
N -0.72978900 -0.83762700 -1.73719500
C -1.72067200 -2.38173800 -3.83987200
C -0.24599100 -0.68676500 -2.98007300
C -0.71570500 -1.44370300 -4.06144400
H -2.11424000 -2.97380700 -4.66033200
H -0.30176100 -1.29242400 -5.05274000
H -3.02207500 -3.24451400 -2.35160800
H -2.58345000 -4.01234600 -0.26851700
C 0.84388100 0.33979000 -3.15411900
H 0.51997400 1.30934300 -2.76344800
H 1.73660400 0.04749000 -2.59074100
H 1.12169800 0.45823500 -4.20387000
C -2.65538400 0.42391100 2.68974700
H -1.65171400 0.86031100 2.70089200
H -3.32172700 1.16141900 2.22980600
H -2.97860200 0.26042700 3.72025300

dmphen

C -3.39042900 -0.70264400 1.50794400
N -2.87969600 -0.71553200 0.28308100
C -2.32462500 -1.86002000 -0.18879700
C -2.26863600 -3.05334200 0.58288500
C -2.81967100 -3.01207100 1.88462400
C -3.37856500 -1.84491500 2.34879600
H -2.79391900 -3.90537700 2.50232200
H -3.80811100 -1.78648100 3.34377300
C -1.76660200 -1.86856400 -1.53250400
C -1.18547800 -3.06989700 -2.02438300
N -1.81964700 -0.73206700 -2.27142400
C -0.65189500 -3.04483000 -3.33381000
C -1.31254700 -0.73458500 -3.49785900
C -0.71295500 -1.88547500 -4.07024100
H -0.19960900 -3.94435400 -3.74194700
H -0.31123000 -1.83968000 -5.07739600
C -1.15139200 -4.24835500 -1.21155900
C -1.67409400 -4.24038900 0.04631000
H -0.69988000 -5.14736200 -1.62100900
H -1.64970500 -5.13277900 0.66494800
C -3.99724800 0.58674800 1.99702700
H -3.47787600 0.94893700 2.89140600
H -3.93349800 1.34831500 1.21854100
H -5.04845100 0.44543300 2.27181200

C -1.39154500 0.54631400 -4.28729700
H -1.88359800 1.31961100 -3.69564700
H -0.39165800 0.89590700 -4.56794500
H -1.95254700 0.39933000 -5.21699500

phen

C -3.31593200 -0.69200700 1.52916900
N -2.82278600 -0.68850100 0.29921000
C -2.30183100 -1.84261600 -0.18400900
C -2.27085400 -3.04227200 0.58287900
C -2.80619900 -3.00278600 1.88940500
C -3.33287700 -1.82295400 2.37036800
H -2.79495400 -3.90333500 2.49658400
H -3.75210400 -1.75399800 3.36821800
C -1.75506400 -1.85778900 -1.53366500
C -1.20895600 -3.07201400 -2.03951400
N -1.78343900 -0.71729100 -2.26527200
C -0.68430700 -3.06189500 -3.35093700
C -1.28173800 -0.74838900 -3.49136100
C -0.71828100 -1.89567700 -4.08545900
H -0.26132600 -3.97394000 -3.76217600
H -0.32491200 -1.84938000 -5.09506800
C -1.20030400 -4.25568400 -1.23026500
C -1.71090300 -4.24134700 0.03100500
H -0.77662600 -5.16421300 -1.64801800
H -1.70407600 -5.13799200 0.64366100
H -3.72652200 0.25074600 1.88735400
H -1.31961100 0.18419800 -4.05216600

DAF

O -7.48897300 15.23785400 20.51363700
N -5.83333400 12.25921600 17.15453700
N -4.43346300 14.99638400 16.83908400
C -6.57549600 11.18701900 17.50445000
H -6.42734600 10.29275400 16.90428500
C -7.49113700 11.16734600 18.56021600
H -8.04615100 10.26045100 18.77187400
C -7.67669100 12.32263600 19.32950000
H -8.37604400 12.35470800 20.15873300
C -6.92036100 13.42914600 18.97971300
C -6.85521700 14.80448200 19.56612000
C -5.84336100 15.53254400 18.73806900
C -5.36781000 16.83140000 18.81189600
H -5.72870500 17.52370800 19.56567800
C -4.40230300 17.20061700 17.86723900
H -3.98119900 18.19956800 17.86024700
C -3.97708700 16.26446200 16.92050000
H -3.22766100 16.54582000 16.18491900
C -5.34836300 14.66529300 17.74400000
C -6.02377300 13.34526900 17.89598100

(py)₂Pd(AcO)₂

Pd -1.99306700 0.93453400 -0.89950300
C -1.85740200 2.58180700 1.44574300
O -2.27539800 2.63563900 0.20563600
C -2.12018100 3.86926600 2.21304000
H -1.67177500 3.81755500 3.20567500
H -1.71640700 4.72563500 1.66593500
H -3.19951500 4.02424700 2.30962100
O -1.31684600 1.60758800 1.97184700
O -1.71071000 -0.76655900 -2.00466600
C -2.12748400 -0.71226100 -3.24517200
O -2.66652300 0.26254000 -3.77174400
C -1.86617800 -2.00036600 -4.01188500
H -2.27945400 -2.85465200 -3.46853600
H -2.30701900 -1.94523500 -5.00771100
H -0.78717000 -2.16207000 -4.10025200
N -0.17763900 1.66998400 -1.56274100
C 0.76998900 0.82737200 -2.01672100
C 0.06287400 2.99504200 -1.54503700
C 2.00008600 1.28843100 -2.47020400
H 0.50425400 -0.22208600 -2.01789700
C 1.26847300 3.52391800 -1.99024600
H -0.73357600 3.61184000 -1.14857700
C 2.25588000 2.65899300 -2.46021200
H 2.73795800 0.57802200 -2.82418200
H 1.42184800 4.59640600 -1.96399500
H 3.20667000 3.04566700 -2.81153700
N -3.80855800 0.19904000 -0.23621700
C -4.04955200 -1.12592000 -0.25517400
C -4.75571600 1.04150800 0.21902400
C -5.25515400 -1.65483100 0.18998100
H -3.25345700 -1.74258000 -0.65256800
C -5.98577600 0.58040600 0.67256500
H -4.48962900 2.09087600 0.22111000
C -6.24206300 -0.79005200 0.66126300
H -5.40891700 -2.72723800 0.16267700
H -6.72324400 1.29071200 1.02759200
H -7.19284100 -1.17675600 1.01258700

(py)₂Pd(BQ)

C -3.22359700 0.80287400 1.67747500
N -2.71411600 0.21448300 0.57907100
C -2.46186500 -1.10716600 0.61538800
C -2.72233000 -1.89009700 1.73567000
C -3.26450200 -1.28251000 2.86775800
C -3.51514700 0.08880600 2.83629600
H -3.48170500 -1.86464200 3.75726300
H -3.92694500 0.60667200 3.69518600
Pd -2.18707000 1.46420900 -1.16287600
C -3.79748800 -0.87721300 -2.56444900
C -4.32293700 -1.64744200 -3.59720000

N -2.97669100 0.16627900 -2.78118800
C -3.98937500 -1.32498300 -4.91211900
C -2.66767900 0.48626100 -4.05280800
C -3.15005100 -0.23546400 -5.14097800
H -4.38079200 -1.90622700 -5.74056800
H -2.87135400 0.06095800 -6.14593300
C -1.19485900 3.20046100 -1.95489800
C -2.23207000 3.79312300 -2.79777100
C -1.25407800 3.28936000 -0.53063200
C -3.36726000 4.45782100 -2.09719200
O -2.20272600 3.75495400 -4.03833400
C -2.37600700 3.96632600 0.12732500
H -0.36711700 3.13005600 0.07577100
C -3.43276600 4.53481900 -0.75671400
H -4.13288400 4.88888300 -2.73636300
O -2.48297600 4.06884900 1.35989300
H -4.25505800 5.03133600 -0.24892100
H -0.26286600 2.95123700 -2.45466100
H -2.04228000 1.36199300 -4.19084400
H -3.37506900 1.87642500 1.62425700
H -2.50128200 -2.95120000 1.71390500
H -4.98078000 -2.47809200 -3.36773100
H -2.03733500 -1.53867000 -0.28474600
H -4.03872500 -1.09126600 -1.52971300

(bpy)Pd(AcO)₂

C -2.88479500 -0.69479100 1.70620400
N -2.35431000 -0.78012000 0.47978200
C -2.22668200 -1.98219400 -0.14138200
C -2.63878600 -3.15070500 0.49729900
C -3.18416300 -3.07125900 1.77746200
C -3.31214000 -1.82752200 2.39248600
H -3.50784700 -3.97336400 2.28448600
H -3.73569200 -1.72708500 3.38440800
Pd -1.73970600 0.82632800 -0.62706900
C -1.26247300 2.65433600 1.50053000
O -2.26152700 2.18175300 0.80230800
C -1.69273000 3.71113900 2.50919900
H -0.83559400 4.04832000 3.09321400
H -2.13860400 4.56295300 1.98695400
H -2.45727000 3.30397700 3.17747300
O -0.08556500 2.30297800 1.39044600
O -1.05455600 2.28052200 -1.87875700
C -1.98133200 2.92376200 -2.53919400
O -3.18991700 2.68203200 -2.49400800
C -1.64083100 -1.93030900 -1.49376100
C -1.39657700 -3.04629200 -2.29256500
N -1.33084800 -0.68536200 -1.94215700
C -0.82818300 -2.87068600 -3.55298500
C -0.77584600 -0.50942200 -3.14792900
C -0.50926500 -1.58609700 -3.98837200

H -0.63422400 -3.73111000 -4.18360100
H -0.06105400 -1.41183200 -4.95900600
C -1.41705500 4.02942800 -3.42182000
H -0.75541000 3.59753800 -4.17923300
H -2.22552000 4.57241600 -3.91264700
H -0.81700500 4.72000900 -2.82260300
H -1.64167700 -4.03907600 -1.93797600
H -2.54045500 -4.10949200 0.00471700
H -0.54906700 0.51751900 -3.40873100
H -2.96037900 0.30799300 2.10980100

(bpy)₂Pd(BQ)

C -1.88535100 0.20179100 1.64709300
N -1.72584600 -0.10438700 0.35321600
C -1.83864000 -1.38545000 -0.06341900
C -2.10435600 -2.40936400 0.85097700
C -2.25805900 -2.09633800 2.19966100
C -2.15296000 -0.76841400 2.60954800
H -2.46328100 -2.88240000 2.91830700
H -2.27498600 -0.48410000 3.64815200
Pd -1.26788200 1.39022300 -1.17714800
C -1.68425400 -1.61504000 -1.52404400
C -1.75426400 -2.88488600 -2.10515800
N -1.48117300 -0.51504400 -2.28682400
C -1.62089900 -3.01381000 -3.48537000
C -1.35810000 -0.64022600 -3.61472100
C -1.42307900 -1.87259000 -4.25976600
H -1.67311200 -3.99409200 -3.94657800
H -1.31950200 -1.92795200 -5.33703200
C -0.78853800 3.33072900 -1.99526900
C -1.94798100 3.66487200 -2.82887200
C -0.87481700 3.38248600 -0.56933000
C -3.21606600 3.99132900 -2.11272100
O -1.91458200 3.69264400 -4.06640700
C -2.13137900 3.73142900 0.10455900
H 0.02297600 3.45024800 0.03946400
C -3.30039100 4.02468800 -0.77130400
H -4.06855900 4.22150000 -2.74603300
O -2.24918500 3.77258500 1.33854900
H -4.22412600 4.28080500 -0.25958800
H 0.17654000 3.36105800 -2.49287900
H -1.20673900 0.28219800 -4.16492100
H -1.80365800 1.25599800 1.89818700
H -2.19620900 -3.43656900 0.52275900
H -1.90954800 -3.76506800 -1.49483200

(dmbpy)Pd(AcO)₂

C -2.50985600 -0.87468800 1.90622400
N -2.19339100 -0.80078000 0.59651800
C -2.45237300 -1.84970300 -0.23535800
C -3.12873200 -2.97896000 0.21778800

C -3.51177900 -3.04546800 1.55448700
C -3.17685800 -2.00184300 2.40424800
H -4.04146000 -3.91481000 1.92825600
H -3.42174400 -2.04040500 3.45902300
Pd -1.62925700 0.88063400 -0.50619900
C -1.48358800 3.01551700 1.36759400
O -2.37710800 2.30757600 0.73701400
C -2.08413300 4.18888500 2.12976900
H -1.29531000 4.85835900 2.47532800
H -2.79334800 4.73489700 1.50301300
H -2.63530500 3.81215000 2.99824100
O -0.27437800 2.76764900 1.41173600
O -1.21316100 2.45706800 -1.72464200
C -2.13325400 2.70016800 -2.61414400
O -3.14909400 2.02328600 -2.80222500
C -1.88678600 -1.75152000 -1.59663300
C -2.00316800 -2.76733300 -2.54048900
N -1.15270500 -0.63230000 -1.85432100
C -1.31732000 -2.64885500 -3.74711300
C -0.42561200 -0.53661700 -2.98500700
C -0.50196900 -1.54687600 -3.95367000
H -1.39772500 -3.42618000 -4.49895900
H 0.08800700 -1.44945700 -4.85753500
C -1.83812200 3.94516500 -3.44140400
H -0.82829200 3.89589700 -3.85851600
H -2.56764100 4.04745800 -4.24567900
H -1.88029100 4.82987700 -2.79839800
H -2.60502500 -3.64312100 -2.34053900
H -3.34186200 -3.80144200 -0.45104600
C 0.49587200 0.62822500 -3.19398100
H 0.03492100 1.37698000 -3.84366000
H 0.74275000 1.11407000 -2.25271200
H 1.40794100 0.27748400 -3.68373900
C -2.13330500 0.24526600 2.82604000
H -1.17191100 0.67725100 2.54498500
H -2.87703900 1.04374900 2.76973800
H -2.08790200 -0.12017100 3.85363800

(dmbpy)Pd(BQ)

C -1.52794000 0.13096600 1.77070100
N -1.54408600 -0.08362300 0.44091800
C -1.96142700 -1.27098500 -0.05768100
C -2.43203500 -2.28131500 0.78468600
C -2.45377400 -2.05891500 2.15825000
C -1.98603300 -0.84954800 2.65830100
H -2.81803200 -2.82957600 2.82930000
H -1.96907500 -0.65470000 3.72433200
Pd -1.24833600 1.47348800 -1.10117300
C -1.83934300 -1.45658900 -1.52854400
C -2.21896300 -2.64072300 -2.16504400
N -1.29232100 -0.43292900 -2.22550900

C -2.00743900 -2.76803700 -3.53473600
C -1.04999400 -0.55762200 -3.54464500
C -1.40398300 -1.72635600 -4.22893000
H -2.29820900 -3.67817000 -4.04859000
H -1.20371400 -1.80482500 -5.29122100
C -1.09874900 3.38162400 -2.05652000
C -2.26155900 3.46919900 -2.94565900
C -1.24443200 3.56244700 -0.64512300
C -3.59339100 3.65536800 -2.30535100
O -2.18263000 3.39979700 -4.18109700
C -2.56028700 3.83861900 -0.05867100
H -0.39125600 3.84244600 -0.03376100
C -3.73047600 3.82526100 -0.98014400
H -4.44431600 3.67426500 -2.98062000
O -2.73333400 4.08029600 1.14493600
H -4.69915400 3.99007700 -0.51655200
H -0.13301100 3.52112800 -2.53400700
H -2.76844200 -3.22896800 0.38655900
H -2.66695700 -3.45410800 -1.61064900
C -0.38310600 0.58843400 -4.24540600
H -1.05811900 1.44539300 -4.33698200
H 0.48397000 0.92371300 -3.66945200
H -0.05631500 0.29245200 -5.24465700
C -0.99398400 1.44349000 2.26209600
H -0.02669800 1.65063400 1.79527700
H -1.66175500 2.26879300 1.99575300
H -0.87030600 1.42792900 3.34711000

(phen)Pd(AcO)₂

C -2.99163500 -0.78153700 1.63829200
N -2.45055300 -0.84084300 0.42632300
C -2.22476500 -2.05240800 -0.15565900
C -2.53139800 -3.26946800 0.48714200
C -3.09890500 -3.18756300 1.77947500
C -3.32906900 -1.94859600 2.34767300
H -3.15736600 0.21369500 2.03415400
H -3.35110400 -4.09801000 2.31323200
H -3.76636500 -1.85767600 3.33460900
Pd -1.89642100 0.72511100 -0.79148800
C -1.53415700 2.63026400 1.28861000
O -2.49373400 2.12720600 0.55724600
C -2.02372800 3.71548800 2.23859300
H -1.20105800 4.07627100 2.85691400
H -2.44395500 4.54760100 1.66573800
H -2.82195000 3.32510100 2.87667300
O -0.34999100 2.28765400 1.24917700
O -1.24942200 2.12242300 -2.12113900
C -2.19075100 2.69084600 -2.82818900
O -3.39076800 2.41117800 -2.77824900
C -1.65714000 -2.05208900 -1.46636200
C -1.38891600 -3.26895500 -2.12646900

N -1.39327700 -0.84015100 -2.03125000
C -0.81892200 -3.18661500 -3.41767500
C -0.85074200 -0.78061200 -3.24257200
C -0.54993500 -1.94757700 -3.96838600
H -0.59533600 -4.09690300 -3.96430500
H -0.65465800 0.21459300 -3.62446700
H -0.11003600 -1.85652600 -4.95415500
C -1.65581600 3.76628000 -3.76489800
H -0.90067500 3.34088100 -4.43249300
H -2.46827600 4.19344500 -4.35371200
H -1.16842200 4.55558700 -3.18488700
C -1.70533600 -4.49783100 -1.45354000
C -2.25362400 -4.49805400 -0.20319200
H -1.49865900 -5.43265900 -1.96363900
H -2.48971400 -5.43304800 0.29365000

(phen)Pd(BQ)

C -1.84991100 0.00348100 1.87635600
N -1.74009400 -0.12313300 0.55765700
C -1.89519300 -1.35488900 -0.00047100
C -2.17052200 -2.50782600 0.77459900
C -2.27641500 -2.34267600 2.17362700
C -2.11676400 -1.08692100 2.72428800
H -2.48478300 -3.20457200 2.79963600
H -2.19480600 -0.92570400 3.79307400
Pd -1.26806900 1.45629500 -0.94067400
C -1.78553600 -1.47562600 -1.43341600
C -1.96567900 -2.73702500 -2.05019700
N -1.52257900 -0.35369800 -2.15160000
C -1.87073300 -2.79090000 -3.45917500
C -1.45077400 -0.42335900 -3.47644800
C -1.61962400 -1.63470300 -4.17197100
H -2.00242700 -3.74119500 -3.96699700
H -1.55069000 -1.64414400 -5.25349400
C -2.23774400 -3.88548500 -1.23413900
C -2.33386600 -3.77521500 0.12082200
H -2.36798400 -4.84632200 -1.72146300
H -2.54110800 -4.64723200 0.73271200
C -0.71316700 3.22394100 -1.95631000
C -1.82002200 3.36292800 -2.91128500
C -0.88005000 3.55140300 -0.57504600
C -3.11581100 3.85604900 -2.36578200
O -1.71605200 3.07794600 -4.11366500
C -2.15458500 4.08359000 -0.08157000
H -0.01639300 3.72914900 0.05921000
C -3.26832200 4.18237200 -1.07063500
H -3.92739600 3.95023300 -3.08211600
O -2.33494000 4.45333900 1.08600400
H -4.21072900 4.55837200 -0.68175600
H 0.27933400 3.14483100 -2.39238600
H -1.26558700 0.51363000 -3.99548900

H -1.72511700 1.00461200 2.27496500

(dmphen)Pd(AcO)₂

C -3.33294300 -0.67514800 1.51145400
N -2.68491700 -0.68934500 0.34254900
C -2.17273600 -1.86786900 -0.13535900
C -2.21940300 -3.07071200 0.60239900
C -2.84043900 -3.02498800 1.87095800
C -3.40694000 -1.85071000 2.30011600
H -2.88792000 -3.92305300 2.47827400
H -3.92635700 -1.79826500 3.24993300
Pd -2.02331800 0.90054600 -0.85646700
C -1.39133700 2.42144200 1.45439300
O -2.27479500 2.39450600 0.49658700
C -1.57274100 3.61399600 2.38445000
H -0.82298500 3.59526900 3.17609900
H -1.48623700 4.54508400 1.81677800
H -2.57432600 3.59481100 2.82462300
O -0.49917000 1.58687100 1.63296800
O -1.11238400 2.36050100 -1.93993600
C -1.91973300 3.19745200 -2.52714400
O -3.14400300 3.06380900 -2.62275900
C -1.62962900 -1.87192300 -1.46065700
C -1.14889900 -3.08075000 -2.01164200
N -1.65384000 -0.69818300 -2.16737100
C -0.70145100 -3.04482300 -3.35050300
C -1.28085100 -0.68968000 -3.45290000
C -0.79042100 -1.87156700 -4.05996300
H -0.31590400 -3.94809300 -3.81228700
H -0.48760000 -1.82764300 -5.09933700
C -1.19477700 4.37240500 -3.16866200
H -0.66312800 4.02399600 -4.06087700
H -1.91012300 5.14179400 -3.46217700
H -0.45139600 4.78967500 -2.48528100
C -1.15793100 -4.27401900 -1.22073200
C -1.67399100 -4.26912700 0.04080700
H -0.76083900 -5.18470100 -1.65655200
H -1.69848000 -5.17558600 0.63632600
C -4.01476100 0.56518300 2.00208400
H -3.42767700 1.02412400 2.80457400
H -4.13564900 1.30003100 1.21124900
H -4.98745400 0.29607000 2.42290400
C -1.38778600 0.56625600 -4.25928800
H -2.31099500 1.09949200 -4.02701600
H -0.55821000 1.23690900 -4.02227700
H -1.35751800 0.32858800 -5.32383600

(dmphen)Pd(BQ)

C -1.44015100 0.06261200 1.81245100
N -1.40973600 -0.10600900 0.48788700
C -1.80273400 -1.29043600 -0.05558600

C -2.29454800 -2.35884600 0.73260000
C -2.35993800 -2.15276300 2.12815200
C -1.92621500 -0.95970400 2.66106400
H -2.73758200 -2.94393600 2.76846800
H -1.94862300 -0.78824300 3.73104100
Pd -1.06733900 1.44680200 -1.05605800
C -1.67431400 -1.46618200 -1.48265400
C -2.04357600 -2.70309500 -2.06437200
N -1.16535700 -0.43955900 -2.21726000
C -1.85837500 -2.84017000 -3.45771500
C -0.96002900 -0.59485000 -3.52779700
C -1.31186600 -1.80146600 -4.17731400
H -2.13502700 -3.76993400 -3.94521600
H -1.14245900 -1.89324500 -5.24394100
C -2.56668300 -3.75256400 -1.24021900
C -2.68735500 -3.58687000 0.10665900
H -2.85562900 -4.68544800 -1.71368200
H -3.07457000 -4.38455100 0.73251100
C -0.84737800 3.35512900 -1.99221800
C -2.00924700 3.49779000 -2.87585000
C -0.98116300 3.52703800 -0.57802500
C -3.33136800 3.72430400 -2.22842400
O -1.93726200 3.44453700 -4.11241100
C -2.28336700 3.84986100 0.01509600
H -0.11616900 3.76929100 0.03297200
C -3.45711300 3.88658500 -0.90128800
H -4.18328000 3.78145000 -2.90030000
O -2.44303900 4.09235900 1.22036100
H -4.41714200 4.08302500 -0.43205600
H 0.12113000 3.46306300 -2.47246600
C -0.33693800 0.53929000 -4.28437900
H -1.01078500 1.40015500 -4.33655600
H 0.56730000 0.87645400 -3.76942900
H -0.07683800 0.23371000 -5.29984100
C -0.93150800 1.35701600 2.37212500
H 0.06493300 1.56721700 1.97241500
H -1.57274300 2.19550800 2.08304200
H -0.87619200 1.31462400 3.46179400

(DAF)Pd(AcO)₂

C -2.81489800 -0.81946100 1.87538800
N -2.36487400 -0.63982400 0.61431400
C -2.16837000 -1.75171100 -0.08622400
C -2.38235000 -3.06297300 0.32225500
C -2.85350600 -3.25447200 1.61506800
C -3.06412600 -2.09749400 2.38784300
H -2.95793600 0.07136300 2.47127100
H -3.04976100 -4.24142800 2.01918100
H -3.42554000 -2.18243200 3.40565200
Pd -1.82560500 1.00242000 -0.65327400
C -1.74907900 2.47777300 1.79285300

O -2.39488900 2.42910100 0.65793000
C -2.20252300 3.63438200 2.67322000
H -1.73820200 3.56119000 3.65721500
H -1.91615000 4.58202900 2.20667100
H -3.29122000 3.63480900 2.77226400
O -0.86478800 1.69462200 2.14797300
O -1.17587400 2.48523500 -1.85945300
C -1.82203000 2.65610300 -2.98244800
O -2.75459500 1.95693200 -3.38602300
C -1.67473700 -1.71484300 -1.43960000
C -1.56371500 -3.00050400 -1.95617600
N -1.39165600 -0.56745800 -2.04721700
C -1.10736300 -3.12065700 -3.26279900
C -0.95442300 -0.67699400 -3.32070900
C -0.80485300 -1.92381400 -3.93814400
H -0.98963000 -4.08301700 -3.74852500
H -0.74003900 0.24575000 -3.84184200
H -0.44922300 -1.95237900 -4.96112000
C -2.01030800 -3.95658900 -0.85577100
O -2.05962500 -5.16513100 -0.90668500
C -1.30281300 3.84460600 -3.78009700
H -0.21409900 3.80155100 -3.86727700
H -1.75726500 3.85744000 -4.77135900
H -1.55305600 4.77210900 -3.25565100

(DAF)Pd(BQ)

C -1.82960200 -0.00830400 1.90779800
N -1.67048400 0.02602000 0.56610900
C -1.78433500 -1.14701000 -0.04732500
C -2.04405800 -2.38131200 0.55228900
C -2.20437600 -2.41593200 1.93050900
C -2.09194300 -1.19039100 2.60806700
H -2.40818900 -3.33903800 2.46236000
H -2.20869100 -1.14592300 3.68453100
Pd -1.22788600 1.57883400 -1.06382400
C -1.65944700 -1.31647900 -1.49109100
C -1.83859300 -2.65969800 -1.82819000
N -1.42020700 -0.31360600 -2.32814300
C -1.76466700 -3.01020300 -3.16918300
C -1.35326300 -0.65385100 -3.63417200
C -1.51701200 -1.96939000 -4.08004500
H -1.89347000 -4.03405900 -3.50327200
H -1.45100400 -2.17431900 -5.14212400
C -0.76882600 3.43022600 -1.99432100
C -1.90710900 3.64230800 -2.90233200
C -0.90652600 3.62956900 -0.58935100
C -3.20806400 4.01687600 -2.27680400
O -1.82155400 3.52555300 -4.13010000
C -2.18955600 4.05928400 -0.01198500
H -0.03323900 3.78607100 0.03786900
C -3.33727400 4.20738800 -0.95326000

H -4.04131900 4.14793900 -2.96154100
O -2.34264800 4.29989700 1.19079500
H -4.28140500 4.50196400 -0.50362100
H 0.21183200 3.43008100 -2.46235700
H -1.16746200 0.15691600 -4.33030400
H -1.74567100 0.94126700 2.42493500
C -2.09212600 -3.42374600 -0.54545600
O -2.29319600 -4.61460200 -0.42336600

[Pd^I(μ -DAF)(AcO)]₂

Pd -0.96475000 -0.80099400 0.17421400
C -4.04250500 -0.61491800 -0.39167100
O -5.11669300 -0.73942500 -0.99623700
O -2.88727100 -0.86772400 -0.92355900
Pd 1.25437700 -0.78057100 1.38756900
C 3.80071200 0.11983700 2.69039900
O 3.25887100 1.24284000 2.64727800
O 3.22026300 -0.99760000 2.41840200
N -0.38974500 0.80343600 -1.00480600
C -1.35929600 1.67137700 -1.39511000
C 0.77742300 0.87296800 -1.65243900
C -1.19513800 2.58310900 -2.43264000
H -2.29777900 1.58841300 -0.86682400
C 0.99187000 1.72696400 -2.74848100
C 0.00249100 2.60406400 -3.15689400
H -2.01442300 3.24604600 -2.68309300
N 0.27091800 -0.77785300 3.20936400
C 0.83904700 -0.07411700 4.22448200
C -0.70409500 -1.63016700 3.53488900
C 0.46961200 -0.24115800 5.55657300
H 1.62223700 0.61423900 3.92332000
C -1.08490600 -1.89078600 4.86194400
C -0.49737200 -1.19242800 5.90329100
H 0.96258400 0.35577400 6.31456200
H -0.77686400 -1.37837100 6.93460600
H 0.15319300 3.26927500 -4.00002100
C 5.27118800 -0.00501400 3.08331900
H 5.84524800 -0.35800400 2.21985100
H 5.67140100 0.95510200 3.41271600
H 5.39155700 -0.74810500 3.87696400
C -4.06351100 -0.16300200 1.07413200
H -4.04423600 -1.04614900 1.72232000
H -3.19057900 0.44483700 1.32898200
H -4.98201100 0.38803600 1.28508400
C -1.52083100 -2.47035300 2.63480200
N -1.58329200 -2.43103500 1.30129000
C -2.31983100 -3.32251000 3.41547600
C -2.40038000 -3.33401400 0.69860200
C -3.16634400 -4.23308900 2.80708300
C -3.17608700 -4.24677200 1.40641100
H -2.45188100 -3.26645800 -0.37947600

H -3.79385300 -4.89692800 3.39158200
H -3.80627600 -4.93626900 0.85791800
C 2.01048000 0.08787700 -1.41848100
C 2.93057900 0.38609000 -2.43895600
N 2.29174700 -0.73965800 -0.40735400
C 4.16252400 -0.24300200 -2.47649100
C 3.49727300 -1.36658900 -0.44449800
C 4.43039900 -1.16292700 -1.45599100
H 4.88237100 -0.02408200 -3.25752500
H 3.71382500 -1.99814600 0.40604000
H 5.36977600 -1.70123500 -1.41906200
C -2.10436200 -2.98999100 4.86280400
O -2.64281300 -3.49997900 5.82569700
C 2.34933400 1.45022200 -3.31849300
O 2.86704200 1.97559600 -4.28480200

A.11 References

1. Bakhmutov, V. I.; Berry, J. F.; Cotton, F. A.; Ibragimov, S.; Murillo, C. A. Non-Trivial Behavior of Palladium Acetate. *Dalton Trans.* **2005**, 1989-1992.
2. Jaworski, J. N.; McCann, S. D.; Guzei, I. A.; S. S. Stahl. Detection of Pd(I) in Aerobic Oxidation Catalysis. *Angew. Chem. Int. Ed.* **2017**, *56*, 3605.
3. Sheldrick, G. M. A Short History of SHELXL. *Acta Cryst.* **2008**, *A64*, 112-122.
4. Dolomanov, O.V.; Bourhis, L.J.; Gildea, R.J.; Howard, J.A.K.; Puschmann, H. OLEX2: A Complete Structure Solution, Refinement and Analysis Program. *J. Appl. Cryst.* **2009**, *42*, 339-341.
5. Guzei, I. A. An Idealized Molecular Geometry Library for Refinement of Poorly Behaved Molecular Fragments with Constraints. *J. Appl. Crystallogr.* **2014**, *47*, 806-809.
6. Frisch, M. J.; Trucks, G. W.; Schlegel, H. B.; Scuseria, G. E.; Robb, M. A.; Cheeseman, J. R.; Scalmani, G.; Barone, V.; Mennucci, B.; Petersson, G. A.; Nakatsuji, H.; Caricato, M.; Li, X.; Hratchian, H. P.; Izmaylov, A. F.; Bloino, J.; Zheng, G.; Sonnenberg, J. L.; Hada, M.; Ehara,

- M.; Toyota, K.; Fukuda, R.; Hasegawa, J.; Ishida, M.; Nakajima, T.; Honda, Y.; Kitao, O.; Nakai, H.; Vreven, T.; Montgomery, J. A., Jr.; Peralta, J. E.; Ogliaro, F.; Bearpark, M.; Heyd, J. J.; Brothers, E.; Kudin, K. N.; Staroverov, V. N.; Kobayashi, R.; Normand, J.; Raghavachari, K.; Rendell, A.; Burant, J. C.; Iyengar, S. S.; Tomasi, J.; Cossi, M.; Rega, N.; Millam, M. J.; Klene, M.; Knox, J. E.; Cross, J. B.; Bakken, V.; Adamo, C.; Jaramillo, J.; Gomperts, R.; Stratmann, R. E.; Yazyev, O.; Austin, A. J.; Cammi, R.; Pomelli, C.; Ochterski, J. W.; Martin, R. L.; Morokuma, K.; Zakrzewski, V. G.; Voth, G. A.; Salvador, P.; Dannenberg, J. J.; Dapprich, S.; Daniels, A. D.; Farkas, Ö.; Foresman, J. B.; Ortiz, J. V.; Cioslowski, J.; Fox, D. J., *Gaussian 09, Revision D.01*, Gaussian, Inc., Wallingford CT, **2009**.
7. Hay, P. J.; Wadt, W. R. Ab Initio Effective Core potentials for Molecular Calculations. Potentials for the Transition Metal Atoms Sc to Hg. *J. Chem. Phys.* **1985**, *82*, 270-283.
 8. Wadt, W. R.; Hay, P. J. Ab Initio Effective Core Potentials for Molecular Calculations. Potentials for Main Group Elements Na to Bi. *J. Chem. Phys.* **1985**, *82*, 284-298.
 9. Becke, A. D. Density-functional Exchange-energy Approximation with Correct Asymptotic Behavior. *Phys. Rev. A* **1988**, *38*, 3098-3100.
 10. Lee, C.; Yang, W.; Parr, R. G. Development of the Colle-Salvetti Correlation-energy Formula into a Functional of the Electron Density. *Phys. Rev. B* **1988**, *37*, 785-789.
 11. Becke, A. D. A New Mixing of Hartree-Fock and Local Density Functional Theories. *J. Chem. Phys.* **1993**, *98*, 1372-1377.
 12. Grimme, S.; Antony, J.; Ehrlich, S.; Krieg, H. A Consistent and Accurate Ab Initio Parametrization of Density Functional Dispersion Correction (DFT-D) for the 94 Elements H-Pu. *J. Chem. Phys.* **2010**, *132*, 154104.

13. Cancès, E.; Mennucci, B.; Tomasi, J. A New Integral Equation Formalism for the Polarizable Continuum Model: Theoretical Background and Applications to Isotropic and Anisotropic Dielectrics. *J. Chem. Phys.* **1997**, *107*, 3032-3041.
14. Mennucci, B.; Tomasi, J. Continuum Solvation Models: A New Approach to the Problem of Solute's Charge Distribution and Cavity Boundaries. *J. Chem. Phys.* **1997**, *106*, 5151-5158.
15. Scalmani, G.; Frisch, M. J. Continuous Surface Charge Polarizable Continuum Models of Solvation. I. General Formalism. *J. Chem. Phys.* **2010**, *132*, 114110.

Appendix B: Supporting Information for Chapter 3

B.1 General Considerations

All manipulations were carried out in a glovebox or using standard Schlenk line technique unless specified otherwise. All chemicals and solvents were purchased from commercially available sources. *Tert*-butylbenzoquinone was purified by sublimation. Chloroform and chloroform-*d*₁ were dried over calcium hydride, stored under inert atmosphere, and distilled prior to use. Palladium acetate was purchased from Sigma-Aldrich and used without further purification, although the purity of the Pd(OAc)₂ was confirmed by ¹H NMR spectroscopic analysis because Pd(OAc)₂ is occasionally contaminated with NO₂ substituting an acetate ligand.¹ (bc)Pd(OAc)₂ was prepared according to the literature.² All NMR spectra were obtained on Bruker-Avance 400, 500, or 600 MHz spectrometers. UV/Vis spectra were obtained on an Agilent Cary 60 spectrometer. UPLC traces were obtained on a Waters Acquity UPLC H-Class PLUS Bio System.

B.2 Kinetic Studies: ⁴F BnOH Oxidation

[⁴F BnOH] dependence: In a glovebox, CHCl₃ stock solutions were prepared as follows: **A:** (bc)Pd(OAc)₂ (43.9 mg, 0.075 mmol, 750 μL); **B:** ⁴F BnOH (50.5 mg, 0.4 mmol, 2000 μL); **C:** ^tBuBQ (32.8 mg, 0.2 mmol, 1000 μL). Into a 4 mL scintillation vial, 100 μL **A**, 50 μL **C**, **B** (variable amount, depending on the [⁴F BnOH] concentration of the experiment), and CHCl₃ were added such that the total volume amounted to 1.0 mL. Aliquots of 100 μL of each solution were added to separate NMR tubes and capped. The tubes were removed from the glovebox and added to an oil bath preheated to 60 °C. Each reaction tube was removed from the heat at a specified time and frozen in a dry ice/acetone bath to quench. The samples were diluted with 100 μL of acetonitrile with 3-methylquinoline as an external standard. Each sample was deposited into the well of a 96-well plate and submitted for UPLC analysis.

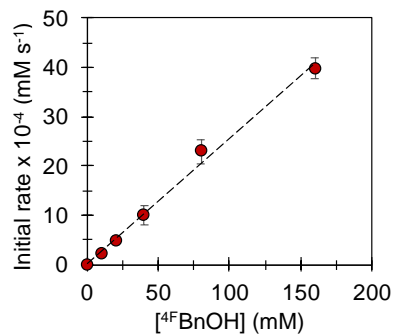


Figure B.1. Initial rate of formation of 4-fluorobenzaldehyde vs $^4\text{F-BnOH}$ concentration

Table B.1. Initial rate data for formation of 4-fluorobenzaldehyde with variable $[\text{}^4\text{F-BnOH}]$

$[\text{}^4\text{F-BnOH}]$ (mM)	Initial rate 4-F-benzaldehyde formation (mM/s)				
	run 1	run 2	run 3	average	std dev
0	0.00E+00	0.00E+00	0.00E+00	0.00E+00	0.00E+00
10	2.29E-04	2.30E-04	1.85E-04	2.15E-04	2.57E-05
20	4.87E-04	5.15E-04	4.72E-04	4.91E-04	2.20E-05
40	1.24E-03	9.22E-04	8.80E-04	1.01E-03	1.97E-04
80	2.55E-03	2.29E-03	2.05E-03	2.30E-03	2.49E-04
160	3.95E-03	3.78E-03	4.21E-03	3.98E-03	2.20E-04

$[(\text{bc})\text{Pd}(\text{OAc})_2]$ dependence: In a glovebox, CHCl_3 stock solutions were prepared as follows: Stock solutions: **A:** $(\text{bc})\text{Pd}(\text{OAc})_2$ (58.5 mg, 0.1 mmol, 1250 μL); **B:** $^4\text{F-BnOH}$ (100.9 mg, 0.8 mmol, 1000 μL); **C:** $^t\text{BuBQ}$ (65.7 mg, 0.4 mmol, 1000 μL). A procedure analogous to above was used with $[\text{}^4\text{F-BnOH}]$ fixed at 40 mM (100 μL **B**) and $[^t\text{BuBQ}]$ fixed at 10 mM (50 μL **C**) while varying $[(\text{bc})\text{Pd}(\text{OAc})_2]$ from 2-15 mM (variable volume of **A**).

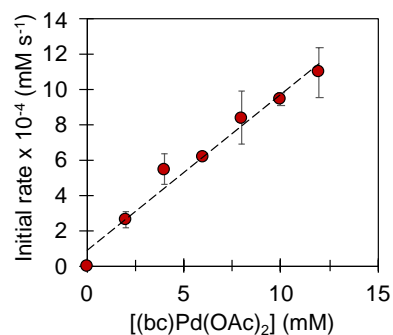
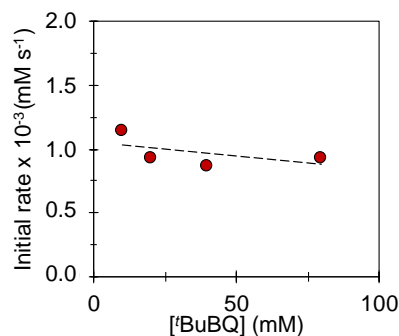


Figure B.2. Initial rate of formation of 4-fluorobenzaldehyde vs $(\text{bc})\text{Pd}(\text{OAc})_2$ concentration

Table B.2. Initial rate data for formation of 4-fluorobenzaldehyde with variable [(bc)Pd(OAc)₂]

[(bc)Pd(OAc) ₂] (mM)	Initial rate 4-F-benzaldehyde formation (mM/s)			
	run 1	run 2	average	std dev
0	0.00E+00	0.00E+00	0.00E+00	0.00E+00
2	2.96E-04	2.30E-04	2.63E-04	4.67E-05
4	4.84E-04	6.06E-04	5.45E-04	8.63E-05
6	6.31E-04	6.07E-04	6.19E-04	1.70E-05
8	9.46E-04	7.36E-04	8.41E-04	1.48E-04
10	9.70E-04	9.18E-04	9.44E-04	3.68E-05
12	1.20E-03	1.00E-03	1.10E-03	1.41E-04

[^tBuBQ] dependence: In a glovebox, CHCl₃ stock solutions were prepared as follows: Stock solutions: **A:** (bc)Pd(OAc)₂ (29.2 mg, 0.5 mmol, 2500 μL); **B:** ⁴Fb₄OH (33.6 mg, 0.27 mmol, 2000 μL); **C:** ^tBuBQ (65.7 mg, 0.4 mmol, 1000 μL). A procedure analogous to above was used with [(bc)Pd(OAc)₂] fixed at 10 mM (500 μL **A**) and [⁴Fb₄OH] fixed at 40 mM (300 μL **B**) while varying the ^tBuBQ concentration from 10-80 mM (variable volume **C**).

**Figure B.3.** Initial rate of formation of 4-fluorobenzaldehyde vs [^tBuBQ]**Table B.3.** Initial rate data for formation of 4-fluorobenzaldehyde with variable [(bc)Pd(OAc)₂]

[^t BuBQ] (mM)	Initial rate 4-F-benzaldehyde formation (mM/s)
10	1.15E-03
20	9.27E-04
40	8.67E-04
80	9.31E-04

B.3 Kinetic Isotope Effect: ^4F BnOH Oxidation

In a glovebox, chloroform stock solutions were prepared as follows: **A**: (bc)Pd(OAc)₂ (11.7 mg, 0.02 mmol, 1000 μL); **B**: *t*BuBQ (12.6 mg, 0.077 mmol, 1000 μL); **C**: ^4F BnOH (6.3 mg, 0.05 mmol, 500 μL); **D**: ^4F PhCD₂OH (6.4 mg, 0.05 mmol, 500 μL). Into a 4 mL scintillation vial 500 μL of **A**, 100 μL **B**, and 400 μL of **C** were added. Into a separate scintillation vial, 500 μL of **A**, 100 μL **B**, and 400 μL of **D** were added. Into separate NMR tubes, 100 μL of each solution were added and the tubes were capped. The tubes were removed from the glovebox and inserted into an oil bath preheated to 60 °C. Tubes were removed at specified times and frozen in a dry ice/acetone bath to quench. The samples were diluted with 100 μL of acetonitrile with 3-methylquinoline as an external standard. Each sample was deposited into the well of a 96-well plate and submitted for UPLC analysis.

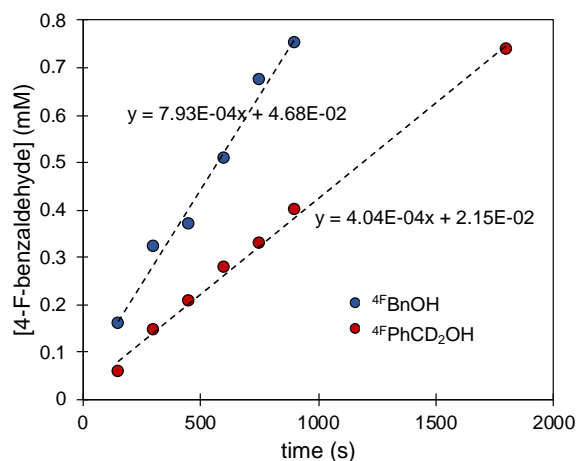


Figure B.4. Kinetic isotope effect: Initial rate of formation of 4-fluorobenzaldehyde from ^4F BnOH and ^4F PhCD₂OH

For the intramolecular competition KIE: In a 4 mL vial, (bc)Pd(OAc)₂ (5.8 mg, 0.01 mmol), *t*BuBQ (1.6 mg, 0.01 mmol), and ^4F PhC(H)(D)OH (5.0 mg, 0.04 mmol) were dissolved in

1.0 mL of CDCl₃. The solution was transferred to an NMR tube and placed in a 60 °C oil bath for 2.5 hours, after which ¹H and ¹⁹F NMR spectra were collected. The relative ratios of deuterio- and proteo-aldehyde formed were used to measure the intramolecular KIE, which was determined to be 2.8.

B.4 Carboxylate Dependence: ⁴F BnOH Oxidation

In a glovebox, chloroform stock solutions were prepared as follows: **A**: (bc)Pd(O₂CR)₂ (0.02 mmol, 1000 μL); **B**: ⁴BuBQ (16.4 mg, 0.1 mmol, 1000 μL); **C**: ⁴F BnOH (37.8 mg, 0.3 mmol, 3000 μL). Into a 4 mL scintillation vial 500 μL of **A**, 100 μL of **B**, and 400 μL of **C** were added. Into separate NMR tubes, 100 μL of each solution were added and the tubes were capped. The tubes were removed from the glovebox and inserted into an oil bath preheated to 60 °C. The tubes were removed at specified times and frozen in a dry ice/acetone bath to quench. The samples were diluted with 100 μL of acetonitrile with 3-methylquinoline as an external standard. Each sample was deposited into the well of a 96-well plate and submitted for UPLC analysis.

Table B.4. Initial rate data for formation of 4-fluorobenzaldehyde with (bc)Pd(O₂CR)₂ complexes

R group on (bc)Pd(O ₂ CR) ₂	Initial rate 4-F-benzaldehyde formation (mM/s)
⁴ CF ₃ Ph	8.69E-05
Ph	1.67E-04
⁴ BuPh	1.75E-04
Me	7.17E-04
⁴ Bu	8.24E-04

B.5 Temperature Dependence: ⁴F BnOH Oxidation

In a nitrogen glovebox, chloroform stock solutions were prepared as follows: **A**: (bc)Pd(OAc)₂ (21.1 mg, 0.036 mmol, 1800 μL); **B**: ⁴BuBQ (16.4 mg, 0.1 mmol, 1000 μL); **C**: ⁴F BnOH (18.9 mg, 0.15 mmol, 1500 μL). Into a 4 mL scintillation vial 1500 μL of **A**, 300 μL **B**, and 1200 μL of **C** were added. Into separate NMR tubes, 100 μL of this solution were added and

the tubes were tightly capped. The reaction tubes were removed from the glovebox and inserted into an oil bath preheated to 60 °C, 50 °C, 40 °C, or 30 °C. Tubes were removed at specified times and frozen in a dry ice/acetone bath to quench. The samples were diluted with 100 μ L of acetonitrile with 3-methylquinoline as an external standard. Each sample was deposited into the well of a 96-well plate and submitted for UPLC analysis.

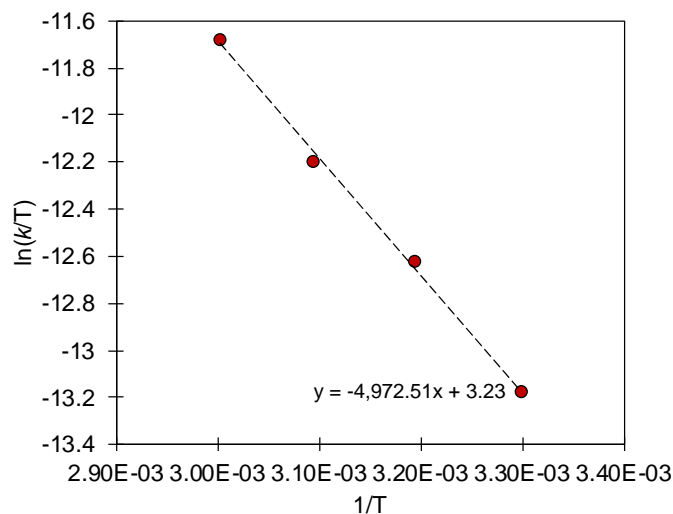


Figure B.5. Eyring plot for (bc)Pd(OAc)₂-mediated ⁴F-BnOH oxidation

B.6 Kinetic Studies: ⁴BuH₂Q Oxidation

[⁴BuH₂Q] Dependence: Chloroform stock solutions were prepared as follows: **A:** (bc)Pd(OAc)₂ (18.3 mg, 0.03 mmol, 25.0 mL); **B:** ⁴BuBQ (8.2 mg, 0.05 mmol, 5000 μ L); **C:** ⁴BuH₂Q (0.005-0.05 mmol, 1000 μ L). Into a septum capped 15 mL vial equipped with a stir bar, a 4000 μ L aliquot of **A** and a 500 μ L aliquot of **B** were injected and cooled to -30 °C with a submersible recirculating chiller. The vial was placed under positive pressure of N₂ and the UV/Vis dip probe was inserted through the septum. Data collection was commenced and a 500 μ L aliquot

of **C** was injected to initiate the reaction. The formation of (bc)Pd(^tBuBQ) was monitored by recording spectral absorbance changes at 420 nm.

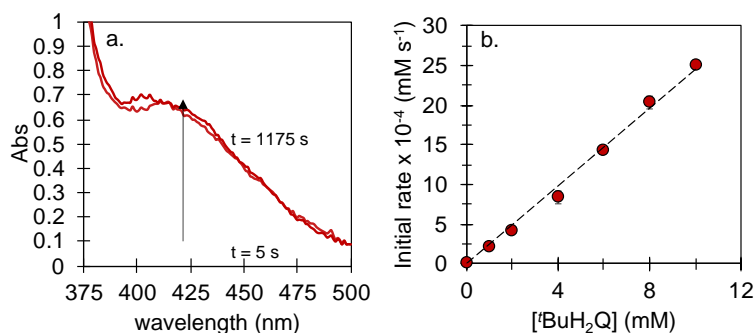


Figure B.6. Dependence of initial rate of formation of (bc)Pd(^tBuBQ) on [^tBuH₂Q]. (a) representative UV/Vis spectral stack for formation of (bc)Pd(^tBuBQ) and (b) initial rate dependence on [^tBuH₂Q]

Table B.5. Initial rate data for formation of (bc)Pd(^tBuBQ) with variable [^tBuH₂Q]

[^t BuH ₂ Q] (mM)	Initial rate (bc)Pd(^t BuBQ) formation (mM/s)				
	run 1	run 2	run 3	average	std dev
0	0.00E+00	0.00E+00	0.00E+00	0.00E+00	0.00E+00
1	2.01E-04	1.98E-04	2.49E-04	2.16E-04	2.86E-05
2	3.91E-04	4.16E-04	4.28E-04	4.12E-04	1.89E-05
4	8.14E-04	7.73E-04	9.26E-04	8.38E-04	7.92E-05
6	--	--	1.43E-03	1.43E-03	0.00E+00
8	2.08E-03	2.08E-03	1.92E-03	2.03E-03	9.24E-05
10	--	--	2.50E-03	2.50E-03	0.00E+00

[(bc)Pd(OAc)₂] dependence: Chloroform stock solutions were prepared as follows: **A**: (bc)Pd(OAc)₂ (11.9 mg, 0.02 mmol, 13.0 mL); **B**: ^tBuBQ (8.2 mg, 0.05 mmol, 5000 μL); **C**: ^tBuH₂Q (33.2 mg, 0.2 mmol, 5000 μL). A procedure analogous to above was used with [^tBuH₂Q] fixed at 4 mM (500 μL **C**) and [^tBuBQ] at 1 mM (500 μL **B**) while varying [(bc)Pd(OAc)₂] from 0.25-1.25 mM by diluting variable volumes of **A** with CHCl₃ to 4.0 mL total volume in order to reach the desired concentration.

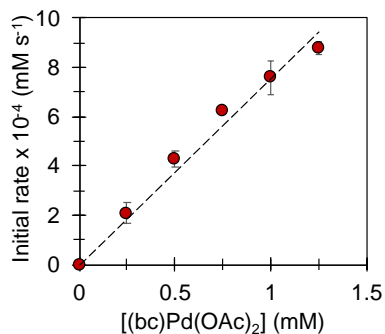


Figure B.7. Initial rate of formation of (bc)Pd('BuBQ) vs [(bc)Pd(OAc)₂].

Table B.6. Initial rate data for formation of (bc)Pd('BuBQ) with variable [(bc)Pd(OAc)₂]

[(bc)Pd(OAc) ₂] (mM)	Initial rate (bc)Pd('BuBQ) formation (mM/s)			
	run 1	run 2	average	std dev
0	0.00E+00	0.00E+00	0.00E+00	0.00E+00
0.25	1.80E-04	2.37E-04	2.09E-04	4.03E-05
0.50	4.50E-04	4.05E-04	4.28E-04	3.18E-05
0.75	6.19E-04	6.31E-04	6.25E-04	8.49E-06
1.00	7.08E-04	8.08E-04	7.58E-04	7.07E-05
1.25	8.57E-04	8.94E-04	8.76E-04	2.62E-05

['BuBQ] Dependence: Chloroform stock solutions were prepared as follows: **A:** (bc)Pd(OAc)₂ (36.6 mg, 0.063 mmol, 40.0 mL); **B:** 'BuBQ (8.2-65.7 mg, 0.05-0.4 mmol, 5000 μL); **C:** 'BuH₂Q (33.2 mg, 0.2 mmol, 5000 μL). An analogous procedure to above was used, except with [(bc)Pd(OAc)₂] fixed at 1 mM (4000 μL **A**) and ['BuH₂Q] fixed at 4 mM (500 μL **C**), while the ['BuBQ] was varied from 1-8 mM (500 μL **C**).

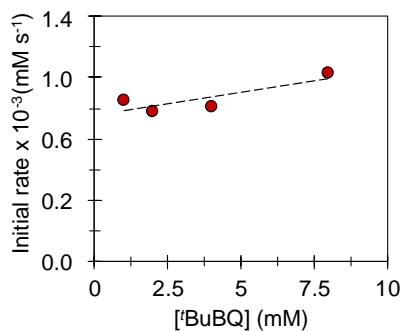


Figure B.8. Initial rate of formation of (bc)Pd('BuBQ) vs ['BuBQ].

Table B.7. Initial rate data for formation of (bc)Pd(^tBuBQ) with variable [^tBuBQ]

[^t BuBQ] (mM)	Initial rate (bc)Pd(^t BuBQ) formation (mM/s)
1	1.05E-03
2	9.73E-04
4	1.01E-03
8	1.22E-03

B.7 Kinetic Isotope Effect: ^tBuH₂Q Oxidation

An NMR tube with a septum cap was flame dried under vacuum and rinsed with D₂O. The D₂O was removed and the NMR tube was flame dried under vacuum again. A 50.0 μL aliquot of ^tBuH₂Q solution in MeOH-*d*₄ (10.0 mg, 0.06 mmol, 500 μL) was added to the tube and the MeOH-*d*₄ was removed under reduced pressure. 50 μL of MeOH-*d*₄ was added to the tube to dissolve the residual ^tBuH₂Q before being removed under reduced pressure. Addition and evaporation of MeOH-*d*₄ was repeated 5 times to ensure complete exchange of the ^tBuH₂Q OH peaks with deuterium. ¹H NMR in dry CDCl₃ confirmed complete exchange of the hydroquinone –OH to –OD.

The NMR tube was transferred to a glovebox and dissolved in 500 μL of dry CDCl₃. In a 4 mL scintillation vial, a 1000 μL stock solution of (bc)Pd(OAc)₂ (17.5 mg, 0.03 mmol) and ^tBuBQ (4.9 mg, 0.03 mmol) was prepared. The NMR tube containing ^tBuH₂Q-*d*₂ was removed from the glovebox and chilled in a dry ice/acetone bath. A 100 μL aliquot of the (bc)Pd(OAc)₂/^tBuBQ solution was injected into the NMR tube, mixed and inserted into a 400 MHz spectrometer chilled to -30 °C before data collection commenced.

For the oxidation of ^tBuH₂Q, a ^tBuH₂Q stock solution was prepared (10.0 mg, 0.06 mmol, 5000 μL CDCl₃). A 500 μL aliquot of the ^tBuH₂Q solution was injected into an NMR tube in a

glovebox, removed, and child in a dry ice acetone bath. The same injection and data collection procedures were performed as above.

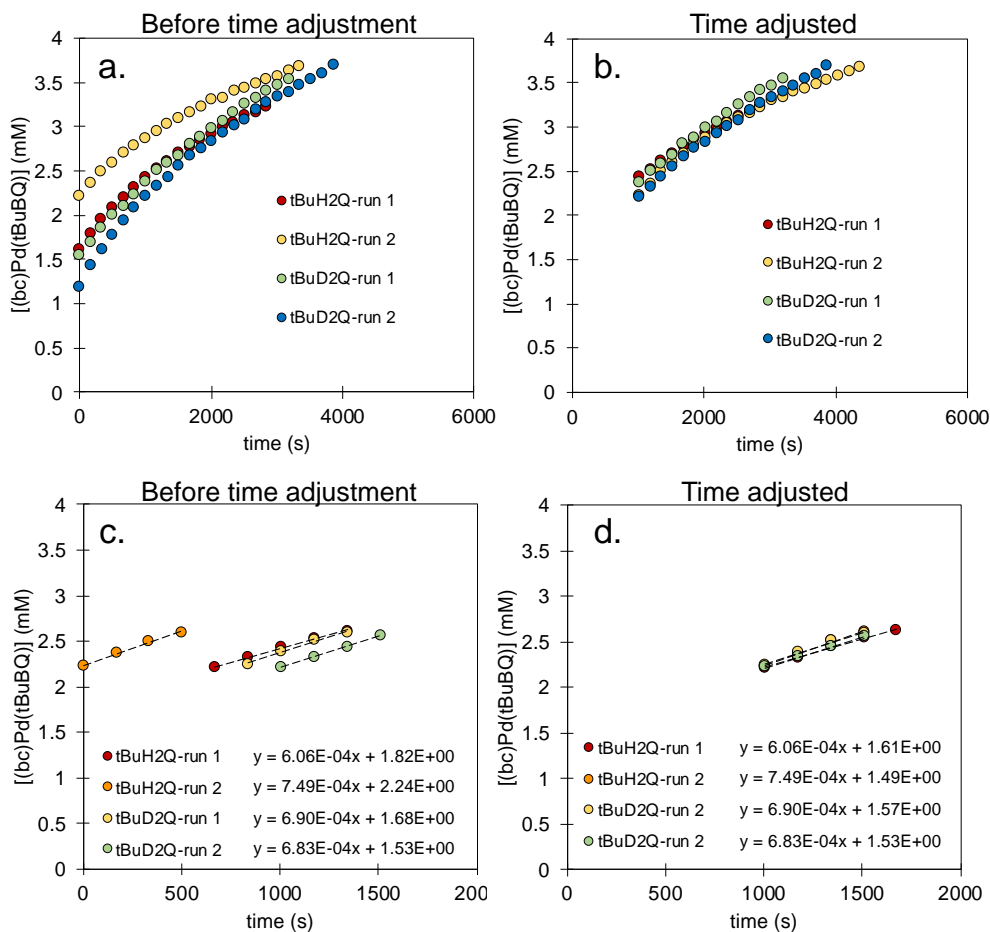


Figure B.9. Time course and initial rate data for formation of (bc)Pd(^tBuBQ) from ^tBuH₂Q and ^tBuD₂Q. (a.) and (c.) represent time course and initial rate data before time adjustment. (b.) and (d.) represent time course and initial rate data after time adjustment

In all runs there was considerable formation of (bc)Pd(^tBuBQ) before the first spectrum was recorded due to the sample warming to an unknown temperature before it could be inserted into the cooled spectrometer. Consequently, the actual time of the first time point is ambiguous. In order to account for this, the traces were time-adjusted such that the rates could be measured

over a regime where the concentrations of all species were identical, thus ensuring the rate measurements were made under identical conditions. This adjustment is represented in Figures S9b and S9d. The kinetic isotope effect was determined to be 1.0.

B.8 Temperature Dependence: $^t\text{BuH}_2\text{Q}$ Oxidation

Chloroform stock solutions were prepared as follows: **A**: (bc)Pd(OAc)₂ (11.0 mg, 15.0 mL); **B**: $^t\text{BuBQ}$ (8.2 mg, 5000 μL); **C**: $^t\text{BuH}_2\text{Q}$ (13.3 mg, 2000 μL). Into a septum capped 15 mL vial equipped with a stir bar, a 4000 μL aliquot of **A** and a 500 μL aliquot of **B** were injected and cooled to -40, -30, -20, -10, or 0 $^\circ\text{C}$ with a submersible recirculating chiller. The vial was placed under positive pressure of N₂ and the UV/Vis dip probe was inserted. Data collection was commenced, and a 500 μL aliquot of **C** was injected. Spectral changes were monitored at 420 nm.

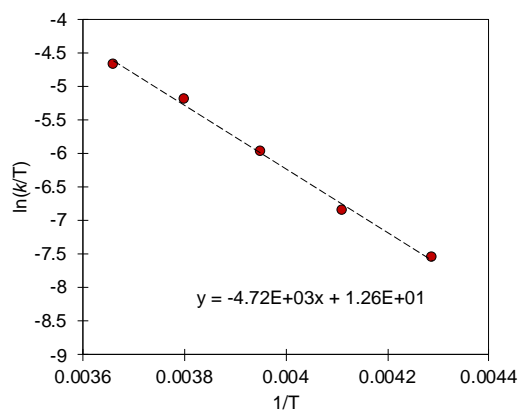


Figure B.10. Eyring plot for (bc)Pd(OAc)₂-mediated $^t\text{BuH}_2\text{Q}$ oxidation

B.9 Carboxylate Dependence: ^tBuH₂Q Oxidation

Chloroform stock solutions were prepared as follows: **A**: (bc)Pd(O₂CR)₂ (0.005 mmol, 4000 μL); **B**: ^tBuBQ (16.4 mg, 10.0 mL); **C**: ^tBuH₂Q (66.5 mg, 10.0 mL). Into a septum capped 15 mL vial equipped with a stir bar, a 4000 μL aliquot of **A** and a 500 μL aliquot of **B** were injected and cooled to -30 °C with a submersible recirculating chiller. The vial was placed under positive pressure of N₂ and the UV/Vis dip probe was inserted. Data collection was commenced, and a 500 μL aliquot of **C** was injected. Spectral changes were monitored at 420 nm.

Table B.8. Initial rate data for formation of (bc)Pd(^tBuBQ) from (bc)Pd(O₂CR)₂ complexes

R group on (bc)Pd(O ₂ CR) ₂	Initial rate (bc)Pd(^t BuBQ) formation (mM/s)
⁴ CF ₃ Ph	2.66E-04
Ph	2.28E-04
⁴ tBuPh	2.80E-04
Me	1.29E-03
^t Bu	1.31E-04

B.10 Estimation of pK_a of 4-trifluoromethylbenzoic acid

A reliable literature value for the pK_a of 4-CF₃-BzOH could not be found and was estimated to be 10.1 based on the fit to a linear regression of the pK_a (in DMSO) of a series of 4-substituted phenols vs the pK_a (in DMSO) of 4-substituted benzoic acids.³⁻⁵

^{13}C NMR (126 MHz, CDCl_3) δ 185.43, 164.93, 150.81, 148.41, 135.71, 129.78, 129.49, 129.17, 126.64, 126.55, 124.25, 39.74, 28.77, 25.03.

(bc)Pd(4'-Bu-C₆H₄CO₂)₂: In a round bottom flask, (bc)Pd(OAc)₂ (200 mg, 0.89 mmol) and 4-tertbutylbenzoic acid (121.9 mg, 1.78 mmol) were dissolved in approximately 5 mL of toluene and stirred at room temperature for several hours. The toluene was removed under reduced pressure, and the remaining solids were again dissolved in approximately 5 mL of toluene and stirred at room temperature for several hours. This procedure was repeated 3-5 times until no (bc)Pd(OAc)₂ starting material remained

Yield: 272 mg, 97% yield

^1H NMR (500 MHz, Chloroform-*d*) δ 7.96 (d, $J = 8.3$ Hz, 4H), 7.81 (s, 2H), 7.60-7.53 (m, 6H), 7.52-7.45 (m, 4H), 7.40 (s, 2H), 7.27 (d, $J = 8.4$ Hz, 4 H), 3.00 (s, 6H), 1.27 (s, 18H)

^{13}C NMR (126 MHz, CDCl_3) δ 173.62, 165.13, 153.47, 150.95, 148.54, 135.67, 132.31, 129.84, 129.78, 129.48, 129.20, 127.08, 126.68, 124.52, 124.36, 34.85, 31.40, 25.28.

(bc)Pd(4'-Bu-C₆H₄CO₂)₂: In a round bottom flask, (bc)Pd(OAc)₂ (200 mg, 0.89 mmol) and 4-tertbutylbenzoic acid (121.9 mg, 1.78 mmol) were dissolved in approximately 5 mL of toluene and stirred at room temperature for several hours. The toluene was removed under reduced pressure, and the remaining solids were again dissolved in approximately 5 mL of toluene and stirred at room temperature for several hours before toluene was removed under reduced pressure. This procedure was repeated 3-5 times until no (bc)Pd(OAc)₂ starting material remained by ^1H NMR.

Yield: 272 mg, 97% yield

^1H NMR (500 MHz, Chloroform-*d*) δ 7.96 (d, J = 8.3 Hz, 4H), 7.81 (s, 2H), 7.60-7.53 (m, 6H), 7.52-7.45 (m, 4H), 7.40 (s, 2H), 7.27 (d, J = 8.4 Hz, 4 H), 3.00 (s, 6H), 1.27 (s, 18H)

^{13}C NMR (126 MHz, CDCl_3) δ 173.62, 165.13, 153.47, 150.95, 148.54, 135.67, 132.31, 129.84, 129.78, 129.48, 129.20, 127.08, 126.68, 124.52, 124.36, 34.85, 31.40, 25.28.

(bc)Pd(OBz)₂: Palladium benzoate (50.4 mg, 0.145 mmol) and bathocuproine (52.1 mg, 0.145 mmol) were dissolved in approximately 5 mL dichloromethane in a 15 mL scintillation vial and stirred at room temperature overnight. Solvent was removed under reduced pressure to yield (bc)Pd(OBz)₂

Yield: 110.8 mg, quant.

^1H NMR (500 MHz, Chloroform-*d*) δ 8.06-8.00 (m, 4H), 7.82 (s, 2H), 7.61-7.53 (m, 6H), 7.51-7.47 (m, 4H), 7.41 (s, 2H), 7.32 (t, J = 7.4 Hz, 2 H), 7.25 (t, J = 7.5, 4H), 3.00 (s, 6H), 2.03 (s, 6H)

^{13}C NMR (126 MHz, CDCl_3) δ 173.64, 165.12, 151.07, 148.55, 135.60, 135.06, 130.45, 129.91, 129.89, 129.48, 129.23, 127.62, 127.14, 126.73, 124.42, 25.21.

(bc)Pd(4-CF₃-C₆H₄CO₂)₂: In a round bottom flask, (bc)Pd(OAc)₂ (200 mg, 0.89 mmol) and 4-trifluoromethylbenzoic acid (130.0 mg, 1.78 mmol) were dissolved in approximately 5 mL of toluene and stirred at room temperature for several hours. The toluene was removed under reduced pressure, and the remaining solids were again dissolved in approximately 5 mL of toluene and stirred at room temperature for several hours before toluene was removed under reduced pressure. This procedure was repeated 3-5 times until no (bc)Pd(OAc)₂ starting material remained by ^1H NMR.

Yield: 284 mg, 98% yield

^1H NMR (500 MHz, Chloroform-*d*) δ 8.11 (d, $J = 8.0$ Hz, 4H), 7.85 (s, 2H), 7.61-7.55 (m, 6H), 7.54-7.47 (m, 8H), 7.44 (s, 2H), 2.97 (s, 6H)

^{13}C NMR (126 MHz, CDCl_3) δ 172.38, 165.21, 151.61, 148.74, 138.20, 135.58, 132.40 (q, $J = 32.2$), 130.29, 130.24, 129.64, 129.49, 127.35, 127.07, 124.96, 124.95, 124.78, 25.30.

^{19}F NMR (377 MHz, CDCl_3) δ -62.69.

B.12 Synthesis of deuterated $^{4\text{F}}\text{BnOH}$ substrates

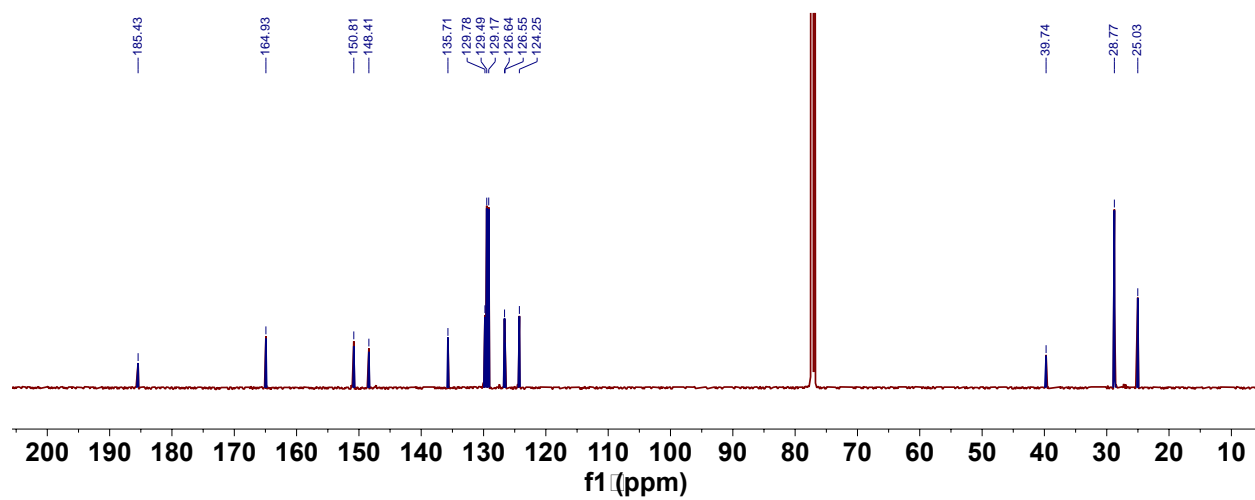
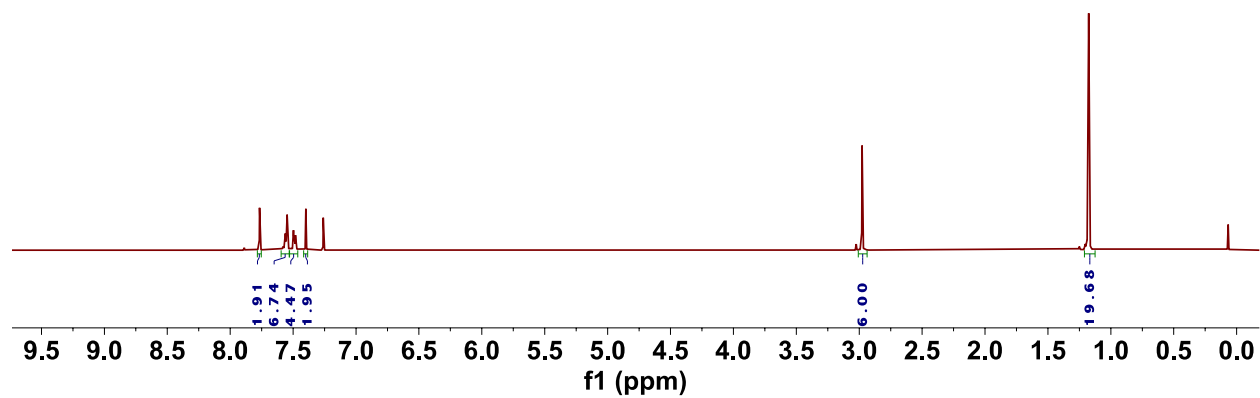
Synthesis of $^{4\text{F}}\text{PhCD}_2\text{OH}$: In a 100 mL 2-neck flask equipped with a stir-bar, LiAlD_4 (208 mg, 5 mmol) was dissolved in 20 mL of THF and capped with rubber septa in a glovebox. The flask was removed from the glovebox and cooled to 0 °C before 4-fluoromethylbenzoate (680 mg, 5 mmol) was added. The reaction was stirred until complete as determined by TLC. When the reaction was complete, 200 μL of water were added dropwise to quench excess LiAlD_4 . Approximately 20 mL of a saturated solution of Rochelle salt was added and the reaction was stirred for 1 h. The reaction was extracted 3 times with ethyl acetate, dried with MgSO_4 , and solvent was removed under reduced pressure. The crude oil was distilled to yield $^{4\text{F}}\text{PhCD}_2\text{OH}$ as a colorless oil (321 mg, 47% yield, 97% D incorporation)

^1H NMR (400 MHz, Chloroform-*d*) δ 7.39-7.29 (m, 2H), 7.10-6.97 (m, 2H), 1.80 (s, 1H)

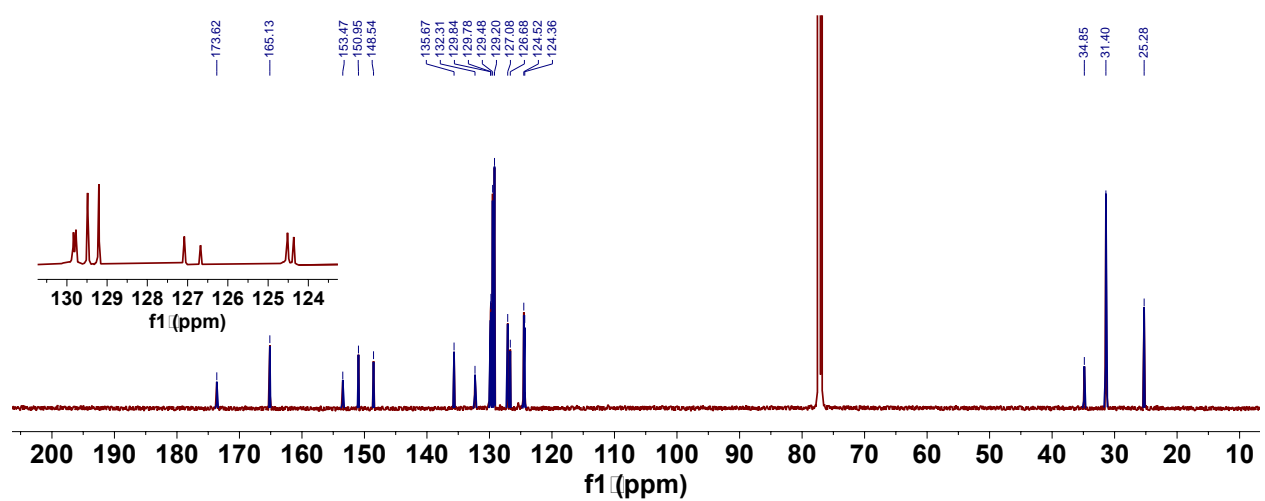
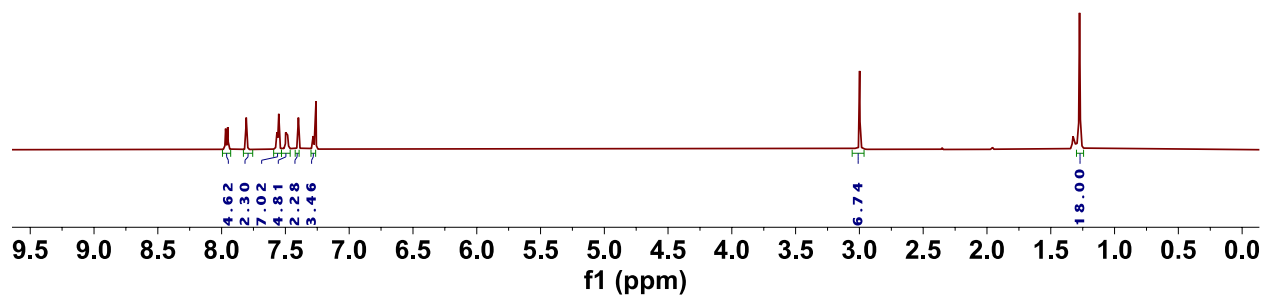
Synthesis of $^{4\text{F}}\text{PhC(H)(D)OH}$: In a 100 mL 2-neck flask equipped with a stir-bar, LiAlD_4 (150 mg, 3.6 mmol) was dissolved in 10 mL of THF and capped with rubber septa in a glovebox. The flask was removed from the glovebox and cooled to 0 °C before 4-fluorobenzaldehyde (1.0 g, 8.1 mmol) was added. The reaction was stirred until complete as determined by TLC. When the reaction was complete, 200 μL of water were added dropwise to quench excess LiAlD_4 . Approximately 20 mL of a saturated solution of Rochelle salt was added and the reaction was

stirred for 1 h. The reaction was extracted 3 times with ethyl acetate, dried with MgSO₄, and solvent was removed under reduced pressure. The crude oil was distilled to yield ⁴FPhC(H)(D)OH as a colorless oil (510 mg, 50% yield >99% D incorporation).

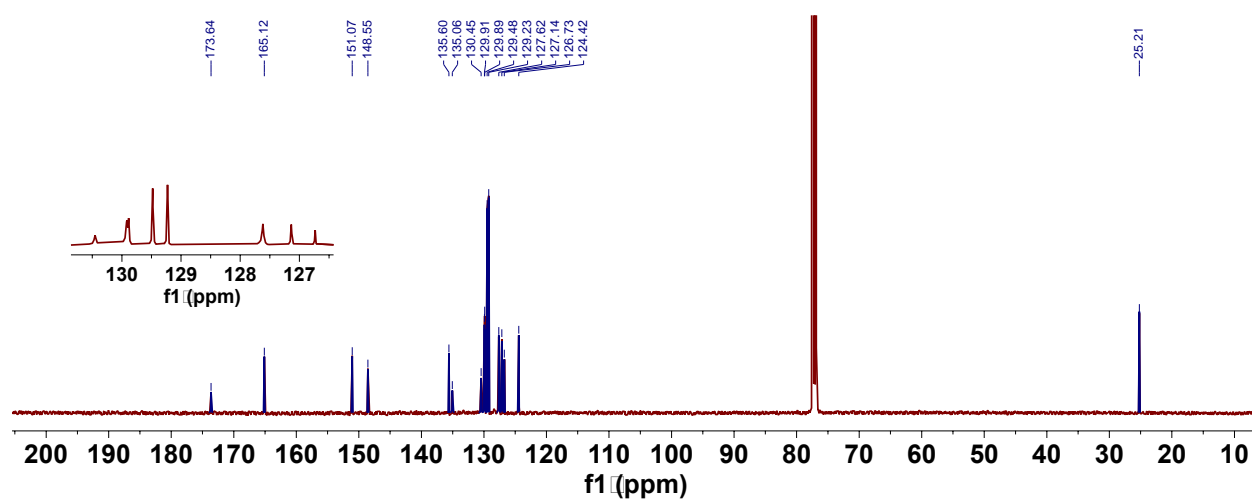
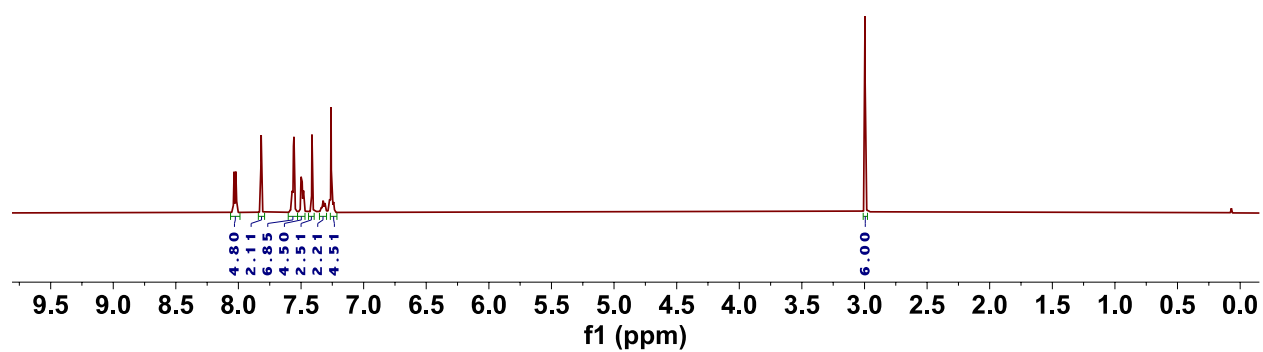
¹H NMR (400 MHz, Chloroform-*d*) δ 7.39-7.29 (m, 2H), 7.10-6.97 (m, 2H), 4.65 (s, 1H), 1.62 (d, *J* = 5.7 Hz, 1H)

B.13 NMR Spectroscopic Data $(bc)Pd(OPiv)_2$ 

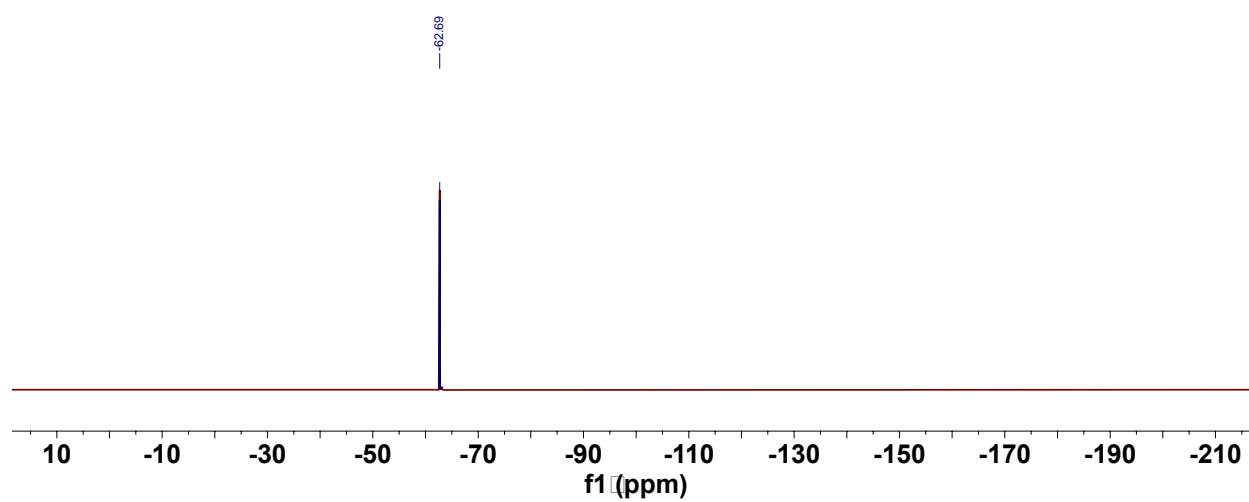
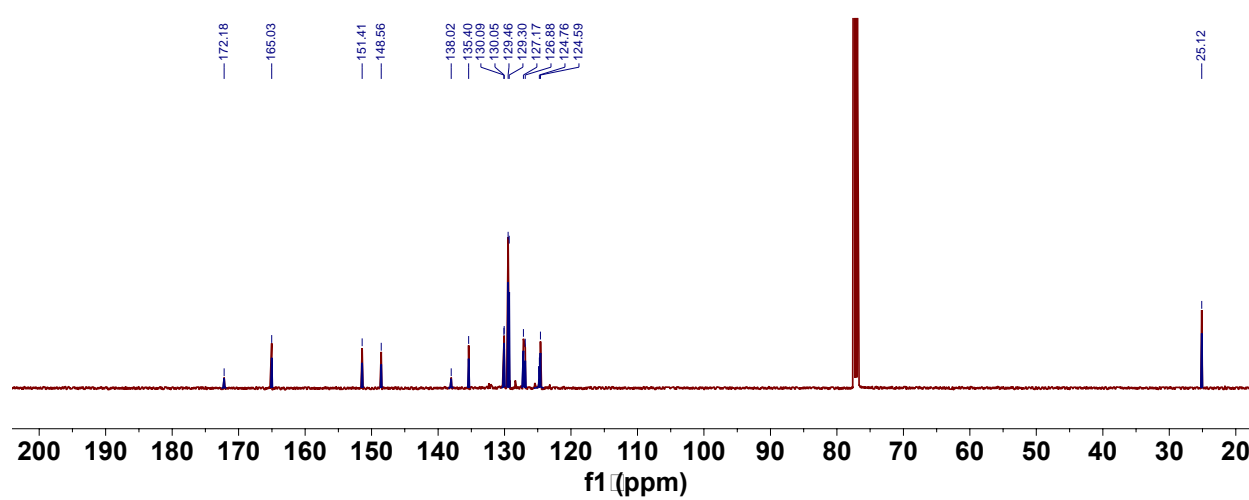
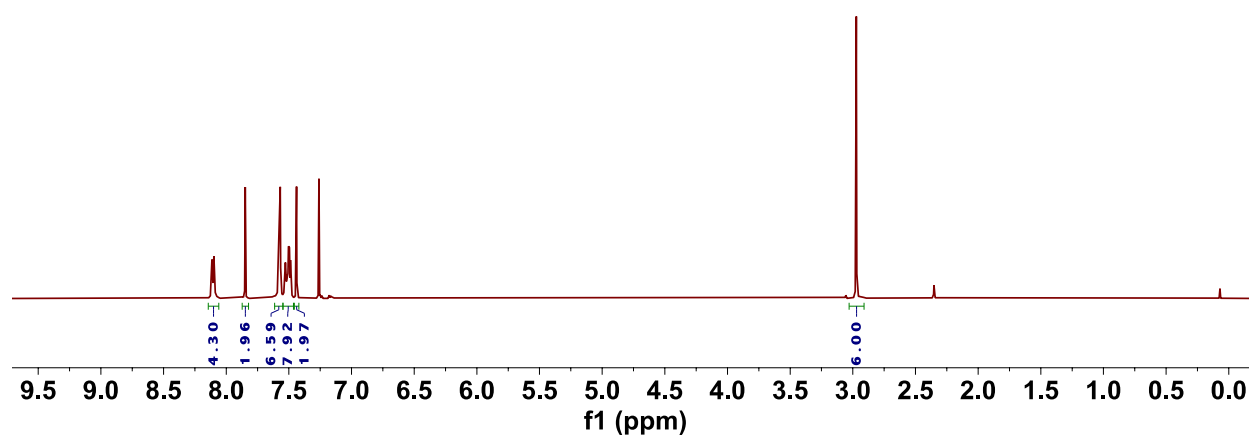
(bc)Pd(4-^tBu-C₆H₄CO₂)₂

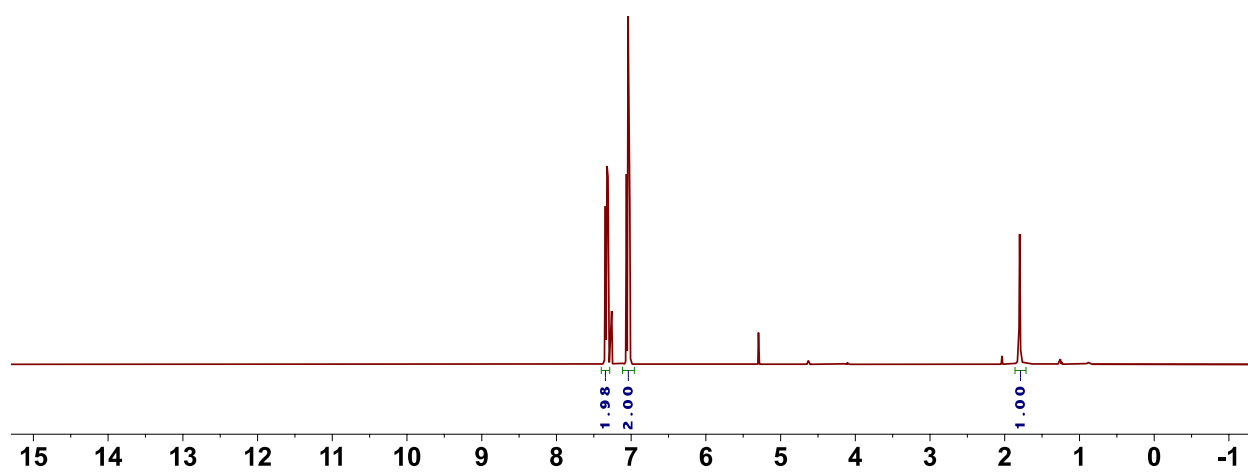
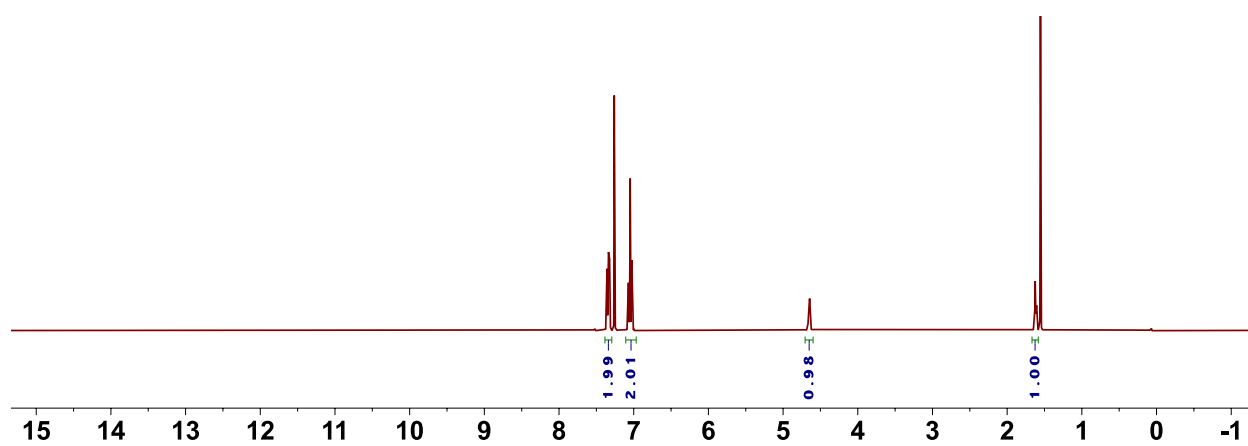


(bc)Pd(OBz)₂



(bc)Pd(4-CF₃-C₆H₄CO₂)₂



$^4\text{FPhCD}_2\text{OH}$  $^4\text{FPhC(H)(D)OH}$ 

B.14 References

1. Bakhmutov, V. I.; Berry, J. F.; Cotton, F. A.; Ibragimov, S.; Murillo, C. A. Non-Trivial Behavior of Palladium Acetate. *Dalton Trans.* **2005**, 1989-1992.
2. Bruns, D. L.; Musaev, D. G.; Stahl, S. S. Can Donor Ligands Make Pd(OAc)₂ a Stronger Oxidant? Access to Elusive Palladium(II) Reduction Potentials and Effects of Ancillary Ligands via Palladium(II)/Hydroquinone redox Equilibria. *J. Am. Chem. Soc.* **2020**, *142*, 19678-19688.
3. Bordwell, F. G.; Cheng, J.-P. Substituent Effects on the Stabilities of Phenoxy Radical Cations and the Acidities of Phenoxy Radical Cations. *J. Am. Chem. Soc.* **1991**, *113*, 1736-1743.
4. Maran, F.; Celadon, D.; Severin, M. G.; Vianello, E. Electrochemical Determination of the pK_a of Weak Acids in *N,N*-Dimethylformamide. *J. Am. Chem. Soc.* **1991**, *113*, 9320-9329.
5. Kulhánek, J.; Decouzon, M.; Gal, J.-F.; Maria, P.-C.; Fiedler, P.; Jiménez, P.; Roux, M.-V.; Exner, O. Steric Effects and Steric Hindrance to Resonance in *tert*-Butylbenzoic Acids in the Gas Phase and in Solution. *Eur. J. Org. Chem.* **1999**, 1589-1594.

Appendix C: Supporting Information for Chapter 4

C.1 General Considerations

All commercially available reagents were purchased from Sigma-Aldrich and used as obtained, except where otherwise noted. $\text{Pd}_2(\text{dba})_3 \cdot \text{CHCl}_3$ was synthesized and recrystallized according to the literature.¹ Substrates **1p**² and **1q**³ were synthesized according to the literature. 3-nitropyridine and 5,5'-Dibromo-4,4'-dihexyl-2,2'-bithiophene **2a** (used for the HPLC calibration curve) were purchased from TCI America. 2-bromo-3-thiophenecarboxylic acid, 2-bromo-3-methylthiophene **1c**, and 4-bromothiazole **1r** were purchased from Combi-Blocks. 1,10-phenanthroline-5,6-dione was purchased from Ark Pharm. 2-Chlorothiophene **1f** was purchased from Matrix Scientific. 2,4-Dibromothiophene **1h** was purchased from Maybridge. 2-Bromo-4-fluorothiophene **1i**, 2-bromo-3-dodecylthiophene **1d**, and 2-chloro-3-hexylthiophene **1b** were purchased from TCI America. 2-Butyloctyl-(2-bromo-3-thiophenecarboxylate) **1l** was synthesized from 2-butyloctanol and 2-bromo-3-thiophenecarboxylic acid according to the literature method for the 2-octyl derivative.⁴ ^1H , $^{19}\text{F}\{^1\text{H}\}$ or ^{19}F , and $^{13}\text{C}\{^1\text{H}\}$ NMR spectra were recorded on a Bruker Avance-400 or Avance-500 NMR spectrometer. Chemical shift values are given in parts per million relative to CDCl_3 (7.26 ppm for ^1H or 77.16 ppm for ^{13}C) or DMSO-d_6 (2.50 ppm for ^1H or 39.52 ppm for ^{13}C). NMR spectra were plotted with MestReNova v10.0.2-15465 (MestreLab Research S. L. 2015). HPLC analyses were performed on a Shimadzu Prominence analytical HPLC with a Kinetex reverse phase LC column (5 μm particle size, XB-C18 phase, 100 Å pore size, 250 x 4.6 mm dimensions, Phenomenex Inc., part number 00G-4605-E0) and a UV detector. Reverse phase column chromatography was performed using an automated Biotage Isolera® with reusable 60 g or 30 g Biotage SNAP® Ultra C-18 cartridges or standard silica cartridges.

Safety note: Use of DMSO as a reaction solvent under O₂ with elevated temperatures is hazardous and proper precautions should be taken.^{5,6}

C.2 Procedures for Aerobic Oxidative Thiophene C–H Thiophene Homocoupling

General Procedure for Aerobic Thiophene C–H Homocoupling: Unless otherwise specified, 1.1 mmol substrate was weighed out into a 13x100 mm borosilicate glass heavy wall test tube. To the test tube, catalyst components (Pd(OAc)₂, Cu(OAc)₂•H₂O, phd, BQ) were added at 3 mol% loading each (0.033 mmol) in stock solutions of DMSO, and enough DMSO was added such that the total volume of the reaction mixture was 1.0 mL. The reaction mixtures were heated at 120 °C temperature for 16 h under 1.1 atm pO₂ with orbital mixing.

Isolations: The reactions were diluted with 10 mL CH₂Cl₂ and filtered through a pad of Celite. The filter cake was washed with CH₂Cl₂ until the washes became colorless. The organic layer was washed 3 times with 25 mL of cold brine. The aqueous washes were combined and extracted 3 times with 10 mL of CH₂Cl₂. The organic layers were combined, dried over Mg₂SO₄, filtered, and the organics were removed to yield the crude product. The crude product was passed through a silica plug with CH₂Cl₂ eluent. The material was then further purified by column chromatography and/or recrystallization. This general isolation procedure was used for all products except **2b** and **2c**. Isolation details are provided below.

NMR yields: After cooling to rt, a known volume of a methyl 3,5-dinitrobenzoate solution in THF was added to the reaction tube. Then, everything was mixed, and the mixture was passed through Celite. The shaker tube was washed with more THF and passed through the filter cake, and then the filter cake was washed with THF until no more color passed through. The filtrate was diluted with more THF. Finally, an aliquot of the mixture was interrogated by ¹H NMR spectroscopy.

C.3 Optimization of Aerobic Oxidative Thiophene C–H Thiophene Homocoupling

Optimization of Aerobic Oxidative Thiophene C–H Thiophene Homocoupling. The individual catalyst components were added to 13x100 mm borosilicate glass heavy wall test tubes as listed with the above conditions. Then, 2-bromo-3-hexylthiophene (67.5 μL , 0.33 mmol) was added to the test tubes. Finally, solvent was added to each test tube. The reactions were then placed in an orbital mixing block with heating element, the block was sealed, the tubes were purged with O_2 for 5 min, and then the reactions were heated to 50 $^\circ\text{C}$ with shaking. After 47 h, the reactions were stopped, and after cooling, dibromomethane (50 μL , 0.71 mmol) was added to each tube along with additional solvent. After filtering through Celite, the reactions were analyzed by ^1H NMR spectroscopy against the dibromomethane standard.

Literature Conditions:

- Wang 2014 Org. Lett. (Aerobic Thiophene Homocoupling): 10 mol% $\text{Pd}(\text{OAc})_2$, 1.0 equiv trifluoroacetic acid, DMSO⁷
- Stahl/Campbell C2 indole arylation: 10 mol% $\text{Pd}(\text{OPiv})_2$, 10 mol% 4,5-diazafluoren-9-one, propionic acid⁸
- Stahl/Izawa o-xylene homocoupling: 10 mol% $\text{Pd}(\text{OAc})_2$, 10 mol% $\text{Cu}(\text{OTf})_2$, 20 mol% 2-fluoropyridine, 13 mol% trifluoroacetic acid, AcOH ⁹

Table C.1. Assessment of Alternative Reaction Conditions: 50 $^\circ\text{C}$

Entry	Reaction Condition	MB (%)	RSM (%)	2a (%)
1	Wang 2014 Org. Lett. ⁷	55	55	Trace
2	Stahl/Campbell C2 Indole Arylation ⁸	81	68	13 ^b
3	Stahl/Izawa o-xylene homocoupling ⁹	68	68	0 ^c

a: Reaction mixtures were quantified by ^1H NMR spectroscopy.

b: It is unclear whether the observed ^1H NMR resonances truly correspond to product **2a**.

c: The peaks in the ^1H NMR spectrum are broad, so ruling out the presence of **2a** is not definitive.

Assessment of Alternative Reaction Conditions: 120 °C. The individual catalyst components were added to 13x100 mm borosilicate glass heavy wall test tubes as listed in the above conditions. Then, 2-bromo-3-hexylthiophene (67.5 μ L, 0.33 mmol) was added to the test tubes. Finally, solvent was added to each test tube. The reactions were then placed in an orbital mixing block with heating element, the block was sealed, the tubes were purged with O₂ for 5 min, and then the reactions were heated to 120 °C with shaking. After 16 h, the reactions were stopped, and after cooling, they were worked up for HPLC analysis.

Table C.2. Assessment of Alternative Conditions: 120 °C

Reaction scheme: 2-bromo-3-hexylthiophene (**1a**) reacts with [Pd] (10 mol%), Additives, and Solvent at 120 °C, 1.1 atm pO₂, 16 hr to form 2,2'-bis(bromomethyl)-5,5'-dihexylthiophene (**2a**). The starting material concentration is 0.67 M (0.33 mmol).

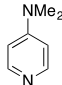
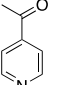
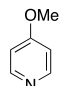
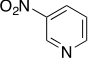
Entry	Reaction Condition	MB (%)	RSM (%)	2a (%)
1	Wang 2014 Org. Lett. ⁷	67	67	0
2	Stahl/Campbell C2 Indole Arylation ⁸	74	72	2
3	Stahl/Izawa <i>o</i> -xylene homocoupling ^{9,a}	70	70	Trace

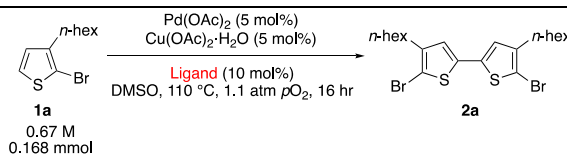
a: Propionic acid instead of AcOH.

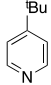
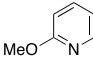
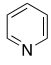
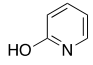
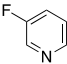
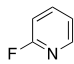
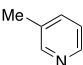
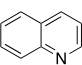
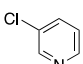
b: Catalyst: Pd(OAc)₂, Cu(OAc)₂·H₂O, phd

Ligand Screening: Monodentate Pyridines. The ligands (10 mol%) were added to 13x100 mm borosilicate glass heavy wall test tubes. Stock solutions of Pd(OAc)₂ (87.8 mg, 0.391 mmol, 39.1 mM) in 10.0 mL DMSO and Cu(OAc)₂•H₂O (78.0 mg, 0.391 mmol, 39.1 mM) in 10.0 mL DMSO were prepared, and 0.215 mL of each stock solution (0.0084 mmol) was added to each tube. Then, 2-bromo-3-hexylthiophene **1a** (34.0 μL, 0.168 mmol) was added to each tube. The reactions were then placed in an orbital mixing block with heating element, the apparatus was sealed and purged with O₂ for 5 min, the cooling water was turned on, and then the purging was stopped, and the block was heated to 110 °C under 1.1 atm *p*O₂. After 16 h, the reactions were stopped, and after cooling, an aliquot of a stock solution of phenanthrene in THF was added to each reaction, followed by filtration through a Celite plug. The reaction test tubes were washed with more THF, which was also passed through the Celite plug. Finally, the Celite plug was washed once more with THF. The filtrates were mixed and then subjected to HPLC analysis (reverse phase column, eluent: 100% acetonitrile, 2 mL/min). Recovered **1a** was also quantified by HPLC analysis against a calibration curve of 2-bromo-3-hexylthiophene **1a** and phenanthrene standard.

Table C.3. Monodentate Pyridine Screening

Entry	Ligand	MB (%)	RSM (%)	2a (%)	Entry	Ligand	MB (%)	RSM (%)	2a (%)
1		78	21	57	8		70	37	33
2		62	15	47	9		36	12	24



3		62	19	43	10		35	10	25
4		54	8	46	11		37	16	21
5		34	5	29	12		31	10	21
6		40	14	26	13		65	30	35
7		35	7	28	14	None	36	13	23

Ligand Screening: Bidentate Ligands. The ligands (5 mol%) were added to 13x100 mm borosilicate glass heavy wall test tubes. The reactions were prepared and run in the same way as Section 0. After 16 h, the reactions were stopped, and after cooling, they were worked up for HPLC analysis.

Table C.4. Bidentate Ligand Screening

Reaction scheme: $2 \text{ 1a} \xrightarrow[\text{DMSO, 110 } ^\circ\text{C, 1.1 atm } p\text{O}_2, 16 \text{ hr}]{\text{Pd(OAc)}_2 \text{ (5 mol\%), Cu(OAc)}_2 \cdot \text{H}_2\text{O (5 mol\%), Ligand (5 mol\%)}$ 2a

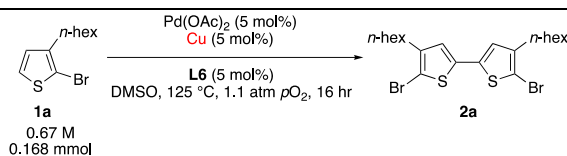
1a: 0.67 M, 0.168 mmol

Entry	Ligand	MB (%)	RSM (%)	2a (%)	Entry	Ligand	MB (%)	RSM (%)	2a (%)
1		40	14	26	8		82	34	48
2		82	38	44	9		87	44	43
3		82	36	46	10		57	21	36
4		88	41	47	11		34	11	23
5		91	44	47	12		58	1	57
6		71	14	57	13		88	8	80
7		44	N/A	44	14	None	36	13	23

Cu Cocatalyst Screening. The copper cocatalysts (5 mol%) were added to 13x100 mm borosilicate glass heavy wall test tubes. The reactions were otherwise prepared and run in the same way as Section 0, except at 125 °C instead of 110 °C. After 16 h, the reactions were stopped, and after cooling, they were worked up for HPLC analysis.

Table C.5. Cu Cocatalyst Screening

Entry	Cu Cocatalyst	MB (%)	RSM (%)	2a (%)
1	Cu(OAc) ₂ ·H ₂ O	90	3	87
2	Cu	92	5	87
3	CuI	59	27	32
4	Cu ₂ O	88	5	83
5	Cu(3-ethylhexanoate)	92	5	84
6	Cu(OTf) ₂	91	71	20
7	Cu(acac) ₂	87	38	49
8	CuBr ₂	89	80	9
9	CuCl ₂	96	75	21
10	CuF ₂	85	5	80
11	Cu(TFA) ₂ ·xH ₂ O	66	38	28
12	CuCl	95	32	63
13	CuBr·SMe ₂	92	47	45
14	Cu(NO ₃) ₂ ·2H ₂ O	86	64	22
15	Cu(OAc)	86	4	82
16	CuO	93	67	26
17	CuCO ₃ ·Cu(OH) ₂	94	47	47



Pd Catalyst Screening. The palladium catalysts (5 mol%) were added to 13x100 mm borosilicate glass heavy wall test tubes. The reactions were otherwise prepared and run in the same way as Section 0, except at 125 °C instead of 110 °C. After 16 h, the reactions were stopped, and after cooling, they were worked up for HPLC analysis.

Table C.6. Pd Catalyst Screening

Reaction scheme showing the coupling of two 5-bromo-2-n-hexylthiophene molecules (1a) to form a biaryl product (2a). The reaction conditions are: Pd (5 mol%), Cu(OAc)₂·H₂O (5 mol%), L6 (5 mol%), DMSO, 125 °C, 1.1 atm pO₂, 16 hr. The starting material 1a is at 0.67 M (0.168 mmol).

Entry	Pd Source	MB (%)	RSM (%)	2a (%)
1	Pd(OAc) ₂	90	3	87
2	Pd(TFA) ₂	90	32	58
3	Pd(O ₂ CC ₂ H ₅) ₂	86	1	85
4	Pd(OPiv) ₂	87	4	83
5	PdI ₂	63	48	15
6	Pd(acac) ₂	86	40	46
7	Pd(OBz) ₂	86	1	85
8	PdO	96	96	0
9	Pd(NO ₃) ₂ ·2H ₂ O	77	58	19
10	Pd ₂ (dba) ₃ ·CHCl ₃	56	3	53

Optimization Leading to Pd(OAc)₂/phd/Cu(OAc)₂·H₂O/BQ Catalyst. Catalyst components at 3 mol% loading (0.033 mmol) were added via stock solution to 13x100 mm borosilicate glass heavy wall test tubes. To each test tube was added 219 μL of 2-bromo-3-hexylthiophene and enough DMSO so that the total volume of each reaction was 1.0 mL. The reactions were heated at 120 °C under an O₂ atmosphere with orbital mixing for 16 h, after which 2.0 mL of a stock solution of 3,5-dinitromethylbenzoate (458.5 mg, 2.02 mmol, in 25.0 mL THF) was added to each reaction as an external standard. The reactions were mixed thoroughly, and aliquots were removed and filtered through cotton into an NMR tube. The reaction mixtures were analyzed by ¹H NMR spectroscopy (8 scans, 10 sec T1 relaxation delay).

Table C.7. Catalyst Component Screening

Reaction scheme: 1a (1.1 M, 1.1 mmol) reacts with 3 mol% catalyst in DMSO at 120 °C and 1.1 atm pO₂ for 16 hr to form 2a.

Entry	Catalyst	MB (%)	RSM (%)	2a (%)
1	Cu	100	100	0
2	Pd	81	76	5
3	Cu/BQ	100	100	0
4	Pd/BQ	92	87	5
5	Cu/phd	100	100	0
6	Pd/phd	99	93	6
7	Pd/Cu	35	20	15
8	Pd/phd/BQ	99	95	4
9	Pd/Cu/BQ	40	18	22
10	Pd/phd/Cu	79	15	64
11	Pd/phd/Cu/BQ	89	4	85

Conditions: 1a (1.1 mmol), 3 mol% catalyst (0.033 mmol), 1.0 mL in DMSO, 1.1 atm pO₂, 120 °C, 16 h.
Pd = Pd(OAc)₂, Cu = Cu(OAc)₂·H₂O.

C.4 Attempted Thiophene C–H Homocoupling with Reported Aerobic Conditions

A stock solution of Pd(OAc)₂ (74.9 mg, 0.33 mmol) and TFAH (510.2 μL) in 10.0 mL DMSO was prepared. Into 13x100 mm borosilicate glass heavy wall test tubes were added 0.5 mmol of each substrate, and 0.75 mL of the Pd(OAc)₂/TFAH stock solution. The reactions were heated at 50 °C under an O₂ atmosphere with orbital mixing for 48 h, after which 1.0 mL of a stock solution of 3,5-dinitromethylbenzoate (183.5 mg, 0.81 mmol, in 10.0 mL THF) was added to each reaction as an external standard. The reaction mixture and standard solution were mixed thoroughly, and aliquots were removed and filtered through cotton into an NMR tube for ¹H NMR spectroscopic analysis (8 scans, 10 sec T1 relaxation delay). Results are shown in Figure C.1 as a comparison to optimized spectroscopic yields from Chapter 4, Figure 4.4.

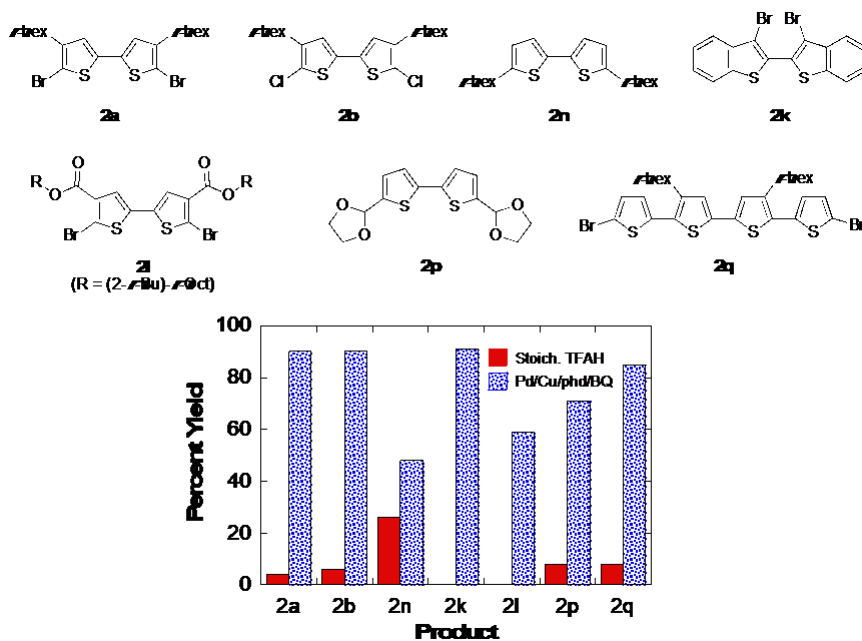


Figure C.1. Comparison of spectroscopic yields of selected substrates from Figure 4.4 to spectroscopic yields from conditions adapted from Wang's aerobic thiophene C–H homocoupling.

C.5 Synthetic Applications: Gram Scale Coupling of 1a and Use of Lower Catalyst Loading

Gram-scale coupling of 2-bromo-3-hexylthiophene: Into a vessel intended for large-scale synthesis on an orbital mixer were weighed Pd(OAc)₂ (37.1 mg, 0.165 mmol), phd (34.8 mg, 0.165 mmol), Cu(OAc)₂ (33.0 mg, 0.165 mmol), and BQ (17.8 mg, 0.165 mmol). The catalyst components were dissolved in 3.9 mL DMSO and moved to the orbital mixer, heated to 120 °C, and purged with O₂ for 5 minutes before 1a (1100 μL, 1.36 g) was added. The reaction was run for 16 h before being removed from the heat and allowed to reach room temperature. The cooled reaction mixture was transferred to a silica column and flushed with pentane. Product 2a was then obtained by removal of pentane under vacuum in 90% yield (1.22 g). *Safety note: Use of DMSO as a reaction solvent under O₂ with elevated temperatures is hazardous and proper precautions should be taken.*^{5,6}

Coupling of 2-bromo-3-hexylthiophene with 0.5 mol% Pd(OAc)₂ and 0.5 mol% phd: Into 13x100 mm borosilicate glass heavy wall test tubes were added Pd(OAc)₂ (0.309 mg, 1.4 x 10⁻³ mmol, 0.5 mol%), phd (0.289 mg, 1.4 x 10⁻³ mmol, , 0.5 mol%), Cu(OAc)₂ (6.6 mg, 0.036 mmol, 13 mol%), BQ (0.892 mg, 8.3 x 10⁻³ mmol, 3 mol%) via stock solutions in DMSO, followed by 1a (55.0 μL, 68.2 mg, 0.275 mmol). Enough DMSO was added to raise the total volume of the reaction to 250 μL. The test tube was moved to an orbital shaker, heated to 120 °C and the headspace purged with O₂ before being sealed and run for 72 h. Analysis of the crude reaction by ¹H NMR mixture revealed formation of 2a in 70% yield.

C.6 Initial Rate Dependence on Catalyst Components

General procedure for initial rate experiments: catalyst components were added via stock solutions in DMSO to 13x100 mm borosilicate glass heavy wall test tubes along with 2-bromo-3-

hexylthiophene and enough DMSO to raise the total reaction volume to 0.5 mL. The reaction mixtures were heated at 120 °C under an O₂ atmosphere for 20 minutes before the reactions were removed and quenched by submerging in an ice bath. To each reaction was added 1.0 mL of a stock solution of 3,5-dinitromethylbenzoate (458.5 mg, 2.02 mmol, in 25.0 mL THF) as an external standard. The reaction mixture was mixed thoroughly, and an aliquot was removed and filtered through cotton for ¹H NMR analysis (8 scans, 10 sec T1 relaxation delay). These single-point experiments were used to approximate initial rate.

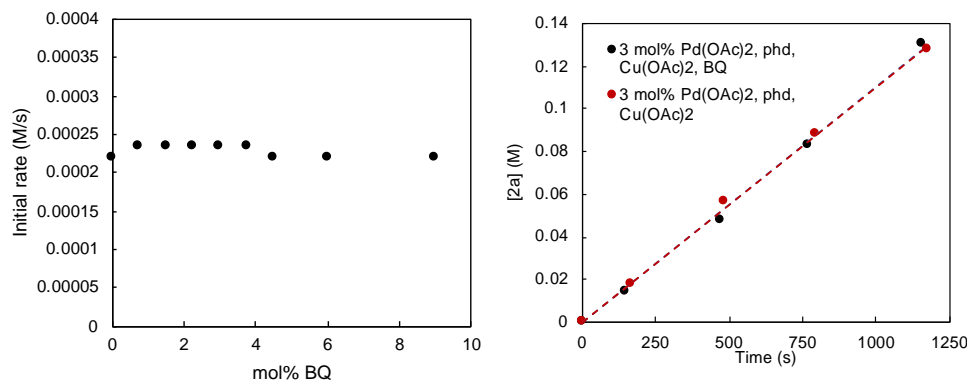


Figure C.2. Dependence on [BQ] and Initial-Rate Time Course. Standard conditions: 33 mM catalyst ([Pd(OAc)₂], [Cu(OAc)₂·H₂O], [phd], [BQ]), 1.1 M [2a] (0.55 mmol), 1.1 atm *p*O₂, 0.50 mL in DMSO, 120 °C. Standard conditions were employed, except for varied [BQ].

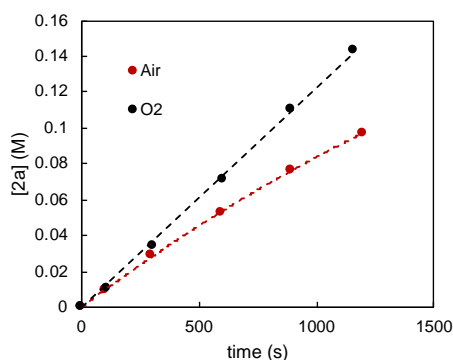


Figure C.3. Rate Dependence on *p*O₂. Conditions: 33 mM catalyst ([Pd(OAc)₂], [Cu(OAc)₂·H₂O], [phd], [BQ]), 1.1 M [2a] (1.1 mmol), 1.1 atm *p*O₂ or ambient air, 1.0 mL in DMSO, 120 °C.

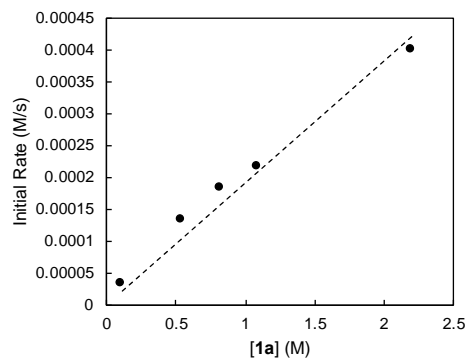


Figure C.4. Rate dependence on 1a. Conditions: 33 mM catalyst ($[\text{Pd}(\text{OAc})_2]$, $[\text{Cu}(\text{OAc})_2 \cdot \text{H}_2\text{O}]$, [phd], [BQ]), varying [2a] (1.1 mmol), 1.1 atm $p\text{O}_2$ or ambient air, 0.5 mL in DMSO, 120 °C.

C.7 Kinetic Isotope Effect Studies

General Procedure for KIE Experiments: Catalyst components (Pd(OAc)₂, phd, and BQ) at 3 mol% loading (0.0165 mmol) and 0.75 mol%, 3 mol% or 10 mol% Cu(OAc)₂ (depending on conditions) in DMSO stock solutions were added to 13x100 mm borosilicate glass heavy wall test tubes. Enough DMSO was added such that the final volume of the reaction mixture was 1.0 mL, and 20 μ L (0.19 mmol) of nitrobenzene was added as an internal standard. The catalyst mixture was heated to 120 °C for 5 minutes under 1.1 atm pO₂ with orbital mixing for 5 minutes before injecting 220 μ L of **1a** or **1a-d₁**. Approximately 50 μ L aliquots of the reaction were taken and quenched by injecting into 0.5 mL of THF in an NMR tube chilled in an ice bath. The samples were centrifuged to bring any precipitate to the bottom of the NMR tube before ¹H NMR analysis (8 scans, 10 second T1 relaxation delay).

Table C.8. Compiled initial rate data for formation of **2a** from **1a** and **1a-d₁** under varying [Cu(OAc)₂].

[Cu(OAc) ₂] (mM)		Rate (mM•s ⁻¹) Run 1	<i>k_H/k_D</i>	Rate (mM•s ⁻¹) Run 2	<i>k_H/k_D</i>	Rate (mM•s ⁻¹) Run 3	<i>k_H/k_D</i>	Avg. <i>k_H/k_D</i>
8.25	H	0.0792	2.4	0.0635	2.4	0.0673	2.3	2.4 ± 0.1
	D	0.0326		0.0268		0.0297		
33	H	0.1122	2.9	0.1239	2.8	--	--	2.9 ± 0.1
	D	0.0381		0.0438		--		
110	H	0.1749	2.5	0.1741	2.4	0.1721	2.8	2.6 ± 0.2
	D	0.071		0.0734		0.0609		

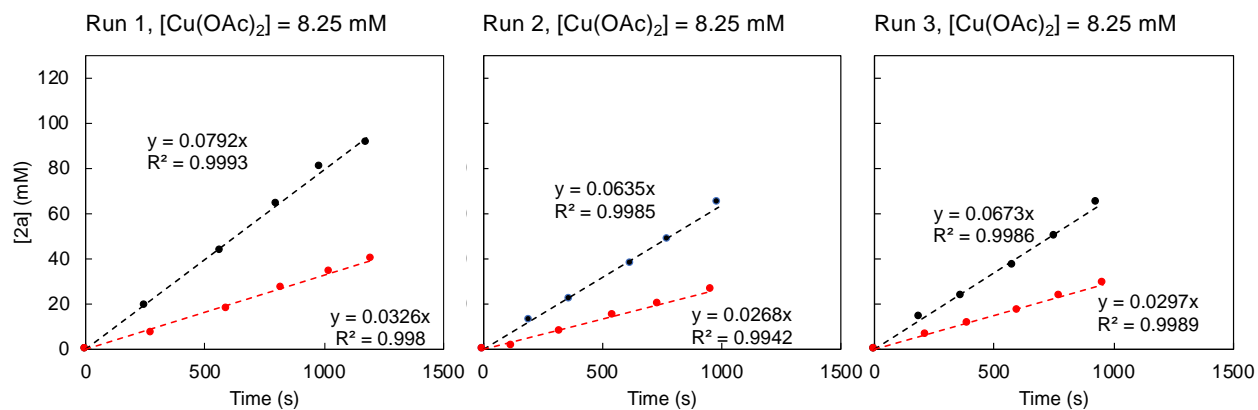


Figure C.5. Initial rate data for formation of **2a** from **1a** (black) or **1a-d₁** (red) at $[\text{Cu}(\text{OAc})_2] = 8.25 \text{ mM}$

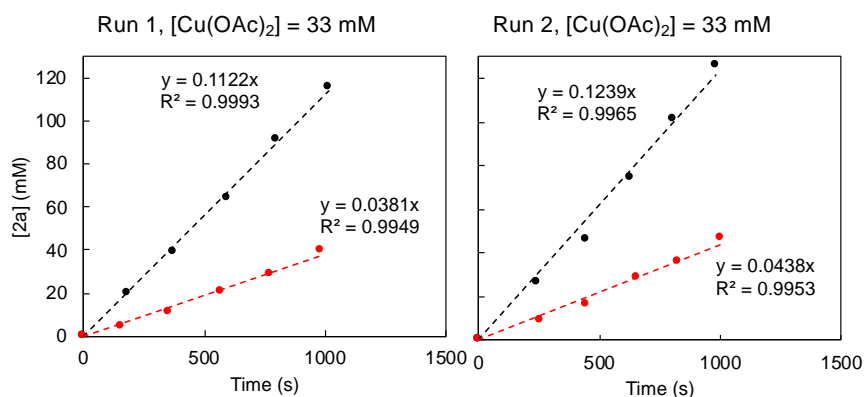


Figure C.6. Initial rate data for formation of **2a** from **1a** (black) or **1a-d₁** (red) at $[\text{Cu}(\text{OAc})_2] = 33 \text{ mM}$

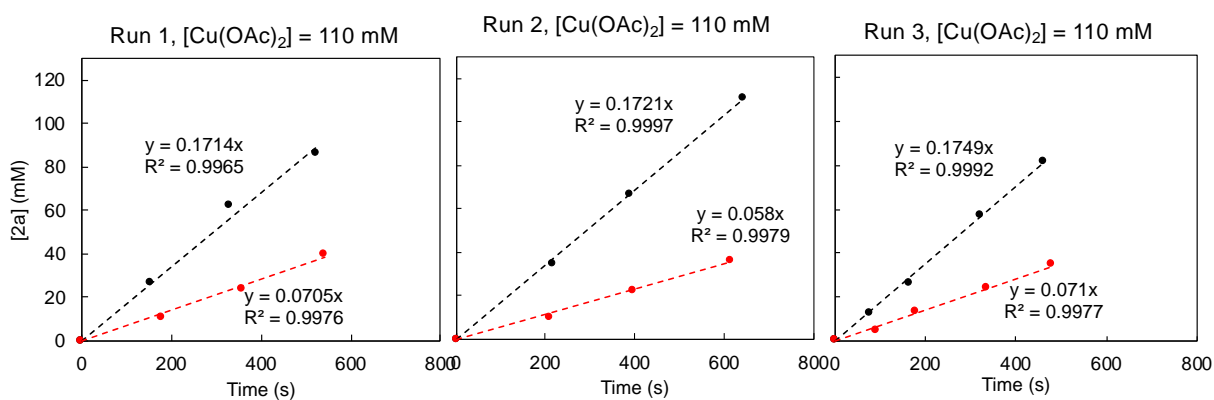


Figure C.7. Initial rate data for formation of **2a** from **1a** (black) or **1a-d₁** (red) at $[\text{Cu}(\text{OAc})_2] = 110 \text{ mM}$

C.8 H/D Exchange Studies

Catalyst components at 3 mol% loading (0.0165 mmol) were added to 13x100 mm borosilicate glass heavy wall test tubes via stock solutions. To each test tube was added 315 μL AcOD (10 equivalents relative to **1a**), 110 μL of **1a**, and enough DMSO such that the final volume of the reaction mixture was 0.5 mL. The reactions were heated at 120 °C under an O₂ atmosphere with orbital mixing for 30 min before they were removed from heat and quenched by submerging in an ice bath. To each reaction was added 200 μL of a stock solution of methyl-3,5-dinitrobenzoate (36.7 mg, 0.16 mmol, in 2.0 mL DMSO) as an external standard and 20 μL of DMSO-*d*₆ was added as an external standard for deuterium quantification. The reaction mixture was mixed thoroughly, and an aliquot was removed and filtered through cotton for ¹H NMR analysis (8 scans, 10 sec T1 relaxation delay). Results are shown in **Error! Reference source not found.** Since the reactions were stopped before completion (30 min) the concentration of **1a-d**₁ at that time serve as the basis for an initial rate measurement.

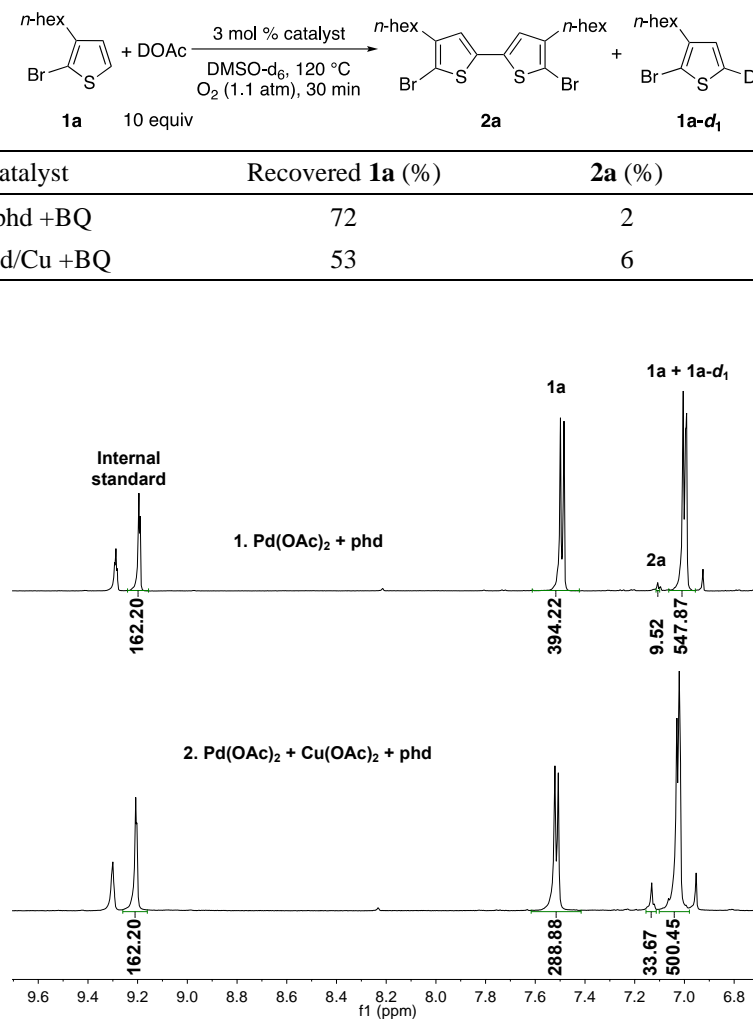
The amount of deuterium incorporation was determined by measuring the decreased intensity of the resonance of the C–H bond at the 5 position of **1a** (alpha to S) relative to the of the C–H bond at the 4 position of **1a** (beta to S). The data in **Error! Reference source not found.** were calculated by this method. %D incorporation can also be calculated by direct integration of deuterated product **1a-d**₁. The results of these each method are commensurate with one another.

Example calculation for %D incorporation by integration of **1a**: $[(547.87 - 394.22)/(547.87)] * 100\% = 28\%$.

Example calculation for %D incorporation by integration of **1a-d**₁ $[(22.97 * 6)/547.87] * 100\% = 25\%$. (Note: 6 is a scaling factor to account for the number of nuclides being integrated in DMSO-*d*₆ vs **1a-d**₁)

Table C.9. Results of H/D Exchange Studies from ^1H NMR Analysis

Entry	Catalyst	Recovered 1a (%)	2a (%)	1a-d₁ (%)
1	Pd/phd +BQ	72	2	28
2	Pd/phd/Cu +BQ	53	6	42

**Figure C.8.** ^1H NMR spectra of the crude reaction mixtures from H/D exchange of **1a** with DOAc.

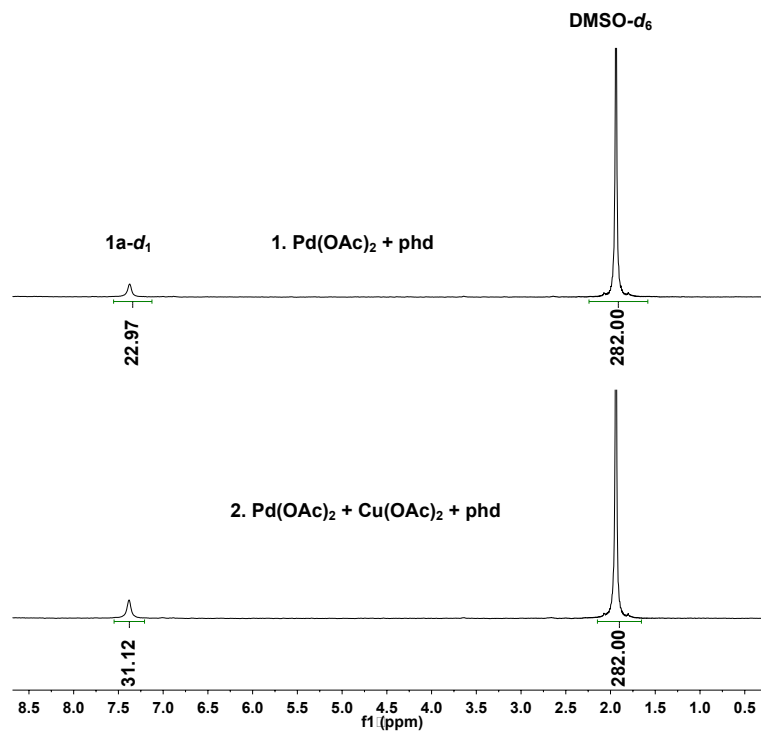
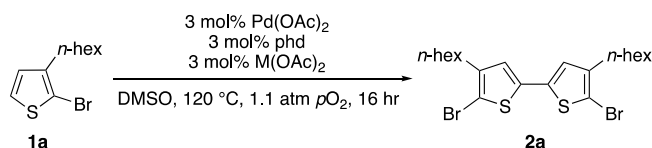


Figure C.9. ^2H NMR spectra of the crude reaction mixtures from H/D exchange of **1a** with DOAc.

C.9 Assessment of Non-Redox Active Metal Acetate Salts

Into 13x100 mm borosilicate glass heavy wall test tubes were added $\text{Pd}(\text{OAc})_2$ (3 mol%), phd (3 mol%), and $\text{M}(\text{OAc})_2$ (3 mol%), via stock solutions in DMSO, followed by **1a** (110.0 μL , 136.4 mg, 0.550 mmol). Enough DMSO was added to raise the total volume of the reaction to 500 μL . The test tube was moved to an orbital shaker, heated to 120 $^\circ\text{C}$ and the headspace purged with O_2 before being sealed and run for 16 h. The reaction mixtures were allowed to cool and a solution of NMR standard in THF was added before being analyzed by ^1H NMR spectroscopy (8 scans, 10 sec T1 relaxation delay).

Table C.10. Acetate Salt Additive Screen



Entry	Metal Acetate	MB (%)	RSM (%)	2a (%)
1	none	99	93	6
2	Mg(OAc) ₂	97	62	35
3	Zn(OAc) ₂	98	68	30
4	Cu(OAc) ₂	81	8	73

C.10 Catalyst Characterization by ¹H NMR Spectroscopy

¹H NMR Spectroscopic Titration of Pd(OAc)₂ with phd. A stock solution of Pd(OAc)₂ (74.1.0 mg, 0.33 mmol) and methyl-3,5-dinitrobenzoate as an internal standard (75.0 mg 0.33 mmol) in 5.0 mL of DCM and a separate stock solution of phd (69.6 mg, 0.32 mmol, in 5.0 mL DCM) were prepared. Into separate vials, 500 μL of the Pd(OAc)₂/ methyl-3,5-dinitrobenzoate solution was deposited. Into each of these was added a portion of the phd stock solution to achieve the Pd(OAc)₂:phd ratio. The DCM was removed *in vacuo*, and the resulting mixtures were dissolved in 1.0 mL of DMSO-d₆ and transferred to an NMR tube for ¹H NMR analysis (8 scans, 2 dummy scans, 10 second T1 relaxation delay).

Table C.11. Concentrations of Species in phd Titration

Entry	Equiv phd added	phd (mM)	Pd(OAc) ₂ (mM)	Pd(OAc) ₂ /phd (mM)	Pd Mass Balance (mM)
1	0	0	30.9	0	30.9
2	0.50	0	15.6	16.8	32.4
3	0.75	0	7.4	24.9	32.3
4	0.90	0	0.9	31.5	32.4
5	1.0	2.1	0	30.9	30.9
6	1.5	18.7	0	30.8	30.8
7	2.0	34.2	0	30.2	30.2

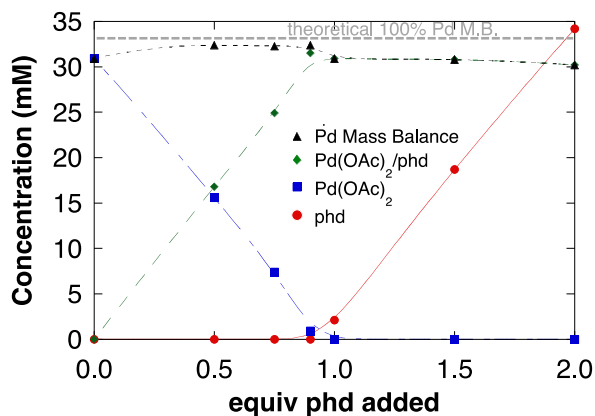


Figure C.10. Plot of titration of Pd(OAc)₂ with phd as monitored by ¹H NMR spectroscopy.

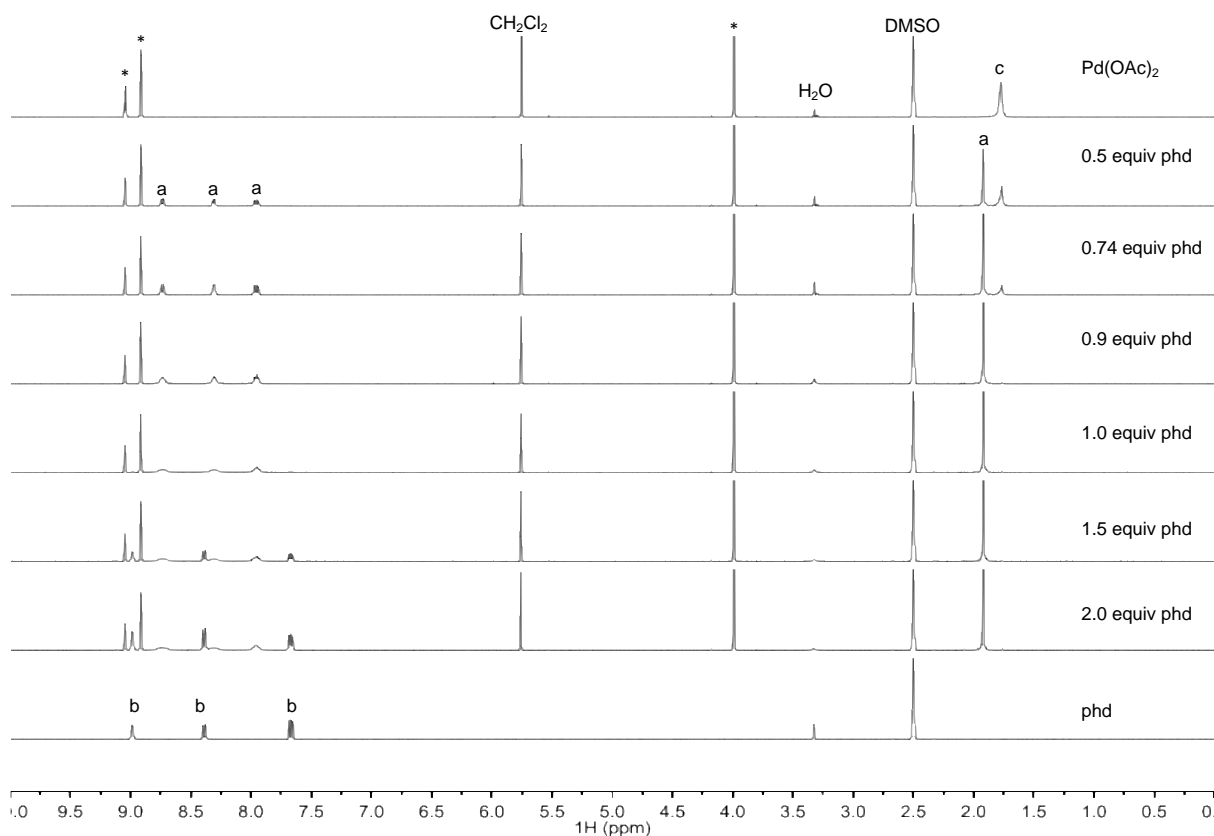


Figure C.11. Titration experiment involving addition of phd into a solution of Pd(OAc)₂ in DMSO. Pd(OAc)₂/phd species is denoted by 'a'; free phd is denoted by 'b'; free Pd(OAc)₂ is denoted by 'c'; * denotes methyl 3,5-dinitrobenzoate internal standard.

¹H NMR Analysis of phd-Pd/Cu(OAc)₂ and phen-Pd/Cu(OAc)₂ mixtures. *Procedure for NMR characterization of phd-Pd/Cu(OAc)₂ and phen-Pd/Cu(OAc)₂ mixtures:* A stock solution of methyl-3,5-dinitrobenzoate (37.3 mg, 0.165 mmol) in 5.0 mL DMSO-d₆ was prepared. Pd(OAc)₂ (22.2 mg, 0.10 mmol), Cu(OAc)₂•H₂O (19.8 mg, 0.10 mmol), and phd (20.8 mg, 0.10 mmol) were each dissolved in 1.0 mL of the methyl-3,5-dinitrobenzoate stock solution. Portions of each of these solutions were mixed such that the desired ratios of the components were achieved, and enough of the methyl-3,5-dinitrobenzoate stock solution was added such that the total volume of the mixture reached 600 μL. The mixtures were transferred to an NMR tube for ¹H NMR analysis. A similar procedure was performed for the phen-Pd/Cu(OAc)₂ mixtures except the internal standard chosen was 1,3,5-trimethoxybenzene.

Interpretation of Pd/Cu(OAc)₂-phd ¹H NMR spectra: From Figure C.12, spectrum 3, it is evident that Pd(OAc)₂ forms a 1:1 complex with phd and no free phd is observed. The mixture of Cu(OAc)₂ and phd (spectrum 2) results in a spectrum with two broad resonances downfield of 10 ppm, consistent with the formation of a paramagnetic Cu(OAc)₂/phd species. Upon addition of Cu(OAc)₂ to Pd(OAc)₂/phd (spectrum 1) the resonances corresponding to Pd(OAc)₂/phd remain, while multiple new resonances are observed in the paramagnetic region of the spectrum and the broad resonances corresponding to Cu(OAc)₂/phd are not observed. Based on integration relative to internal standard, 76% of the major Pd(OAc)₂/phd species can be accounted for. It is thus proposed that the new resonances that appear upon addition of Cu(OAc)₂ correspond to (1) free Cu(OAc)₂ and (2) a unique heterometallic paramagnetic species, designated Pd(OAc)₂/phd/Cu(OAc)₂, that accounts for at least some of the missing 24% mass balance.

Interpretation of Pd/Cu(OAc)₂-phen ¹H NMR spectra and Comparison to Pd/Cu(OAc)₂-phd ¹H NMR spectra: From Figure C.13, spectrum 3, it is evident that Pd(OAc)₂ forms a 1:1

complex with phen; no free phen is observed. The mixture of $\text{Cu}(\text{OAc})_2$ and phen (spectrum 2) results in the formation of three broad resonances downfield of 10 ppm, consistent with the formation of a paramagnetic $\text{Cu}(\text{OAc})_2/\text{phen}$ species. Addition of $\text{Cu}(\text{OAc})_2$ to $\text{Pd}(\text{OAc})_2/\text{phen}$ results in a spectrum consistent with a mixture of $\text{Cu}(\text{OAc})_2$ and $\text{Pd}(\text{OAc})_2/\text{phen}$. No new resonances are observed, and the $[\text{Pd}(\text{OAc})_2/\text{phen}]$ measured relative to internal standard is 33 mM, accounting for 100% of the $\text{Pd}(\text{OAc})_2$ and phen concentrations. These observations suggest that phen selectively binds $\text{Pd}(\text{OAc})_2$ in the presence of $\text{Cu}(\text{OAc})_2$ and that phen does not facilitate the formation of a paramagnetic heterometallic species like phd. It is therefore proposed that the *o*-quinone moiety of phd facilitates the formation of this heterometallic species.

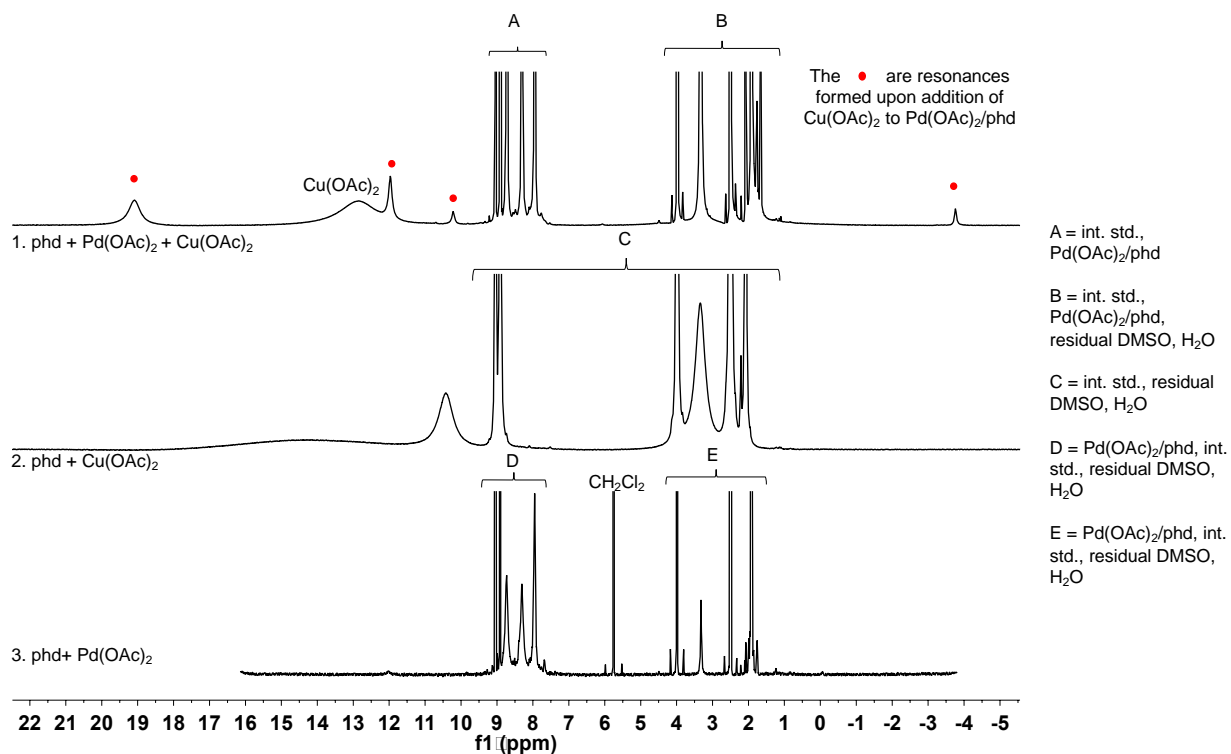


Figure C.12. ^1H NMR Spectral Studies of phd- $\text{Pd}/\text{Cu}(\text{OAc})_2$ Mixtures ^1H NMR spectra of mixtures of (1) phd + $\text{Pd}(\text{OAc})_2$ + $\text{Cu}(\text{OAc})_2$; (2) phd + $\text{Cu}(\text{OAc})_2$; (3) phd + $\text{Pd}(\text{OAc})_2$ in $\text{DMSO}-d_6$ (all components 33 mM). Spectra are clipped vertically to amplify the phd resonances. NMR parameters =500 MHz, $\text{DMSO}-d_6$, 8 scans, 2 dummy scans, T1 relaxation delay: 10 seconds

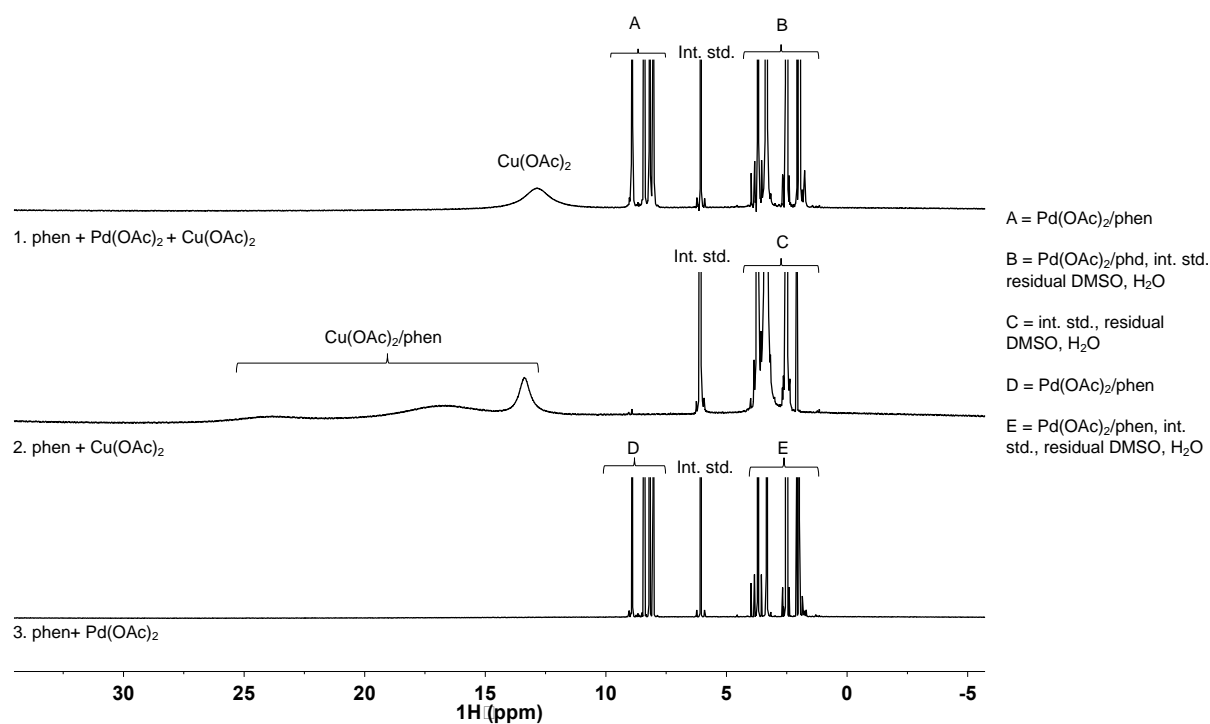
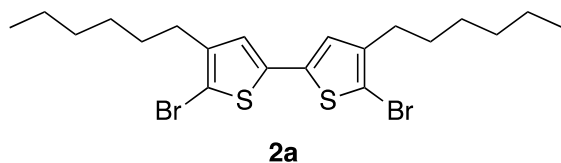


Figure C.13. ¹H NMR spectra of mixtures of (1) phen + Pd(OAc)₂ + Cu(OAc)₂; (2) phen + Cu(OAc)₂; (3) phen + Pd(OAc)₂ in DMSO-*d*₆ (all components 33 mM). Spectra are clipped vertically to amplify the phd resonances. NMR parameters =500 MHz, DMSO-*d*₆, 8 scans, 2 dummy scans, T1 relaxation delay: 10 seconds

C.11 Synthetic Procedures and Characterization Data



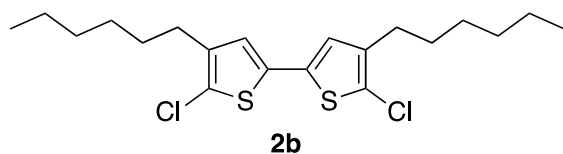
2a: Prepared from **1a** (1.1 mmol, 271.92 mg) according to general procedure in Section II except the work-up utilized pentanes instead of CH₂Cl₂.

Purified by reversed phase column chromatography using a 0-100% acetonitrile gradient in MeOH to give **2a** in 75% yield (0.202 g) as a pale-yellow oil.

¹H NMR: (500 MHz, CDCl₃) δ 6.77 (s, 2H), 2.55 – 2.48 (m, 4H), 1.58 (m, 4H), 1.39 – 1.24 (m, 12H), 0.92 – 0.86 (m, 6H).

^{13}C NMR: (126 MHz, CDCl_3) δ 143.12, 136.30, 124.61, 108.01, 31.74, 29.75, 29.70, 29.03, 14.24.

HRMS (ASAP-MS) Calculated for $\text{C}_{20}\text{H}_{28}\text{Br}_2\text{S}_2$ ($[\text{M}+\text{H}]^+$): 491.0072, measured 491.0067

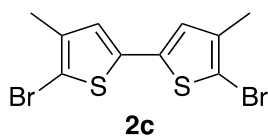


2b: After cooling to rt, 5 mL EtOAc was added to the shaker tube. The crude product mixture was mixed, and everything was filtered through a glass frit. The shaker tube was washed with more EtOAc and passed through the frit, and then the frit was washed with EtOAc until no more color passed through it. The filtrate was diluted to ~15 mL w/EtOAc. It then was extracted twice with ice-chilled brine. The brine layers were combined and back extracted with EtOAc until there was little color left in the brine layers. The organic layers were combined, dried w/ MgSO_4 , and filtered through a glass frit. The filtrate was rotovapped. The residue was dissolved in minimal pentanes and passed through a silica plug (100% CH_2Cl_2 eluent). Fractions were collected until a red band was about to elute. The fractions were combined. The solid was dissolved in minimal CH_2Cl_2 and purified by reverse phase column chromatography (100% MeOH to 55% MeOH/45% CH_3CN gradient). Fractions enriched in product were collected, rotovapped, and dried *in vacuo* to give 77% yield (0.170 g).

^1H NMR: (500 MHz, CDCl_3) δ 6.76 (s, 2H), 2.53 (t, $J = 7.6$ Hz, 4H), 1.62 – 1.52 (m, 4H), 1.39 – 1.25 (m, 12H), 0.89 (t, $J = 6.7$, 6H).

^{13}C NMR: (126 MHz, CDCl_3) δ 140.36, 133.24, 123.42, 31.74, 29.66, 29.03, 28.19, 22.74, 14.24.

HRMS (ASAP-MS) Calculated for $\text{C}_{20}\text{H}_{28}\text{Cl}_2\text{S}_2$ ($[\text{M}+\text{H}]^+$): 403.1082, measured 403.1074

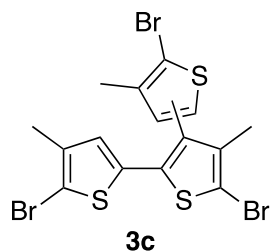


2c: After cooling to rt, 5 mL EtOAc was added to the shaker tube. The crude product mixture was mixed, and everything was filtered through a glass frit. The shaker tube was washed with more EtOAc and passed through the frit, and then the frit was washed with EtOAc until no more color passed through it. The filtrate was diluted to ~15 mL w/EtOAc. It then was extracted twice with ice-chilled brine. The brine layers were combined and back extracted with EtOAc until there was little color left in the brine layers. The organic layers were combined, dried w/ MgSO_4 , and filtered through a glass frit. The filtrate was rotovapped. The residue was dissolved in minimal CH_2Cl_2 and passed through a silica plug (100% CH_2Cl_2 eluent). Fractions were collected until a red band was about to elute. The fractions were combined. The solid was dissolved in minimal CH_2Cl_2 and purified by reverse phase column chromatography (100% MeOH to 55% MeOH/45% CH_3CN gradient). Fractions enriched in product were collected, rotovapped, and dried *in vacuo* to give 69% yield (0.141 g).

2c: ^1H NMR: (500 MHz, CDCl_3) δ 6.76 (s, 2H), 2.17 (s, 6H).

2c: ^{13}C NMR: (126 MHz, CDCl_3) δ 138.21, 135.98, 125.59, 108.50, 15.38.

2c: HRMS (ASAP-MS) Calculated for $\text{C}_{10}\text{H}_8\text{Br}_2\text{S}_2$ ($[\text{M}+\text{H}]^+$): 350.8507, measured 350.8505

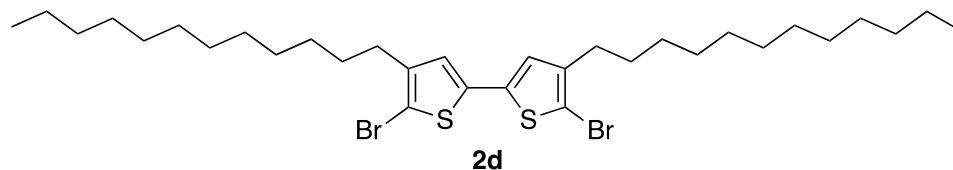


3c: This was enriched relative to **2c** in fractions from reverse phase column chromatography that eluted after the most pure fractions of **2c**. Yield: 6.9 mg (4%).

3c: $^1\text{H NMR}$ (500 MHz, CDCl_3) δ 6.73 (s, 1H), 6.63 (s, 1H), 2.23 (s, 3H), 2.12 (s, 3H), 2.02 (s, 3H).

3c: $^{13}\text{C NMR}$ (126 MHz, CDCl_3) δ 138.84, 137.79, 137.21, 135.52, 134.94, 134.26, 131.25, 130.26, 127.88, 111.14, 111.00, 108.19, 15.48, 15.26, 15.13.

3c: **HRMS (ASAP-MS)** Calculated for $\text{C}_{15}\text{H}_{11}\text{Br}_3\text{S}_3$ ($[\text{M}+\text{H}]^+$): 524.7646, measured 524.7641



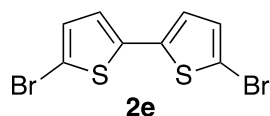
2d: Prepared from **1d** (1.1 mmol, 329.9 mg) according to general procedure in Section II except the solvent used was a 1.2:1 mixture of cyclohexyl acetate:DMSO and the work-up utilized pentanes instead of DCM.

Purified by reversed phase column chromatography using a 0-100% THF gradient in MeOH. The resulting material was passed through a plug of silica gel eluting with pentanes to remove plasticizer that was leached from the reversed phase column to give **2d** in 74% yield (0.267 g) as a yellow solid.

$^1\text{H NMR}$: (500 MHz, CDCl_3) δ 6.77 (s, 2H), 2.57 – 2.46 (m, 4H), 1.57 (s, 4H), 1.39 – 1.17 (m, 36H), 0.88 (t, $J = 6.9$ Hz, 6H).

$^{13}\text{C NMR}$: (126 MHz, CDCl_3) δ 143.13, 136.30, 124.62, 108.00, 32.08, 29.82, 29.79, 29.77, 29.70, 29.54, 29.51, 29.34, 22.85, 14.28.

HRMS (ASAP-MS) Calculated for $\text{C}_{32}\text{H}_{52}\text{Br}_2\text{S}_2$ ($[\text{M}+\text{H}]^+$): 659.1950, measured 659.1946

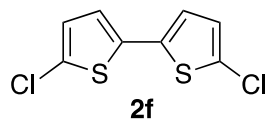


2e: Prepared from **1e** (1.1 mmol, 179.3 mg) according general procedure in Section II, except the crude reaction mixture was taken directly to plug silica gel (~10 inches of silica, 1 inch diameter column) eluted with CH_2Cl_2 . A yellow band was collected until an orange band began to elute. The yellow band was found to be the product **2e** in 63% yield (0.112 g) as a yellow solid.

$^1\text{H NMR}$: (500 MHz, CDCl_3) δ 6.96 (d, $J = 3.8$ Hz, 2H), 6.85 (d, $J = 3.8$ Hz, 2H).

$^{13}\text{C NMR}$: (126 MHz, CDCl_3) δ 137.93, 130.82, 124.31, 111.67.

HRMS (ASAP-MS) Calculated for $\text{C}_8\text{H}_4\text{Br}_2\text{S}_2$ ($[\text{M}+\text{H}]^+$): 322.8194, measured 322.8191

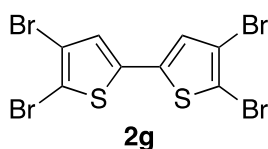


2f: Prepared from **1f** (1.1 mmol, 130.4 mg) according general procedure in Section II, except the crude reaction mixture was taken directly to a plug of silica gel (~10 inches of silica, 1 inch diameter column) eluted with pentanes. Eluent was collected until a yellow band began to elute. The early fractions were found to be **2f** in 37% yield (0.048 g) as a pale yellow solid.

¹H NMR: (500 MHz, CDCl₃) δ 6.85 (d, *J* = 3.8 Hz, 2H), 6.82 (d, *J* = 3.9 Hz, 2H).

¹³C NMR: (126 MHz, CDCl₃) δ 135.17, 129.33, 127.05, 123.21.

HRMS (ASAP-MS) Calculated for C₈H₄Cl₂S₂ ([M+H]⁺): 234.9204 measured 234.9202

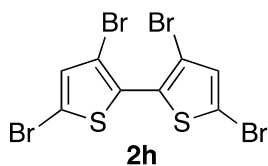


2g: Prepared from **1g** (1.1 mmol, 266.1 mg) according general procedure in Section II, except the crude reaction mixture was taken directly to a plug of silica gel (~10 inches of silica, 1 inch diameter column) eluted with CH₂Cl₂. A yellow band eluted first, which was collected and found to be enriched in product **2g**. The crude product was purified by column chromatography on silica gel with a 0-10% EtOAc gradient in pentane to yield **2g** in 50% yield (0.132 g) as a pale-yellow solid.

¹H NMR: (500 MHz, CDCl₃) δ 6.93 (s, 2H).

¹³C NMR: (126 MHz, CDCl₃) δ 136.50, 126.91, 114.92, 111.28.

HRMS (ASAP-MS) Calculated for C₈H₂Br₄S₂ ([M+H]⁺): 478.6404, measured 478.6397

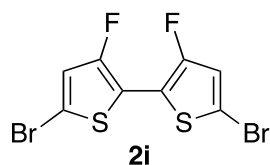


2h: Prepared from **1h** (1.1 mmol, 266.1 mg) according general procedure in Section II, except the crude reaction mixture was taken directly to a plug of silica gel (~10 inches of silica, 1 inch diameter column) eluted with CH₂Cl₂. A yellow band eluted first, which was collected and found to be enriched in product **2g**. The crude product was purified by silica gel column chromatography with a 0-10% EtOAc gradient in pentane to yield **2g** in 57% yield (0.152 g) as a white solid.

¹H NMR: (500 MHz, CDCl₃) δ 7.05 (s, 2H).

¹³C NMR: (126 MHz, CDCl₃) δ 133.13, 129.69, 114.97, 112.27.

HRMS (ASAP-MS) Calculated for C₈H₂Br₄S₂ ([M+H]⁺): 478.6404, measured 478.6398



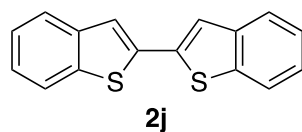
2i: Prepared from **1i** (1.1 mmol, 199.1 mg) according general procedure in Section II, except the crude reaction mixture was taken directly to a plug of silica gel (~10 inches of silica, 1 inch diameter column) eluted with pentanes. Eluent was collected until a yellow band began to elute. The fraction collected prior to elution of the yellow band was found to be product **2i** in 73% yield (0.144 g) as a pale yellow solid which required no more purification.

¹H NMR: (500 MHz, CDCl₃) δ 6.87 (s, 2H)

¹³C NMR: (126 MHz, CDCl₃) δ 152.16 (d, *J* = 266.6 Hz), 120.26 (d, *J* = 27.2 Hz), 112.58-112.40 (m), 111.74-111.58 (m)

¹⁹F NMR: (377 MHz, CDCl₃) δ -123.21.

HRMS (ASAP-MS) Calculated for C₈H₂Br₂F₂S₂ ([M+H]⁺): 358.8006, measured 358.8002

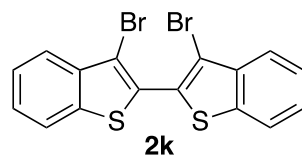


2j: Prepared from **1j** (1.1 mmol, 147.6 mg) according general procedure in Section II. Purified by silica gel column chromatography with a 0-5% EtOAc gradient in pentanes to yield impure **2j** that was further purified by recrystallization from EtOH/CH₂Cl₂ to give **2j** in 15% yield as a tan solid.

¹H NMR: (500 MHz, CDCl₃) δ 7.81 (d, *J* = 7.6 Hz, 2H), 7.77 (d, *J* = 8.2 Hz, 2H), 7.52 (s, 2H), 7.39 – 7.30 (m, 4H).

¹³C NMR: (126 MHz, CDCl₃) δ 140.34, 139.61, 137.35, 125.08, 124.95, 123.87, 122.34, 121.56.

HRMS (ASAP-MS) Calculated for C₁₆H₁₀S₂ ([M+H]⁺): 267.0297, measured 267.0294

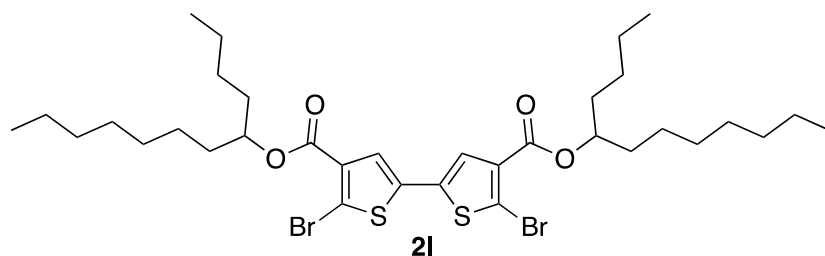


2k: Prepared from **1k** (1.1 mmol, 234.4 mg) according general procedure in Section II. Purified by silica gel column chromatography with a 0-5% EtOAc gradient in pentanes to yield impure **2k** that was further purified by recrystallization from EtOH/DCM to give **2k** in 73% yield (0.172 g) as a tan solid.

¹H NMR: (500 MHz, CDCl₃) δ 7.88 – 7.82 (m, 2H), 7.80 – 7.74 (m, 2H), 7.51 – 7.35 (m, 4H).

¹³C NMR: (126 MHz, CDCl₃) δ 139.29, 138.24, 129.51, 126.49, 125.62, 124.19, 122.42, 111.01.

HRMS (ASAP-MS) Calculated for C₁₆H₈Br₂S₂ ([M+H]⁺): 422.8507, measured 422.8502



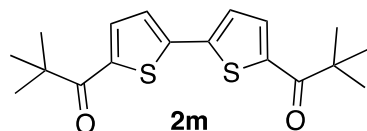
2l: Prepared from **1l** (1.1 mmol, 412.9 mg) according to general procedure in Section II except the work-up utilized pentanes instead of DCM.

Purified by reversed phase column chromatography using a 0-5% acetonitrile gradient in MeOH to give **2l** in 59% yield (0.242 g) as a yellow oil. Product contains a small amount of unidentified impurity (~7%, assuming ^1H NMR resonances at 7.42, 7.45, and 7.64 ppm correspond to 1 proton).

^1H NMR: (500 MHz, CDCl_3) δ 7.35 (s, 2H), 4.22 (d, $J = 5.6$ Hz, 4H), 1.75 (m, 5.9 Hz, 2H), 1.50 – 1.13 (m, 32H), 0.89 (m, 12H).

^{13}C NMR: (126 MHz, CDCl_3) δ 161.85, 135.42, 132.46, 126.19, 119.09, 68.24, 37.46, 31.98, 31.52, 31.19, 29.77, 29.10, 26.87, 23.13, 22.81, 14.26, 14.24.

HRMS (ASAP-MS) Calculated for $\text{C}_{34}\text{H}_{52}\text{O}_4\text{Br}_2\text{S}_2$ ($[\text{M}+\text{H}]^+$): 747.1747, measured 747.1751

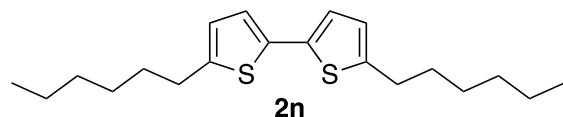


2m: Prepared from **1m** (1.1 mmol, 185.1 mg) according general procedure in Section II. Purified by silica gel column chromatography with a 0-30% EtOAc gradient in pentanes to yield impure **2m** that was further purified by recrystallization from EtOH/DCM to give **2m** in 55% yield (0.102 g).

^1H NMR: (500 MHz, CDCl_3) δ 7.69 (d, $J = 4.0$ Hz, 2H), 7.27 (d, $J = 4.0$ Hz, 2H), 1.41 (s, 18H).

^{13}C NMR: (126 MHz, CDCl_3) δ 198.76, 142.79, 142.46, 132.83, 125.65, 44.05, 28.27.

HRMS (ASAP-MS) Calculated for $\text{C}_{18}\text{H}_{22}\text{O}_2\text{S}_2$ ($[\text{M}+\text{H}]^+$): 335.1134, measured 335.1129

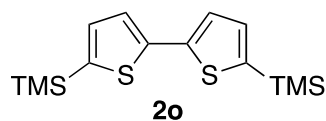


2n: Prepared from **1n** (1.1 mmol, 362.2 mg) according general procedure in Section II, except the crude reaction mixture was taken directly to a plug of silica gel and eluted with CH_2Cl_2 . An orange/brown band eluted which was collected and found to be enriched in product **2n**. The crude product was purified by reversed phase column chromatography with a 0-100% acetonitrile gradient in MeOH to yield impure **2n**. Impure **2n** was recrystallized in EtOH/ CH_2Cl_2 to yield **2n** in 36% yield (0.067 g).

^1H NMR: (500 MHz, CDCl_3) δ 6.89 (d, $J = 3.5$ Hz, 2H), 6.64 (dt, $J = 3.5, 1.0$ Hz, 2H), 2.81 – 2.73 (m, 4H), 1.66 (p, $J = 7.5$ Hz, 4H), 1.42 – 1.32 (m, 4H), 1.35 – 1.24 (m, 8H), 0.93 – 0.85 (m, 6H).

^{13}C NMR: (126 MHz, CDCl_3) δ 144.83, 135.45, 124.70, 122.72, 31.72, 30.30, 28.90, 22.73, 14.24.

HRMS (ASAP-MS) Calculated for $\text{C}_{20}\text{H}_{30}\text{S}_2$ ($[\text{M}+\text{H}]^+$): 335.1862, measured 335.1856

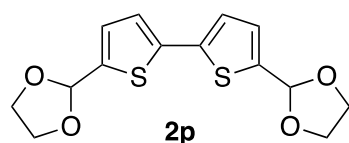


2o: Prepared from **1o** (1.1 mmol, 172.0 mg) according general procedure in Section II. Purified by silica gel column chromatography with pentanes to yield **2o** in 62% yield (0.106 g).

¹H NMR: (500 MHz, CDCl₃) δ 7.23 (d, *J* = 3.4 Hz, 2H), 7.13 (d, *J* = 3.4 Hz, 2H), 0.33 (s, 18H).

¹³C NMR: (126 MHz, CDCl₃) δ 142.56, 139.92, 134.87, 125.20, 0.04.

HRMS (ASAP-MS) Calculated for C₁₄H₂₂S₂Si₂ ([M+H]⁺): 311.0774, measured 311.0770

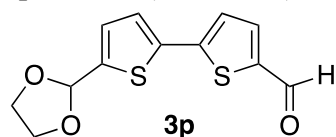


2p and 3p: Prepared from **1p** (1.1 mmol, 171.8 mg) according general procedure in Section II, except the crude reaction mixture was taken directly to a plug of silica gel and eluted with CH₂Cl₂. A yellow band eluted which was collected and found to be enriched in product **2p**. The crude product was purified by silica gel column chromatography with a 10-100% EtOAc gradient in pentanes to yield a mixture of product **2p** and **3p** in a ratio of 8.8:1 **2p**:**3p** in combined 53% yield (0.090 g) as a tan solid.

2p: **¹H NMR:** (500 MHz, CDCl₃) δ 7.06 (d, *J* = 3.7 Hz, 2H), 7.03 (d, *J* = 3.7 Hz, 2H), 6.08 (s, 2H), 4.20 – 4.09 (m, 4H), 4.07 – 3.98 (m, 4H).

2p: **¹³C NMR:** (126 MHz, CDCl₃) δ 141.05, 138.32, 127.09, 123.64, 100.34, 65.42.

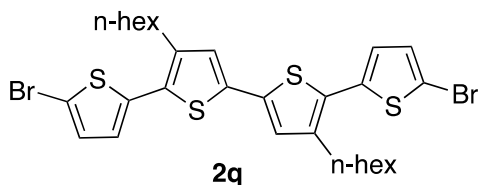
2p: **HRMS (ASAP-MS)** Calculated for C₁₄H₁₄S₂O₄ ([M+H]⁺): 311.0406, measured 311.0410



4p: **¹H NMR:** (500 MHz, CDCl₃) δ 9.86 (s, 1H), 7.67 (d, *J* = 3.9 Hz, 1H), 7.24 (dd, *J* = 3.8, 2.4 Hz, 2H), 7.12 (d, *J* = 3.7 Hz, 1H), 6.10 (s, 1H), 4.21 – 3.97 (m, 4H).

4p: **¹³C NMR:** (126 MHz, CDCl₃) δ 182.71, 147.04, 143.84, 142.14, 137.41, 136.91, 127.38, 125.86, 124.59, 100.07, 65.50.

4p: **HRMS (ASAP-MS)** Calculated for C₁₂H₁₀S₂O₃ ([M+H]⁺): 267.0144, measured 267.1043

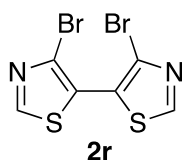


2q: Prepared from **1h** (1.1 mmol, 362.2 mg) according general procedure in Section II, except the crude reaction mixture was taken directly to a plug of silica gel and eluted with CH₂Cl₂. An orange band eluted which was collected and found to be enriched in product **2q**. The crude product was recrystallized from EtOH/DCM to give **2q** as a bright orange solid in 64% yield (0.233 g).

¹H NMR: (500 MHz, CDCl₃) δ 7.02 (d, *J* = 3.8 Hz, 2H), 6.97 (s, 2H), 6.86 (d, *J* = 3.8 Hz, 2H), 2.71 – 2.64 (m, 4H), 1.63 (ddd, *J* = 12.8, 10.3, 6.5 Hz, 4H), 1.42 – 1.32 (m, 4H), 1.31 (m, 8H), 0.92 – 0.83 (m, 6H).

¹³C NMR: (126 MHz, CDCl₃) δ 141.09, 137.50, 135.29, 130.41, 128.88, 126.62, 126.22, 112.08, 31.78, 30.67, 29.46, 29.33, 22.75, 14.24.

HRMS (ASAP-MS) Calculated for C₂₈H₃₂Br₂S₄ ([M+H]⁺): 654.9806, measured 654.9834

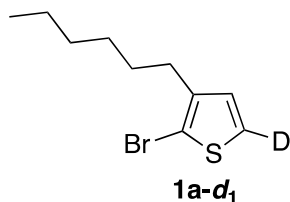


2r: Prepared from **1m** (1.1 mmol, 180.4 mg) according general procedure in Section II. Purified by reversed phase column chromatography with a gradient of acetonitrile in MeOH to give **2r** in 29% yield (0.052 g) as a yellow solid.

¹H NMR: (500 MHz, CDCl₃) δ 8.88 (s, 2H).

¹³C NMR: (126 MHz, CDCl₃) δ 154.63, 129.25, 122.48.

HRMS (ASAP-MS) Calculated for C₆H₂Br₂S₂N₂ ([M+H]⁺): 324.8100, measured 324.8099



1a-d₁: To 40 mL of Et₂O in an oven-dried 100 mL Schlenk flask under N₂, 16.0 mL of *n*-butyllithium (2.5 M in hexanes) was added and cooled to -78 °C. To the *n*-BuLi solution, 2,5-dibromo-3-hexylthiophene (3.3 mL, 15.4 mmol) was added and stirred for 30 minutes while the reaction mixture took a gelatin-like consistency. The reaction temperature was raised to 0 °C, and excess D₂O was added to quench the reaction. Upon addition of D₂O, the reaction mixture lost its gelatin-like consistency and was stirred for 30 minutes. Water was added to dissolve salts that formed, and the aqueous layer was separated from the organic layer. The organics were removed *in vacuo* to yield the 2,5-dideutero-3-hexylthiophene. The reaction was taken to directly to the next step without further work-up. The 2,5-dideutero-3-hexylthiophene was added to an oven-dried 100 mL round-bottom flask, put under an atmosphere of N₂, dissolved in 25 mL of THF from a solvent still, and cooled to 0 °C. Freshly recrystallized N-bromosuccinimide (2.74 g 15.4 mmol) was added and the reaction was stirred for 4 h and allowed to warm to RT. The reaction mixture was washed with 25 mL of 10% aqueous Na₂S₂O₃ and twice with 25 mL of

water. The aqueous layer was separated and extracted 3 times with 10 mL of pentanes. The organic layers were combined and dried over MgSO_4 , filtered, and removed *in vacuo*. The crude pale-yellow oil was distilled *in vacuo* to yield 3.65 g of 2-bromo-3-hexyl-5-deuteriothiophene (**1a-d₁**) (96% yield over two steps).

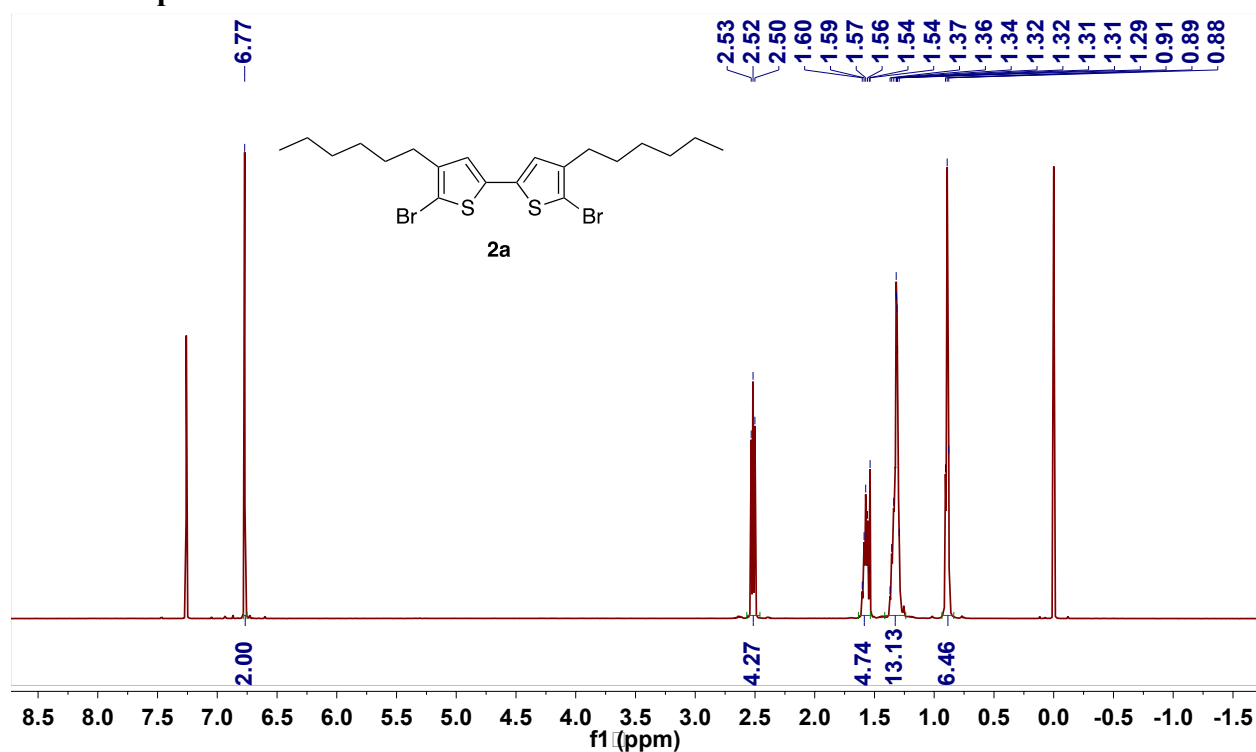
$^1\text{H NMR}$ (500 MHz, CDCl_3) δ 6.79 (s, 1H), 2.59 – 2.52 (m, 2H), 1.61 – 1.53 (m, 2H), 1.38 – 1.26 (m, 6H), 0.92 – 0.85 (m, 3H).

$^{13}\text{C NMR}$ (126 MHz, CDCl_3) δ 141.98, 128.09, 126.43 – 122.57 (m), 108.68, 31.62, 29.71, 29.40, 28.89, 22.60, 14.09.

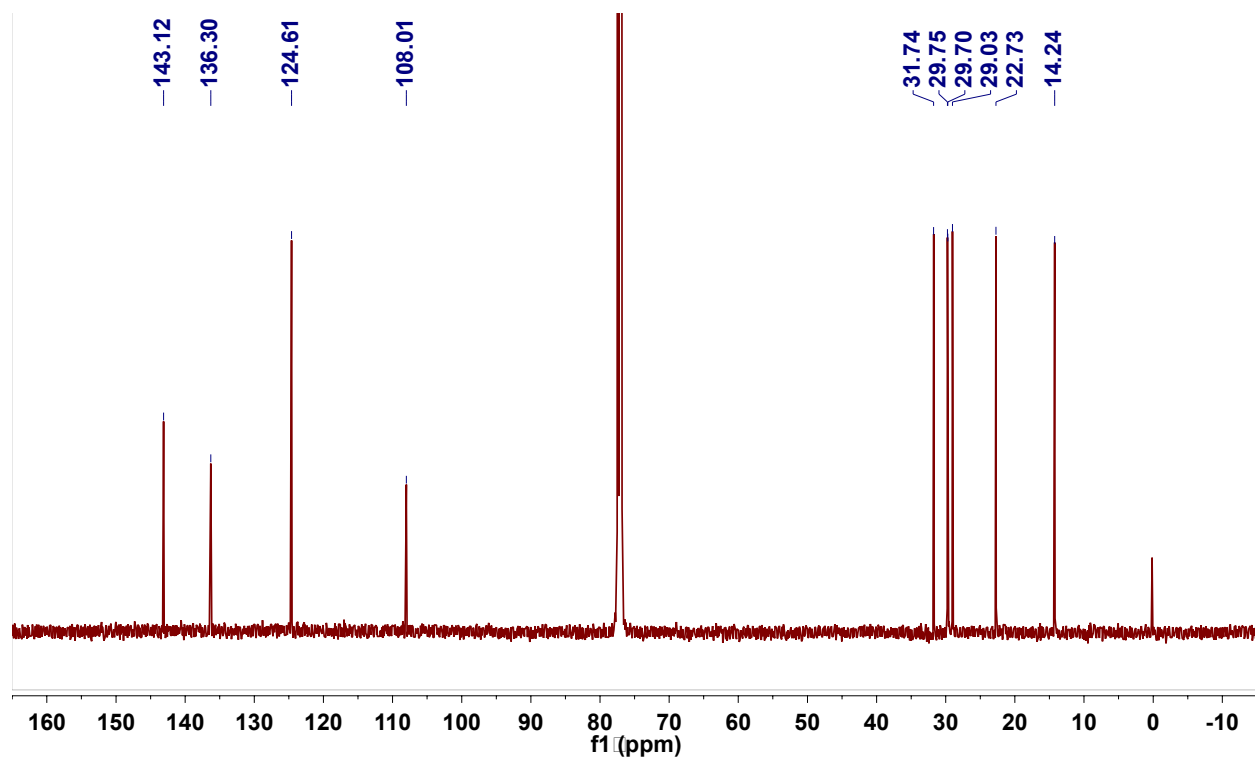
HRMS (ESI) Calculated for $\text{C}_{10}\text{H}_{14}\text{DBrS}_2$ ($[\text{M}+\text{H}]^+$): 248.0213, measured 248.0208

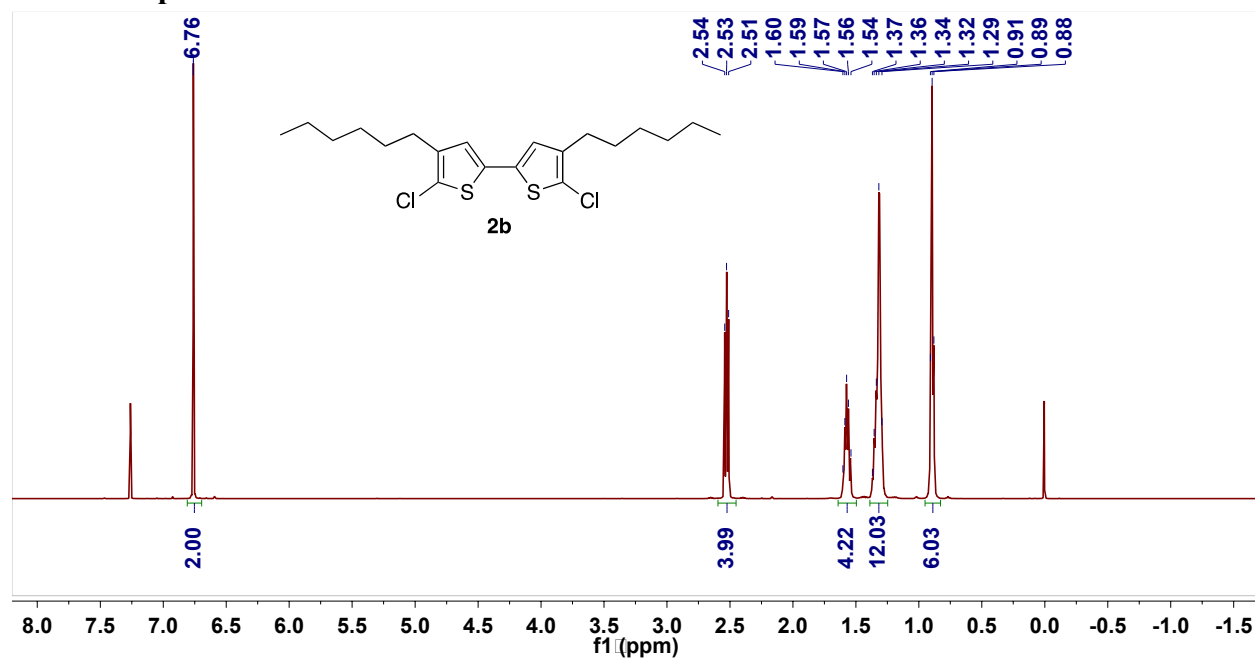
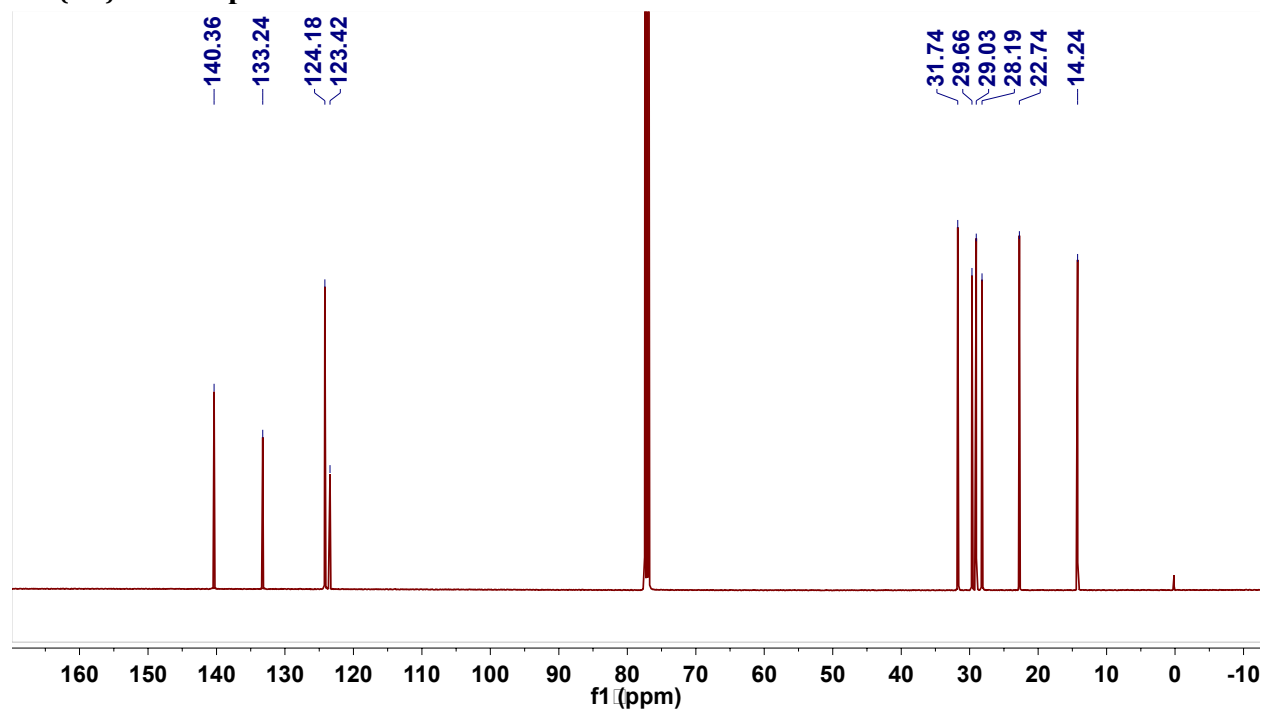
C.12 NMR Spectra of Isolated Products

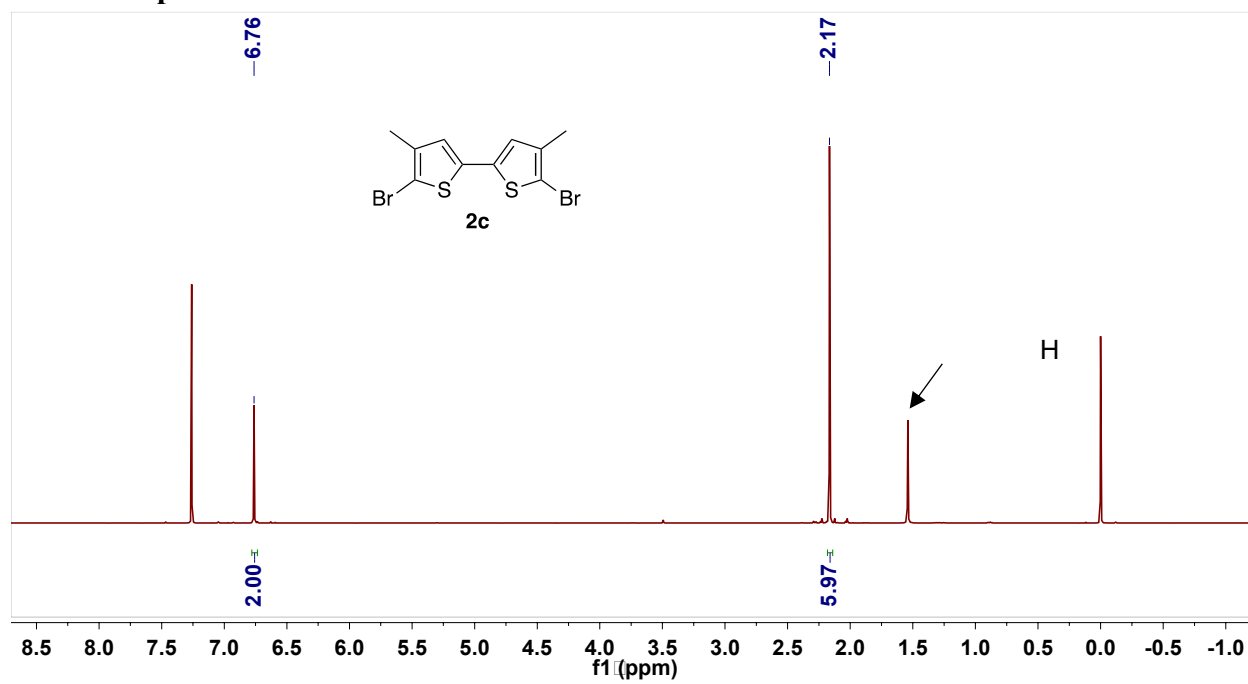
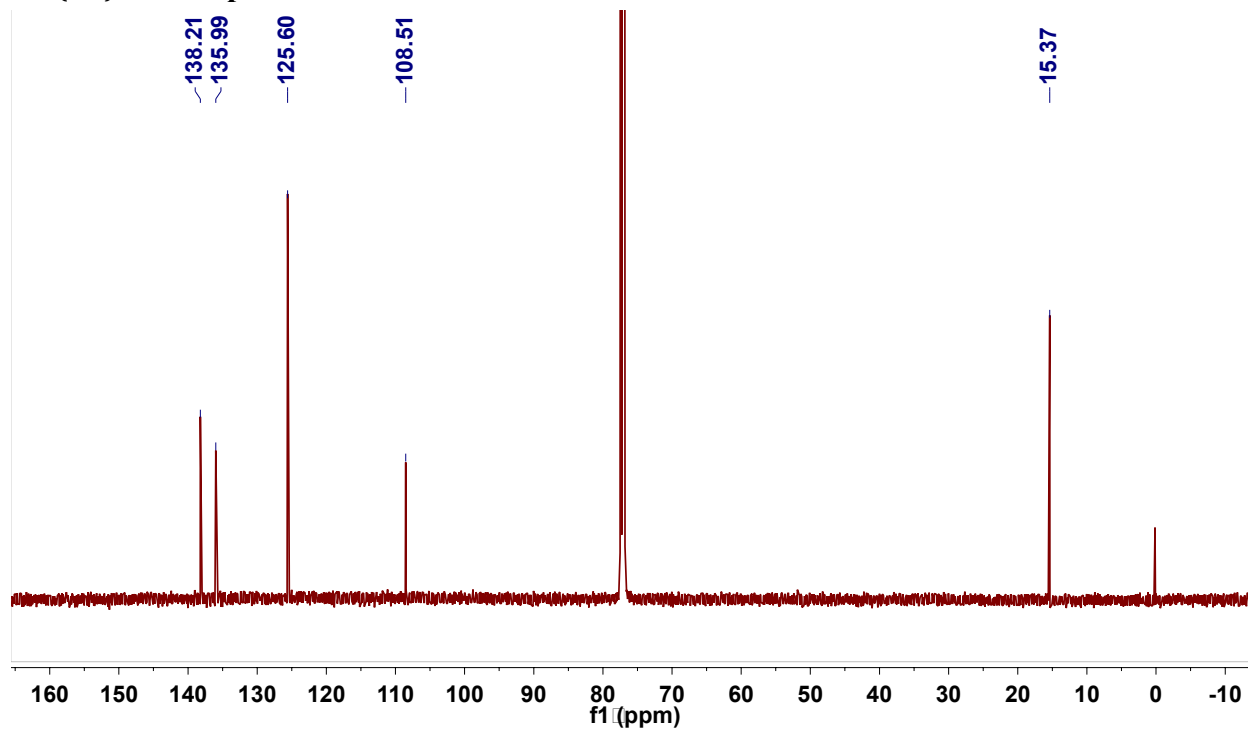
$^1\text{H NMR}$ Spectrum of **2a**

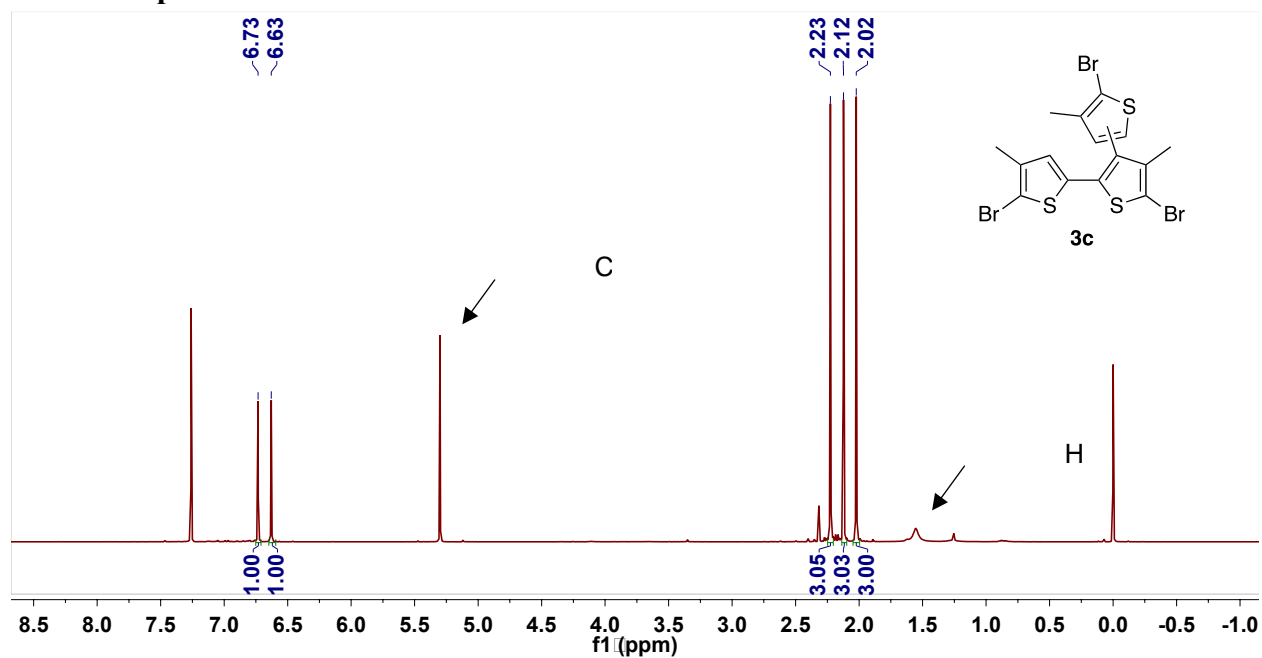
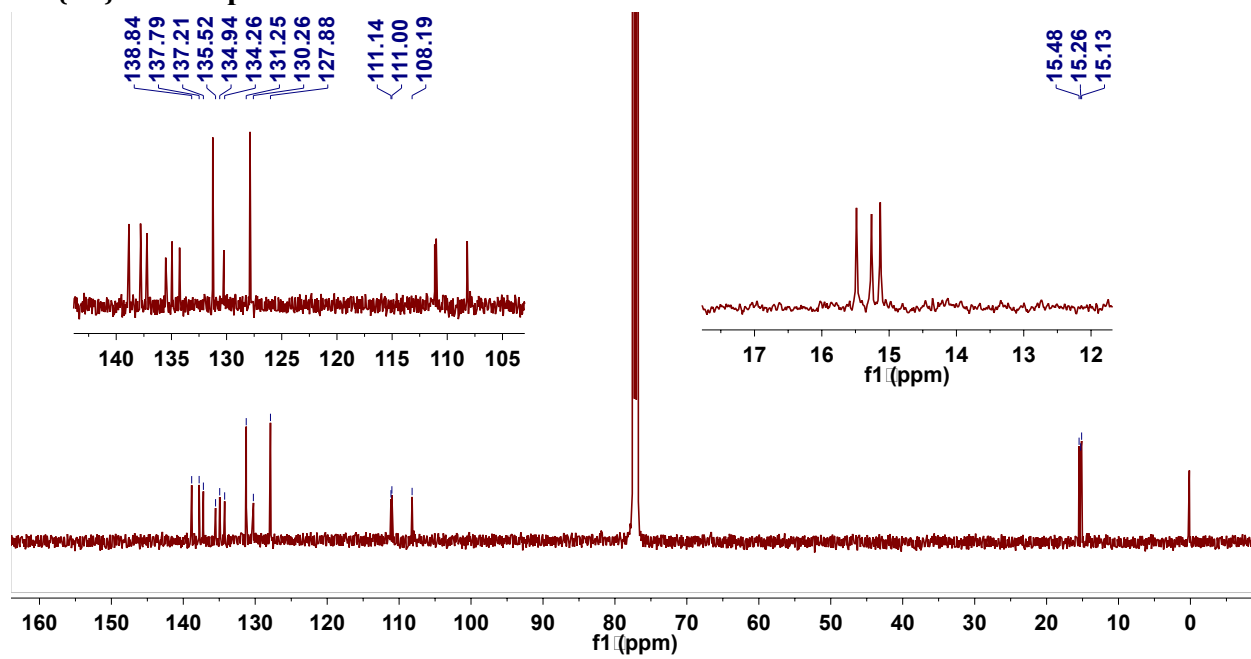


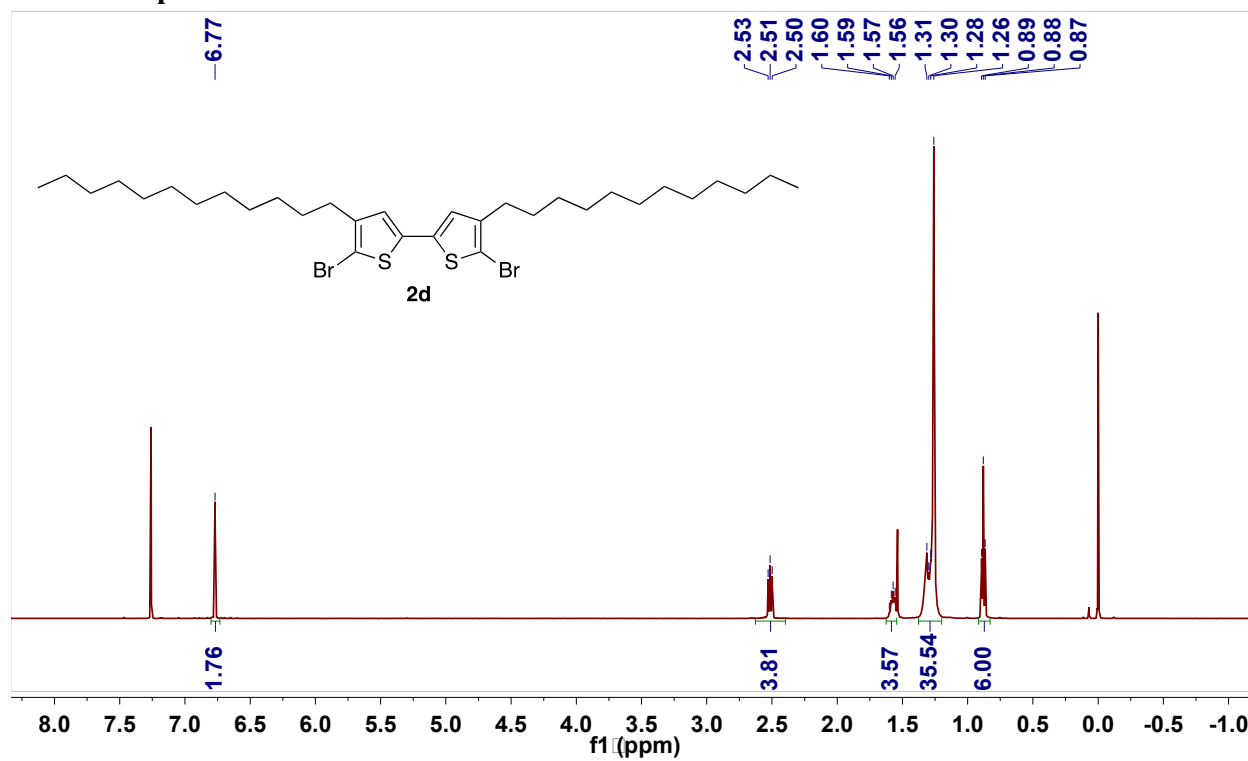
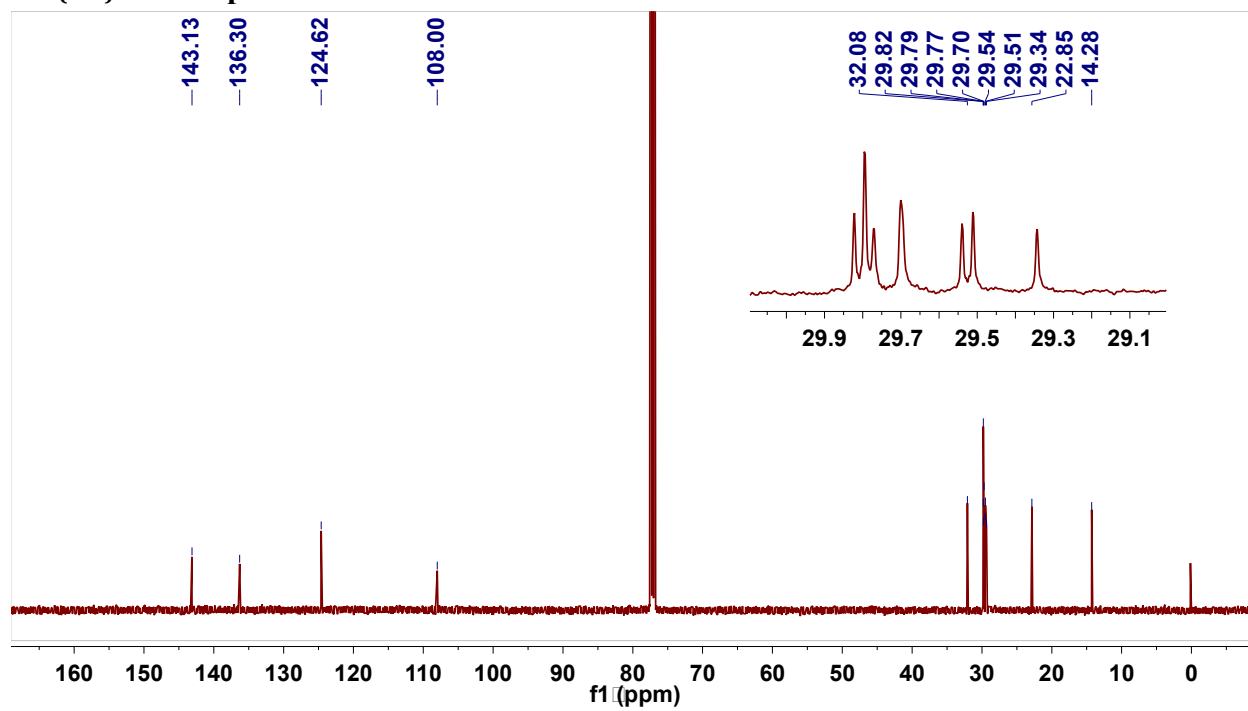
$^{13}\text{C}\{^1\text{H}\}$ NMR Spectrum of **2a**

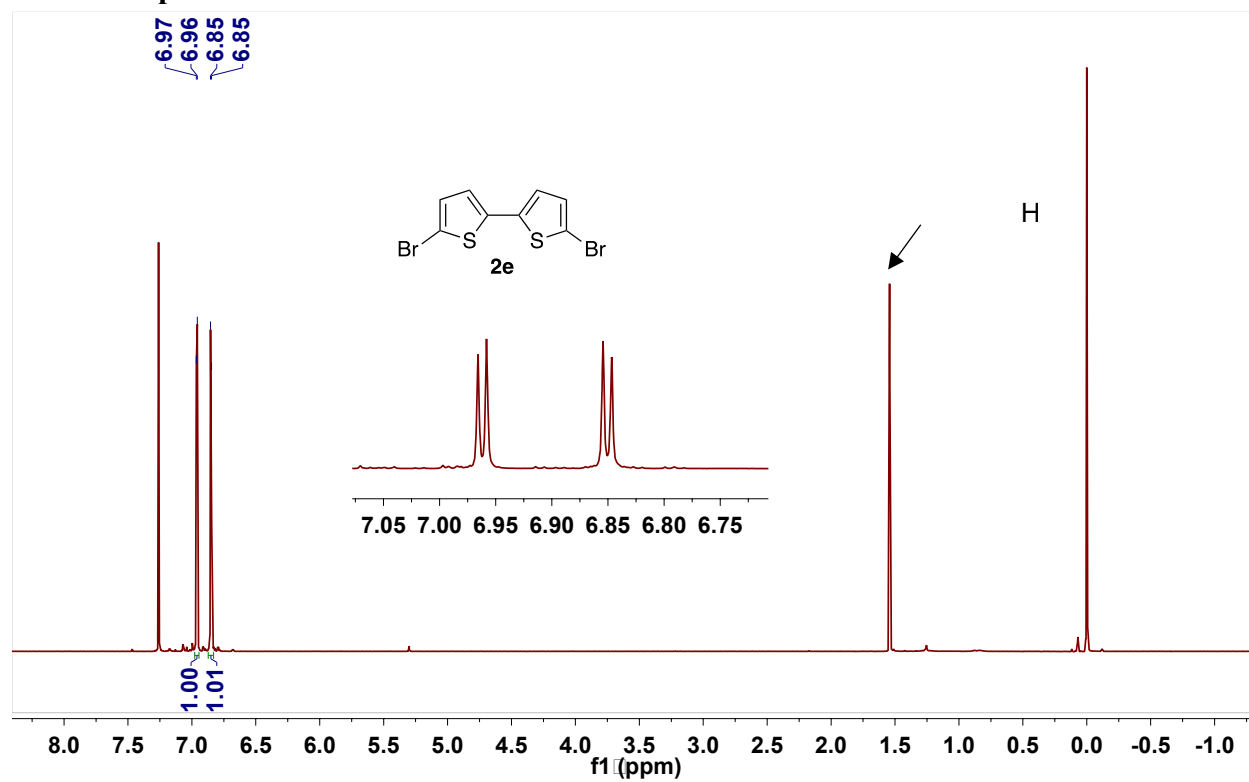
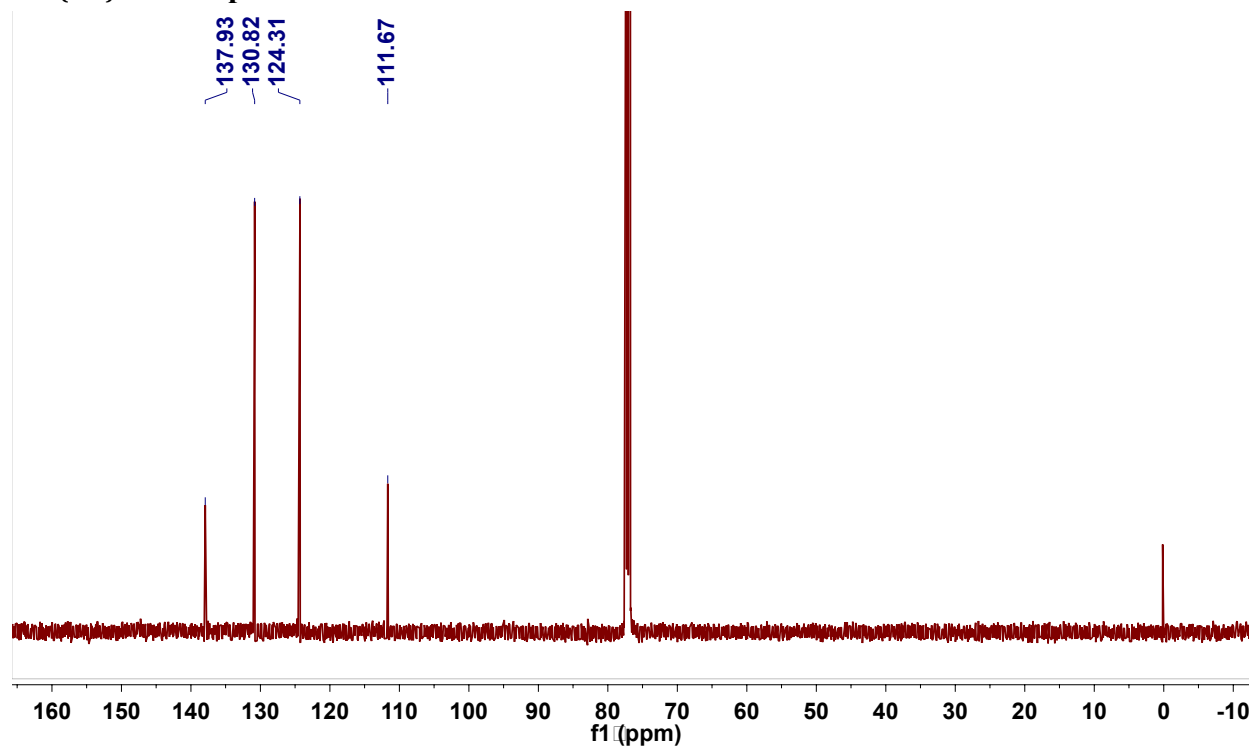


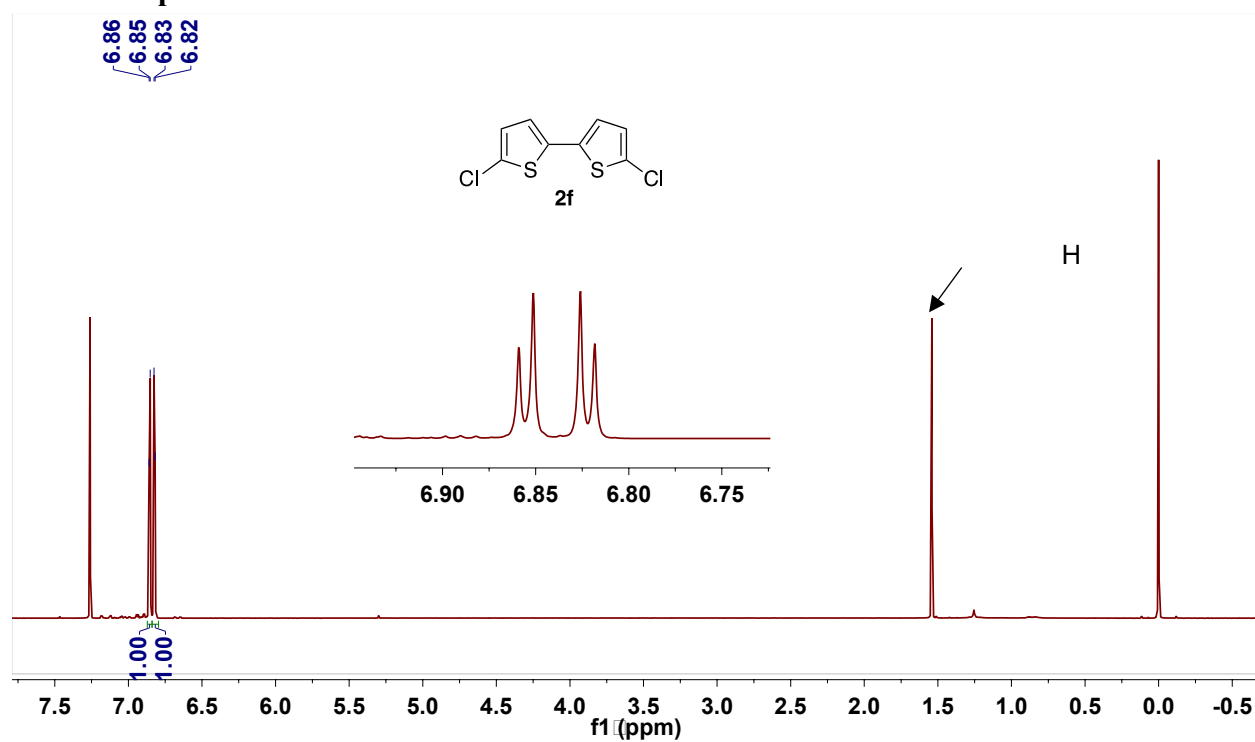
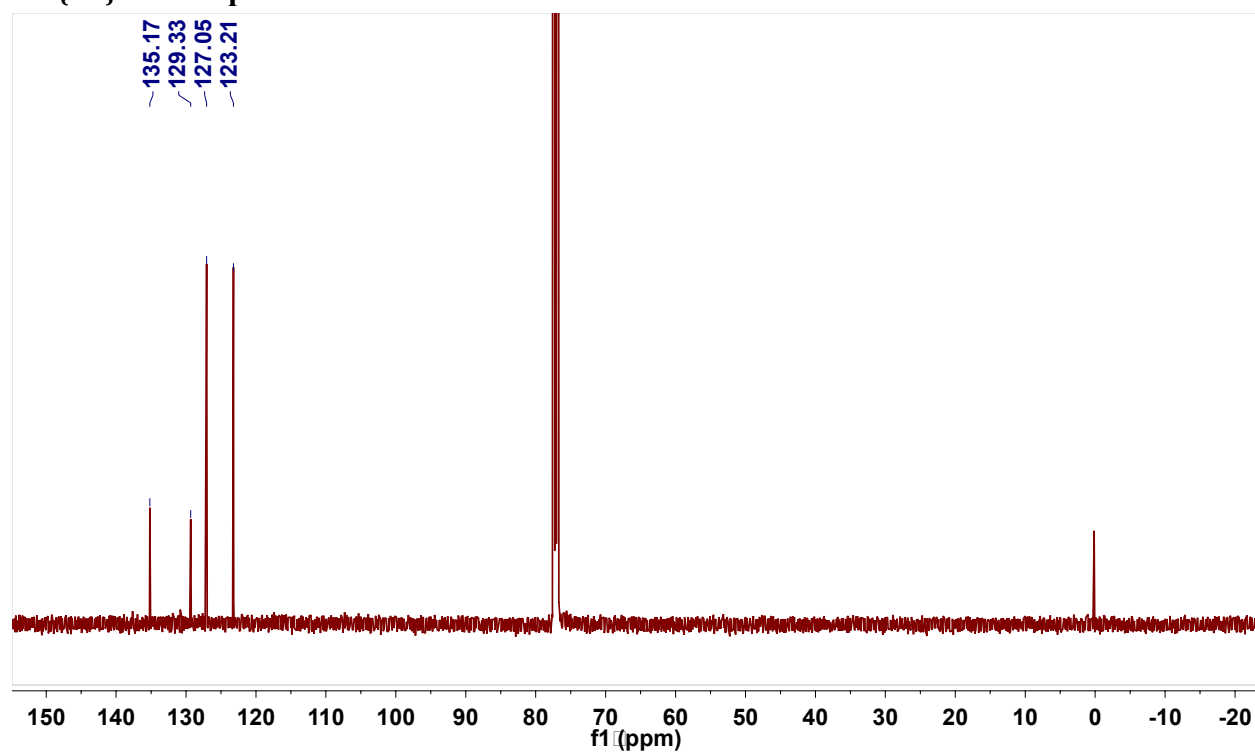
^1H NMR Spectrum of 2b **$^{13}\text{C}\{^1\text{H}\}$ NMR Spectrum of 2b**

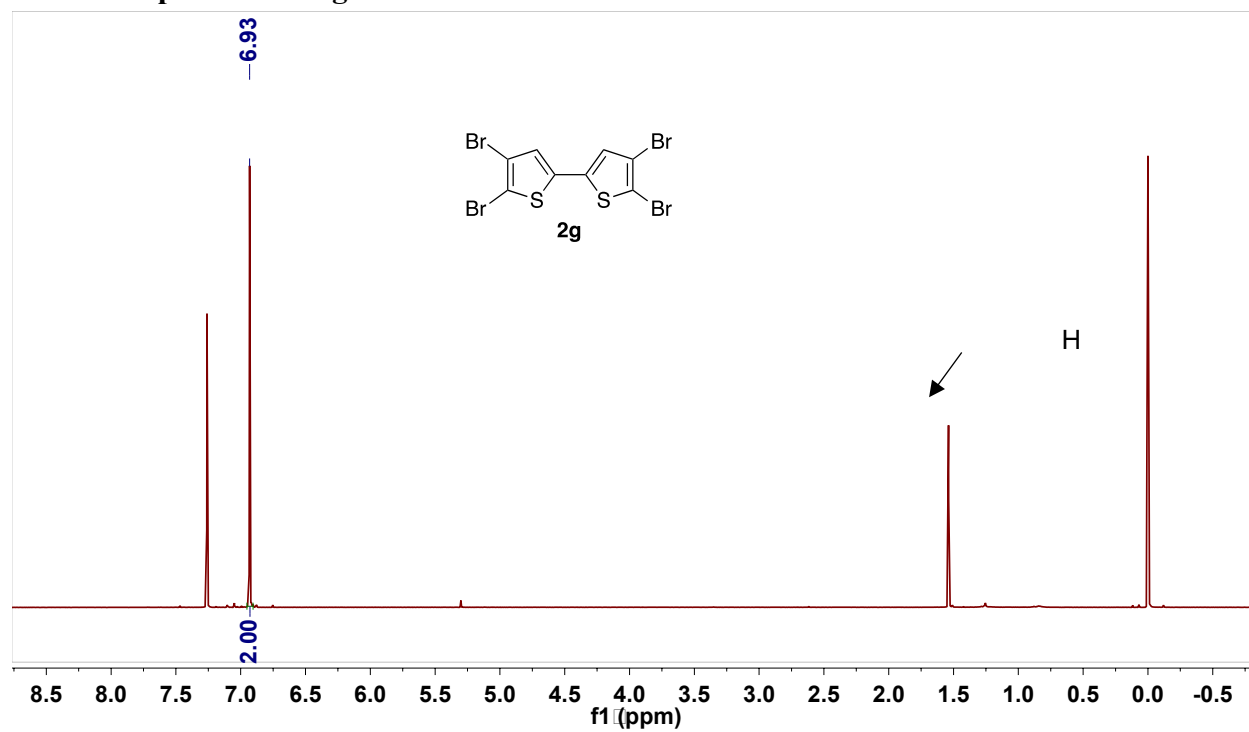
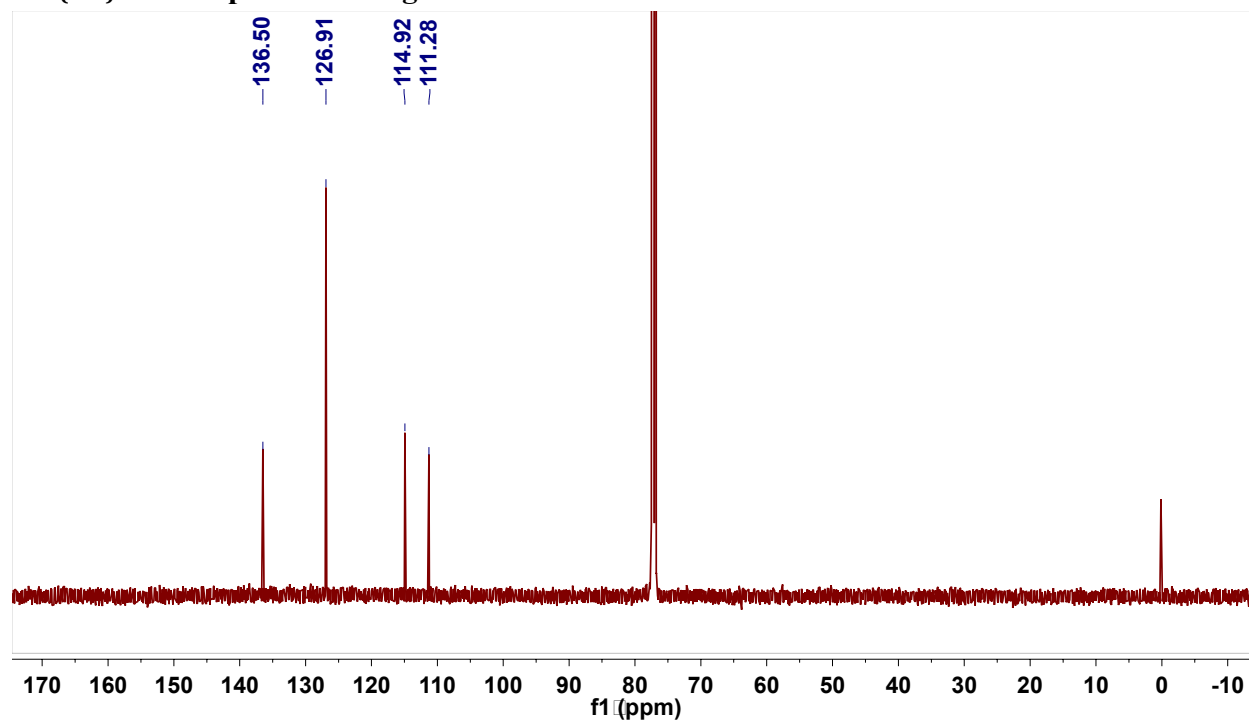
^1H NMR Spectrum of 2c **$^{13}\text{C}\{^1\text{H}\}$ NMR Spectrum of 2c**

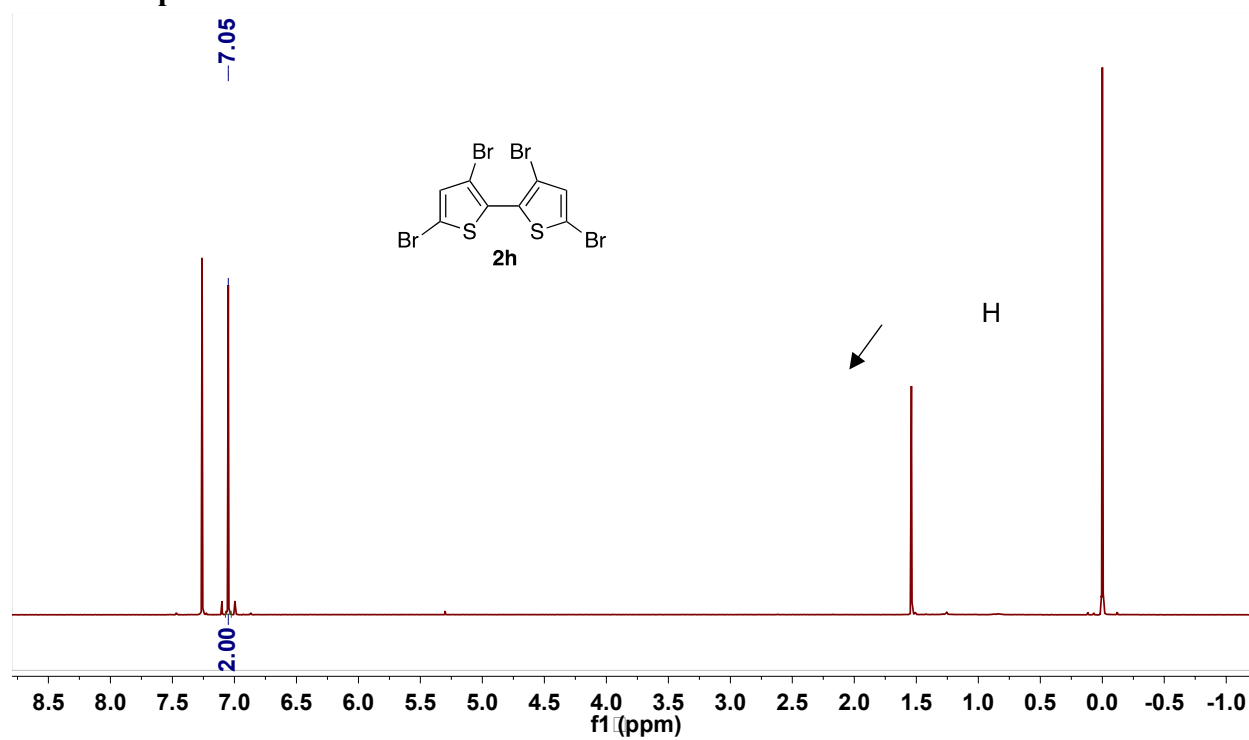
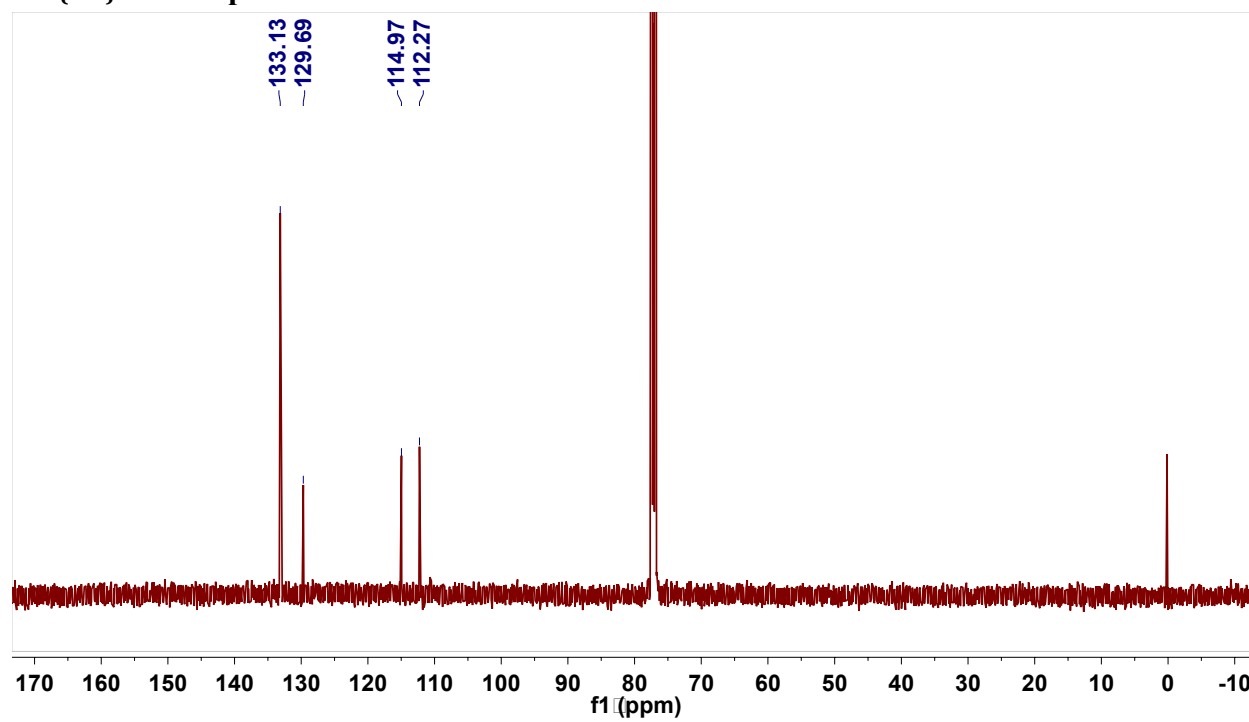
^1H NMR Spectrum of 3c **$^{13}\text{C}\{^1\text{H}\}$ NMR Spectrum of 3c**

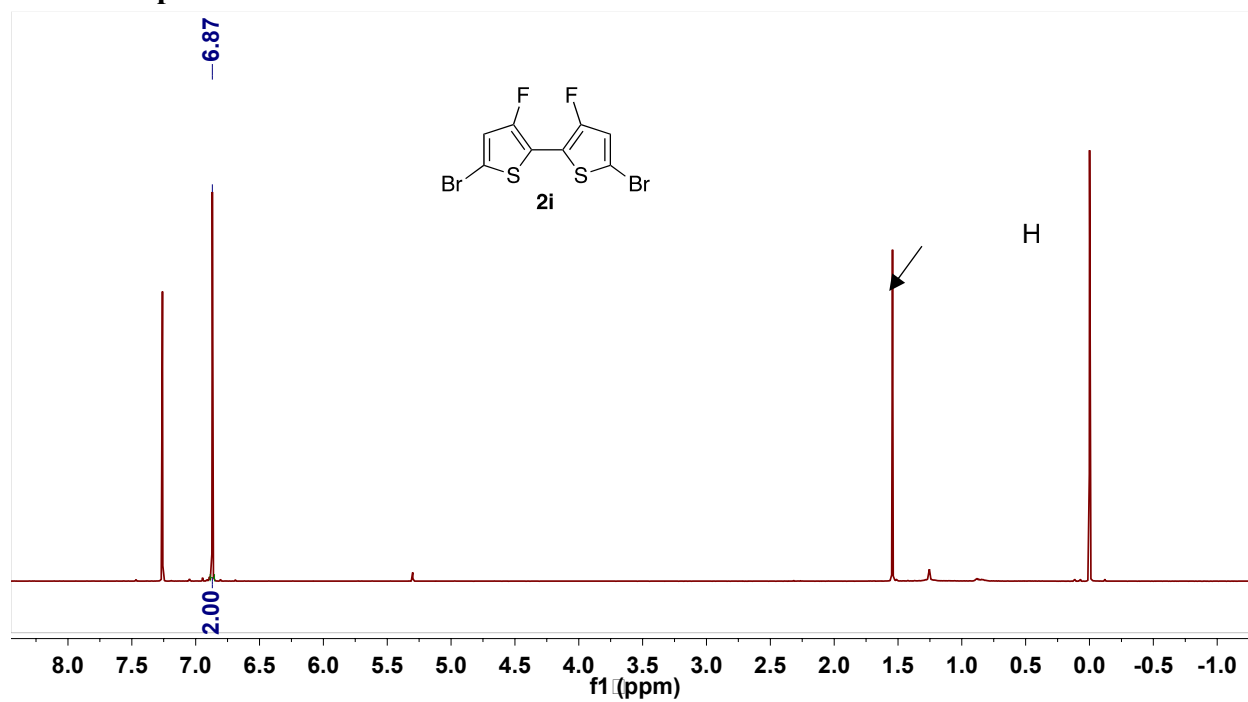
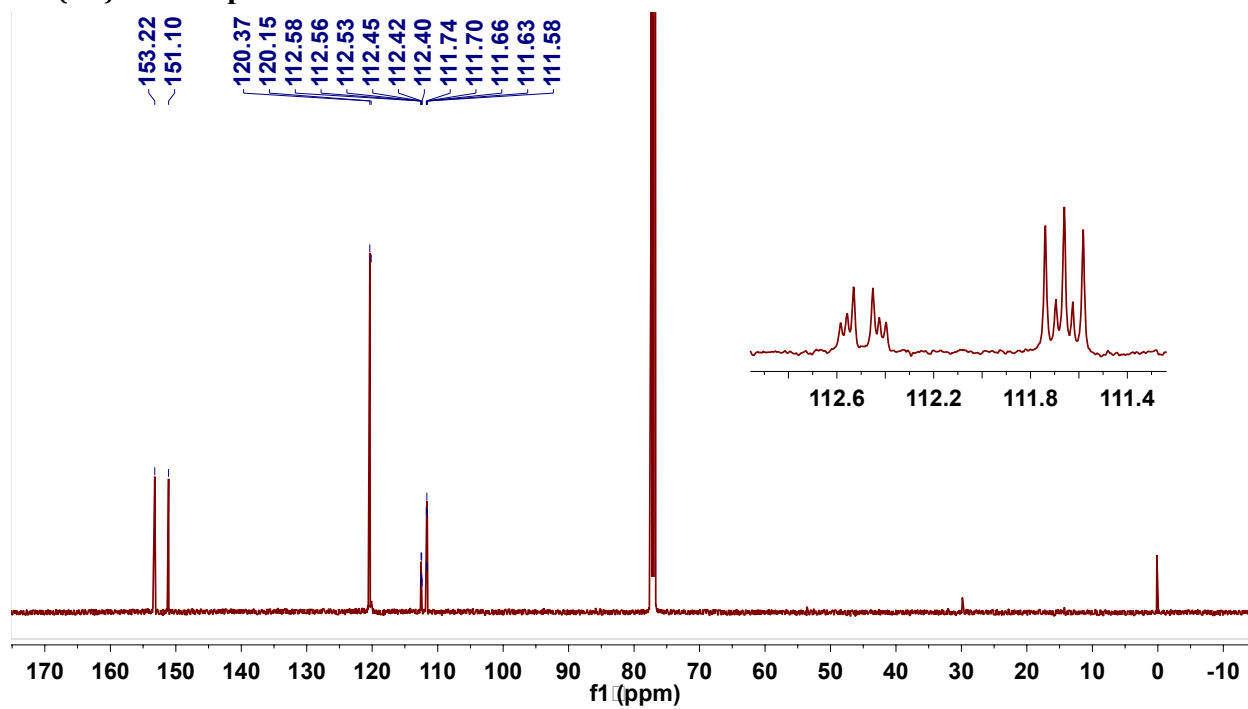
^1H NMR Spectrum of 2d **$^{13}\text{C}\{^1\text{H}\}$ NMR Spectrum of 2d**

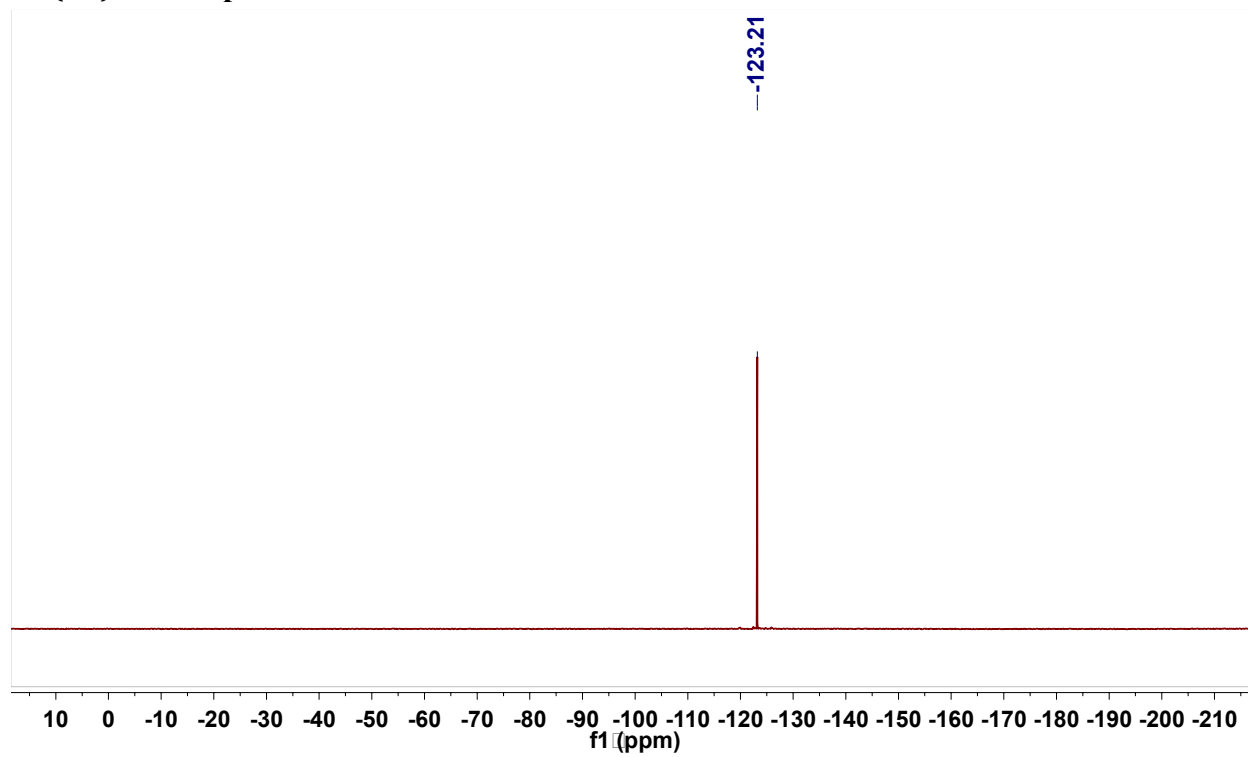
^1H NMR Spectrum of 2e **$^{13}\text{C}\{^1\text{H}\}$ NMR Spectrum of 2e**

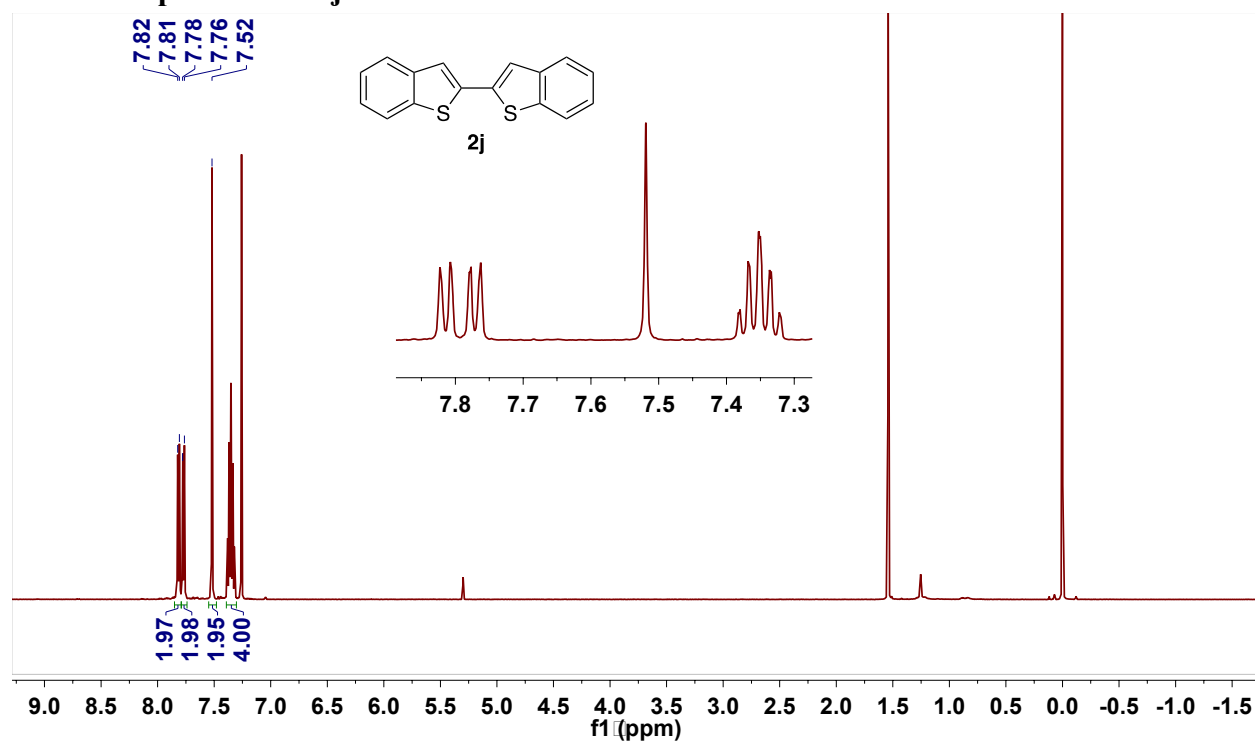
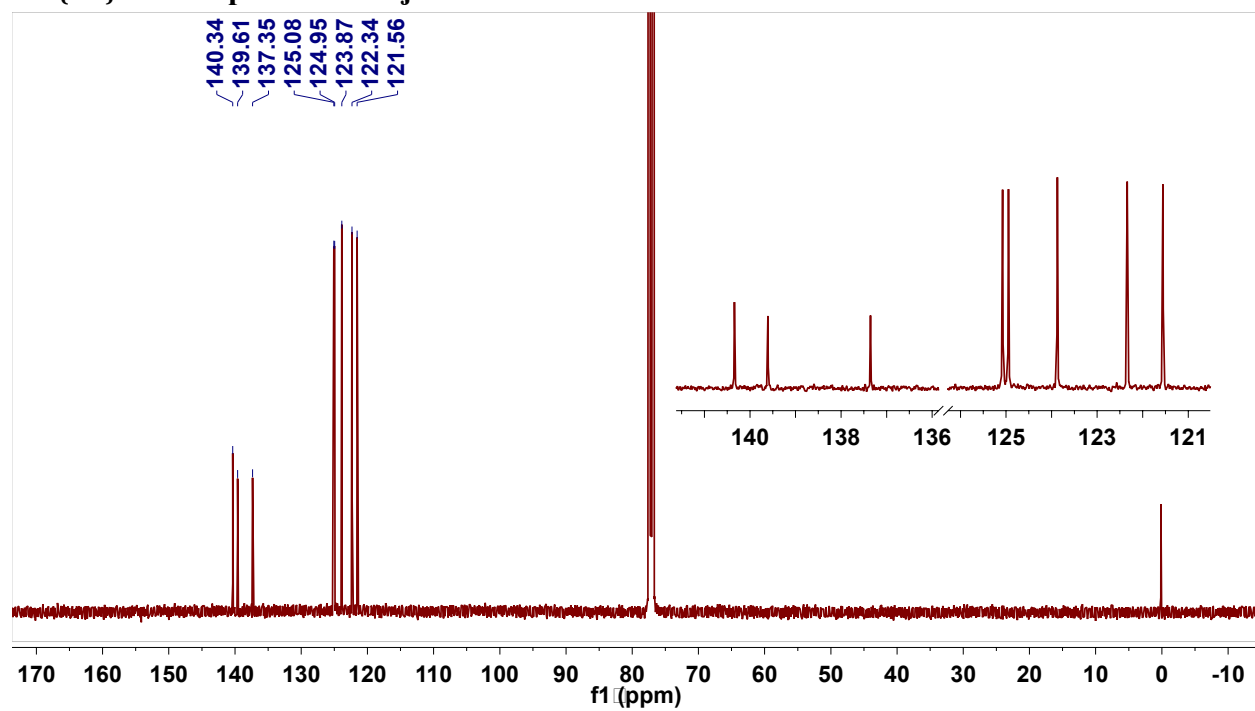
^1H NMR Spectrum of 2f **$^{13}\text{C}\{^1\text{H}\}$ NMR Spectrum of 2f**

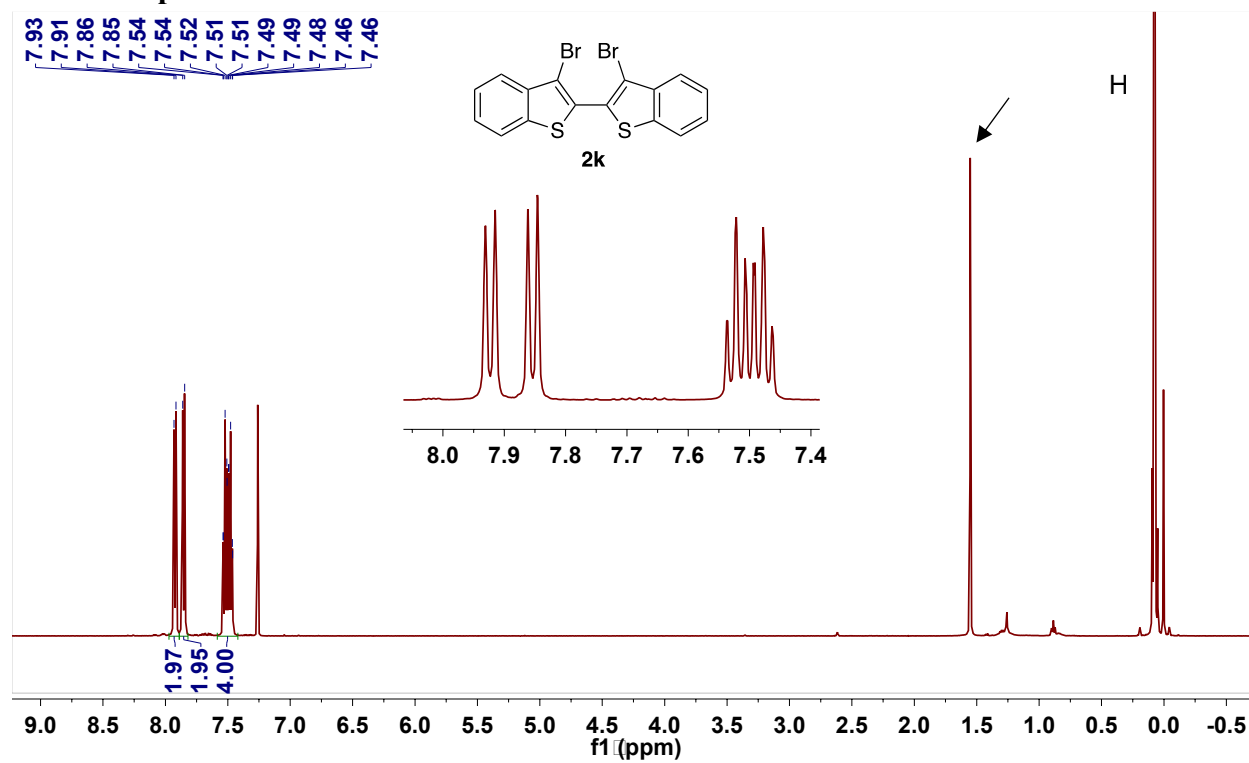
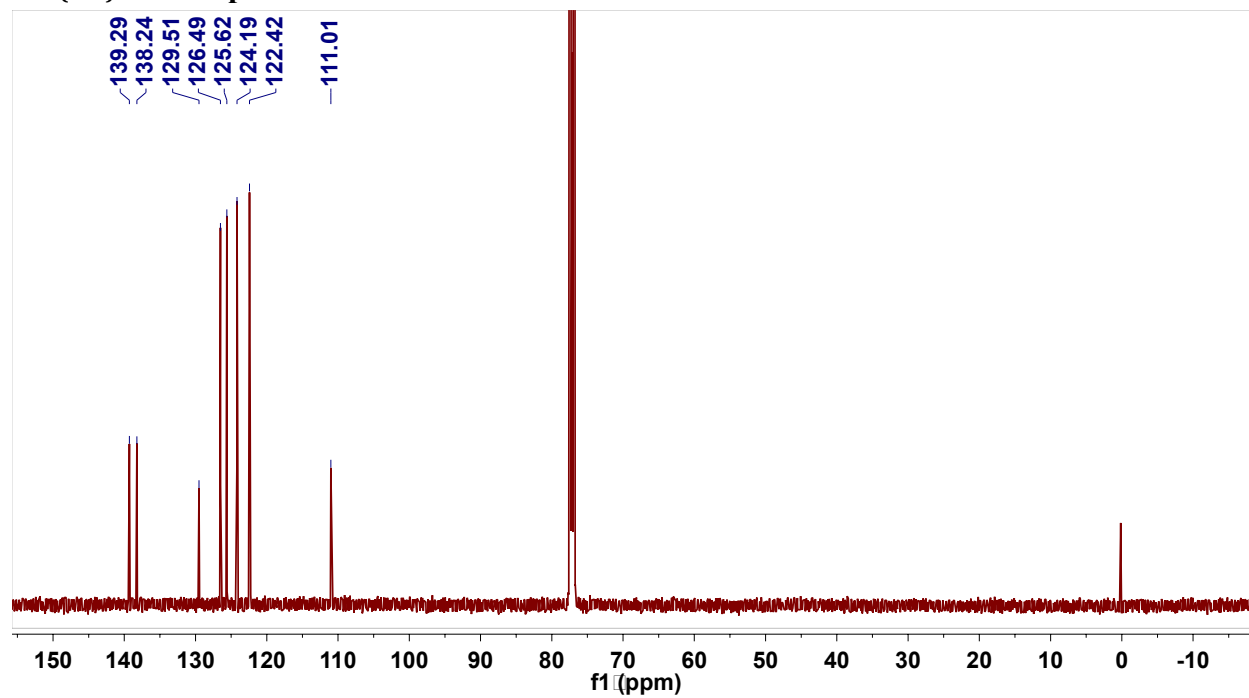
¹H NMR Spectrum of 2g**¹³C{¹H} NMR Spectrum of 2g**

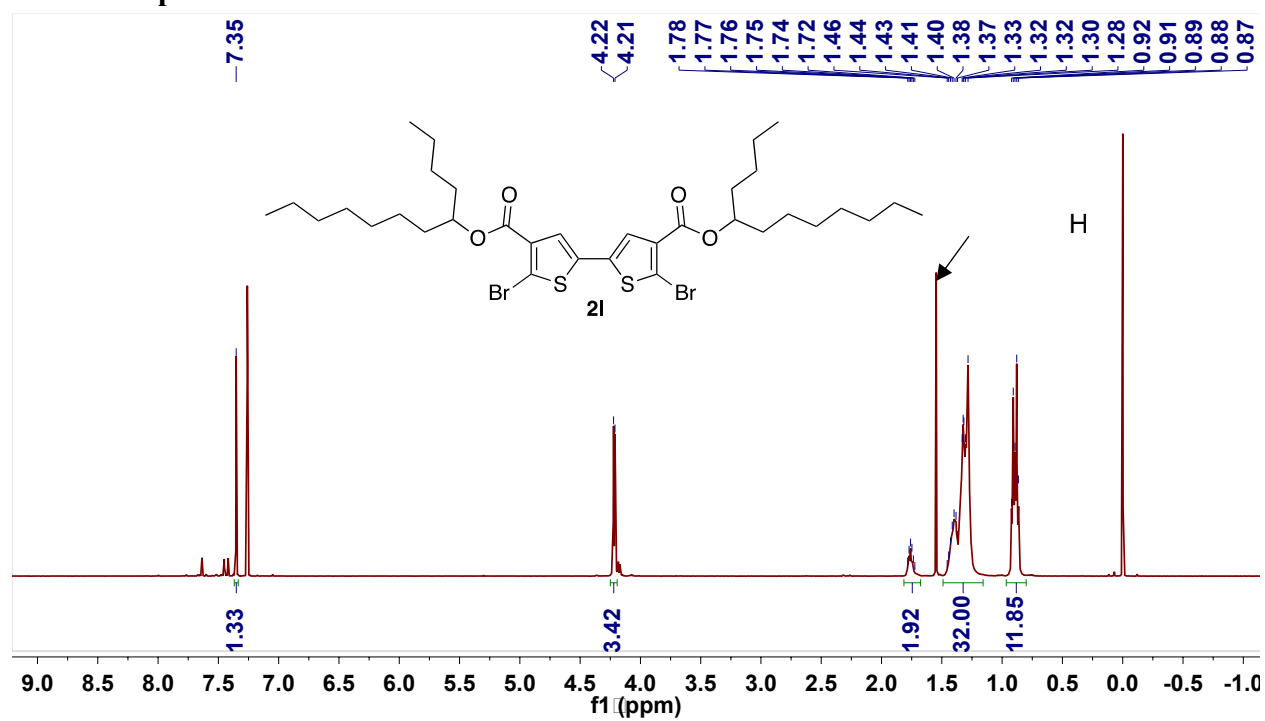
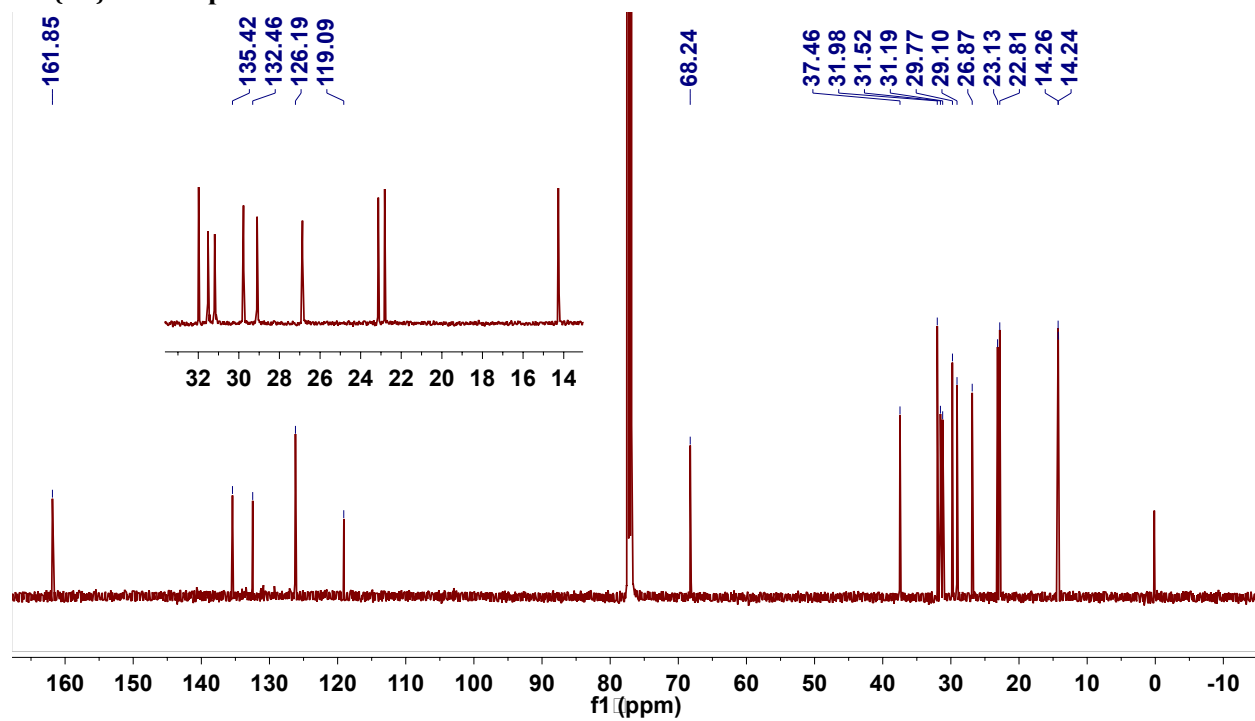
¹H NMR Spectrum of 2h**¹³C{¹H} NMR Spectrum of 2h**

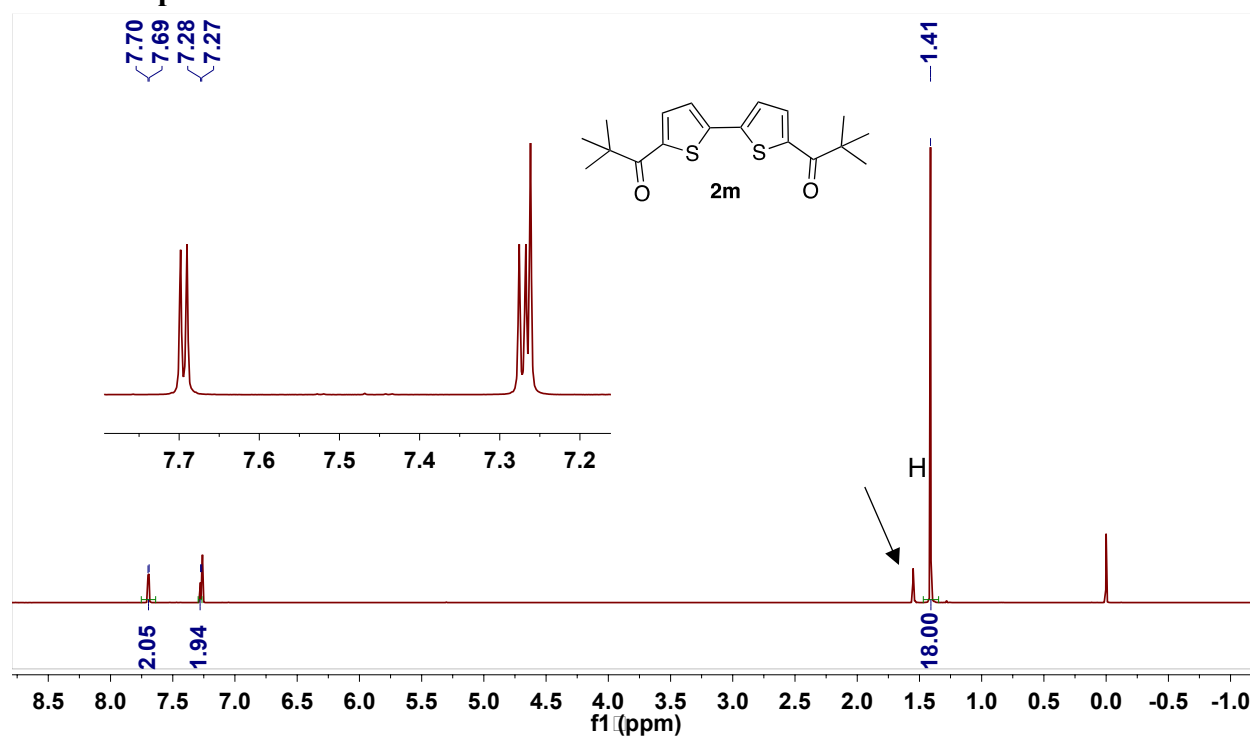
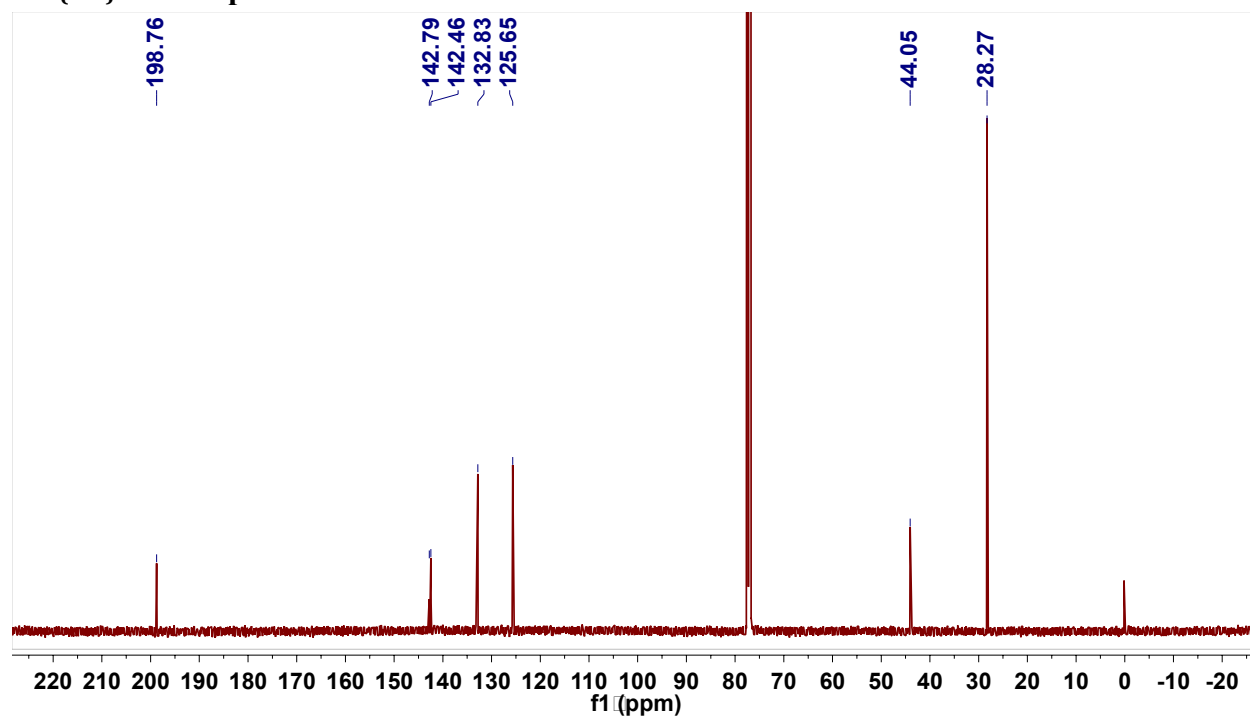
^1H NMR Spectrum of 2i **$^{13}\text{C}\{^1\text{H}\}$ NMR Spectrum of 2i**

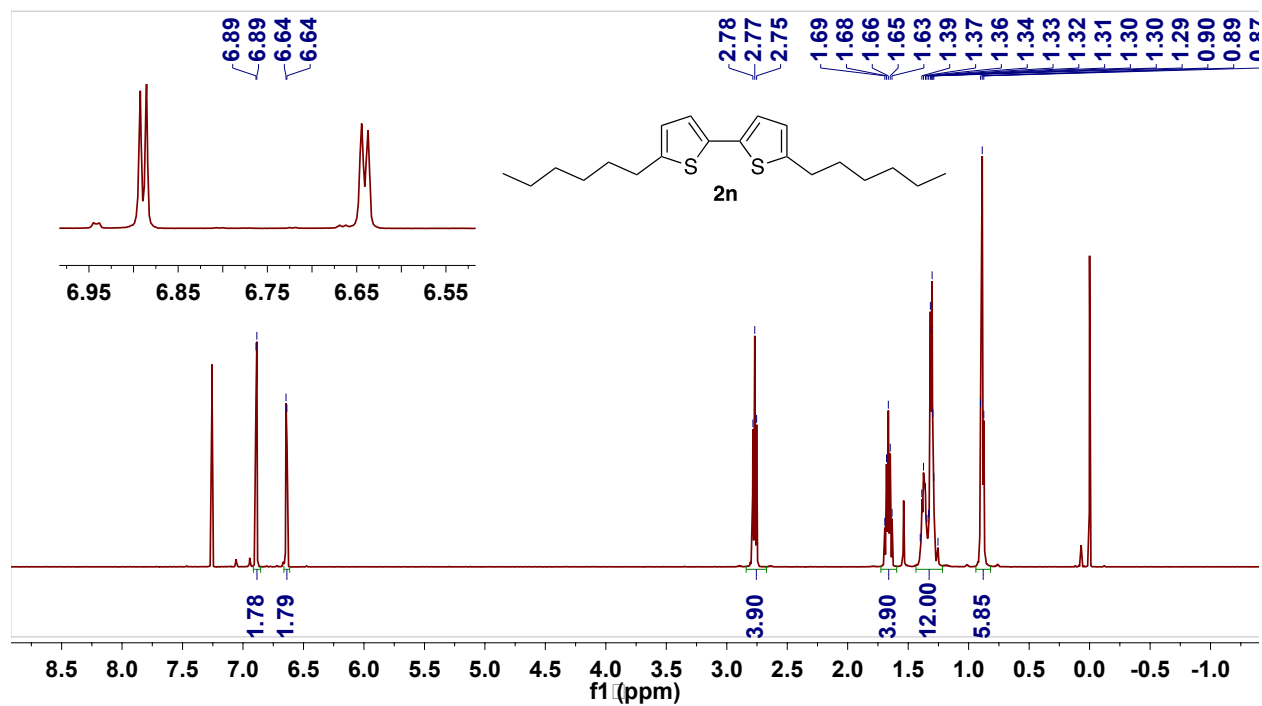
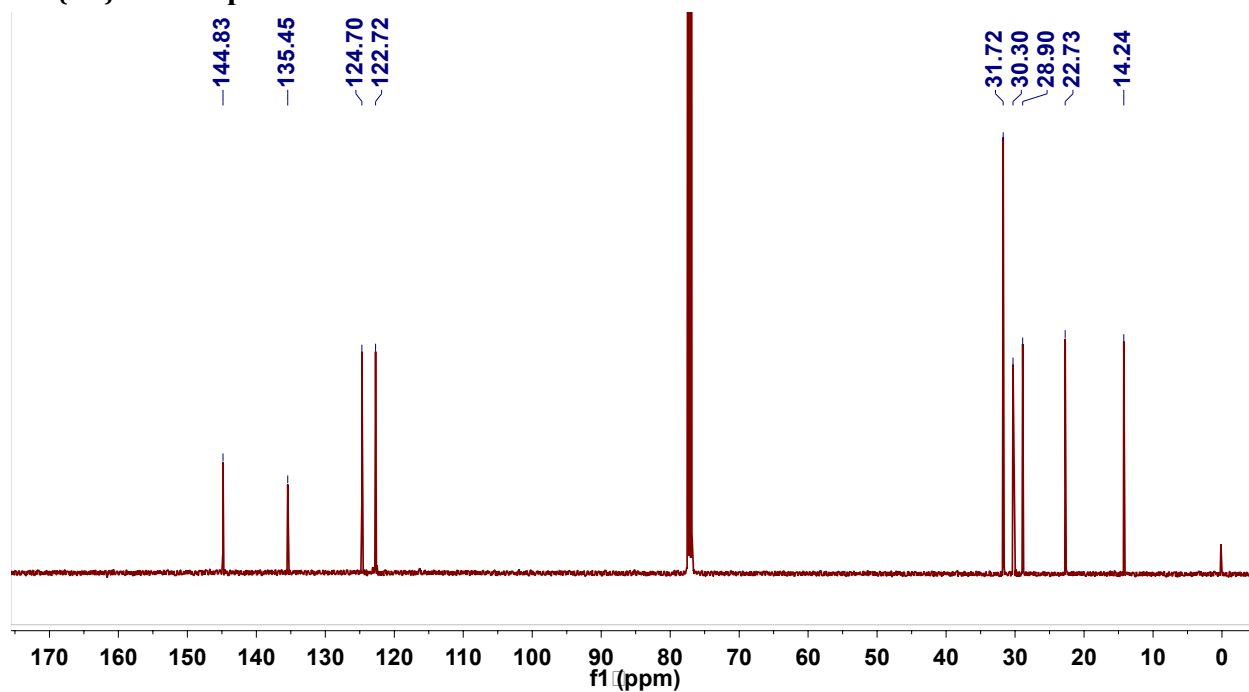
$^{19}\text{F}\{^1\text{H}\}$ NMR Spectrum of 2i

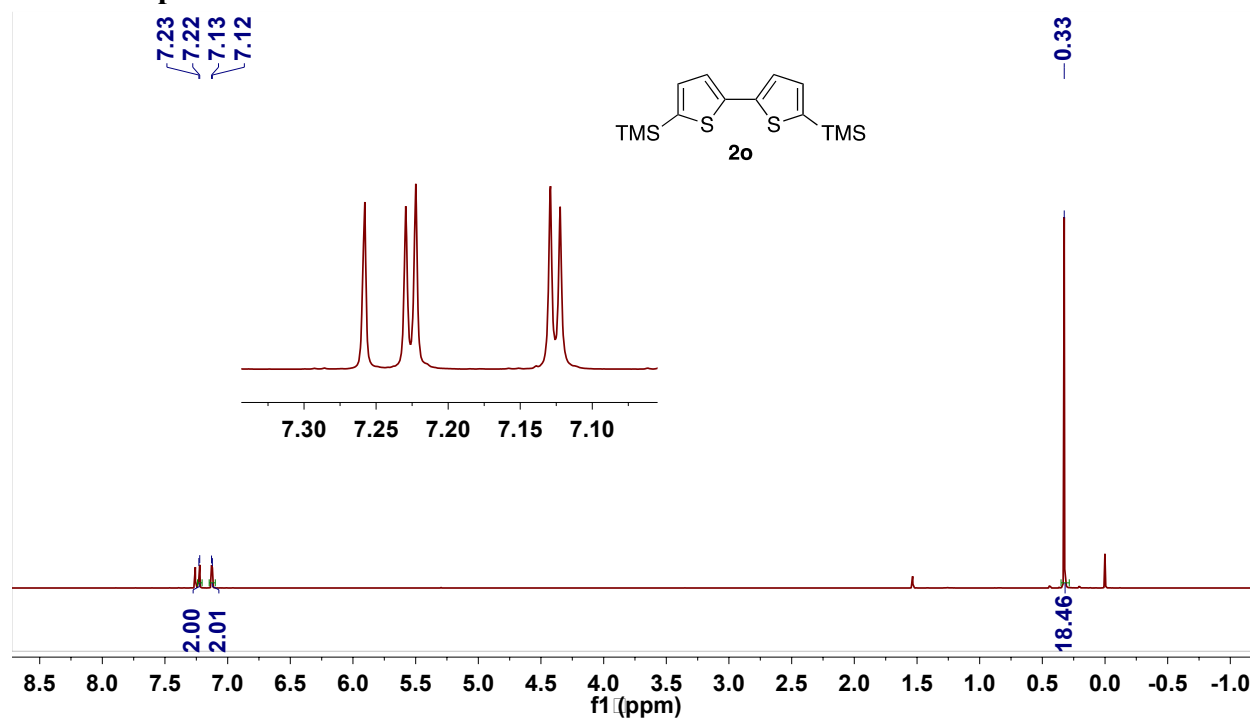
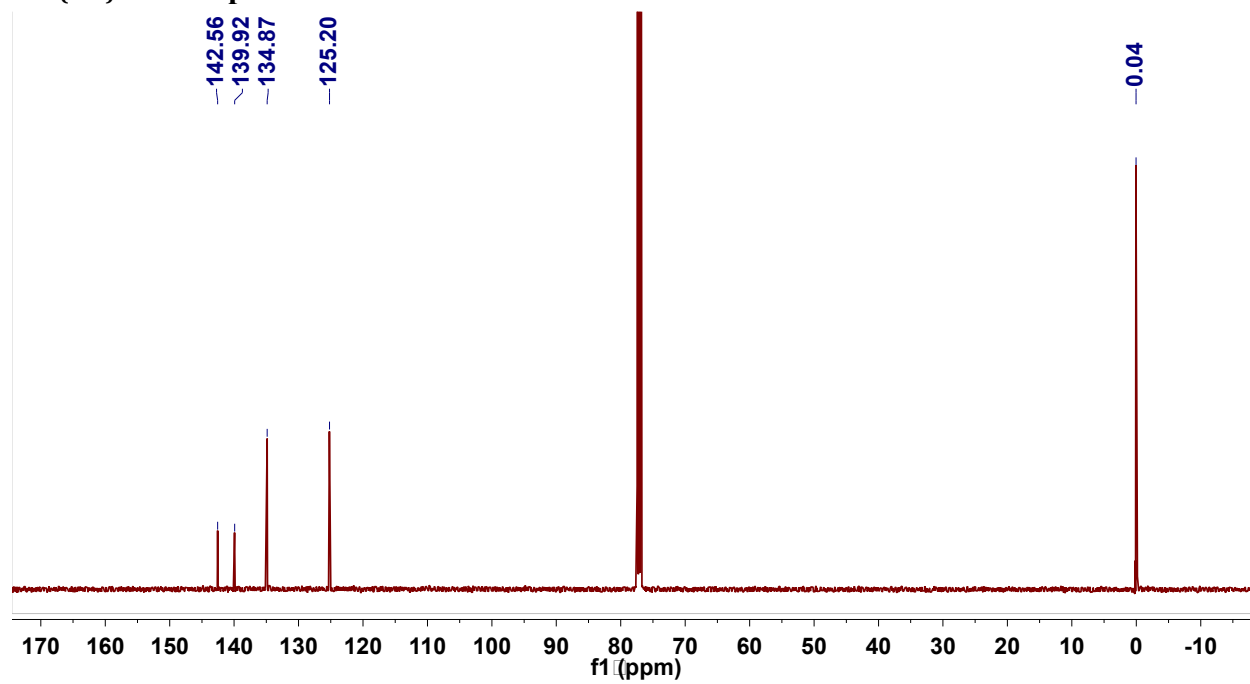
^1H NMR Spectrum of 2j **$^{13}\text{C}\{^1\text{H}\}$ NMR Spectrum of 2j**

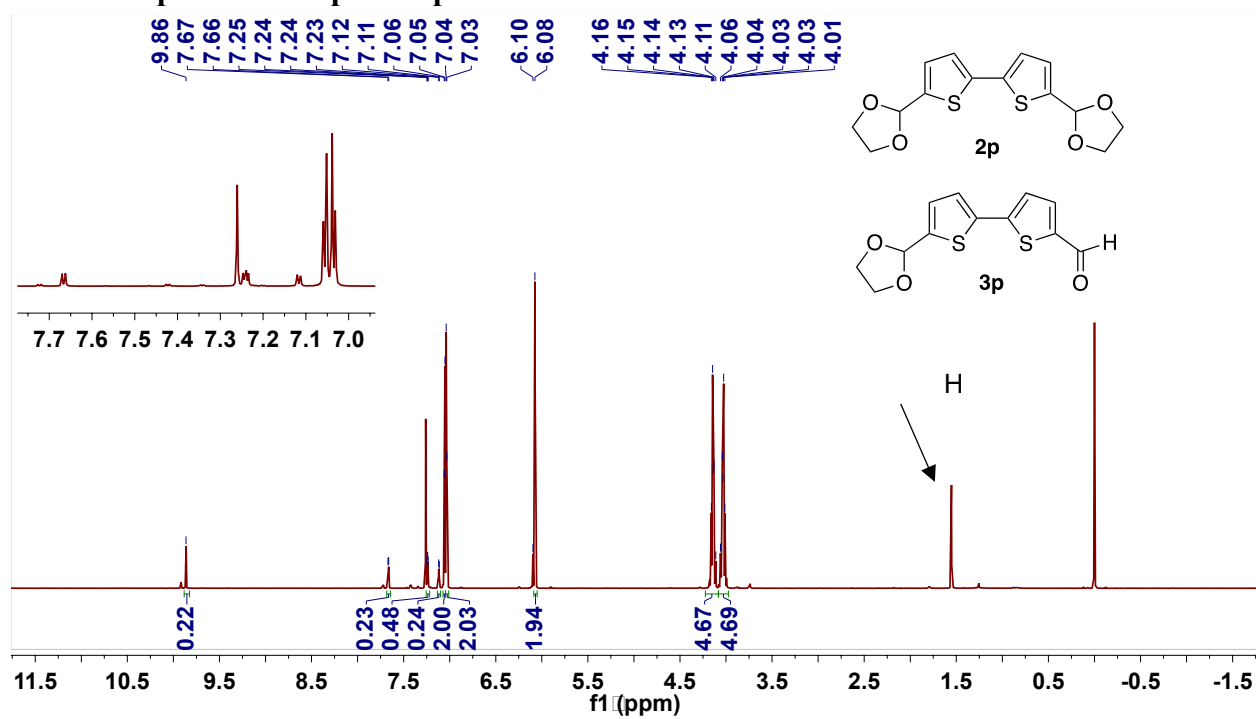
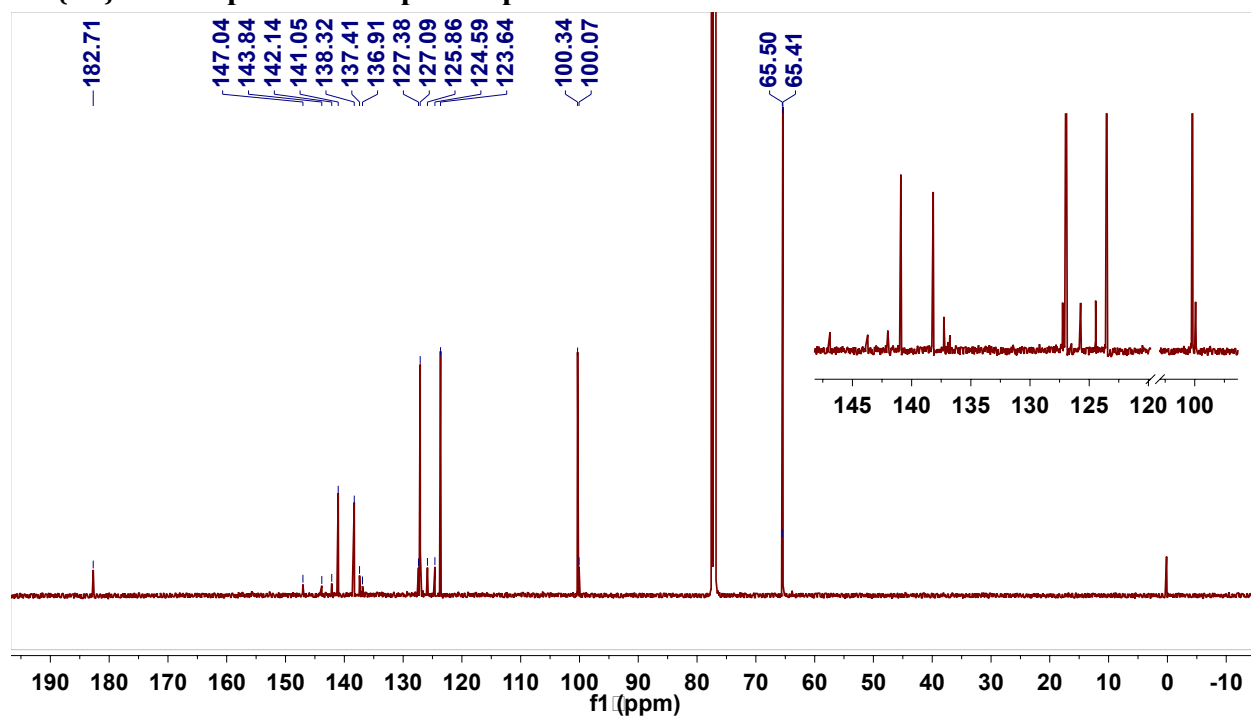
¹H NMR Spectrum of 2k**¹³C{¹H} NMR Spectrum of 2k**

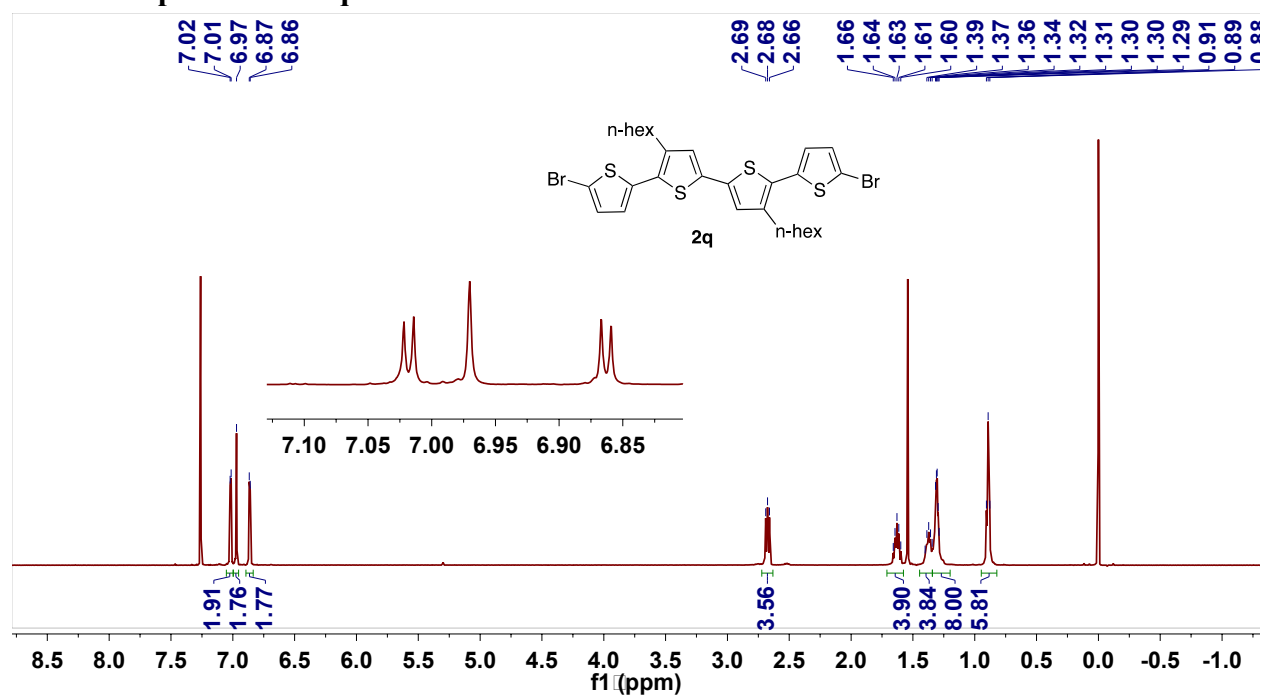
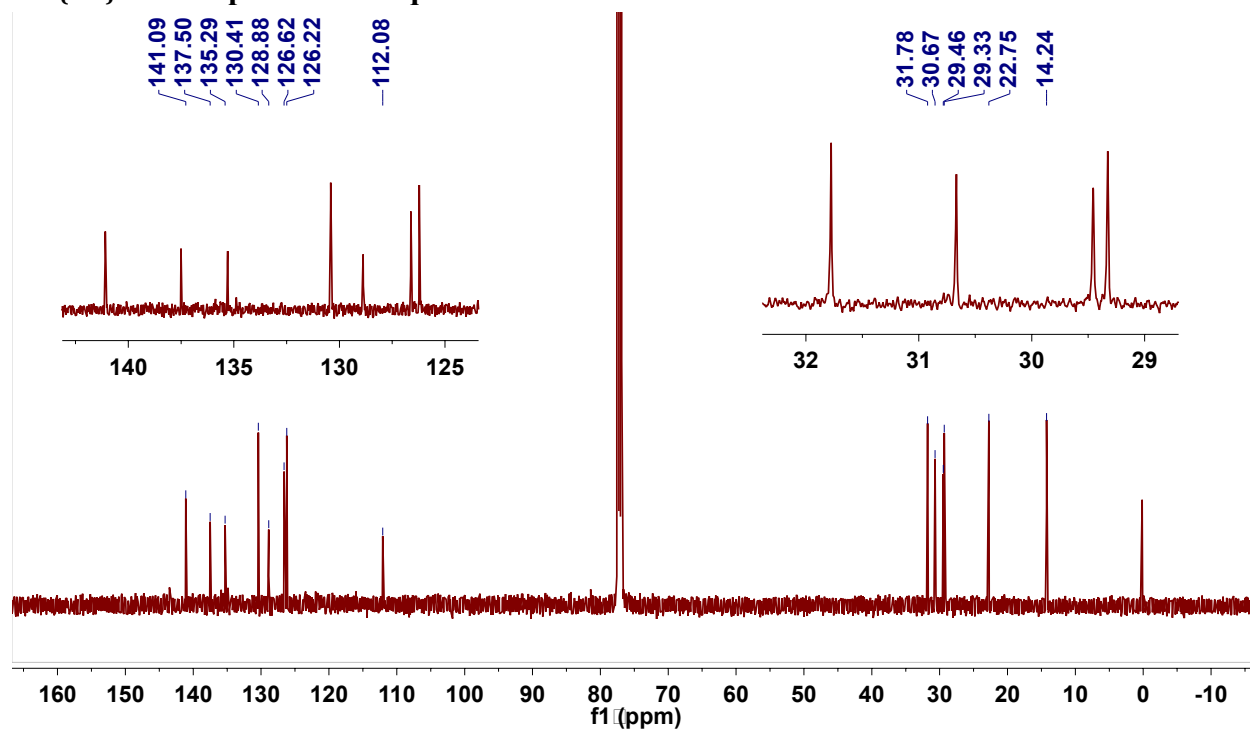
^1H NMR Spectrum of 21 $^{13}\text{C}\{^1\text{H}\}$ NMR Spectrum of 21

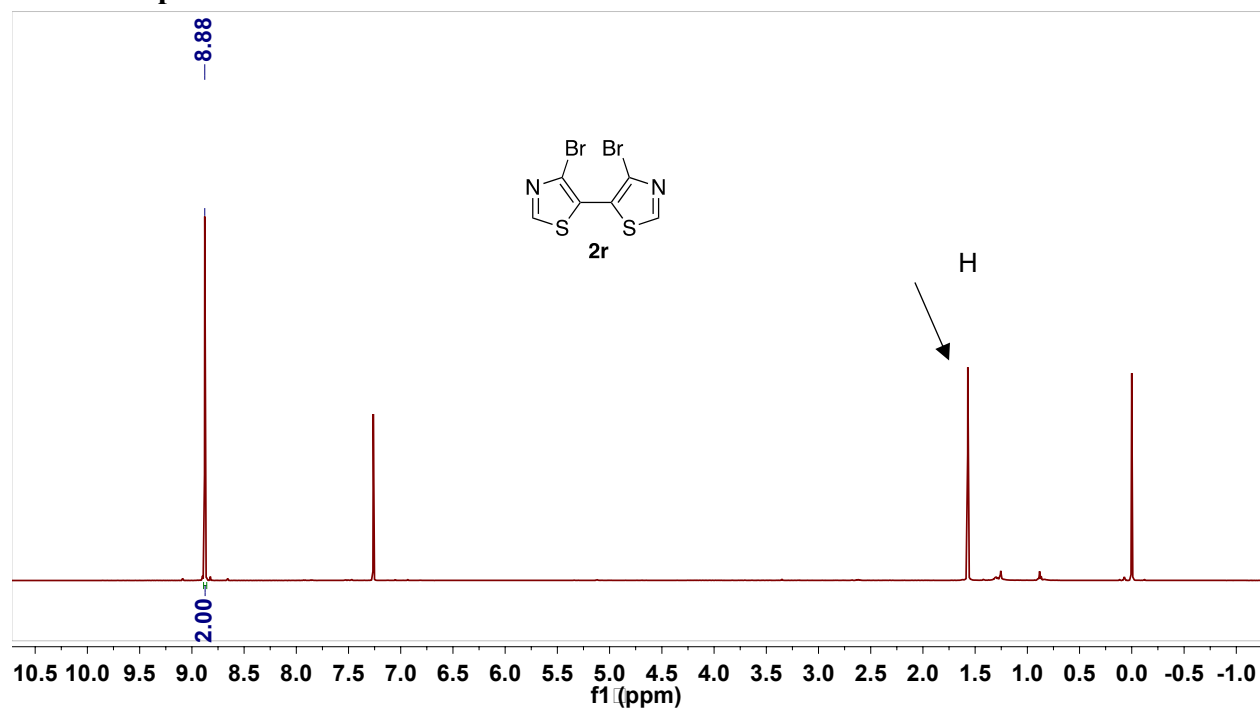
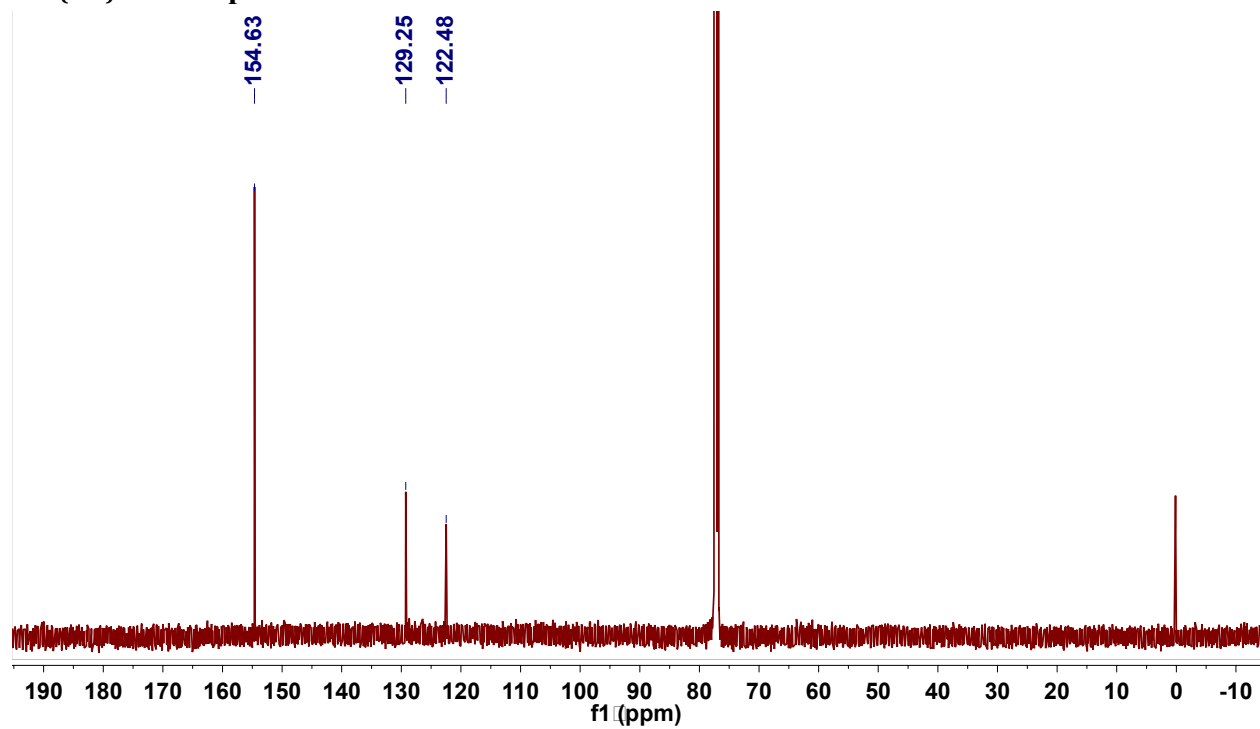
^1H NMR Spectrum of 2m **$^{13}\text{C}\{^1\text{H}\}$ NMR Spectrum of 2m**

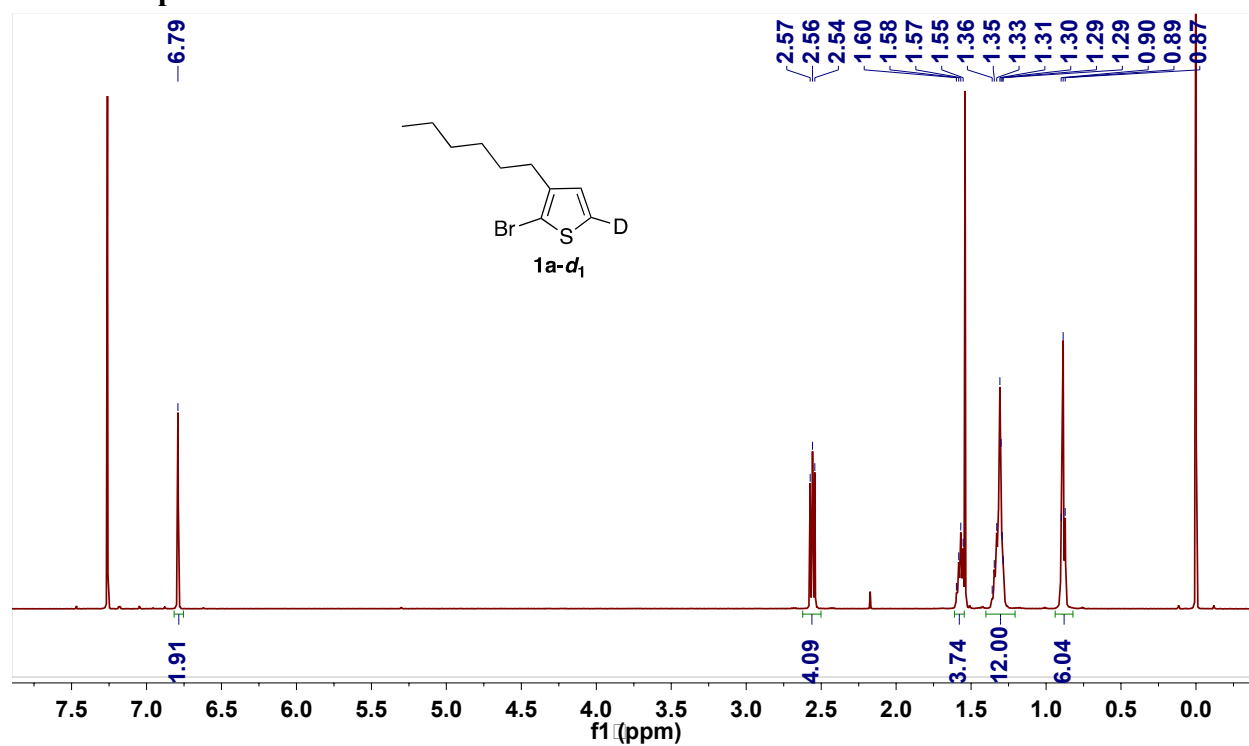
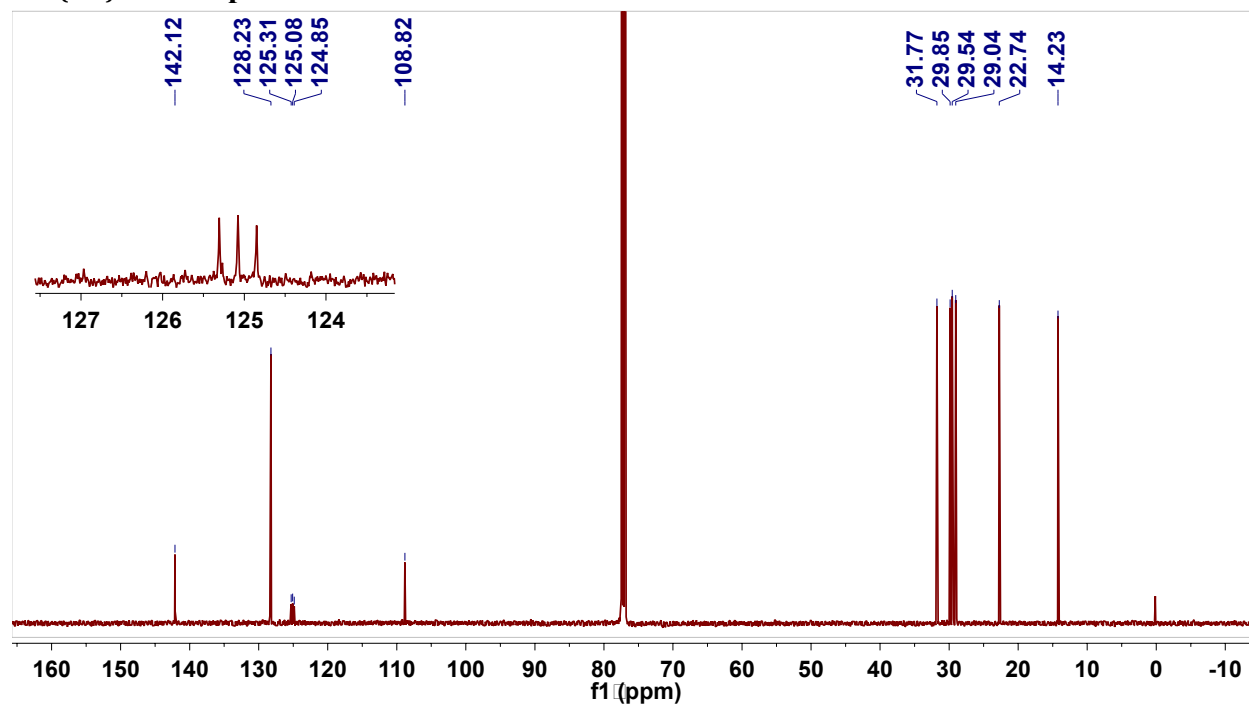
^1H NMR Spectrum of 2n **$^{13}\text{C}\{^1\text{H}\}$ NMR Spectrum of 2n**

¹H NMR Spectrum of 2o**¹³C{¹H} NMR Spectrum of 2o**

^1H NMR Spectrum of 2p and 3p **$^{13}\text{C}\{^1\text{H}\}$ NMR Spectrum of 2p and 3p**

^1H NMR Spectrum of 2q **$^{13}\text{C}\{^1\text{H}\}$ NMR Spectrum of 2q**

^1H NMR Spectrum of 2r **$^{13}\text{C}\{^1\text{H}\}$ NMR Spectrum of 2r**

¹H NMR Spectrum of 1a-d₁**¹³C{¹H} NMR Spectrum of 1a-d₁****C.13 References**

1. Kapdi, A. R.; Whitwood, A. C.; Williamson, D. C.; Lynam, J. M.; Burns, M. J.; Williams, T. J.; Reay, A. J.; Holmes, J.; Fairlamb, I. J. S. The Elusive Structure of Pd₂(dba)₃. Examination by Isotopic Labeling, NMR Spectroscopy, and X-ray Diffraction Analysis: Synthesis and Characterization of Pd₂(dba-Z)₃ Complexes. *J. Am. Chem. Soc.* 2013, *135*, 8388-8399.
2. Steinberger, S.; Mishra, A.; Reinold, E.; Mena-Osteritz, E.; Müller, H.; Uhrich, C.; Pfeiffer, M.; Bäuerle, P. Synthesis and Characterization of Red/Near-IR Absorbing A–D–A–D–A-Type Oligothiophenes Containing Thienothiadiazole and Thienopyrazine Central Units. *J. Mater. Chem.* 2012, *22*, 2701-2712.
3. Fachetti, A.; Yoon, M.-H.; Stern, C. L.; Hutchison, G. R.; Ratner, M. A.; Marks, T. J. Building Blocks for N-Type Molecular and Polymeric Electronics. Perfluoroalkyl- versus Alkyl-Functionalized Oligothiophenes (nTs; $n = 2-6$). Systematic Synthesis, Spectroscopy, Electrochemistry, and Solid-State Organization. *J. Am. Chem. Soc.* 2004, *126*, 13480-13501.
4. Amarasekara, A. S.; Pomerantz, M. Synthesis and Study of Head-to-Tail Regioregular Poly(alkyl thiophene-3-carboxylates). *Synthesis* 2003, 2255-2258.
5. Osterberg, P. M.; Niemeier, J. K.; Welch, C. J.; Hawkins, J. M.; Martinelli, J. R.; Johnson, T. E.; Root, T. W.; Stahl, S. S. Experimental Limiting Oxygen Concentrations for Nine Organic Solvents at Temperatures and Pressures Relevant to Aerobic Oxidations in the Pharmaceutical Industry. *Org. Process Rev. Dev.* 2015, *19*, 1537–1543.
6. Yang, Q.; Shend, M.; Li, X.; Tucker, C.; Céspedes, S. V.; Webb, N. J.; Whiteker, G. T.; Yu, J. Potential Explosion Hazards Associated with the Autocatalytic Thermal Decomposition of Dimethyl Sulfoxide and Its Mixtures. *Org. Process Rev. Dev.* 2020, *24*, 916–939.

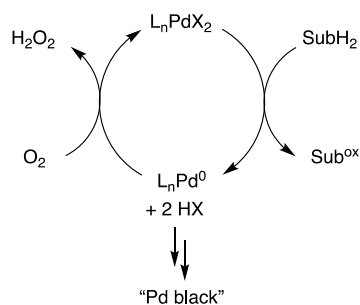
7. Li, N.-N.; Zhang, Y.-L.; Mao, S.; Gao, Y.-R.; Guo, D.-D.; Wang, Y.-Q. Palladium-Catalyzed C–H Homocoupling of Furans and Thiophenes Using Oxygen as the Oxidant. *Org. Lett.* 2014, *16* (10), 2732–2735.
8. Campbell, A. N.; Meyer, E. B.; Stahl, S. S. Regiocontrolled Aerobic Oxidative Coupling of Indoles and Benzene Using Pd Catalysts with 4,5-Diazafluorene Ligands. *Chem. Commun.* 2011, *47*, 10257–10259.
9. Izawa, Y.; Stahl, S. S. Aerobic Oxidative Coupling of O-Xylene: Discovery of 2-Fluoropyridine as a Ligand to Support Selective Pd-Catalyzed C–H Functionalization. *Adv. Synth. Catal.* 2010, *352*, 3223–3229.

**Appendix D: A Thermodynamically Stable Palladium
Catalyst for the Aerobic Oxidation of Organic Molecules**

D.1 Introduction

Palladium catalyzed aerobic oxidation reactions are a powerful class of methods for the synthesis of organic molecules.¹ They proceed via the general mechanism depicted in Scheme D.1, where a PdX₂ salt, which may be supported by an ancillary ligand, reacts with substrate (SubH₂) to form product (Sub_{ox}), Pd⁰, and two equivalents of HX. Palladium(0) reacts with O₂ and 2 equivalents of HX to generate H₂O₂ and regenerate the PdX₂ catalyst to close the catalytic cycle.²³ Despite their synthetic utility, they are plagued by significant limitations, the most glaring of which are high catalyst loadings and low turnover numbers (TONs).⁴ The former is a direct consequence of the latter, which is commonly attributed to the instability of Pd(0) with respect to the irreversible formation of catalytically inactive Pd black (cf. Scheme D.1).

There are numerous strategies to mitigate Pd black formation and thereby extend catalyst lifetimes, most notably the addition of ancillary ligands such as pyridine, bipyridine, or phenanthroline derivatives, *N*-heterocyclic carbenes, amines, and, to a lesser extent, phosphines.¹ Ancillary ligands work principally by slowing agglomeration of Pd(0) relative to catalyst reoxidation. Other catalytic additives, particularly benzoquinone (BQ) and derivatives thereof, are especially effective at prolonging catalyst lifetimes by binding to Pd(0) to retard catalyst precipitation. BQ also serves as a terminal or cocatalytic oxidant for Pd, accelerating catalyst oxidation and slowing degradation.⁵⁶



Scheme D.1. Generic mechanism of Pd catalyzed aerobic oxidation reaction

While these strategies have proven somewhat effective for the development of catalyst systems with high TON (~ 2000),⁶ they have not proven general. Perhaps more significantly, kinetic strategies—however effective they may be at generating high TON catalysts—are ultimately doomed to fail precisely because they rely on kinetic phenomenon. That is, their success is tied to the relative rates of Pd reoxidation (k_{ox}) and Pd black formation (k_{deg}), the latter of which is irreversible. Even in the scenario where $k_{ox} \gg k_{deg}$, it is only a matter of time before all the catalyst dies.

An alternative strategy for the generation of a long lived Pd oxidation catalyst relies on the development of conditions under which the formation of Pd black is thermodynamically unfavorable, resulting in an effectively "immortal" catalyst. Such a catalyst would be especially attractive in large-scale chemical applications, where catalyst loadings and lifetimes have significant pecuniary implications. Indeed, the Wacker process, the Pd-catalyzed aerobic oxidative coupling of water and ethylene to acetaldehyde, utilizes just such a catalyst to produce billions of pounds of acetaldehyde per year.⁷ A Pourbaix analysis of Pd (

Figure D.1) reveals that under typical Wacker conditions—acidic aqueous conditions with high concentrations of chloride anions—are sufficiently corrosive such that formation of Pd metal is thermodynamically unfavorable, thus ensuring effective "immortality" of Pd catalyst.

Inspired by the Wacker process, we sought to develop a Pd catalyst system for the aerobic oxidation of organic molecules where the decomposition of the Pd catalyst to metallic Pd is thermodynamically unfavorable, producing an "immortal" catalyst system. Herein is reported early progress toward this goal.

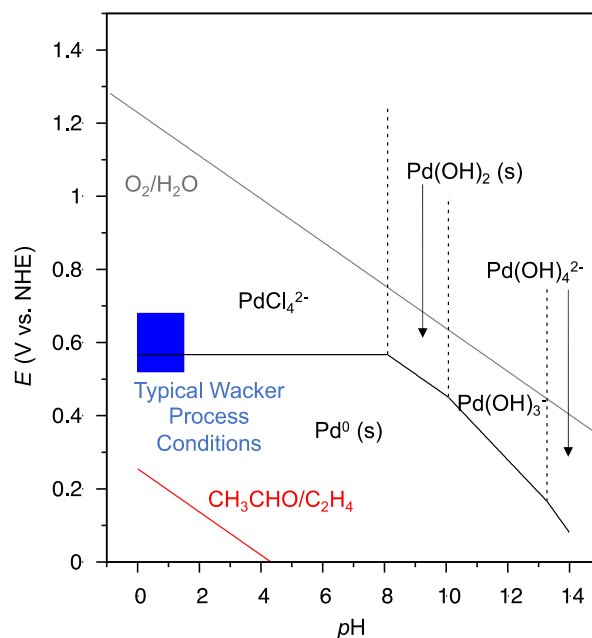
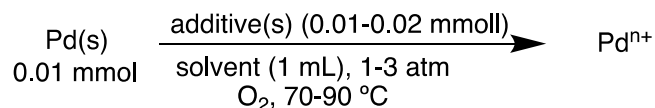


Figure D.1. Pourbaix Diagram for Pd and acetaldehyde, with relevant Wacker Process conditions

D.2 Results and Discussion

The general experimental plan was organized thusly: Experiments were conducted to identify conditions capable of corroding Pd metal. Upon identification of sufficiently corrosive conditions, a variety of organic substrates were subjected to the resulting corroded Pd solution to evaluate whether they were catalytically active.



Equation D.1. General reaction scheme for Pd dissolution experiments

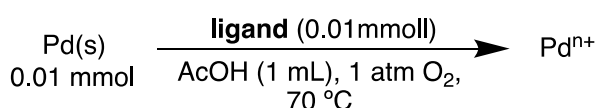
Initial experiments were conducted to identify conditions for the dissolution of Pd metal (in the form of Pd powder) under conditions relevant to the aerobic oxidation of organic molecules. General reaction conditions utilized throughout the following screens are depicted in Equation D.1. These conditions included: organic solvents, ancillary ligands, benzoquinone derivatives, first-row transition metal salt additives, temperatures, O₂ pressures, and combinations thereof. Dissolution studies were performed by depositing a known amount of Pd powder into a reaction tube with solvent and other additives and subjecting the mixture to the reaction conditions. The amount of dissolved Pd was quantified by inductively coupled plasma-optical emission spectroscopy (ICP-OES) calibrated to known standards.

D.2.1 Ligand screens

A variety of ancillary ligands, including pyridine, bipyridine, phenanthroline, and phosphine derivatives (0.01 mmol) were mixed with Pd powder (0.01 mmol) in acetic acid (1 mL) and stirred under 1 atm of O₂ at 70 °C overnight. The results of this screen are shown in Table D.1. A few trends emerge. Most notably, bidentate and tridentate ligands are more effective at promoting Pd corrosion than monodentate ligands, such as pyridine derivatives, consistent with the enhanced stability conferred by the chelate effect. Electron-rich monodentate ligands (e.g. 4-methoxypyridine) tend to perform better than electron poor varieties (e.g. 4-trifluoromethylpyridine), probably a consequence of their stronger sigma donor capabilities and consequent tendency to stabilize Pd^{II}. Bidentate nitrogen donor ligands (e.g. bipyridine) with steric bulk *ortho* to the nitrogen donors are less effective, likely due to destabilizing steric interactions

in the ligand-supported Pd^{II} complex (cf. Chapter 2).⁸ A notable exception to this is 6-methyl-2,2'-dipyridyl, which is among the most effective ligands at promoting corrosion, although the reason is unclear at this point. It should be noted that the three entries with lowest amounts of Pd—bathocuproine, *rac*-BINAP, and 4,4'-dinonyl-2,2'-dipyridyl—formed considerable amounts of precipitate when diluted with aqueous acid for ICP-OES analysis, so the value for dissolved Pd may be higher. Overall, these results suggest that future ligand screens should focus on chelating, nitrogen donor ligands. Phosphines could be explored further, as this screen was limited to only one phosphine ligand (*rac*-BINAP), although most phosphine ligands are expected to be rapidly oxidized to phosphine oxides under the reaction conditions.⁹

To ensure a wide chemical space was evaluated in future screens, a selection of the top-performing ligands of structural diversity were selected to use as ligands in subsequent additive and reaction conditions screens, including 1,10-phenanthroline (*phen*), 2,2'-bipyridine-4,4'-dicarboxylate (4,4'-(CO₂Me)₂-bpy), 6-methyl-2,2'-dipyridyl (6-Me-bpy), tris(2-pyridylmethyl)amine (TPA), 2-(2-pyridyl)imidazole, and 2-pyrazol-1-yl-pyridine,.



Equation D.2. Reaction scheme for ligand screen

Table D.1. Ligand screen for Pd corrosion

Ligand	% corroded Pd
1,10-Phenanthroline (<i>phen</i>)	110*
6-Methyl-2,2'-dipyridyl	110*
5,5'-Dimethyl-2,2'-dipyridyl	95
4,7-Dimethoxy-1,10-phenanthroline	77
4,4'-Di-tert-butyl-2,2'-dipyridyl	76
3,4,7,8-Tetramethyl-1,10-phenanthroline	72
2-Pyrazol-1-yl-pyridine	69
2,2'-bipyridine-4,4'-dicarboxylate	48
2-(2-Pyridyl)imidazole	48

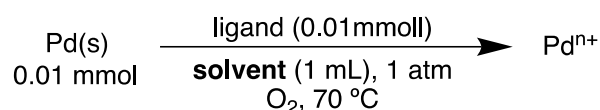
4,4,4-Tri-tert-butyl-2,2:6,2-terpyridine	47
Tris(2-pyridylmethyl)amine (TPA)	44
6,6'-Dimethyl-2,2'-bipyridine	41
4,7-Dimethyl-1,10-phenanthroline	37
4-Methoxypyridine	27
2,2'-Bipyridyl	26
4,4'-Dimethyl-2,2'-bipyridyl	25
4-methyl pyridine	25
4,4'-Dimethoxy-2,2'-bipyridyl	25
4-Morpholinopyridine	22
4-Dimethylaminopyridine	19
3-Chloropyridine	15
1,10-Phenanthroline-5,6-dione	12
pyridine-2-carboxamide	12
<i>N,N'</i> -Di-tert-butylethylenediamine	10
4-Pyrrolidinopyridine	9
2-Chloro-6-methoxypyridine	9
4,5-Diazafluoren-9-one	8
4-Pyridinecarbonitrile	6
4-(Trifluoromethyl)pyridine	6
4-Phenylpyridine	5
2-Chloro-4-(trifluoromethyl)pyridine	5
2-(2-Pyridyl)benzimidazole	5
4,7-Dichloro-1,10-phenanthroline	4
5-Bromo-2-methoxypyridine	3
(<i>S,S</i>)-2,2'-Methylenebis(4-tert-butyl-2-oxazoline)	3
2,2'-Methylenebis[3a,8a-dihydro-8H-indeno[1,2-d]oxazole]	2
2,2'-Biquinoline	2
none	1
1,8-Naphthyridine	1
2-Bromopyrimidine	1
4-Piperidinopyridine	1
2-bromo-4-chloro-6-methoxypyridine	1
Bathocuproine	1
4,4'-Diamino-2,2'-bipyridyl	0
4,4'-Dinonyl-2,2'-dipyridyl	0
Bathophenanthroline	0
rac-BINAP	0

*Exceeds 100%. This is likely because Pd powder is deposited into reaction via slurry, which introduces some uncertainty in initial amount of Pd added.

D.2.2 Solvent screens

Solvents including acetic acid (AcOH), *N*-methyl-2-pyrrolidone (NMP), dimethylsulfoxide (DMSO), toluene, 1,4-dioxane, and tert-amyl alcohol (*t*AmylOH) were evaluated with a selection

of top-performing ligands. The results are tabulated in Table D.2. Only AcOH was demonstrated to be effective at dissolving Pd in appreciable amounts. The reason for this observation is three-fold. First, a source of protons is required for the O₂ reduction product (H₂O₂ or H₂O) formed on oxidation of Pd. Second, an anion is needed to accompany the oxidized Pd species. Third, the surface of the Pd metal is likely covered in a variety of Pd-oxide and -hydroxide species, and protons are needed to remove those species to expose a fresh surface. AcOH provides a source of protons for O₂ reduction and cleaning the Pd surface, and anions for Pd oxidation.



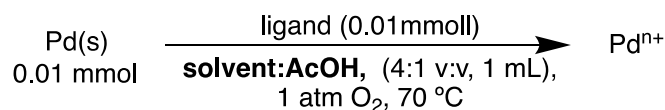
Equation D.3. Reaction scheme for solvent screen

Table D.2. Solvent screen for Pd corrosion

Solvent	ligand	% corroded Pd
AcOH	1,10-Phenanthroline	62
	2,2'-bipyridine-4,4'-dicarboxylate	27
	6-Methyl-2,2'-dipyridyl	86
	2-(2-Pyridyl)imidazole	47
	2-Pyrazol-1-yl-pyridine	67
	4,4'-Di-tert-butyl-2,2'-dipyridyl	77
	Tris(2-pyridylmethyl)amine	42
	blank	0
DMSO	1,10-Phenanthroline	2
	2,2'-bipyridine-4,4'-dicarboxylate	1
	6-Methyl-2,2'-dipyridyl	0
	2-(2-Pyridyl)imidazole	3
	2-Pyrazol-1-yl-pyridine	1
	4,4'-Di-tert-butyl-2,2'-dipyridyl	1
	Tris(2-pyridylmethyl)amine	6
	blank	0
NMP	1,10-Phenanthroline	0
	2,2'-bipyridine-4,4'-dicarboxylate	0
	6-Methyl-2,2'-dipyridyl	0
	2-(2-Pyridyl)imidazole	0
	2-Pyrazol-1-yl-pyridine	0
	4,4'-Di-tert-butyl-2,2'-dipyridyl	0
	Tris(2-pyridylmethyl)amine	0
		0

	blank	0
Dioxane	1,10-Phenanthroline	1
	2,2'-bipyridine-4,4'-dicarboxylate	0
	6-Methyl-2,2'-dipyridyl	0
	2-(2-Pyridyl)imidazole	0
	2-Pyrazol-1-yl-pyridine	0
	4,4'-Di-tert-butyl-2,2'-dipyridyl	0
	Tris(2-pyridylmethyl)amine	0
	blank	0
toluene	1,10-Phenanthroline	0
	2,2'-bipyridine-4,4'-dicarboxylate	0
	6-Methyl-2,2'-dipyridyl	0
	2-(2-Pyridyl)imidazole	0
	2-Pyrazol-1-yl-pyridine	0
	4,4'-Di-tert-butyl-2,2'-dipyridyl	0
	Tris(2-pyridylmethyl)amine	0
	blank	0
tAmylOH	1,10-Phenanthroline	0
	2,2'-bipyridine-4,4'-dicarboxylate	0
	6-Methyl-2,2'-dipyridyl	0
	2-(2-Pyridyl)imidazole	0
	2-Pyrazol-1-yl-pyridine	0
	4,4'-Di-tert-butyl-2,2'-dipyridyl	0
	Tris(2-pyridylmethyl)amine	4
	blank	0

Accordingly, another solvent screen was performed with mixtures of the aforementioned solvents and AcOH in 4:1 v/v ratios with the same ligands. Significant increases in Pd dissolution were observed (Table D.3). These results reveal that strongly polar/coordinating solvents, (DMSO, NMP) hinder Pd dissolution relative to less polar/coordinating solvents. Strongly coordinating solvents are known to induce the formation of Pd nanoparticles,¹⁰ a presumed intermediate in the formation of bulk Pd metal. Such solvents are therefore not likely to be good candidates for a thermodynamically stable Pd catalyst system.



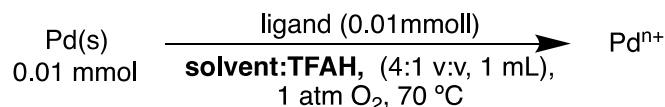
Equation D.4. Reaction scheme for AcOH cosolvent screen

Table D.3. Solvent screen with AcOH cosolvent for Pd corrosion

solvent	ligand	% corroded Pd
AcOH:AcOH (4:1)	1,10-Phenanthroline	47
	2,2'-bipyridine-4,4'-dicarboxylate	33
	6-Methyl-2,2'-dipyridyl	87
	2-(2-Pyridyl)imidazole	55
	2-Pyrazol-1-yl-pyridine	58
	4,4'-Di-tert-butyl-2,2'-dipyridyl	77
	Tris(2-pyridylmethyl)amine	75
	blank	0
DMSO:AcOH (4:1)	1,10-Phenanthroline	10
	2,2'-bipyridine-4,4'-dicarboxylate	3
	6-Methyl-2,2'-dipyridyl	4
	2-(2-Pyridyl)imidazole	8
	2-Pyrazol-1-yl-pyridine	5
	4,4'-Di-tert-butyl-2,2'-dipyridyl	6
	Tris(2-pyridylmethyl)amine	3
	blank	1
NMP:AcOH (4:1)	1,10-Phenanthroline	4
	2,2'-bipyridine-4,4'-dicarboxylate	2
	6-Methyl-2,2'-dipyridyl	4
	2-(2-Pyridyl)imidazole	6
	2-Pyrazol-1-yl-pyridine	2
	4,4'-Di-tert-butyl-2,2'-dipyridyl	3
	Tris(2-pyridylmethyl)amine	5
blank	1	
Dioxane:AcOH (4:1)	1,10-Phenanthroline	4
	2,2'-bipyridine-4,4'-dicarboxylate	5
	6-Methyl-2,2'-dipyridyl	26
	2-(2-Pyridyl)imidazole	3
	2-Pyrazol-1-yl-pyridine	7
	4,4'-Di-tert-butyl-2,2'-dipyridyl	11
	Tris(2-pyridylmethyl)amine	2
blank	2	
toluene:AcOH (4:1)	1,10-Phenanthroline	6
	2,2'-bipyridine-4,4'-dicarboxylate	15
	6-Methyl-2,2'-dipyridyl	35
	2-(2-Pyridyl)imidazole	11
	2-Pyrazol-1-yl-pyridine	28
	4,4'-Di-tert-butyl-2,2'-dipyridyl	16
Tris(2-pyridylmethyl)amine	17	

	blank	0
tAmylOH:AcOH (4:1)	1,10-Phenanthroline	15
	2,2'-bipyridine-4,4'-dicarboxylate	12
	6-Methyl-2,2'-dipyridyl	48
	2-(2-Pyridyl)imidazole	6
	2-Pyrazol-1-yl-pyridine	12
	4,4'-Di-tert-butyl-2,2'-dipyridyl	29
	Tris(2-pyridylmethyl)amine	23
	blank	1

A second screen was performed in which trifluoroacetic acid (TFAH) was used as a cosolvent in a 4:1 v/v ratio of solvent:TFAH. The results are summarized in Table D.4. Overall, there are substantially greater amounts of Pd dissolution relative to screens with AcOH. This can be attributed to the greater proton activity with the more acidic TFAH, facilitating O₂ reduction and more effectively helping expose fresh Pd surfaces to the reaction conditions. Similar dissolution trends are observed with TFAH as with AcOH: non-polar solvents are superior for the dissolution of Pd metal, likely for the same reason as above.



Equation D.5. Reaction scheme for TFAH cosolvent screen

Table D.4. Solvent screen with TFAH cosolvent for Pd corrosion

solvent	ligand	% corroded Pd
AcOH:TFAH (4:1)	1,10-Phenanthroline	61
	2,2'-bipyridine-4,4'-dicarboxylate	63
	6-Methyl-2,2'-dipyridyl	62
	2-(2-Pyridyl)imidazole	54
	2-Pyrazol-1-yl-pyridine	68
	4,4'-Di-tert-butyl-2,2'-dipyridyl	70
	Tris(2-pyridylmethyl)amine	45
	blank	0
DMSO:TFAH (4:1)	1,10-Phenanthroline	13
	2,2'-bipyridine-4,4'-dicarboxylate	9
	6-Methyl-2,2'-dipyridyl	7
	2-(2-Pyridyl)imidazole	8

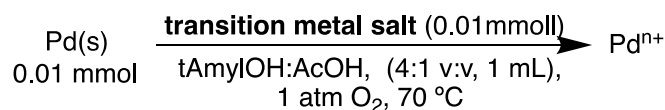
	2-Pyrazol-1-yl-pyridine	29
	4,4'-Di-tert-butyl-2,2'-dipyridyl	6
	Tris(2-pyridylmethyl)amine	4
	blank	5
NMP:TFAH (4:1)	1,10-Phenanthroline	8
	2,2'-bipyridine-4,4'-dicarboxylate	11
	6-Methyl-2,2'-dipyridyl	22
	2-(2-Pyridyl)imidazole	19
	2-Pyrazol-1-yl-pyridine	16
	4,4'-Di-tert-butyl-2,2'-dipyridyl	16
	Tris(2-pyridylmethyl)amine	20
	blank	2
Dioxane:TFAH (4:1)	1,10-Phenanthroline	25
	2,2'-bipyridine-4,4'-dicarboxylate	8
	6-Methyl-2,2'-dipyridyl	52
	2-(2-Pyridyl)imidazole	22
	2-Pyrazol-1-yl-pyridine	32
	4,4'-Di-tert-butyl-2,2'-dipyridyl	46
	Tris(2-pyridylmethyl)amine	8
	blank	1
toluene:TFAH (4:1)	1,10-Phenanthroline	44
	2,2'-bipyridine-4,4'-dicarboxylate	94
	6-Methyl-2,2'-dipyridyl	50
	2-(2-Pyridyl)imidazole	28
	2-Pyrazol-1-yl-pyridine	72
	4,4'-Di-tert-butyl-2,2'-dipyridyl	36
	Tris(2-pyridylmethyl)amine	7
	blank	0
<i>t</i> AmylOH:TFAH (4:1)	1,10-Phenanthroline	12
	2,2'-bipyridine-4,4'-dicarboxylate	22
	6-Methyl-2,2'-dipyridyl	81
	2-(2-Pyridyl)imidazole	68
	2-Pyrazol-1-yl-pyridine	91
	4,4'-Di-tert-butyl-2,2'-dipyridyl	55
	Tris(2-pyridylmethyl)amine	94
	blank	1

Overall, these experiments suggest that future optimization of Pd corrosion conditions should focus on weakly polar/coordinating solvents with added acid. The lower limit to the amount of acid that could be employed remains to be tested. Neat AcOH or *t*AmylOH:AcOH (4:1) were selected as the optimal conditions for future screens. Although TFAH proved superior at

facilitating Pd corrosion, many substrates would likely not tolerate solvent quantities of TFAH under catalytic conditions, and it was largely excluded from future screens.

D.2.3 Metal additive screens

First-row transition metal additives feature prominently in Pd-catalyzed aerobic oxidation reactions as a redox active cocatalysts, of which Cu is the most notable, particularly in the Wacker process. In the absence of ancillary ligands, a variety of first-row transition metal salts (0.01 mmol) were mixed with Pd (0.01 mmol additive) in 4:1 tAmylOH:AcOH as additives for the oxidation of Pd metal, the results shown in Table D.5. Most metal additives had at least a small positive influence on Pd corrosion relative to no added metal salt. Since the metals were screened at stoichiometric amounts relative to Pd, whether the promotional effect is a result of the additives acting as redox mediators for O₂-mediated Pd oxidation or stoichiometric oxidants is unclear. Additional experiments should be performed using sub-stoichiometric amounts of metals to elucidate the effect. A variety of Mn, Fe, and Cu salts, including Mn(OAc)₃, FeBr₃, CuCl, and CuBr₂, emerged as the most effective at promoting Pd dissolution, and all these metals have been featured as stoichiometric or cocatalytic additives in Pd-catalyzed aerobic oxidation reactions.¹¹¹² There appears to be an effect on the anion of the metal additive, chloride and bromide ions tending to be the most effective. The relative ineffectiveness of other anions may be a consequence of anion exchange between dissolved Pd ions and metal additive ions, resulting in the formation of insoluble or otherwise unstable PdX₂ species. Overall, these results suggest that metal additives, especially metal chlorides and bromides, are a promising direction for developing a thermodynamically stable catalyst system and warrant further exploration.



Equation D.6. Reaction scheme for transition metal salt additive screen

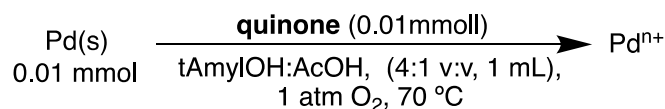
Table D.5. Metal additive screen for Pd corrosion

Metal additive	% corroded Pd	Metal additive	% corroded Pd
Co(acac) ₃	60	Fe(NO ₃) ₂ •9H ₂ O	1
Mn(OAc) ₃ •2H ₂ O	52	Cu(TFA) ₂	1
FeBr ₃	48	CuI	1
MnBr ₂	38	Ni(acac) ₂	1
CuCl	29	Mn ₂ O ₃	1
CuBr ₂	9	CoBr ₂	1
Cr(NO ₃) ₃ •9H ₂ O	7	Fe(OTf) ₂	1
Co(NO ₃) ₂ •6H ₂ O	7	Ni(CO ₃) ₂	1
FeCl ₂ •4H ₂ O	3	Fe(OAc) ₂	1
CoF ₂	3	NiF ₂	1
CuO	3	Mn(CO ₃) ₂ •H ₂ O	1
FeF ₃	2	NiBr ₂	1
NiCl ₂ •6H ₂ O	2	NiO	0
Cu(CO ₃) ₂	2	Co ₃ O ₄	0
Ni(OAc) ₂	2	Ni(NO ₃) ₂ •6H ₂ O	0
Fe ₂ O ₃	2	AgF	0
Mn(acac) ₂	2	CoPc	0
AgCl	2	Cu(NO ₃) ₂ •2.5H ₂ O	0
(MeCN)Cu(OTf)	2	AgOAc	0
MnF ₂	2	AgClO ₄	0
Fe(acac) ₃	2	Co(salophen)	0
CoCl ₂	1	none	0

D.2.4 Quinone screens

As discussed above, quinones are common additives in Pd-catalyzed oxidation reactions, where they are proposed to stabilize Pd⁰ intermediates. Accordingly, a variety of BQ derivatives were screened (0.01 mmol) for their effect of Pd corrosion in 4:1 tAmylOH:AcOH, and the results are displayed in Table D.6. In general, BQ derivatives show no improvement relative to no quinone ("blank"), and in some cases have a deleterious effect. Quinones are known to decompose under acidic conditions,¹³ and the reduction of corroded Pd by quinone decomposition products could account for the negative effect observed in some instances. These results suggest little merit in

further investigation of quinones as additives for immortal catalyst systems. Their tendency to degrade under the reaction conditions also indicate that any positive effect they may impart would be mitigated over the course of time.



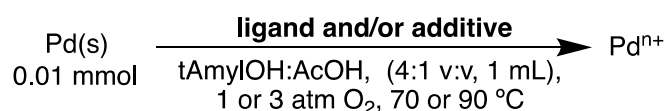
Equation D.7. Reaction scheme for quinone screen

Table D.6. Quinone screen for Pd corrosion

Quinone	ligand	% corroded Pd	Quinone	ligand	% corroded Pd
BQ	blank	1	2-MeOBQ	blank	0
	6-Me-bpy	1		6-Me-bpy	20
	4,4'-(CO ₂ Me) ₂ -bpy	3		4,4'-(CO ₂ Me) ₂ -bpy	5
	TPA	6		TPA	42
2-CIBQ	blank	0	(Me) ₄ BQ	blank	0
	6-Me-bpy	7		6-Me-bpy	1
	4,4'-(CO ₂ Me) ₂ -bpy	4		4,4'-(CO ₂ Me) ₂ -bpy	4
	TPA	29		TPA	26
2-'BuBQ	blank	1	2,6-Me ₂ BQ	blank	0
	6-Me-bpy	1		6-Me-bpy	1
	4,4'-(CO ₂ Me) ₂ -bpy	2		4,4'-(CO ₂ Me) ₂ -bpy	2
	TPA	1		TPA	3
2,5-Me ₂ BQ	blank	0	2-PhBQ	blank	0
	6-Me-bpy	26		6-Me-bpy	1
	4,4'-(CO ₂ Me) ₂ -bpy	5		4,4'-(CO ₂ Me) ₂ -bpy	2
	TPA	49		TPA	1
2,5-CIBQ	blank	0	2,6-Cl ₂ BQ	blank	0
	6-Me-bpy	3		6-Me-bpy	24
	4,4'-(CO ₂ Me) ₂ -bpy	12		4,4'-(CO ₂ Me) ₂ -bpy	4
	TPA	84		TPA	47
2,6-'BuBQ	blank	0	blank	blank	0
	6-Me-bpy	23		6-Me-bpy	33
	4,4'-(CO ₂ Me) ₂ -bpy	5		4,4'-(CO ₂ Me) ₂ -bpy	5
	TPA	45		TPA	49

D.2.5 Temperature, O₂ pressure, time, and added glass bead screens

A series of screens were conducted to assess the effect of temperature, O₂ pressure, and the effect of glass beads using a selection of the best ligands and metal additives (ligands in a 1:1 molar ratio with Pd, metals in a 2:1 molar ratio with Pd)—and combinations thereof—the results of which are presented in Table D.7. The data reveal that higher temperatures and pressures generally facilitate greater Pd dissolution, indicating that dissolution conditions could stand to be further optimized. The combination of ligands and metal additives are not particularly effective, which is probably a consequence of the 2:1 molar ratio in which they are used: excess metal additive will bind to all free ligand, leaving no ligand remaining to bind to Pd. The screens should be repeated with excess ligand to circumvent this problem. Glass beads also promote Pd corrosion, likely serving to mechanically break up aggregates of Pd, increasing surface area available to be corroded. These results suggest that future dissolution screens should employ glass beads with higher temperatures and O₂ pressures, although there are safety considerations that should be taken into account when considering the latter.



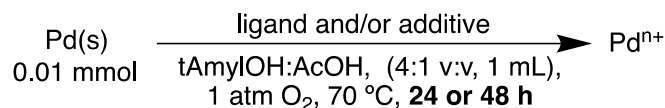
Equation D.8. Reaction scheme for temperature, O₂ pressure and glass beads

Table D.7. Temperature, O₂ pressure, and glass bead screen with best corrosion conditions

ligand	additive	% corroded Pd		
		70 °C, 1 atm O ₂	90 °C, 1 atm O ₂	70 °C, 3 atm O ₂
none		0	5	3
1,10-phen		57	90	89
6-methyl-2,2'-bpy		54	67	99
5,5'-dimethyl-2,2'-bpy		78	108	115
4,4'-ditBu-2,2'-bpy		71	16	104
2-pyrazol-1-yl pyridine		54	7	86
TPA		12	11	3
none	Mn(OAc) ₃ ·2(H ₂ O)	7	3	103

none	FeBr ₃	0	0	0
none	CuCl ₂	49	4	15
6-methyl-2,2'-bpy	Mn(OAc) ₃ •2(H ₂ O)	5	6	9
6-methyl-2,2'-bpy	FeBr ₃	12	23	8
6-methyl-2,2'-bpy	CuCl ₂	54	42	53
none	3 glass beads	1	21	13

A separate dissolution screen with 3 ligands and Mn(OAc)₃•H₂O (0.01 mmol ligand, 0.005 mmol Mn(OAc)₃, 0.005 mmol Pd; stoichiometries adjusted to address the issue mentioned above regarding M/L/Pd ratios) was also performed to assess the extent of dissolution as a function of time, the results shown in Table D.8. The data reveal that there are significantly greater amounts of Pd dissolution after 48 hr relative to 24 hr, indicating that dissolution is rather sluggish. Optimal dissolution conditions should therefore err toward longer reaction times.



Equation D.9. Reaction scheme for time reaction time screen

Table D.8. Effect of time on Pd corrosion

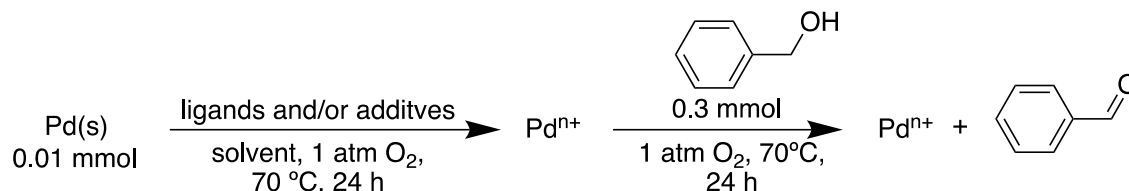
additive	ligand	% corroded Pd (24 h)	% corroded Pd (48 h)
none	none	1	1
Mn(OAc) ₃ •H ₂ O	1,10-phen	4	19
	6-methyl-2,2'-bpy	32	40
	5,5'-dimethyl-2,2'-bpy	21	59

D.2.6 Organic oxidation screen

The most promising Pd corrosion conditions from the above screens were identified and served as the basis for catalyst systems for three aerobic oxidation reactions: benzyl alcohol oxidation, oxidative coupling of water and styrene, and α,β -dehydrogenation of 4-phenylcyclohexanone. Pd powder (0.01 mmol) was subject to the standard dissolution procedure

with the ligands, solvents, and additives shown in Tables D.9-D.10 below. After 24 h, substrates (0.3 mmol) were added to the reaction tubes and allowed to mix for an additional 24 h, after which the reaction mixtures were assayed by UPLC.

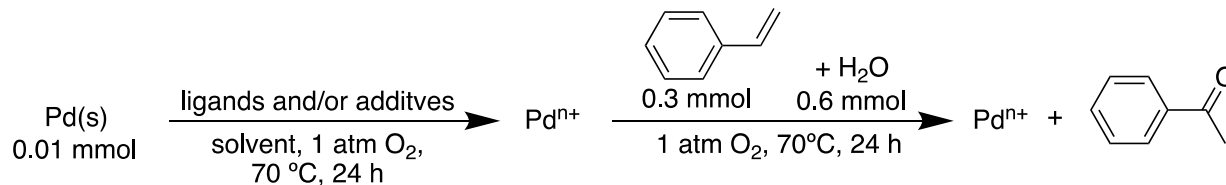
Little to no (<5%) conversion of benzyl alcohol to benzaldehyde was observed for the reactions containing benzyl alcohol (Table D.9). The minimal oxidation observed may be a consequence of the solvent-level AcOH concentration, which is known to be inhibitory in Pd-catalyzed aerobic alcohol oxidation reactions.¹⁴ There was likewise little to no acetophenone observed in the reactions containing styrene (Table D.10). The failure to produce measurable amounts of acetophenone from styrene may be a consequence of the low water concentration (2 equiv relative to styrene). Future screens should use greater water concentration.



Equation D.10. Reaction scheme for corrosion-oxidation sequence with benzyl alcohol substrate

Table D.9. Benzyl alcohol oxidation to benzaldehyde by corroded Pd solutions

condition	ligand	solvent	additive	% yield
1	none	tAmylOH/AcOH (3:2)	CuCl ₂	2
2	phen	AcOH		2
3	6-Me-bpy	AcOH		3
4	6-Me-bpy	Tol/AcOH (3:2)		4
5	6-Me-bpy	tAmylOH/AcOH (3:2)		5
6	6-Me-bpy	Tol/TFAH (3:2)		0
7	6-Me-bpy	tAmylOH/TFAH (3:2)		0
8	4,4'-(<i>t</i> Bu) ₂ -bpy	Tol/AcOH (3:2)		3
9	4,4'-(<i>t</i> Bu) ₂ -bpy	tAmyl/AcOH (3:2)		2
10	4,4'-(<i>t</i> Bu) ₂ -bpy	AcOH		2
11	TPA	tAmylOH/TFAH (3:2)		0
12	TPA	tAmylOH/AcOH (3:2)	CuCl ₂	1
13	TPA	tAmylOH/AcOH (3:2)	2,6- <i>t</i> Bu ₂ BQ	2
14	2-Pyrazol-1-yl-pyridine	Tol/TFAH (3:2)		2
15	2-Pyrazol-1-yl-pyridine	tAmylOH/TFAH (3:2)		4
16	2-Pyrazol-1-yl-pyridine	AcOH		3



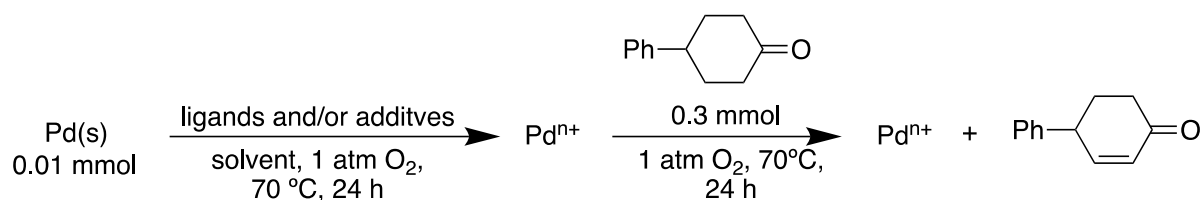
Equation D.11. Reaction scheme for corrosion-oxidation sequence with styrene substrate

Table D.10. Styrene oxidation to acetophenone by corroded Pd solutions

condition	ligand	solvent	additive	% LC area
1	none	tAmylOH/AcOH (3:2)	CuCl ₂	<1
2	phen	AcOH		<1
3	6-Me-bpy	AcOH		<1
4	6-Me-bpy	Tol/AcOH (3:2)		<1
5	6-Me-bpy	tAmylOH/AcOH (3:2)		<1
6	6-Me-bpy	Tol/TFAH (3:2)		<1
7	6-Me-bpy	tAmylOH/TFAH (3:2)		<1
8	4,4'-(<i>t</i> Bu) ₂ -bpy	Tol/AcOH (3:2)		<1
9	4,4'-(<i>t</i> Bu) ₂ -bpy	tAmyl/AcOH (3:2)		<1
10	4,4'-(<i>t</i> Bu) ₂ -bpy	AcOH		<1
11	TPA	tAmylOH/TFAH (3:2)		<1
12	TPA	tAmylOH/AcOH (3:2)	CuCl ₂	<1
13	TPA	tAmylOH/AcOH (3:2)	2,6- <i>t</i> Bu ₂ BQ	<1
14	2-Pyrazol-1-yl-pyridine	Tol/TFAH (3:2)		<1
15	2-Pyrazol-1-yl-pyridine	tAmylOH/TFAH (3:2)		<1
16	2-Pyrazol-1-yl-pyridine	AcOH		<1

In contrast to benzyl alcohol and styrene oxidation, reasonable quantities (20-54 LC area %) of 4-phenylcyclohexenone were produced in several of the conditions evaluated (Table D.11). Condition 5 in Table D.11 produced 54 LC area % of 4-phenylcyclohexenone, corresponding to approximately 10% yield by preliminary ¹H NMR analysis. It should be noted that the corrosion of Pd was not complete after 24 h under these conditions, as confirmed visually. This implies that the catalyst loading was lower than 3.3 mol% (the theoretical maximum based on initial stoichiometry). Longer dissolution conditions would increase the initial concentration of dissolved Pd and likely increase product yields. An important experiment to determine the stability of this catalyst system is to measure the concentration of Pd before the addition of substrate and after

stopping the reaction. Increased levels of Pd after addition of substrate would indicate that net corrosion continues even in the presence of a reductant (i.e. substrate), while decreased Pd concentrations would indicate the system has reached a point where the rate of corrosion is exceeded by substrate-induced decomposition. Overall, the success of this initial screen for α,β -dehydrogenation of 4-phenylcyclohexanone is promising and commends further optimization and exploration of additional ketone substrates.



Equation D.12. Reaction scheme for corrosion-oxidation sequence with 4-phenylcyclohexanone substrate

Table D.11. 4-phenylcyclohexanone dehydrogenation to 4-phenylcyclohexenone by corroded Pd solutions

condition	ligand	solvent	additive	% LC area
1	none	tAmylOH/AcOH (3:2)	CuCl ₂	9
2	phen	AcOH		2
3	6-Me-bpy	AcOH		11
4	6-Me-bpy	Tol/AcOH (3:2)		14
5	6-Me-bpy	tAmylOH/AcOH (3:2)		54
6	6-Me-bpy	Tol/TFAH (3:2)		0
7	6-Me-bpy	tAmylOH/TFAH (3:2)		4
8	4,4'-(<i>t</i> Bu) ₂ -bpy	Tol/AcOH (3:2)		2
9	4,4'-(<i>t</i> Bu) ₂ -bpy	tAmyl/AcOH (3:2)		5
10	4,4'-(<i>t</i> Bu) ₂ -bpy	AcOH		1
11	TPA	tAmylOH/TFAH (3:2)		0
12	TPA	tAmylOH/AcOH (3:2)	CuCl ₂	4
13	TPA	tAmylOH/AcOH (3:2)	2,6-'Bu ₂ BQ	0
14	2-Pyrazol-1-yl-pyridine	Tol/TFAH (3:2)		0
15	2-Pyrazol-1-yl-pyridine	tAmylOH/TFAH (3:2)		0
16	2-Pyrazol-1-yl-pyridine	AcOH		20

D.3 Conclusions and future directions

The above results show that, in general, Pd corrosion is facilitated by the presence of chelating nitrogen-donor ligands in acidified weakly polar/coordinating organic solvents. Quinones seem to have minimal or even detrimental effects on the amounts of Pd dissolution. The effect of metal additives is ambivalent, especially in the presence of ancillary ligands. Higher temperatures and pressures of O₂ generally favor increased rates of Pd corrosion, as does mechanical agitation (i.e. glass beads). Promising preliminary conditions utilizing 6-methyl-2,2'-bipyridine as the ligand and tAmylOH:AcOH 3:2 v/v solvent have been identified for the oxidative dehydrogenation of 4-phenylcyclohexanone to 4-phenylcyclohexenone. This is especially encouraging, since α,β -dehydrogenation of ketones represents a useful method for introducing complexity into organic molecules.

The above data represent an important entry point into the development of a Pd catalyst capable of achieving selective aerobic oxidation of organic molecules with indefinitely many TONs. Further experiments must be performed remain to further develop this research. An expanded exploration of chemical space of ligand structure is warranted. Among the most effective ligands are alkyl substituted bipyridine ligands such as 6-methyl-2,2'-bipyridine and 5,5'-dimethyl-2,2'-bipyridine. The effectiveness of these ligands may be attributed to enhanced Van der Waals interactions between the surface of metallic Pd and the ligands, facilitating dissolution. Replacing the methyl groups on these ligands for longer chain alky groups (e.g. butyl) may further enhance these proposed Van der Waals interactions and result in greater Pd dissolution. With regards to substrate oxidation, a greater variety of organic substrates should be evaluated to determine whether the corroded Pd solutions are effective catalysts for a wider array of oxidation reactions. Classes of oxidations include allylic oxidation (e.g. acetoxylation), oxidative C–H/C–H biaryl

coupling, benzylic oxidation, and α,β -dehydrogenation of ketones (linear, 5- and 7+-membered rings). It will be important to evaluate whether the conditions developed are indeed effective at corroding Pd in the presence of substrates, and experiments should be performed to determine the amount of Pd in solution before and after substrate oxidation has occurred. Finally, it should be noted that "Pd black" is not necessarily a monolithic substance composed entirely of Pd metal. Making such an assumption may fatally derail any progress in the development of "immortal" Pd oxidation catalysts. Work should be undertaken to determine the compositions of the types of Pd black that form during a variety of homogeneous Pd-catalyzed oxidation reactions and evaluate whether the dissolution conditions developed are even efficacious for corrosion of a plurality of forms of Pd black.

D.4 Experimental

General Considerations: Pd metal (Aldrich, powder, $<1 \mu\text{M}$, $\geq 99.9\%$ trace metal basis, lot # MKBT9910V, PCode 1001993337) was purchased from Sigma-Aldrich. All reagents were purchased from commercial suppliers. Reactions were carried out in 13x100 mm borosilicate glass heavy wall test tube on a heated multi-well reactor with orbital mixing. An Agilent 5110 ICP-OES was used for determination of Pd content calibrated to a set of standards of known Pd concentration.

Pd calibration standards were prepared as follows. A solution of $\text{Pd}(\text{OAc})_2$ (6.4 mg, 0.029 mmol) in acetic acid (2.0 mL) was prepared. Serial dilutions were performed with the initial solution (1.0 mL diluted to 2.0 mL with AcOH) to prepare 2 mL solutions of 1.6, 0.8, and 0.4 mg/mL. A 200 μL aliquot of each of these solutions was diluted to 10.0 mL with an aqueous solution of 2% AcOH and 5% HNO_3 . The diluted aliquots represent standards of 32, 16, 8, and 4

ppm Pd(OAc)₂. Since Pd(OAc)₂ is 47% Pd by mass, these standards are 15.04, 7.52, 3.76, and 1.88 ppm Pd, respectively. These solutions served as the basis for the calibration curve.

General procedure for dissolution screens: Pd powder (1.0 mg, 0.01 mmol) was added to a 13x100 mm borosilicate glass heavy wall test tube as a 0.5 mL slurry. Additives (screen-dependent; 0.01-0.02 mmol) were as stock solutions to the test tubes charged with Pd powder such that the total volume was 1 mL. The mixtures were stirred overnight at 70 °C under 1 atm of O₂. After allowing undissolved Pd powder to settle to the bottom of the tube, 200 μL aliquots of each tube were added to 25 mL centrifuge tubes and diluted to 10.0 mL with an aqueous solution of 2% AcOH and 5% HNO₃ before being submitted for ICP-OES analysis. Precipitate formed in some of the aqueous solutions and those samples were passed through a syringe filter before being submitted for ICP-OES analysis. This procedure was adapted accordingly for variations in additive stoichiometry, etc.

Organic oxidation screens: Reaction tubes were prepared as above for the dissolution reactions according to the conditions reported in Tables D.9, D.10 and D.11. After reacting for 24 h, substrates (benzyl alcohol, 4-phenylcyclohexanone, styrene, 0.3 mmol each) were added to the reaction tubes and allowed to mix for an additional 24 h. For styrene oxidation 2 equivalents of water were added. The reactions were stopped, aliquots of each reaction were removed, and submitted for UPLC analysis. Benzyl alcohol conversion to benzaldehyde was determined against calibrated standards. Styrene and 4-phenylcyclohexanone conversions were assayed by LC area % of the products.

D.5 References

1. Wang, D.; Weinstein, A. B.; White, P. B.; Stahl, S. S. Ligand-Promoted Palladium-Catalyzed Aerobic Oxidation Reactions. *Chem. Rev.* **2018**, *118*, 2636-2679.
2. Stahl, S. S. Palladium Oxidase Catalysis: Selective Oxidation of Organic Chemicals by Direct Dioxygen-Coupled Turnover. *Angew. Chem. Int. Ed.* **2004**, *43*, 3400-3420.
3. Stahl, S. S. Palladium-Catalyzed Oxidation of Organic Chemicals with O₂. *Science* **2005**, *309*, 1824-1826.
4. Salazar, C. A. Mechanistic Insights Support the Development of Efficient Palladium Catalysts for Oxidative C–H Arylation with O₂. PhD Dissertation, University of Wisconsin-Madison, Madison, WI, 2021.
5. Vasseur, A.; Muzart, J.; Le Bras, J. Ubiquitous Benzoquinones, Multitalented Compounds for Palladium-Catalyzed Oxidative Reactions. *Eur. J. Org. Chem.* **2015**, 4053-4069.
6. Salazar, C. A.; Flesch, K. N.; Zhou, P. S.; Musaev, D. G.; Stahl, S. S. Palladium-Catalyzed C–H Oxidative Arylation Accessing High Turnover with O₂. *Science* **2020**, *370*, 1454-1460.
7. Jira, R. Acetaldehyde from Ethylene—A Retrospective on the Discovery of the Wacker Process. *Angew. Chem. Int. Ed.* **2009**, *48*, 9034-9037.
8. Bruns, D. L.; Musaev, D. J.; Stahl, S. S. Can Donor Ligands Make Pd(OAc)₂ a Stronger Oxidant? Access to Elusive Palladium(II) Reduction Potentials and Effects of Ancillary Ligands via Palladium(II)/Hydroquinone Redox Equilibria. *J. Am Chem. Soc.* **2020**, *142*, 19678-19688.
9. Tereniak, S. J.; Stahl, S. S. Are Phosphines Viable Ligands for Pd-Catalyzed Aerobic Oxidation Reactions? Contrasting Insights from a Survey of Six Reactions. *ACS Catal.* **2018**, *8*, 3708-3714.

10. See this citation and citations herein: Pun, D.; Diao, T.; Stahl, S. S. Aerobic Dehydrogenation of Cyclohexanone to Phenol Catalyzed by Pd(TFA)₂/2-Dimethylaminopyridine: Evidence for the Role of Pd Nanoparticles. *J. Am. Chem. Soc.* **2013**, *135*, 8213-8221.
11. Wang, D.; Stahl, S. S. Pd-Catalyzed Aerobic Oxidative Biaryl Coupling: Non-Redox Cocatalysis by Cu(OTf)₂ and Discovery of Fe(OTf)₃ as a Highly Effective Cocatalyst. *J. Am. Chem. Soc.* **2017**, *139*, 5704-5707.
12. Liu, J.; Gudmunsson, A.; Bäckvall, J.-E. Efficient Aerobic Dehydrogenation of Organic Molecules by Multistep Electron Transfer. *Angew. Chem. Int. Ed.* **2021**, *60*, 15686-15704.
13. Erdtman, H.; Högberg, H.-E. The Acid-Catalyzed Oligomerisation of *p*-Benzoquinone. *Tetrahedron* **1979**, *35*, 535-540.
14. Mueller, J. A.; Goller, C. P.; Sigman, M. S. Elucidating the Significance of β-Hydride Elimination and the Dynamic Role of Acid/Base Chemistry in a Palladium-Catalyzed Aerobic Oxidation of Alcohols. *J. Am. Chem. Soc.* **2004**, *126*, 9724-9734.